YUKAWA INSTITUTE FOR THEORETICAL PHYSICS

DOCTORAL THESIS

Extended Nielsen-Ninomiya theorem for Floquet and non-Hermitian systems

Author: Takumi BESSHO

A thesis submitted in fulfillment of the requirements for the degree of Doctor of Science and the WISE Program

in the

Department of Physics
Kyoto University

February 8, 2022

Abstract

Recently, the study of topological phases has made remarkable progress on highly-controlled non-equilibrium systems: Floquet and non-Hermitian systems. Floquet systems are dynamical systems governed by time-periodic Hamiltonians. Non-Hermitian systems are non-equilibrium and open systems, where effective Hamiltonians become non-Hermitian. Floquet and non-Hermitian systems provide desirable platforms for realizing the topological phenomena proposed in equilibrium. Furthermore, it has become clear that Floquet and non-Hermitian systems can realize novel topological phenomena that cannot occur in equilibrium. One such unique physics is the breakdown of the Nielsen-Ninomiya theorem [1, 2]. Nielsen-Ninomiya theorem was initially proposed as a no-go theorem for the lattice realization of the Standard Model in particle physics, which assures the pair-wise existence of gapless fermions. However, in Floquet systems, two schemes to realize a single Weyl fermion were proposed [3, 4]. Moreover, in non-Hermitian systems, a general procedure to obtain an anomalous single gapless mode was proposed [5].

In this paper, we establish an extended version of the Nielsen-Ninomiya theorem for Floquet and non-Hermitian systems that is valid even in the presence of anomalous single gapless modes above. The extended Nielsen-Ninomiya theorem relates the anomalous gapless modes with bulk topological invariants intrinsic to dynamical systems. we also see applications of this theorem for both Floquet systems and non-Hermitian systems.

1. Extended Nielsen-Ninomiya theorem [6]

In this chapter, we find and prove formulae that relate anomalous gapless modes and topological invariants in Floquet and non-Hermitian systems in a unified manner. First, for non-Hermitian systems, we refine an observation given by Lee, *et al.* [5] into formulae of extended Nielsen-Ninomiya theorem for non-Hermitian systems. Then, for Floquet systems, we establish a topological duality between Floquet and non-Hermitian systems for energy gaps, symmetries, and topological charges of gapless modes. Then, we apply the duality to the formula in non-Hermitian systems to obtain the extended Nielsen-Ninomiya theorem for Floquet systems.

2. Non-Hermitian chiral magnetic effect [6]

Applying the extended Nielsen-Ninomiya theorem for non-Hermitian systems, we propose a non-Hermitian version of the chiral magnetic effect. Chiral magnetic effect is an occurrence of electric current proportional to an applied magnetic field in the presence of chemical potential unbalance in Weyl fermions [7]. The effectively single Weyl fermion in non-Hermitian systems can be a platform to realize the chiral magnetic effect. We also find a formula, which assures the number of right-going modes is proportional to an applied magnetic field.

3. Extrinsic topology in Floquet anomalous edge states in quantum walks [8]

Applying the extended Nielsen-Ninomiya theorem for Floquet systems, we propose extrinsic topological nature in quantum walks. Quantum walk is a quantum version of random walks, and a time-periodic series of unitary operators describe its dynamics. We give a topological classification of boundary states in quantum walks. We show that the boundary states depend not only on bulk topology through bulk-boundary correspondence but also on boundary topology.

Contents

List of Publications

Papers related to the thesis

1. Takumi Bessho and Masatoshi Sato,
   Nielsen-Ninomiya Theorem with Bulk Topology: Duality in Floquet and Non-Hermitian Systems,
   Physical Review Letters **127**, 196404 (2021).
   © 2021 American Physical Society

2. Takumi Bessho, Ken Mochizuki, Hideaki Obuse and Masatoshi Sato,
   Extrinsic Topology of Floquet Anomalous Edge States in Quantum Walks,
   arXiv:2112.03167.

Published papers not included in the thesis

1. Kohei Kawabata, Takumi Bessho, and Masatoshi Sato,
   Classification of Exceptional Points and Non-Hermitian Topological Semimetals,
   Physical Review Letters **123**, 066405 (2019).
   © 2019 American Physical Society

2. Takumi Bessho, Kohei Kawabata, and Masatoshi Sato,
   Topological Classificaton of Non-Hermitian Gapless Phases: Exceptional Points and Bulk Fermi Arcs,
   JPS Conference Proceeding **30**, 011098 (2020).
   © 2019 The Physical Society of Japan

3. Ken Mochizuki, Takumi Bessho, Masatoshi Sato, and Hideaki Obuse,
   Topological quantum walk with discrete time-glide symmetry,
   Physical Review B **102**, 035418 (2020).
   © 2020 American Physical Society

List of Abbreviations

BZ	**B**rillouin **Z**one
PBC	**P**eriodic **B**oundary **C**onditions
OBC	**O**pen **B**oundary **C**onditions
AZ	**A**ltland-**Z**irnbauer
TRS	**T**ime **R**eversal **S**ymmetry
PHS	**P**article **H**ole **S**ymmetry
CS	**C**hiral **S**ymmetry
CME	**C**hiral **M**agnetic **E**ffect
SLS	**S**ub-**L**attice **S**ymmetry
pH	**p**seudo-**H**ermiticity
SSH	**S**u-**S**chrieffer-**H**eefer
DOS	**D**ensity **O**f **S**tates

Chapter 1

Introduction

In the last two decades, the study of topological phases has encountered great progress in condensed matter physics. The quantization of Hall conductance was firstly observed in 1980 [9]. This *integer quantum Hall effect* is now used for SI units. Later, it was found that the quantized Hall conductance is rewritten as the Chern number, a topological invariant in two dimensions [10, 11]. After these works, there has been little progress in the study of topological insulators for a long time. In 2005, however, the prediction of quantum spin Hall effect paved a new way [12]. Through this study, it was found that symmetries enrich topological phases, and many researchers started to study in this direction: the topological condensed matter physics. The studies of symmetry-enriched topological phases have been summarized in a periodic table of topological insulators and superconductors [13–18], which shows the presence or absence of $\mathbb{Z}, \mathbb{Z}_2$ topological invariants in each symmetry class and dimensions. [1]

Recently, the topological phases have also been widely investigated in non-equilibrium systems. We discuss two uprising fields of non-equilibrium systems: Floquet systems and non-Hermitian systems. In Sec. 1.1, we review the topological classifications and some examples in Floquet systems. In Sec. 1.2, we review the topological classification and some examples in non-Hermitian systems. Finally, we explain the organization of this thesis in Sec. 1.3.

1.1 Overview of recent studies on Floquet topological phases

In this section, we review the recent studies of Floquet topological phases from the perspective of classifications. Floquet systems are periodically driven systems governed by a time-periodic Hamiltonian $H(t) = H(t + T)$, where T is the one-cycle time period of the system. The stroboscopic dynamics of such systems can be understood by a time-averaged Hamiltonian as effectively time-independent dynamics. Its key ingredient is the Floquet theorem with time translation symmetry, which leads to energy periodicity [19, 20], an analog of Bloch theorem with translation symmetry leading to momentum periodicity. In experiments, for example, by using appropriate lasers that induce a time-periodic part of the original Hamiltonian, we can obtain the targeted Hamiltonian which is difficult to realize in equilibrium; such a scheme is called *Floquet engineering*.

Then, Floquet systems can be a desirable platform of topological insulators and superconductors [21–24], where the effective Hamiltonian can be approximately evaluated by *high-frequency expansion* [25]. Beyond the high-frequency approximation, it was found that Floquet systems can realize novel edge states that have no counterpart in equilibrium, called *Floquet anomalous*

[1] This classification table explains the topological phases without interactions. In this thesis, we focus on topological phases without interactions. Even in the presence of strong interactions, many of these topological phases are known to survive.

edge states [26–31]: Remarkably, we can realize robust chiral edge modes without the Chern number in Floquet systems.

We can also realize novel bulk topology in Floquet systems. Thouless pumping [32], the time-periodic Hamiltonian of which pumps one particle in one cycle, is actually a typical example. The quasi-energy spectrum of the effective time-independent Hamiltonian evaluated from the Thouless pumping model indicates the existence of unpaired chiral modes. The net number of the chiral modes in the effective Hamiltonian indicates the number of pumped particles in one cycle. A three-dimensional counterpart with unpaired Weyl fermions enables the chiral magnetic effect [7], an occurrence of current by an applied magnetic field, in Floquet systems [3, 4].

Recently, various studies on Floquet topological phases have been summarized as topological classifications [3, 33]. These classifications have clarified the presence or absence of non-trivial topological phases in each symmetry class and dimensions.

In Sec. 1.1.1, we review the classification of Floquet topological insulators and superconductors [33]. In Sec. 1.1.2, we review the concrete topological invariants and models of Floquet topological insulators and superconductors for class A $d = 2$ [27], class AIII $d = 1$ [30], and class D $d = 1$ [28]. In Sec. 1.1.3, we review the topological classification of Floquet gapless phases [3]. In Sec. 1.1.4, we review the concrete topological invariants and models of Floquet gapless phases for class A $d = 1$ [32, 34] and $d = 3$ [3, 4, 26]

1.1.1 Classification of Floquet topological insulators

In this subsection, we review the classification theory on Floquet topological insulators. The stroboscopic dynamics in Floquet systems can be described by the one-cycle time evolution operator, sometimes called the *Floquet operator*,

$$U_F(\boldsymbol{k}) = \mathcal{T} \exp[-i \int_0^T dt H(\boldsymbol{k}, t)]. \tag{1.1}$$

The effective time-independent Hamiltonian, called the *Floquet Hamiltonian*, is defined by $U_F(\boldsymbol{k}) = e^{-iH_F(\boldsymbol{k})T}$ or equivalently,

$$H_F(\boldsymbol{k}) = \frac{i}{T} \log U_F(\boldsymbol{k}). \tag{1.2}$$

Quasi-energy spectrum of $H_F(\boldsymbol{k})$ has $2\pi/T$ periodicity which comes from the uncertainty of logarithm for a complex phase.

We next introduce symmetries. In equilibrium, we have ten-fold Altland-Zirnbauer (AZ) symmetry classes as local symmetry classes [15, 35]. Hamiltonians H possible satisfies time-reversal symmetry (TRS), particle-hole symmetry (PHS) and/or chiral symmetry (CS):

$$THT^{-1} = H, \tag{1.3}$$
$$CHC^{-1} = -H, \tag{1.4}$$
$$\Gamma H \Gamma^{-1} = -H. \tag{1.5}$$

Here, T and C are anti-unitary operators with $T^2 = \pm 1$ and $C^2 = \pm 1$, and Γ is a unitary operator with $\Gamma^2 = 1$. If the Hamiltonian has translational symmetry, Bloch (BdG) Hamiltonians obey

$$TH(\boldsymbol{k})T^{-1} = H(-\boldsymbol{k}), \tag{1.6}$$
$$CH(\boldsymbol{k})C^{-1} = -H(-\boldsymbol{k}), \tag{1.7}$$
$$\Gamma H(\boldsymbol{k})\Gamma^{-1} = -H(\boldsymbol{k}). \tag{1.8}$$

Similarly, in Floquet systems, TRS, PHS, and CS are given as

$$TH(\boldsymbol{k},t)T^{-1} = H(-\boldsymbol{k},-t), \tag{1.9}$$
$$CH(\boldsymbol{k},t)C^{-1} = -H(-\boldsymbol{k},t), \tag{1.10}$$
$$\Gamma H(\boldsymbol{k},t)\Gamma^{-1} = -H(\boldsymbol{k},-t). \tag{1.11}$$

These symmetries reproduce the original TRS, PHS, and CS for the effective Hamiltonian $H_F(\boldsymbol{k})$:

$$TH_F(\boldsymbol{k})T^{-1} = H_F(-\boldsymbol{k}), \tag{1.12}$$
$$CH_F(\boldsymbol{k})C^{-1} = -H_F(-\boldsymbol{k}), \tag{1.13}$$
$$\Gamma H_F(\boldsymbol{k})\Gamma^{-1} = -H_F(\boldsymbol{k}). \tag{1.14}$$

If there are PHS and/or CS, there is a symmetry constraint $\epsilon_n = -\epsilon_m \pmod{2\pi}$ for some energy bands n, m. Then, we obtain high-symmetric Fermi energy levels $\epsilon = 0, \pi$.

We first review the classification of Floquet topological insulators and superconductors given by Roy and Harper [33]. We assume two energy gaps both at high-symmetric energies $\epsilon = 0$ and $\epsilon = \pi/T$ are open. A Floquet system is given by a microscopic Hamiltonian $H(\boldsymbol{k},t)$, but we consider the topological classification of time evolution operators $U(\boldsymbol{k},t)$ because it has the same information as the original microscopic Hamiltonians. We rewrite the TRS, PHS, and CS as those for time evolution operator $U(\boldsymbol{k},t)$:

$$TU(\boldsymbol{k},t)T^{-1} = U(-\boldsymbol{k},-t), \tag{1.15}$$
$$CU(\boldsymbol{k},t)C^{-1} = U(-\boldsymbol{k},t), \tag{1.16}$$
$$\Gamma U(\boldsymbol{k},t)\Gamma^{-1} = U(\boldsymbol{k},-t). \tag{1.17}$$

We next decompose the time evolution operator $U(\boldsymbol{k},t)$ into two parts:

$$C(\boldsymbol{k},t) := e^{-iH_F(\boldsymbol{k})t},\ L(\boldsymbol{k},t) := U(\boldsymbol{k},t)C(\boldsymbol{k},t)^{-1}. \tag{1.18}$$

We call $C(\boldsymbol{k},t)$ *constant time evolution* and $L(\boldsymbol{k},t)$ *loop unitary*. Here, we implicitly supposed that $H_F(\boldsymbol{k})$ is gapped at $\epsilon = 0,\ \pi/T$ and the branch cut is taken at $\epsilon = \pi/T$. We note that this decomposition is unique up to homotopy equivalence [33]. Thus, the topological classification problem of the time evolution operator $U(\boldsymbol{k},t)$ becomes the topological classification problem of constant time evolution $C(\boldsymbol{k},t)$ and loop unitary $L(\boldsymbol{k},t)$.

The topological classification of $C(\boldsymbol{k},t)$ is equivalent to that of $H_F(\boldsymbol{k})$, which can be seen as ordinary Hamiltonian with a gap at $\epsilon = 0$. Thus, the periodic table of $C(\boldsymbol{k},t)$ is equivalent to that of ordinary topological insulators and superconductors in equilibrium.

The topological classification of $L(\boldsymbol{k},t)$ also becomes the same as that of ordinary topological insulators and superconductors, but for different reasons. We introduce a *doubled Hamiltonian* $H_L(\boldsymbol{k},t)$ as

$$H_L(\boldsymbol{k},t) := \begin{pmatrix} 0 & L(\boldsymbol{k},t) \\ L^\dagger(\boldsymbol{k},t) & 0 \end{pmatrix}. \tag{1.19}$$

We note that $H_L(\boldsymbol{k},t)$ is Hermitian, has eigenvalues ± 1 due to $H_L(\boldsymbol{k},t)^2 = \hat{1}$, periodic both in k_j and t, and obeys proper chiral symmetry:

$$\Sigma_z H_L(\boldsymbol{k},t)\Sigma_z = -H_L(\boldsymbol{k},t),\ \Sigma_z := \begin{pmatrix} \hat{1} & 0 \\ 0 & -\hat{1} \end{pmatrix}. \tag{1.20}$$

Therefore, $H_L(\boldsymbol{k},t)$ can be regarded as a Hamiltonian of topological insulators and superconductors with "momentum" $(\boldsymbol{k},t)$ on the Brillouin zone $\mathbb{T}^{d+1} = [-\pi/a,\pi/a]^d \times [-T/2,T/2]$. Here a is lattice constant. $L(\boldsymbol{k},t)$ obey the same symmetries as $U(\boldsymbol{k},t)$ in Eqs. (1.15)-(1.17), and thus $H_L(\boldsymbol{k},t)$ obeys

$$\tilde{T} H_L(\boldsymbol{k},t)\tilde{T}^{-1} = H_L(-\boldsymbol{k},-t),\ \tilde{T} := \begin{pmatrix} T & 0 \\ 0 & T \end{pmatrix}, \tag{1.21}$$

$$\tilde{C} H_L(\boldsymbol{k},t)\tilde{C}^{-1} = H_L(-\boldsymbol{k},t),\ \tilde{C} := \begin{pmatrix} C & 0 \\ 0 & C \end{pmatrix}, \tag{1.22}$$

$$\tilde{\Gamma} H_L(\boldsymbol{k},t)\tilde{\Gamma}^{-1} = H_L(\boldsymbol{k},-t),\ \tilde{\Gamma} := \begin{pmatrix} \Gamma & 0 \\ 0 & \Gamma \end{pmatrix}. \tag{1.23}$$

These symmetries have the form of two-fold crystalline symmetries [17, 18, 36, 37], and thus we can calculate the topological classification by the methods developed in equilibrium. One systematic classification method depends on K-theory firstly established by Kitaev [14]. Another systematic method depends on the extension problem of Clifford algebra, which is also firstly proposed by Kitaev and later developed by Morimoto, Furusaki, Chiu, Schnyder, and Shinsei, *et al.*, [15, 17, 36, 37]. We explain the classification method of Clifford algebra in Chap. 2. Then, we can find that the topological classification of $L(\boldsymbol{k},t)$ coincides with the topological classification of ordinary insulators and superconductors in equilibrium.

As a result, the periodic table of Floquet topological insulators and superconductors is the same as that of ordinary topological insulators and superconductors except for the doubling of topological numbers [Table 1.1].

The bulk-boundary correspondence in Floquet systems is summarized as [2]

$$\begin{cases} \displaystyle\sum_{\epsilon_\alpha=0} \nu_\alpha^0 = n_C + n_L, \\ \displaystyle\sum_{\epsilon_\alpha=\pi/T} \nu_\alpha^\pi = (-1)^d n_L, \end{cases} \tag{1.24}$$

[2] We note that this formula is sometimes meaningless because some convenient Floquet topological invariants are defined from the combinations of n_C and n_L. One nontrivial result from this form is that the Floquet anomalous topological phases — the topological phases that have nontrivial gapless states but has trivial bulk topological invariants $n_C = 0$ of the Floquet Hamiltonian $H_F(\boldsymbol{k})$ — have net n_L gapless states at $\epsilon = 0$ and net $(-1)^d n_L$ gapless states at $\epsilon = \pi/T$.

TABLE 1.1: Periodic table of Floquet topological insulators and superconductors in Altland-Zirnbauer (AZ) symmetry classes with two gaps $\epsilon = 0$ and $\epsilon = \pi/T$.

AZ class	T	C	Γ	$d=1$	2	3
A	0	0	0	0	$\mathbb{Z}\oplus\mathbb{Z}$	0
AIII	0	0	1	$\mathbb{Z}\oplus\mathbb{Z}$	0	$\mathbb{Z}\oplus\mathbb{Z}$
AI	$+1$	0	0	0	0	0
BDI	$+1$	$+1$	1	$\mathbb{Z}\oplus\mathbb{Z}$	0	0
D	0	$+1$	0	$\mathbb{Z}_2\oplus\mathbb{Z}_2$	$\mathbb{Z}\oplus\mathbb{Z}$	0
DIII	-1	$+1$	1	$\mathbb{Z}_2\oplus\mathbb{Z}_2$	$\mathbb{Z}_2\oplus\mathbb{Z}_2$	$\mathbb{Z}\oplus\mathbb{Z}$
AII	-1	0	0	0	$\mathbb{Z}_2\oplus\mathbb{Z}_2$	$\mathbb{Z}_2\oplus\mathbb{Z}_2$
CII	-1	-1	1	$2\mathbb{Z}\oplus 2\mathbb{Z}$	0	$\mathbb{Z}_2\oplus\mathbb{Z}_2$
C	0	-1	0	0	$2\mathbb{Z}\oplus 2\mathbb{Z}$	0
CI	$+1$	-1	1	0	0	$2\mathbb{Z}\oplus 2\mathbb{Z}$

where n_C is the topological invariant of $C(\boldsymbol{k},t)$ or equivalently $H_F(\boldsymbol{k})$, and n_L is the topological invariant of $L(\boldsymbol{k})$. $\nu_\alpha^{0,\pi}$ is the topological charge of gapless states of α-th Fermi surface at $\epsilon = 0$ or π/T. We note that the explicit form of $\nu_\alpha^{0,\pi}$ is defined to become one for the gapless Dirac Hamiltonian $H_{\text{Dirac}}(\boldsymbol{k}) = \sum_j k_j\Gamma_j + \epsilon_F\hat{1}$ of the symmetry class and the dimensions, where $\epsilon_F = 0, \pi/T$ and we introduced the gamma matricies $\{\Gamma_i, \Gamma_j\} = 2\delta_{ij}$. [3] The $(-1)^d$ sign factor does not exist in the previous works [33], but this sign is naturally appears to be compatible with the topological charge defined from the primitive Dirac Hamiltonian $H_{\text{Dirac}}(\boldsymbol{k}) = \sum_j k_j\Gamma_j$. we found this $(-1)^d$ factor by studying Floquet anomalous gapless states [8].

For class A, AI, and AII, we can take energy gaps different from $\epsilon = 0, \pi/T$ because there is no symmetry constraint of the form $\epsilon_n = -\epsilon_m$. If there are l energy gaps $\epsilon = \mu_i$ $(i = 1, \dots, l)$, the topological classification [Table 1.1] change as $\mathbb{Z}\oplus\mathbb{Z} \to \oplus_l\mathbb{Z}$, $\mathbb{Z}_2\oplus\mathbb{Z}_2 \to \oplus_l\mathbb{Z}_2$, $2\mathbb{Z}\oplus 2\mathbb{Z} \to \oplus_l 2\mathbb{Z}$.

In the following sections, we review previous studies based on the classification table.

1.1.2 Examples of Floquet topological insulators

We review examples of Floquet topological insulators appearing in Table 1.1.

Class A $d = 2$: Floquet anomalous Chern insulator

Class A 2D systems have $\mathbb{Z}\oplus\mathbb{Z}$ topological invariants according to Table 1.1, which indicates the existence of two integer-valued topological invariants. One $\mathbb{Z}$ topological invariant is the Chern number Ch calculated from the effective Hamiltonian $H_F(\boldsymbol{k})$.

Here, for completeness, we explain the definition of the Chern number in detail. For a Bloch wave function satisfying $H(\boldsymbol{k})\,|u(\boldsymbol{k})\rangle = E(\boldsymbol{k})\,|u(\boldsymbol{k})\rangle$, We define Berry connection (gauge

[3]This is because the gapless Dirac Hamiltonian is a primitive nontrivial gapless model from the perspective of topological classifications. For example, for the Weyl Hamiltonian $H(\boldsymbol{k}) = k_x\sigma_x + k_y\sigma_y + k_z\sigma_z$ has unit topological charge $\nu = 1$, where the explicit form of ν is given by the Chern number on S^2 surrounding $\boldsymbol{k} = \boldsymbol{0}$. Another example is the 2D chiral-symmetric Dirac Hamiltonian $H(\boldsymbol{k}) = k_x\sigma_x + k_y\sigma_y$ satisfying $\sigma_x H\sigma_x = -H$, which has unit topological charge $\nu = 1$ given by a winding number $\nu = \int_{S_1}\frac{id\boldsymbol{k}}{2\pi}\cdot \mathrm{tr}[H^{-1}\nabla H]$ on S^1 surrounding $\boldsymbol{k} = \boldsymbol{0}$.

potential) and Berry curvature (field strength) as

$$\boldsymbol{A}(\boldsymbol{k}) := -i \langle u(\boldsymbol{k})| \frac{\partial}{\partial \boldsymbol{k}} |u(\boldsymbol{k})\rangle , \quad F_{k_x k_y} := \partial_{k_x} A_y - \partial_{k_y} A_x. \tag{1.25}$$

Then, the Chern number is defined as the integration of Berry curvature on the whole Brillouin zone (BZ)

$$Ch := \int_{\mathrm{BZ}} \frac{\mathrm{d}^2 k}{2\pi} F_{k_x k_y}. \tag{1.26}$$

Remarkably, the Chern number is invariant under gauge transformation. We can arbitrarily change the complex phase factor of Bloch wave function (gauge transformation) as

$$|u(\boldsymbol{k})\rangle \to e^{i\theta(\boldsymbol{k})} |u(\boldsymbol{k})\rangle . \tag{1.27}$$

Under the gauge transformation, Berry connection changes but Berry curvature does not change [4]

$$\boldsymbol{A}(\boldsymbol{k}) \to \boldsymbol{A}(\boldsymbol{k}) + \partial_{\boldsymbol{k}}\theta(\boldsymbol{k}), \quad F_{k_x k_y} \to F_{k_x k_y} + \partial_{k_x}\partial_{k_y}\theta(\boldsymbol{k}) - \partial_{k_y}\partial_{k_x}\theta(\boldsymbol{k}) = F_{k_x k_y}. \tag{1.28}$$

Thus the Chern number is a gauge independent quantity [5]. Moreover, the Chern number Ch takes only integer values. We suppose the Brillouin zone is split into two patches S_1 and S_2. On each patch, we take different gauges such that $F_{k_x k_y}$ is well-defined (do not have singularity). The gauge transformation on the boundary $\partial S_1 = -\partial S_2$ is given by some gauge transformation $\boldsymbol{A}_2(\boldsymbol{k}) = \boldsymbol{A}_1(\boldsymbol{k}) + \partial_{\boldsymbol{k}}\theta(\boldsymbol{k})$. Then, from Green's theorem, Ch reduces into

$$Ch = \int_{\partial S_1} \boldsymbol{A}^1(\boldsymbol{k}) \cdot \frac{\mathrm{d}\boldsymbol{k}}{2\pi} + \int_{\partial S_2} \boldsymbol{A}^2(\boldsymbol{k}) \cdot \frac{\mathrm{d}\boldsymbol{k}}{2\pi} = \int_{\partial S_2} [-\boldsymbol{A}^1(\boldsymbol{k}) + \boldsymbol{A}^2(\boldsymbol{k})] \cdot \frac{\mathrm{d}\boldsymbol{k}}{2\pi} = \int_{\partial S_2} \partial_{\boldsymbol{k}}\theta(\boldsymbol{k}) \cdot \frac{\mathrm{d}\boldsymbol{k}}{2\pi}. \tag{1.29}$$

The phase $\theta(\boldsymbol{k})$ can change only $2\pi\times$integer after one cycle along ∂S_2. Thus, Ch takes integer values. If there are multiple energy bands below Fermi energy, we take the summation of them as a gap-protected topological invariant

$$Ch = \sum_{E_n < E_F} Ch_n. \tag{1.30}$$

Another $\mathbb{Z}$ topological invariant is the three-dimensional winding number [27]:

$$\begin{aligned} W_\pi[L(\boldsymbol{k}, t = k_z)] := &\int_0^{2\pi} \mathrm{d}k_x \int_0^{2\pi} \mathrm{d}k_y \int_0^{T} \mathrm{d}k_z \\ &\varepsilon^{\alpha\beta\gamma} \mathrm{tr}\left[(L^{-1}\partial_{k_\alpha} L)(L^{-1}\partial_{k_\beta} L)(L^{-1}\partial_{k_\gamma} L)\right], \end{aligned} \tag{1.31}$$

where $L(\boldsymbol{k}, t)$ is the loop unitary in Eq. (1.18).

In class A $d = 2$, Eq. (1.24) holds for $n_C = Ch$ and $n_L = W[L]$.

[4] If the gauge transformation has singularity, the Berry curvature may change. One example is $\theta = \tan(k_y/k_x)$, which changes Berry curvature by delta function $\delta(k_x, k_y)$.

[5] When calculating the Chern number, we consider multiple patches covering the manifold BZ $\approx \mathbb{T}^2$. Berry curvature (field strength) should be well-defined (do not have singularity) on each patch of them.

One nontrivial example is given by Rudner, *et al.*, [27]:

$$H(t) = H_j,\ t \in [(j-1)T/5, jT/5], \tag{1.32}$$

$$\begin{cases} H_j = Je^{i\boldsymbol{b}_j\cdot\boldsymbol{k}}\sigma_+ + Je^{-i\boldsymbol{b}_j\cdot\boldsymbol{k}}\sigma_- + \delta_{AB}\sigma_z \text{ for } j = 1,2,3,4 \\ H_5 = \delta_{AB}\sigma_z. \end{cases} \tag{1.33}$$

Here, the hopping directions are given by $\boldsymbol{b}_1 = -\boldsymbol{b}_3 = (a, 0)$ and $\boldsymbol{b}_2 = -\boldsymbol{b}_4 = (0, a)$.

The energy spectrum and the phase diagram are shown in Fig. 1.1. This model has chiral edge modes not only at $\epsilon = 0$ but also at $\epsilon = \pi/T$. The existence of chiral edge modes can be easily understood by considering simple parameters. When $JT/5 = \pi/2$ and $\delta_{AB} = 0$, each time-evolution operator becomes:

$$\begin{cases} e^{-iH_jT/5} = -i(e^{i\boldsymbol{b}_j\cdot\boldsymbol{k}}\sigma_+ + e^{-i\boldsymbol{b}_j\cdot\boldsymbol{k}}\sigma_-) \\ e^{-iH_5T/5} = 1. \end{cases} \tag{1.34}$$

Then, the bulk Floquet operator becomes trivial: $U_F = \hat{1}$, while the boundary hosts nontrivial chiral modes [Fig. 1.2]. The spin up edge mode at $y = 1$ move in the $+x$-direction with the eigenvalue $\lambda = -e^{-2ik_y}$, i.e., $\epsilon = 2(k_y + \pi/2)/T$. The spin down edge mode at $y = L_y$ move in the $-x$-direction with the eigenvalue $\lambda = -e^{2ik_y}$, i.e., $\epsilon = -2(k_y + \pi/2)/T$. These edge modes exist even if we modify the parameters δ_{AB} and J as long as the energy gaps at $\epsilon = 0, \pi/T$ are open.

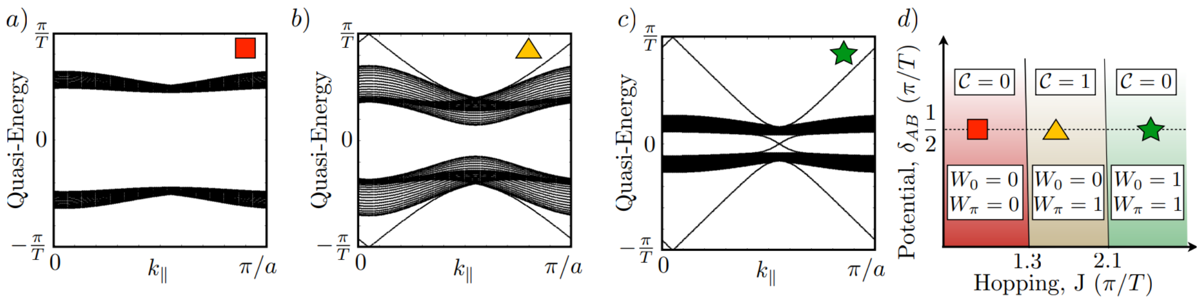

FIGURE 1.1: Energy spectra and the phase diagram of the model Eq. (1.32). Energy spectra for (a) $(JT, \delta_{AB}T) = (0.5\pi, 0.5\pi)$, (b) $(JT, \delta_{AB}T) = (1.5\pi, 0.5\pi)$, and (c) $(JT, \delta_{AB}T) = (2.5\pi, 0.5\pi)$. (d) C represents the Chern number and W_π represents the winding number $W[L]$. W_0 is obtained by taking the branch cut of H_F at $\epsilon = 0$ for $W[L]$. The three topological invariants are unnecessary to characterize the topological phases and obey the relation $W_\pi - W_0 = \mathcal{C}$.
Reproduced from Fig. 3 of Ref. [27]. © 2013 by the American Physical Society.

Class AIII $d = 1$: chiral symmetric quantum walk

Class AIII 1D systems have $\mathbb{Z} \oplus \mathbb{Z}$ topological invariants according to Table 1.1, which indicates the existence of two integer-valued topological invariants. The convenient form of the topological invariants is constructed by Asboth and Obuse [30] in the context of the quantum walk, a quantum version of the random walk. Quantum walk has been studied as a Floquet

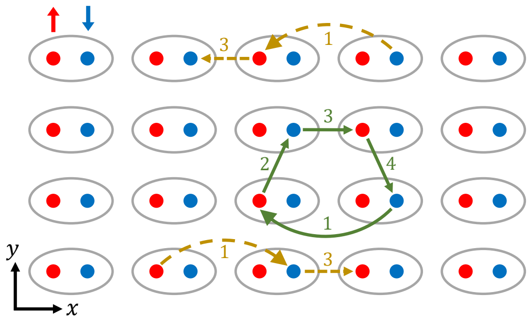

FIGURE 1.2: One cycle dynamics of the model Eq. (1.32) at $JT/5 = \pi/2$ and $\delta_{AB} = 0$. This model has bipartite lattice structure with spin up (red) and spin down (blue). After one-cycle time evolution, bulk states come back to the same states, while spin up edge states along $y = 1$ go in the $+x$-direction and spin down edge states along $y = L_y$ go in the $-x$-direction.

system with the time period $T = 1$. We first consider the time evolution operators in the high-symmetric time domains:

$$U_1(k) := \mathcal{T}\exp\left[-i\int_0^{T/2} \mathrm{d}t H(k,t)\right], \quad U_2(k) := \mathcal{T}\exp\left[-i\int_{T/2}^{T} \mathrm{d}t H(k,t)\right]. \tag{1.35}$$

For simplicity, we take the basis

$$\Gamma = \begin{pmatrix} 1_{p\times p} & 0 \\ 0 & -1_{p\times p} \end{pmatrix}, \; U_1 = \begin{pmatrix} a & b \\ c & d \end{pmatrix}. \tag{1.36}$$

We introduce a topological winding number w_1 defined for unitary operators $U(k)$ in 1D,

$$w_1[U(k)] := \int_0^{2\pi} \frac{i\mathrm{d}k}{2\pi} \mathrm{tr}[U^\dagger \partial_k U]. \tag{1.37}$$

If the band gap at $\epsilon = 0$ ($\epsilon = \pi$) is open, topological invariants $w_1[b]$ and $w_1[c]$ ($w_1[a]$ and $w_1[d]$) are well-defined [38]. Then, the bulk-boundary correspondence is given as

$$\begin{cases} \displaystyle\sum_{\epsilon_\alpha = 0} \nu_\alpha^0 = \frac{w_1[a] - w_1[d]}{2} = w^0, \\ \displaystyle\sum_{\epsilon_\alpha = \pi} \nu_\alpha^\pi = \frac{w_1[c] - w_1[b]}{2} = w^\pi, \end{cases} \tag{1.38}$$

Here, $\nu_\alpha^{0,\pi}$ is the topological charge of gapless boundary states at $\epsilon = 0, \pi/T$. Let us consider the eigenstate of U_F with the eigenvalue ϵ_n as

$$H_F |u_n\rangle = \epsilon_n |u_n\rangle \Leftrightarrow U_F |u_n\rangle = \lambda_n |u_n\rangle, \lambda_n = e^{-i\epsilon_n}. \tag{1.39}$$

Then, CS implies

$$\begin{aligned} H_F[\Gamma |u_n\rangle] &= -\Gamma H_F |u_n\rangle \\ &= -\epsilon_n[\Gamma |u_n\rangle]. \end{aligned} \tag{1.40}$$

Thus, when the eigenstates localized at the boundary are gapless, i.e., $\epsilon_n = 0$ or $\epsilon_n = \pi$, $\Gamma |u_n\rangle$ and $|u_n\rangle$ have the same eigenvalue. In this case, they satisfy [6]

$$\Gamma |u_n\rangle = \pm |u_n\rangle . \tag{1.41}$$

The chirality $\nu^{0,\pi}$ of the gapless states is given by

$$\nu^{0,\pi} = \langle u_n| \Gamma |u_n\rangle . \tag{1.42}$$

One simple nontrivial example is the split step quantum walk model [39–41]:

$$\begin{aligned} &U_F = U_2 U_1, \\ &U_1 = R_2^{1/2} S_- R_1^{1/2},\ U_2 = R_1^{1/2} S_+ R_2^{1/2}. \end{aligned} \tag{1.43}$$

Here, S_+, S_- are shift operators and $R_j := R(\theta_j)$ is a spin rotation operator defined as

$$S_+(k) := \begin{pmatrix} e^{-ik} & 0 \\ 0 & 1 \end{pmatrix},\ S_-(k) := \begin{pmatrix} 1 & 0 \\ 0 & e^{ik} \end{pmatrix}, \tag{1.44}$$

$$R(\theta) := e^{-i\theta\sigma_2} = \begin{pmatrix} \cos\theta & -\sin\theta \\ \sin\theta & \cos\theta \end{pmatrix}. \tag{1.45}$$

Strictly speaking, this model cannot be realized as a time evolution of any time-dependent Hamiltonian as discussed in Chapter 5, but it is known that the bulk-boundary correspondence still holds. We note the chiral symmetry Eq. (1.11) leads to

$$\Gamma U_1 \Gamma^{-1} = U_2^\dagger. \tag{1.46}$$

Split step quantum walk obeys this decomposed chiral symmetry with $\Gamma = \sigma_x$.

If we apply a unitary transformation such that the chiral symmetry operator becomes $\Gamma = \sigma_z$ to take the basis Eq. (1.36) [7], we can use the bulk-boundary correspondence for chiral-symmetric 1D quantum walks in Eq. (1.38). Therefore, the split step quantum walk in Eq. (1.43) obeys the phase diagram [Fig. 1.3 (a)].

In the following, we especially consider a systems where a left chain $(\theta_1^L, \theta_2^L) = (0, \pi/4)$ with length N and a right chain $(\theta_1^R, \theta_2^R) = (0, -\pi/4)$ with the same length N are joined at two edges [Fig. 1.3 (b)]. The eigenenergy spectrum, dynamics, and boundary states are shown in Fig. 1.4. The eigenvalue spectrum of $U_{\mathrm{QW}} |\psi\rangle = \lambda |\psi\rangle$ [Fig. 1.4 (a)] has two $\epsilon = 0$ and $\epsilon = \pi$ modes. The two modes with $\epsilon = \pi$ ($|\psi^{\epsilon=\pi}_{x\approx 1}\rangle$ and $|\psi^{\epsilon=\pi}_{x\approx N+1}\rangle$) [Fig. 1.4 (c),(d)] and the two modes with $\epsilon = 0$ ($|\psi^{\epsilon=0}_{x\approx 1}\rangle$ and $|\psi^{\epsilon=0}_{x\approx N+1}\rangle$) [Fig. 1.4 (e),(f)] are localized at one of two boundaries $x \approx 1$ or $x \approx N+1$ with nontrivial chiralities defined in Eq. (1.42). We can see that the chiralities of the boundary states are compatible with the bulk-boundary correspondence,

$$\begin{cases} \nu_0^R - \nu_0^L = \langle \psi^{\epsilon=0}_{x\approx N+1}| \Gamma |\psi^{\epsilon=0}_{x\approx N+1}\rangle = -1, \\ \nu_\pi^R - \nu_\pi^L = \langle \psi^{\epsilon=\pi}_{x\approx N+1}| \Gamma |\psi^{\epsilon=\pi}_{x\approx N+1}\rangle = 1, \end{cases} \tag{1.47}$$

[6] If there are more than two gapless states at $\epsilon = 0$ or $\epsilon = \pi$, we need to choose an appropriate basis to obtain this form in general.

[7] It is explicitly given by $U^\dagger \sigma_x U = \sigma_z$ with the unitary operator $U := e^{-i\frac{\pi}{4}\sigma_y}$.

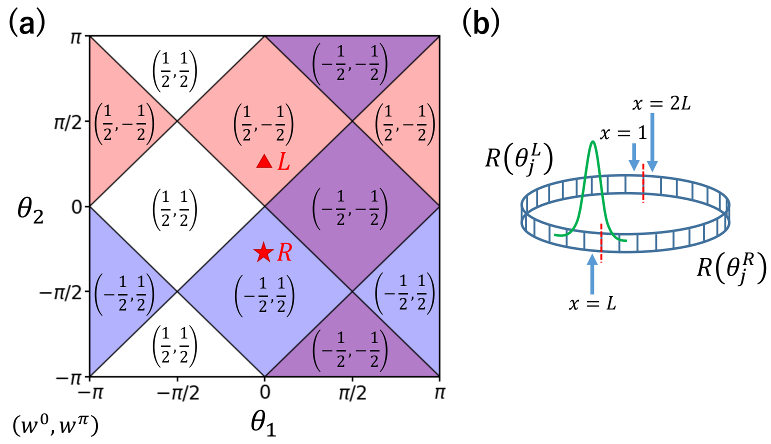

FIGURE 1.3: (a) Phase diagram of split step quantum walk. (w^0, w^π) represents the bulk topological invariant given as Eq.(1.38). Red triangle and star represent the parameters of the left chain $(\theta_1^L, \theta_2^L) = (0, \pi/4)$ and right chain $(\theta_1^R, \theta_2^R) = (0, -\pi/4)$. (b) Setup of a quantum walk system to study the bulk-boundary correspondence. Left quantum walk and right quantum walk are joined at two edges.

where the topological invariants for the right and left chain are $(w_R^0, w_R^\pi) = (0, 1)$ and $(w_L^0, w_L^\pi) = (1, 0)$ from Fig. 1.3 (a). Due to the existence of boundary localized states $|\psi_{x\approx N+1}^{\epsilon=0}\rangle$ and $|\psi_{x\approx N+1}^{\epsilon=\pi}\rangle$, the wave packet initially localized at $x = N+1$ stays localized after time evolutions [Fig. 1.4 (b)].

Class D $d = 1$: Floquet Majorana states

Class D 1D systems have $\mathbb{Z}_2 \oplus \mathbb{Z}_2$ topological invariants according to Table 1.1, which indicates the existence of two binary topological invariants. It is constructed by Jiang, *et al.*, [28]. We remember the PHS for Floquet systems in Eq. (1.10),

$$\mathcal{C}H^*(\boldsymbol{k}, t)\mathcal{C}^{-1} = -H(-\boldsymbol{k}, t), \tag{1.48}$$

where we redefined as $C = \mathcal{C}K$ with K representing complex conjugation and $\mathcal{C}\mathcal{C}^* = 1$. Then, the bulk boundary correspondence is given as

$$\begin{cases} (-1)^{\nu_0+\nu_\pi} = \mathrm{Pf}[H_F(0)\mathcal{C}] \cdot \mathrm{Pf}[H_F(\pi/a)\mathcal{C}], \\ (-1)^{\nu_0} = \mathrm{Pf}[H_F^h(0)\mathcal{C}] \cdot \mathrm{Pf}[H_F^h(0)\mathcal{C}]. \end{cases} \tag{1.49}$$

Here, the $\mathbb{Z}_2$ topological charges ν_0, ν_π (mod 2) are the numbers of gapless boundary modes. a is lattice constant and

$$H_F(k) := \frac{i}{T} \ln U(k, T), \quad H_F^h(k) := \frac{i}{T} \ln \sqrt{U(k, T)}. \tag{1.50}$$

We note that $H_F(k)$ is a usual Floquet Hamiltonian while the half Hamiltonian $H_F^h(k)$ is determined by the analytic continuation from the history of $U(k, T)$.

For 2×2 microscopic Hamiltonian $H(k, t)$, the topological invariants become simple. Let us consider a general 2×2 Hamiltonian:

$$H(k, t) = R_0(k, t)1_{2\times 2} + R_x(k, t)\sigma_x + R_y(k, t)\sigma_y + R_z(k, t)\sigma_z, \; R_\mu \in \mathbb{R}. \tag{1.51}$$

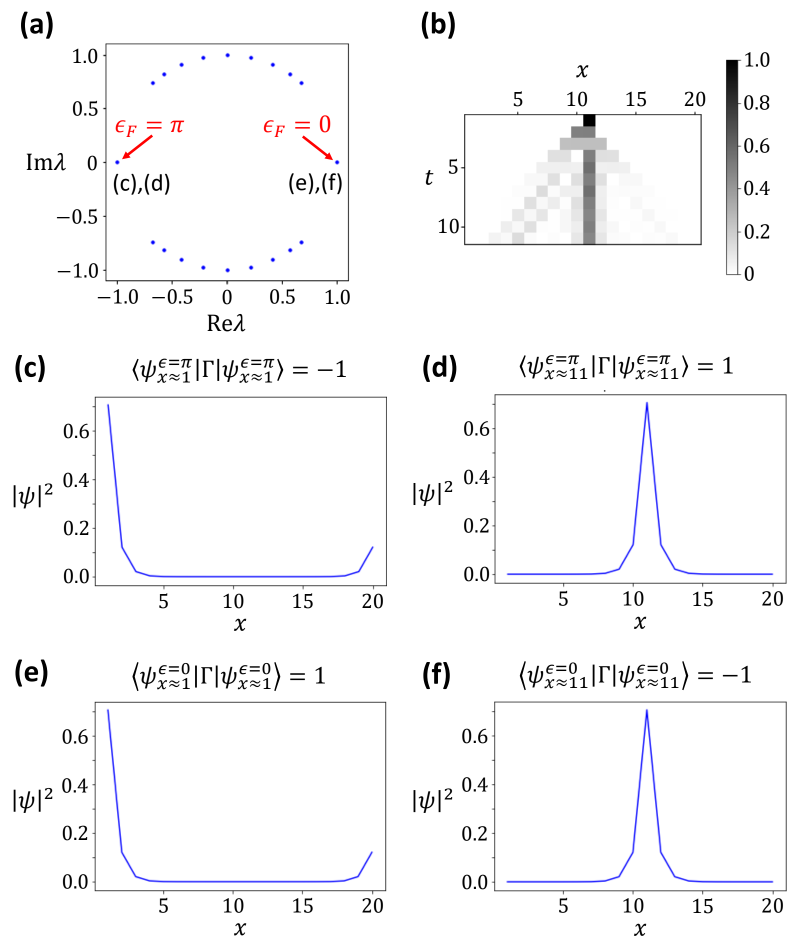

FIGURE 1.4: (a) Energy spectrum, (b) dynamics, and (c-f) eigenstates of the split step walk. Total system size is $2N = 20$. The left half chain are $(\theta_1^L, \theta_2^L) = (0, \pi/4)$, while the right half chain are $(\theta_1^R, \theta_2^R) = (0, -\pi/4)$. The initial state is $|x = 11, \downarrow\rangle$. The chirality of the $\epsilon = 0$ edge mode is minus the chirality of the $\epsilon = \pi$ edge mode.

We take $\mathcal{C} = \sigma_x$ for the PHS in Eq. (1.48), then, we obtain

$$R_0(-k) = -R_0(k),\ R_x(-k) = -R_x(k),\ R_y(-k) = -R_y(k),\ R_z(-k) = R_z(k). \tag{1.52}$$

At the time reversal invariant momenta $k_{\text{inv}} = 0, \pi/a$, the Hamiltonian becomes

$$H(k_{\text{inv}}, t) = R_z(k_{\text{inv}})\sigma_z, \tag{1.53}$$

and thus the time evolution operator becomes

$$U(k_{\text{inv}}, t) = \begin{pmatrix} e^{-i\int_0^t \mathrm{d}t R_z(k_{\text{inv}})} & 0 \\ 0 & e^{i\int_0^t \mathrm{d}t R_z(k_{\text{inv}})} \end{pmatrix}. \tag{1.54}$$

Therefore we have

$$H_F(k_{\text{inv}}) = \int_0^T \mathrm{d}t R_z(k_{\text{inv}})\sigma_z, \quad H_F^h(k_{\text{inv}}) = \frac{1}{2}\int_0^T \mathrm{d}t R_z(k_{\text{inv}})\sigma_z, \tag{1.55}$$

where we need to take the branch $\int_0^T \mathrm{d}tR_z(k_{\text{inv}}) \in [-\pi/T, \pi/T]$ and $\frac{1}{2}\int_0^T \mathrm{d}tR_z(k_{\text{inv}}) \in [-\pi/T, \pi/T]$ for each. Then, we obtain

$$\mathrm{Pf}[H_F(k_{\text{inv}})\mathcal{C}] = \mathrm{sgn}\left[\int_0^T \mathrm{d}tR_z(k_{\text{inv}})\right], \quad \mathrm{Pf}[H_F^h(k_{\text{inv}})\mathcal{C}] = \mathrm{sgn}\left[\frac{1}{2}\int_0^T \mathrm{d}tR_z(k_{\text{inv}})\right]. \tag{1.56}$$

Let us consider a simple model

$$H(k,t) = [J\cos k - \mu(t)]\sigma_z + \Delta \sin k\sigma_x, \ \mu(t) = \mu_0[1-\cos(2\pi t)], \tag{1.57}$$

where J is the hopping amplitude, $\mu(t)$ is the time-dependent chemical potential, and Δ is the order parameter of a superconductor. The quasi-energy spectrum for $T = 1$, $J = 0.8\pi$ and $\Delta = 0.8\pi$ and $\mu_0 \in [0, 4\pi]$ is Fig. 1.5. This model has zero-energy modes for $\mu_0 \in [1.2\pi, 2.8\pi]$ (mod 2π) and π-energy modes for $\mu_0 \in [0.2\pi, 1.8\pi]$ (mod 2π). We can see that this is compatible with the bulk boundary correspondence in Eq. (1.49), where Pfaffians are given by Eq. (1.56) and

$$\int_0^T \mathrm{d}tR_z(0) = (J-\mu_0)T, \quad \int_0^T \mathrm{d}tR_z(\pi/a) = (-J-\mu_0)T. \tag{1.58}$$

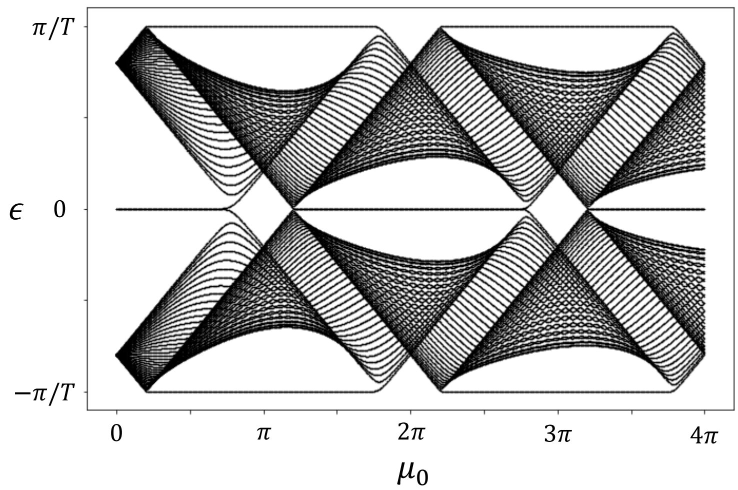

FIGURE 1.5: Quasi-energy spectrum of Eq. (1.57). We take the time period $T = 1$. The hopping amplitude is $J = 0.8\pi$, the order parameter is $\Delta = 0.8\pi$, and $\mu_0 \in [0, 4\pi]$. This model has zero-energy modes for $\mu_0 \in [1.2\pi, 2.8\pi]$ (mod 2π) and π-energy modes for $\mu_0 \in [0.2\pi, 1.8\pi]$ (mod 2π).

1.1.3 Classification of Floquet gapless phases

Until now, we have discussed the Floquet topological insulators, i.e., Floquet gapped phases. In the following two sections, we review the Floquet "gapless" phases. Here, we review the classification of Floquet unitary operators [3], or equivalently the *Floquet gapless phases* [42]. Remarkably, Floquet unitary operators can have nontrivial topology without imposing band gaps, which leads to unique gapless structures that are impossible in equilibrium.

We rewrite the TRS, PHS, and CS as those for one-cycle time evolution operators,

$$TU_F(\boldsymbol{k})T^{-1} = U_F(-\boldsymbol{k})^\dagger, \tag{1.59}$$

$$CU_F(\boldsymbol{k})C^{-1} = U_F(-\boldsymbol{k}), \tag{1.60}$$

$$\Gamma U_F(\boldsymbol{k})\Gamma^{-1} = U_F(\boldsymbol{k})^\dagger. \tag{1.61}$$

We introduce a doubled Hamiltonian $H_U(\boldsymbol{k})$ as

$$H_U(\boldsymbol{k}) := \begin{pmatrix} 0 & U_F(\boldsymbol{k}) \\ U_F^\dagger(\boldsymbol{k}) & 0 \end{pmatrix}. \tag{1.62}$$

We note that $H_U(\boldsymbol{k})$ is Hermitian, has eigenvalues ± 1 because of $H_U(\boldsymbol{k})^2 = \hat{1}$, and obeys the proper chiral symmetry

$$\Sigma_z H_U(\boldsymbol{k})\Sigma_z = -H_U(\boldsymbol{k}),\ \Sigma_z := \begin{pmatrix} \hat{1} & 0 \\ 0 & -\hat{1} \end{pmatrix}. \tag{1.63}$$

Therefore, $H_U(\boldsymbol{k})$ can be regarded as an ordinary topological insulators and superconductors with an additional chiral symmetry in Eq. (1.63). TRS, PHS, and CS for $U_F(\boldsymbol{k})$ in Eqs. (1.59)-(1.61) lead to the following constraints for $H_U(\boldsymbol{k})$ as

$$\tilde{T} H_U(\boldsymbol{k})\tilde{T}^{-1} = H_U(-\boldsymbol{k}),\ \tilde{T} := \begin{pmatrix} 0 & T \\ T & 0 \end{pmatrix}, \tag{1.64}$$

$$\tilde{C} H_U(\boldsymbol{k})\tilde{C}^{-1} = H_U(-\boldsymbol{k}),\ \tilde{C} := \begin{pmatrix} C & 0 \\ 0 & C \end{pmatrix}, \tag{1.65}$$

$$\tilde{\Gamma} H_U(\boldsymbol{k})\tilde{\Gamma}^{-1} = H_U(\boldsymbol{k}),\ \tilde{\Gamma} := \begin{pmatrix} 0 & \Gamma \\ \Gamma & 0 \end{pmatrix}. \tag{1.66}$$

Both Eqs. (1.64) and (1.65) take the form of ordinary TRS and Eq. (1.66) is a commutation relation. Thus we can use the classification methods developed in equilibrium. We explain the classification method by Clifford algebra in Chap. 2. Then, we find that the topological classification of $U(\boldsymbol{k})$ in $(d-1)$-dimension coincides with the topological classification of ordinary insulators and superconductors in d-dimension [Table 1.2]. In other words, the topological classification of $U(\boldsymbol{k})$ coincides with the topological classification of gapless boundary states of topological insulators and superconductors. Therefore, we can expect the topology of Floquet unitary operators $U(\boldsymbol{k})$ is closely related to bulk gapless structures.

In the next section, we see the nontrivial topology of $U(\boldsymbol{k})$ is actually related to the novel bulk gapless structures that is impossible in equilibrium.

1.1.4 Examples of Floquet gapless phases

In this section, we review examples of the Floquet gapless phases in Table 1.2.

Class A $d = 1$: Thouless pump

Class A 1D systems have a $\mathbb{Z}$ topological invariant according to Table 1.2, which indicates the existence of an integer-valued topological invariant. The topological invariant is the energy

TABLE 1.2: Periodic table of Floquet gapless phases in Altland-Zirnbauer symmetry classes. This table shows the presence or absence of $\mathbb{Z}$ or $\mathbb{Z}_2$ topological invariant defined for unitary operators $U(\boldsymbol{k})$.

AZ class	T	C	Γ	$d=0$	1	2	3
A	0	0	0	0	$\mathbb{Z}$	0	$\mathbb{Z}$
AIII	0	0	1	$\mathbb{Z}$	0	$\mathbb{Z}$	0
AI	$+1$	0	0	0	0	0	$2\mathbb{Z}$
BDI	$+1$	$+1$	1	$\mathbb{Z}$	0	0	0
D	0	$+1$	0	$\mathbb{Z}_2$	$\mathbb{Z}$	0	0
DIII	-1	$+1$	1	$\mathbb{Z}_2$	$\mathbb{Z}_2$	$\mathbb{Z}$	0
AII	-1	0	0	0	$\mathbb{Z}_2$	$\mathbb{Z}_2$	$\mathbb{Z}$
CII	-1	-1	1	$2\mathbb{Z}$	0	$\mathbb{Z}_2$	$\mathbb{Z}_2$
C	0	-1	0	0	$2\mathbb{Z}$	0	$\mathbb{Z}_2$
CI	$+1$	-1	1	0	0	$2\mathbb{Z}$	0

winding number,

$$w_1[U_F(k)] := \int_0^{2\pi} \frac{i\mathrm{d}k}{2\pi} \mathrm{tr}[U_F^\dagger \partial_k U_F]. \tag{1.67}$$

Strictly speaking, the winding number always becomes zero $w_1[U_F(k)] = 0$ for ordinary Floquet systems. This is because the time-evolution operator $U(k,t)$ continuously deforms $U(k,T) = U_F(k)$ into $U(k,0) = \hat{1}$, and the topological invariant does not change during this deformation: $w_1[U_F(k)] = w_1[\hat{1}]$. Instead of U_F itself, we consider a decomposed Floquet unitary

$$U_F = \begin{pmatrix} U_1 & 0 \\ 0 & U_2 \end{pmatrix}, \tag{1.68}$$

then $w_1[U_1(k)]$ can takes nonzero values. There are several schemes to realize such a decomposed Floquet unitary operators [42]. One is to consider an adiabatic process of insulators. According to the adiabatic theorem, if there is a large energy gap between the conduction band (the upper band) and the valence band (the lower band) of $H(t)$ for all $t \in [0,T]$, the many-body ground state occupying all the lower bands of $H(t=0)$ becomes the many-body ground state occupying all the lower bands of $H(t=T) = H(0)$ after one-cycle time evolution in the adiabatic limit. This implies that the time-evolution operator in the adiabatic limit takes the form of Eq. (1.68), where U_2 indicates the upper bands and U_1 indicates the lower bands. Another way to realize the block diagonal Floquet unitary operator is to fine-tune the microscopic Hamiltonian.

The most famous example in class A 1D is Thouless pumping, an adiabatic transport of particles under a time-periodic Hamiltonian [32]. Let us suppose the system is described by a 1D time-periodic Hamiltonian $H(k,t)$ and the Chern number for the occupied bands of $H(k = k_x, t = k_y)$ is nontrivial. Then, the system shows a quantized transport after one cycle time evolution, and the number of transported charges equals the Chern number.

We see that the Chern number is equivalent to the winding number $w_1[U_F(k)]$ in the following. We can also show that the winding number $w_1[U_F(k)]$ equals the displacement in one cycle as shown in Chapter 5 (for example, Eq. (5.116)). From these two results, the nontrivial Chern number of $H(k = k_x, t = k_y)$ equals to the number of transported particles in one cycle.

For simplicity, we especially consider the case that all the lower bands are separated from each other. We first prepare the occupied eigenstate of $H(k,t=0)$ as $|u_n(k,t=0)\rangle$ for occupied bands $n=1,\cdots,N_1$, and we consider the states after time evolutions as

$$|u_n(k,t)\rangle := U(k,t)\,|u_n(k,t=0)\rangle\,. \tag{1.69}$$

In the adiabatic limit, $|u_n(k,t)\rangle$ is also the eigenstate of $H(k,t)$ for each t. We suppose the $U_1(k)$ block of Eq. (1.68) is composed from the basis $n=1,\ldots,N_1$. When $t=T$,

$$|u_n(k,T)\rangle = U_F(k)\,|u_n(k,0)\rangle = e^{-i\epsilon_n(k)T}\,|u_n(k,0)\rangle\,. \tag{1.70}$$

We consider the Berry connection

$$A_k^n(k,t) = \langle u_n(k,t)|i\partial_k|u_n(k,t)\rangle\,, \tag{1.71}$$

especially at $t=T$, it becomes

$$A_k^n(k,T) = \langle u_n(k,T)|i\partial_k|u_n(k,T)\rangle \tag{1.72}$$
$$= \langle u_n(k,t=0)|e^{i\epsilon_n(k)T}i\partial_k e^{-i\epsilon_n(k)T}|u_n(k,t=0)\rangle \tag{1.73}$$
$$= A_k^n(k,0) + \partial_k\epsilon_n(k)T. \tag{1.74}$$

We consider integration in the whole Brillouin zone and summation of the lower bands,

$$\sum_{n=1}^{N_1}\int_0^{2\pi}\frac{\mathrm{d}k}{2\pi}[A_k^n(k,T)-A_k^n(k,0)] = \sum_{n=1}^{N_1}\int_0^{2\pi}\frac{\mathrm{d}k}{2\pi}\partial_k\epsilon_n(k)T. \tag{1.75}$$

The left hand side becomes

$$\text{l.h.s.} = \sum_{n=1}^{N_1}\int_0^{2\pi}\frac{\mathrm{d}k}{2\pi}\int_0^T \mathrm{d}t\partial_t A_k^n(k,t) \tag{1.76}$$
$$= \sum_{n=1}^{N_1}\int_0^{2\pi}\frac{\mathrm{d}k}{2\pi}\int_0^T \mathrm{d}t[\partial_t A_k^n(k,t) - \partial_k A_t^n(k,t)], \tag{1.77}$$

where $A_t^n(k,t)$ is defined as

$$A_t^n(k,t) := \langle u_n(k,t)|i\partial_t|u_n(k,t)\rangle\,, \tag{1.78}$$

and it satisfies

$$\int_0^{2\pi}\frac{\mathrm{d}k}{2\pi}\partial_k A_t(k,t) = A_t(k=2\pi,t) - A_t(k=0,t) = 0. \tag{1.79}$$

The right hand side of Eq. (1.75) becomes

$$\text{r.h.s} = \sum_{n=1}^{N_1}\int_0^{2\pi}\frac{\mathrm{d}k}{2\pi}\partial_k\epsilon_n(k)T = \int_0^{2\pi}\frac{i\mathrm{d}k}{2\pi}\partial_k \ln\det U_1(k) \tag{1.80}$$
$$= \int_0^{2\pi}\frac{\mathrm{d}k}{2\pi}\mathrm{tr}\left[U_1^\dagger i\partial_k U_1(k)\right]. \tag{1.81}$$

Therefore, we obtain

$$\sum_{n=1}^{N_1}\int_0^{2\pi}\frac{\mathrm{d}k}{2\pi}\int_0^T \mathrm{d}t[\partial_t A_k^n(k,t)-\partial_k A_t^n(k,t)] = w_1[U_1(k)]. \tag{1.82}$$

We can rewrite it as

$$\int_0^{2\pi}\frac{\mathrm{d}k}{2\pi}\int_0^T \mathrm{d}t\mathrm{tr}[\partial_t \boldsymbol{A}_k(k,t)-\partial_k \boldsymbol{A}_t(k,t)] = w_1[U_1(k)]. \tag{1.83}$$

Here, we introduced the $N_1\times N_1$ matrix of

$$A_t^{m,n}(k,t) := \langle u_m(k,t)|i\partial_t|u_n(k,t)\rangle\,, \quad A_k^{m,n}(k,t) := \langle u_m(k,t)|i\partial_k|u_n(k,t)\rangle\,. \tag{1.84}$$

We note that the both sides of Eq. (1.83) is well-defined even if the lower bands are touching each other. For any general Hamiltonian $H(k,t)$ that has gaps between conduction and valence bands, the lower bands of $H(k,t)$ can be continuously deformed into the ones separated from each other. During the deformation, the topological invariants on the both sides of Eq. (1.83) does not change. Therefore, Eq. (1.83) is valid for general gapped Hamiltonians $H(k,t)$.

A famous model for Thouless pumping is the Rice-Mele model [43],

$$H_{\mathrm{RM}}(t) = \sum_{j=1}^{L}[J_+(t)b_j^\dagger a_j + J_-(t)a_{j+1}^\dagger b_j + h.c] + \Delta(t)[a_j^\dagger a_j - b_j^\dagger b_j], \tag{1.85}$$

or equivalently, the Bloch Hamiltonian of it is

$$H_{\mathrm{RM}}(k,t) = \begin{pmatrix} \Delta(t) & J_+ + J_- e^{-ik} \\ J_+ + J_- e^{ik} & -\Delta(t)\end{pmatrix}. \tag{1.86}$$

The parameters are takes as $J_\pm = J_0 \pm \delta_0\cos\varphi(t)$, $\Delta(t) = \Delta_0 \sin\varphi(t)$ and $\varphi = \Omega t$. We can see the Chern number of this model takes unit integer. For a general two band model

$$H(k_x,k_y) = R_x\sigma_x + R_y\sigma_y + R_z\sigma_z, \tag{1.87}$$

the Chern number is equivalent to the wrapping number around $\boldsymbol{R} = \boldsymbol{0}$ on $(k_x,k_y)\in[-\pi/a,\pi/a]^2$. The proof can be found in many textbooks such as [44, 45], and was originally given in Ref. [46]. The wrapping number for $H_{\mathrm{RM}}(k,t)$ is 1 because

$$\begin{cases} R_x = J_0 + \delta_0\cos\Omega t + [J_0 - \delta_0\cos\Omega t]\cos k \\ R_y = [J_0 - \delta_0\cos\Omega t]\sin k \\ R_z = \Delta_0 \sin\Omega t \end{cases} \tag{1.88}$$

wraps around $\boldsymbol{R} = \boldsymbol{0}$ [Fig. 1.6] once. The energy winding number for $H_{\mathrm{RM}}(k,t)$ is numerically obtained in Fig. 1.7. The thick energy spectrum has two right-going mode at $\epsilon = 0$ and one left-going mode at $\epsilon = \pi$.

class A $d = 3$: Floquet chiral magnetic effect

Class A 3D systems have $\mathbb{Z}$ topological invariants according to Table 1.2, which indicates the existence of an integer-valued topological invariant. The topological invariant is given by

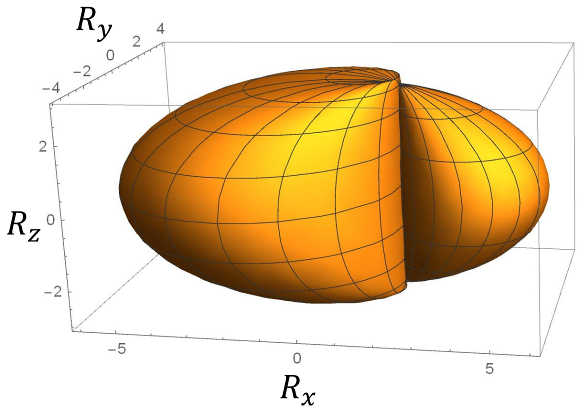

FIGURE 1.6: The manifold of $\boldsymbol{R}(k,t)$ on $(k,t) \in [-\pi/a, \pi/a] \times [0,T]$. The manifold wraps the $\boldsymbol{R} = \boldsymbol{0}$ once. The parameters are takes as $J_0 = 1$, $\Delta_0 = 3$ and $\delta_0 = 1$.

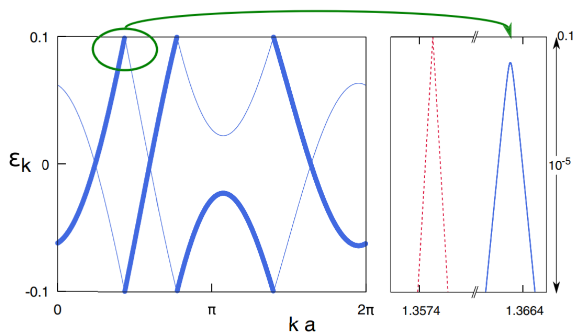

FIGURE 1.7: Quasi-energy spectrum of the Floquet Hamiltonian calculated from Eq. (1.86). The parameters are $\Delta_0 = 3J_0$, $\delta_0 = J_0$ and $\Omega = 2\pi/T = 0.2J_0$. We can see the thick curve (the lower band) has energy winding number 1, but has a small energy gap because of incomplete adiabaticity.
Reproduced from Fig. 1 of Ref. [34]. © 2018 by the American Physical Society.

the 3D winding number [3, 4, 26],

$$w_3[U(\boldsymbol{k})] = -\frac{1}{24\pi^2}\int_{\mathrm{BZ}} \mathrm{tr}[U^\dagger \mathrm{d}U]^3, \tag{1.89}$$

Strictly speaking, the 3D winding number always becomes zero $w_3[U_F(k)] = w_3[U(k, t=0)] = 0$ for ordinary Floquet systems. Thus, we need to consider a decomposed Floquet operator in Eq. (1.68).

One way of making a nontrivial model is to consider the adiabatic limit of the 4D Chern insulator model [4]. Another way is to utilize the sub-lattice structure [3]. In this work, they consider the sublattice structure as

$$L_C := \left\{ \left(m_1, m_2, \frac{m_3}{2} \right) \mid m_1, m_2, m_3 \in \mathbb{Z} \right\}. \tag{1.90}$$

They introduced spin-selective pumps,

$$\mathcal{U}_j^{\pm} := \sum_{x\alpha,\beta} \left[\left(P_j^{\pm}\right)^{\alpha\beta} c^\dagger_{x\pm e_j,\alpha} c_{x,\beta} + \left(P_j^{\mp}\right)^{\alpha\beta} c^\dagger_{x,\alpha} c_{x,\beta} \right], \tag{1.91}$$

and the half version of it is

$$\mathcal{U}_{h,3}^{\pm} := \sum_{x,\alpha,\beta} \left[\left(P_j^{\pm}\right)^{\alpha\beta} c^\dagger_{x\pm(e_3/2),\alpha} c_{x,\beta} + \left(P_j^{\mp}\right)^{\alpha\beta} c^\dagger_{x,\alpha} c_{x,\beta} \right]. \tag{1.92}$$

Then the sequence of these pumps are

$$\mathcal{U}_F^{\mathrm{wh}} := \mathcal{U}_1^{-}\mathcal{U}_{h,3}^{-}\mathcal{U}_2^{-}\mathcal{U}_{h,3}^{+}\mathcal{U}_1^{+}\mathcal{U}_{h,3}^{-}\mathcal{U}_2^{+}\mathcal{U}_{h,3}^{+} \tag{1.93}$$

gives nontrivial model with $w_3[\mathcal{U}_F^{\mathrm{wh}}] = 1$ for $\boldsymbol{k} \in [-\pi/a, \pi/a]^3$. This model has a Weyl fermion at $\boldsymbol{k} = \boldsymbol{0}$ with energy $\epsilon = 0$,

$$H_F(\boldsymbol{k}) = \boldsymbol{k}\cdot\boldsymbol{\sigma} + O(k^2). \tag{1.94}$$

Under magnetic field $B_z = -2\pi\phi$, the Weyl fermion becomes the chiral mode of $\epsilon = k_z$, and the Floquet operator has charge pump proportional to magnetic field $\Delta Q = \phi/2$ in one cycle. The energy spectrum is Fig. 1.8.

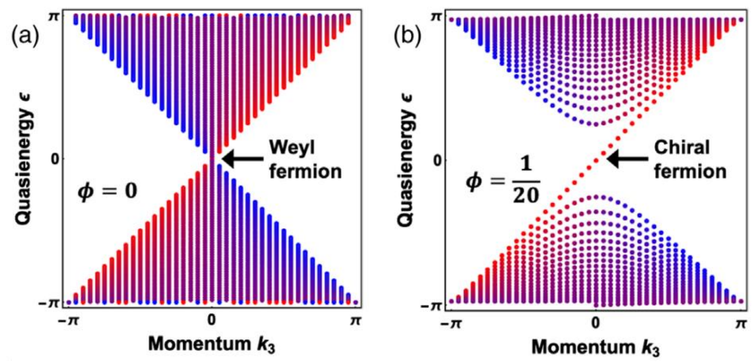

FIGURE 1.8: Quasi-energy spectrum of the model in Eq. (1.93) (a) without and (b) with the magnetic field $B_z = -2\pi\phi$. We can see the Weyl fermion at $\boldsymbol{k} = \mathbf{0}$ changes into a chiral mode under the magnetic field.
Reproduced from Fig. 2 of Ref. [3]. © 2019 by the American Physical Society.

1.2 Overview of non-Hermitian topological phases

In this section, we review the recent studies of non-Hermitian systems. Non-Hermitian systems are the systems that are effectively described by non-Hermitian Hamiltonians $H^\dagger \neq H$. Such non-Hermitian Hamiltonians are realized in open quantum and classical systems, where dissipation or enhancement leads to non-Hermiticity. For example, photonic systems [47, 48], cold atomic systems [**Takasu20**, 49], strongly correlated electron systems [50–54], and electric circuits [55, 56] are known to realize non-Hermitian systems.

Historically, non-Hermitian systems were studied in the context of radiative decay of nucleus in scattering process [57–60]. Later, C. M. Bender proposed PT-symmetric quantum mechanics as a natural extension of Hermitian quantum mechanics [61], where PT symmetry is a combination of inversion symmetry (P) and time-reversal symmetry (T). Non-Hermitian Hamiltonians generally have complex eigenenergies, but PT symmetry keeps the eigenenergies real unless PT symmetry is broken. Thus, PT-symmetric quantum systems can be regarded as ordinary quantum systems where the quantum states conserve norms during dynamics.

Recently, non-Hermitian systems have been studied from the perspective of topological phases. In non-Hermitian systems, the bulk-boundary correspondence does not hold in the normal sense [62, 63]. The bulk topological invariant calculated in periodic boundary conditions (PBC) does not always coincide with the number of boundary gapless states in open boundary conditions (OBC). This is because the energy spectrum in PBC and that in OBC are very different for non-Hermitian Hamiltonians. All the eigenstates in OBC may be localized at one boundary while the eigenstates in PBC are distributed throughout the system due to translational symmetry, so-called the *skin effect*. Later, it was found that the bulk-boundary correspondence holds for bulk topological invariants calculated in OBC [64–66]. In OBC, Bloch momentum k is ill-defined, but we can consider a natural extension of momentum as $\beta = re^{-ik}$, where r indicates exponential localization factor to one boundary. On the other hand, the skin effect itself was found to be related to topological invariants unique to non-Hermitian systems [67]. Typical skin effect occurs for non-symmetric hoppings, which may conflict with the Anderson localization, i.e., the localization of all eigenstates [68].

Another important topic in non-Hermitian systems is the exceptional point. The exceptional point is an energy degeneracy where eigenstates also coalesce. Exceptional points occur with various novel physics unique to non-Hermitian systems: unidirectional invisibility [69–72], enhanced sensitivity [73–76], etc. The PT symmetry breaking point is also a typical exceptional point.

General theories for such non-Hermitian topological phenomena are summarized as topological classifications [68, 77, 78]. In non-Hermitian systems, eigenvalues are complex: $E_n \in \mathbb{C}$, and thus we can consider two types of energy gaps: *point gap* and *line gap*. Point gap is a constraint that the energy bands do not cross a base energy point E_B, while line gap is a constraint that the energy bands do not cross a base energy line. Real line gap $\mathrm{Re}E_n(\boldsymbol{k}) \neq 0$ especially can be regarded as a natural generalization of the Hermitian energy gap $E_n(\boldsymbol{k}) \neq 0$. Topological classification of non-Hermitian Hamiltonians are given for these two gaps [68, 77, 78]. From the perspective of gap structures, the gapped topology about the real line gap is related to bulk-boundary correspondence, while the gapped topology about the point gap is related to skin effect and localization-delocaliation transition of the Anderson Hamiltonian [Fig. 1.9]. The extended Nielsen-Ninomiya theorem we propose in this thesis gives the relations between point-gapped structures and line-gapless structures.

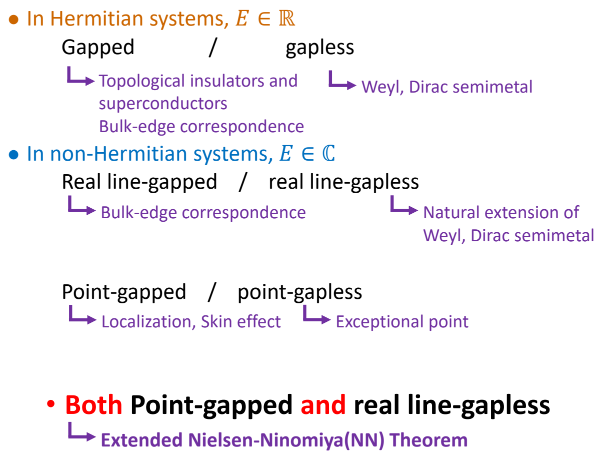

FIGURE 1.9: Relations between energy gaps and topological phenomena.

In Sec. 1.2.1, we review the classification of non-Hermitian gapped topological phases for point gap and line gap [33]. We also review the abundant symmetries in non-Hermitian systems. We also mention PT symmetry. In Sec. 1.2.2, we review a phenomenon related to line-gapped topological phases: bulk-boundary correspondence. We especially explain the non-Hermitian SSH chain in detail. In Sec. 1.2.3, we review a phenomenon related to point-gapped topological phases: skin effect and localization-delocalization transition of the Anderson Hamiltonian. We especially explain the Hatano-Nelson model which was first proposed to describe the depinning of flux lines in type-II superconductors [79–81]. In Sec. 1.2.4, we review a phenomenon related to point-gapless topological states: exceptional points. We also give classifications of exceptional points. In Sec. 1.2.5, we review experimental realizations of non-Hermitian Hamiltonians. We especially explain (i) cold atoms where Lindblad equation with post-selection leads to effective non-Hermitian Hamiltonian, and (ii) strongly correlated or disordered electron systems where Green's functions lead to effective non-Hermitian Hamiltonian, etc.

1.2.1 Classification of non-Hermitian gapped topological phases

In this subsection, we review the non-Hermitian topological classification theory [68, 77, 78]. We first review energy gap structure [Fig. 1.10]. For Hermitian Hamiltonians, the energy spectrum is real: $E \in \mathbb{R}$, and we thus take an energy gap at some Fermi energy $E_F \in \mathbb{R}$. Under symmetry constraints particle-hole symmetry (PHS) and/or chiral symmetry (CS), we have energy constraints $E_n = -E_m$, and thus we need to take a high-symmetric energy gap at $E_F = 0$. For non-Hermitian Hamiltonians, however, the energy spectrum is complex: $E \in \mathbb{C}$, and thus we can consider two types of energy gaps: point gap and line gap. As for point gaps, energy bands do not cross an energy point $E_P \in \mathbb{C}$. Under some symmetry constraints, we need to take the point gap at $E_P = 0$. As for line gaps, energy bands do not cross a line in a complex energy plane. Under some symmetry constraints, we need to choose the line as Re$E = 0$ (*real line gap*) or Im$E = 0$ (*imaginary line gap*).

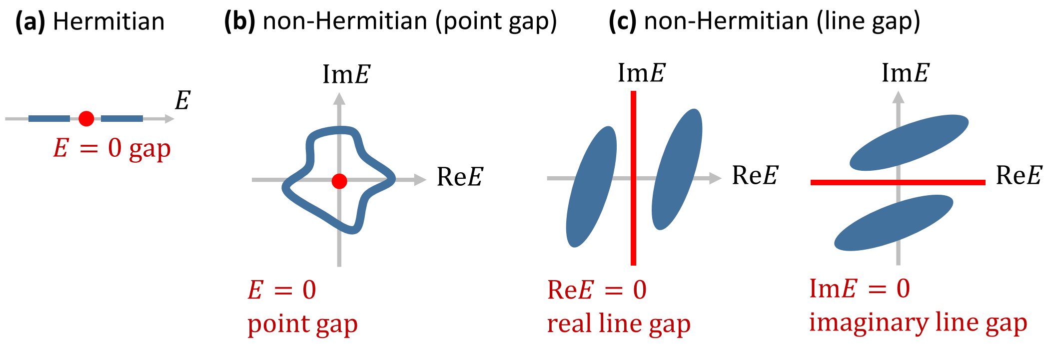

FIGURE 1.10: Energy gaps for (a) Hermitian and (b,c) non-Hermitian Hamiltonians.

We next review symmetries for non-Hermitian Hamiltonians. In Ref. [77], non-Hermitian TRS, PHS, and CS are defined as

$$TH(\boldsymbol{k})T^{-1} = H(-\boldsymbol{k}), \tag{1.95}$$
$$CH^{\dagger}(\boldsymbol{k})C^{-1} = -H(-\boldsymbol{k}), \tag{1.96}$$
$$\Gamma H^{\dagger}(\boldsymbol{k})\Gamma^{-1} = -H(\boldsymbol{k}). \tag{1.97}$$

Non-Hermiticity $H \neq H^{\dagger}$ differentiate the above symmetries from TRS†, PHS† and sub-lattice symmetry (SLS),

$$T'H^{\dagger}(\boldsymbol{k})T'^{-1} = H(-\boldsymbol{k}), \tag{1.98}$$
$$C'H(\boldsymbol{k})C'^{-1} = -H(-\boldsymbol{k}), \tag{1.99}$$
$$SH(\boldsymbol{k})S = -H(\boldsymbol{k}). \tag{1.100}$$

In non-Hermitian systems, the pseudo-Hermiticity is also regarded as a symmetry,

$$\eta H(\boldsymbol{k})\eta^{\dagger} = H(\boldsymbol{k}). \tag{1.101}$$

The above seven symmetries constitute 38-fold symmetry classes [77].

We review the classification of non-Hermitian gapped topological phases. We first explain the case of point-gapped topological phases. For simplicity, we take the gap at $E_P = 0$. If a Hamiltonian is point-gapped $E_n(\boldsymbol{k}) \neq 0$, the determinant becomes nonzero $\det[H(\boldsymbol{k})] \neq 0$. We introduce a doubled Hamiltonian

$$\bar{H}(\boldsymbol{k}) := \begin{pmatrix} 0 & H(\boldsymbol{k}) \\ H^{\dagger}(\boldsymbol{k}) & 0 \end{pmatrix}. \tag{1.102}$$

Then, $\bar{H}(\boldsymbol{k})$ is Hermitian, gapped due to $\det[\bar{H}(\boldsymbol{k})] = -\det[H(\boldsymbol{k})H(\boldsymbol{k})^{\dagger}] \neq 0$, and obeys the proper chiral symmetry

$$\Sigma_z \bar{H}(\boldsymbol{k})(\boldsymbol{k})\Sigma_z = -\bar{H}(\boldsymbol{k}),\ \Sigma_z := \begin{pmatrix} \hat{1} & 0 \\ 0 & -\hat{1} \end{pmatrix}. \tag{1.103}$$

Therefore, $\bar{H}(\boldsymbol{k})$ can be regarded as a Hamiltonian of topological insulators and superconductors with an additional chiral symmetry. The seven symmetries Eqs. (1.95)-(1.101) for the doubled Hamiltonian $\bar{H}(\boldsymbol{k})$ have the form of 2-fold crystalline symmetries, and thus we can calculate the topological classification by the methods developed in equilibrium. We explain the classification method by Clifford algebra in Chapter. 2. Then, some of the periodic tables are given as follows [Tables 1.3-1.5].

We next explain the case of line-gapped topological phases. When a non-Hermitian Hamiltonian is gapped about the real line gap $\mathrm{Re}E(\boldsymbol{k}) \neq 0$, we can continuously deform the non-Hermitian Hamiltonian into a Hermitian Hamiltonian with gap $E(\boldsymbol{k}) \neq 0$. Thus, the classification table becomes the same as that in equilibrium. When a non-Hermitian Hamiltonian $H(\boldsymbol{k})$ is gapped about imaginary line gap $\mathrm{Im}E(\boldsymbol{k}) \neq 0$, multiplying imaginary unit $H(\boldsymbol{k}) \to iH(\boldsymbol{k})$ changes the imaginary line gap into real line gap $\mathrm{Re}E(\boldsymbol{k}) \neq 0$, and the classification problem becomes the same as the case of real line gap. If there are no symmetry constraints that differentiate real line gap and imaginary line gap, the topological classification with real line gap and that with imaginary line gap becomes the same.

As a result, some of the periodic tables of gapped topological phases with point gap or line gap become Table 1.3-1.5. As for other symmetry classes, see Ref. [77].

TABLE 1.3: Periodic table of non-Hermitian gapped topological phases in AZ symmetry classes. ± 1, 1 and 0 in the T, C, and Γ columns show the presence or absence of $T^2 = \pm 1$, $C^2 = \pm 1$, and $\Gamma^2 = 1$. P represents point gap and L represents line gap. Under some symmetry classes, real line gap L_r and imaginary line gap L_i give different topological phases.

AZ class	T	C	Γ	Gap	$d=0$	$d=1$	$d=2$	$d=3$
A	0	0	0	P	0	$\mathbb{Z}$	0	$\mathbb{Z}$
				L	$\mathbb{Z}$	0	$\mathbb{Z}$	0
AIII	0	0	1	P	$\mathbb{Z}$	0	$\mathbb{Z}$	0
				$\mathrm{L_r}$	0	$\mathbb{Z}$	0	$\mathbb{Z}$
				$\mathrm{L_i}$	$\mathbb{Z}\oplus\mathbb{Z}$	0	$\mathbb{Z}\oplus\mathbb{Z}$	0
AI	$+1$	0	0	P	$\mathbb{Z}_2$	$\mathbb{Z}$	0	0
				$\mathrm{L_r}$	$\mathbb{Z}$	0	0	0
				$\mathrm{L_i}$	$\mathbb{Z}_2$	$\mathbb{Z}_2$	$\mathbb{Z}$	0
BDI	$+1$	$+1$	1	P	$\mathbb{Z}_2$	$\mathbb{Z}_2$	$\mathbb{Z}$	0
				$\mathrm{L_r}$	$\mathbb{Z}_2$	$\mathbb{Z}$	0	0
				$\mathrm{L_i}$	$\mathbb{Z}_2\oplus\mathbb{Z}_2$	$\mathbb{Z}_2\oplus\mathbb{Z}_2$	$\mathbb{Z}\oplus\mathbb{Z}$	0
D	0	$+1$	0	P	0	$\mathbb{Z}_2$	$\mathbb{Z}_2$	$\mathbb{Z}$
				L	$\mathbb{Z}_2$	$\mathbb{Z}_2$	$\mathbb{Z}$	0
DIII	-1	$+1$	1	P	$2\mathbb{Z}$	0	$\mathbb{Z}_2$	$\mathbb{Z}_2$
				$\mathrm{L_r}$	0	$\mathbb{Z}_2$	$\mathbb{Z}_2$	$\mathbb{Z}$
				$\mathrm{L_i}$	$\mathbb{Z}$	0	$\mathbb{Z}$	0
AII	-1	0	0	P	0	$2\mathbb{Z}$	0	$\mathbb{Z}_2$
				$\mathrm{L_r}$	$2\mathbb{Z}$	0	$\mathbb{Z}_2$	$\mathbb{Z}_2$
				$\mathrm{L_i}$	0	0	$2\mathbb{Z}$	0
CII	-1	-1	1	P	0	0	$2\mathbb{Z}$	0
				$\mathrm{L_r}$	0	$2\mathbb{Z}$	0	$\mathbb{Z}_2$
				$\mathrm{L_i}$	0	0	$2\mathbb{Z}\oplus 2\mathbb{Z}$	0
C	0	-1	0	P	0	0	0	$2\mathbb{Z}$
				L	0	0	$2\mathbb{Z}$	0
CI	$+1$	-1	1	P	$\mathbb{Z}$	0	0	0
				$\mathrm{L_r}$	0	0	0	$2\mathbb{Z}$
				$\mathrm{L_i}$	$\mathbb{Z}$	0	$\mathbb{Z}$	0

TABLE 1.4: Periodic table of non-Hermitian gapped topological phases in AZ† symmetry classes. ±1, 1 and 0 in the T, C, and Γ columns shows the presence or absence of $T'^2 = \pm1$, $C'^2 = \pm1$, and $\Gamma^2 = 1$. P represents point gap and L represents line gap. Under some symmetry classes, real line gap L_r and imaginary line gap L_i give different topological phases.

AZ† class	T'	C'	Γ	Gap	$d=0$	$d=1$	$d=2$	$d=3$
AI†	$+1$	0	0	P	0	0	0	$2\mathbb{Z}$
				L	$\mathbb{Z}$	0	0	0
BDI†	$+1$	$+1$	1	P	$\mathbb{Z}$	0	0	0
				L_r	$\mathbb{Z}_2$	$\mathbb{Z}$	0	0
				L_i	$\mathbb{Z}\oplus\mathbb{Z}$	0	0	0
D†	0	$+1$	0	P	$\mathbb{Z}_2$	$\mathbb{Z}$	0	0
				L_r	$\mathbb{Z}_2$	$\mathbb{Z}_2$	$\mathbb{Z}$	0
				L_i	$\mathbb{Z}$	0	0	0
DIII†	-1	$+1$	1	P	$\mathbb{Z}_2$	$\mathbb{Z}_2$	$\mathbb{Z}$	0
				L_r	0	$\mathbb{Z}_2$	$\mathbb{Z}_2$	$\mathbb{Z}$
				L_i	$\mathbb{Z}$	0	$\mathbb{Z}$	0
AII†	-1	0	0	P	0	$\mathbb{Z}_2$	$\mathbb{Z}_2$	$\mathbb{Z}$
				L	$2\mathbb{Z}$	0	$\mathbb{Z}_2$	$\mathbb{Z}_2$
CII†	-1	-1	1	P	$2\mathbb{Z}$	0	$\mathbb{Z}_2$	$\mathbb{Z}_2$
				L_r	0	$2\mathbb{Z}$	0	$\mathbb{Z}_2$
				L_i	$2\mathbb{Z}\oplus2\mathbb{Z}$	0	$\mathbb{Z}_2\oplus\mathbb{Z}_2$	$\mathbb{Z}_2\oplus\mathbb{Z}_2$
C†	0	-1	0	P	0	$2\mathbb{Z}$	0	$\mathbb{Z}_2$
				L_rr	0	0	$2\mathbb{Z}$	0
				L_i	$2\mathbb{Z}$	0	$\mathbb{Z}_2$	$\mathbb{Z}_2$
CI†	$+1$	-1	1	P	0	0	$2\mathbb{Z}$	0
				L_r	0	0	0	$2\mathbb{Z}$
				L_i	$\mathbb{Z}$	0	$\mathbb{Z}$	0

TABLE 1.5: Periodic table of non-Hermitian gapped topological phases under sub-lattice symmetry (SLS) and chiral symmetry. The subscript of $S_\pm$ represents the commutation (+) or anticommutation (-) relation with chiral symmetry $\Gamma S_\pm = \pm S_\pm \Gamma$. These unitary symmetry operators obey $\Gamma^2 = 1$ and $S^2 = 1$. P represents point gap and L represents line gap. Under some symmetry classes, real line gap L_r and imaginary line gap L_i give different topological phases.

SLS	AZ class	Gap	$d=0$	$d=1$	$d=2$	$d=3$
SLS$_+$	AIII	P	0	$\mathbb{Z}$	0	$\mathbb{Z}$
		L_r	0	$\mathbb{Z}\oplus\mathbb{Z}$	0	$\mathbb{Z}\oplus\mathbb{Z}$
		L_i	0	$\mathbb{Z}\oplus\mathbb{Z}$	0	$\mathbb{Z}\oplus\mathbb{Z}$
SLS	A	P	0	$\mathbb{Z}\oplus\mathbb{Z}$	0	$\mathbb{Z}\oplus\mathbb{Z}$
		L	0	$\mathbb{Z}$	0	$\mathbb{Z}$
SLS$_-$	AIII	P	$\mathbb{Z}\oplus\mathbb{Z}$	0	$\mathbb{Z}\oplus\mathbb{Z}$	0
		L_r	$\mathbb{Z}$	0	$\mathbb{Z}$	0
		L_i	$\mathbb{Z}$	0	$\mathbb{Z}$	0

In the following, we review previous studies based on the above classification tables.

1.2.2 Examples of line-gapped topological phases

In this section, we review a phenomenon related to line-gapped topological phases: bulk-boundary correspondence. We especially explain the non-Hermitian SSH chain in detail [Fig. 1.11(a)],

$$H(k) = d_x\sigma_x + (d_y + i\gamma/2)\sigma_y, \tag{1.104}$$

where $d_x = t_1 + t_2 \cos k$ and $d_y = t_2 \sin k$. This model obeys sub-lattice symmetry $\sigma_z H(k)\sigma_z = -H(k)$.

The energy spectrum in open boundary conditions becomes Fig. 1.11(b). We note that the energy spectrum in PBC is very different from that in OBC. The topological transition point in PBC and that in OBC are also different. The bulk topological invariant changes during the topological transition point at $t_1 = \pm t_2 \pm \gamma/2$ in PBC, but the topological transition point in OBC is $t_1 = \pm\sqrt{t_2^2 + (\gamma/2)^2}$. As for PBC energy spectrum, the eigenvalues are given as $E_\pm = \pm\sqrt{d_x^2 + (d_t + i\gamma/2)^2}$.

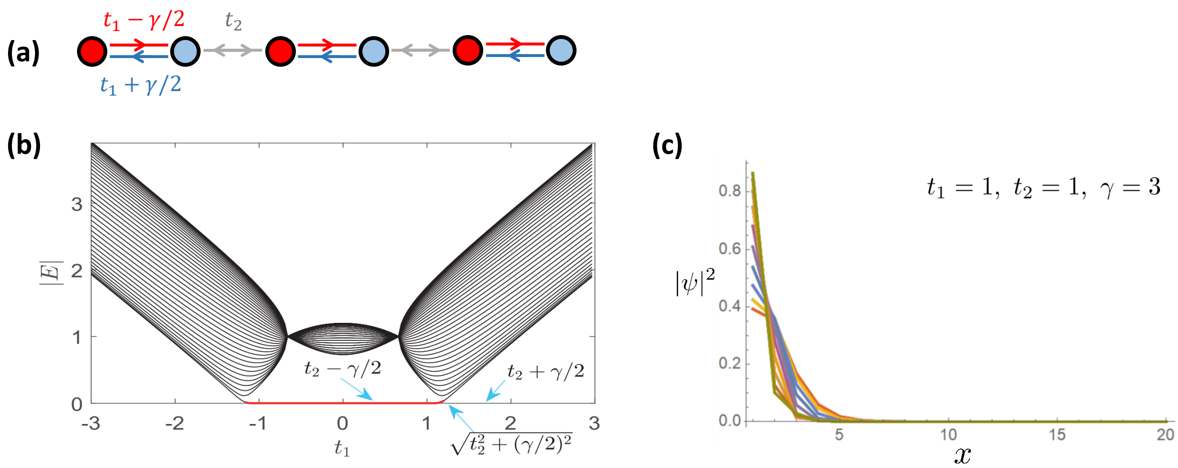

FIGURE 1.11: (a) Sketch of the non-Hermitian SSH model, (b) Energy spectrum, and (c) all the wave-functions of Eq. (1.104). Parameters are $t_2 = 1$, $\gamma = 4/3$, and the system size is (a) $L = 40$ and (b) $L = 20$. (b) Two-fold degenerate zero-energy modes are shown in red. (c) All the eigenstates are localized at one boundary.
Fig. (b) is reproduced from Fig. 2 of Ref. [64]. © 2018 by the American Physical Society.

We review how to obtain the wave functions in OBC, firstly proposed in Rev. [64]. In Hermitian systems, it is known that the eigenvalues and the properties of eigenfunctions do not change a lot between PBC and OBC. But, in non-Hermitian systems, the eigenvalues and eigenfunctions dramatically change [Fig. 1.11(c)]. In non-Hermitian systems, all the eigenstates are exponentially localized at one boundary. Therefore, we can expect the wave function of the form $\psi \propto c_1 e^{-ikx} + c_2 e^{ikx}$in equilibrium changes into $\psi \propto c_1(re^{-ik})^x + c_2(re^{ik})^x$, where $r \in \mathbb{R}$ is the exponential localization factor [8]. We note that both the right-going wave and the left-going wave are needed to construct a standing wave. From this observation, we consider the following form of the eigenfunction,

$$|\psi\rangle = \sum_n \psi_{n,A} c_{n,A}^\dagger |0\rangle + \psi_{n,B} c_{n,B}^\dagger |0\rangle, \quad \psi_{n,A} = \beta^n \phi_A,\ \psi_{n,B} = \beta^n \phi_B, \tag{1.105}$$

[8] r depends on k in general

where we expect $\beta = re^{-ik}$. Then, the Schrodinger equation $H|\psi\rangle = E|\psi\rangle$ is rewritten as

$$\left[\left(t_1 + \frac{\gamma}{2}\right) + t_2\beta^{-1}\right]\phi_B = E\phi_A, \quad \left[\left(t_1 - \frac{\gamma}{2}\right) + t_2\beta\right]\phi_A = E\phi_B, \tag{1.106}$$

and thus we have

$$\left[\left(t_1 + \frac{\gamma}{2}\right) + t_2\beta^{-1}\right]\left[\left(t_1 - \frac{\gamma}{2}\right) + t_2\beta\right] = E^2. \tag{1.107}$$

We have two unknown numbers $\beta, E \in \mathbb{C}$ for one equation, and we cannot solve this equation. Thus, we need to use the standing wave condition. Firstly, equation (1.107) can be seen as a quadratic equation for β and we can introduce two roots β_1, β_2 depending on E. If the solution of Eq. (1.107) has the form $\psi \propto c_1(re^{-ik})^x + c_2(re^{ik})^x = c_1\beta^x + c_2(\beta^*)^x$, we can expect the relation $|\beta_1| = |\beta_2|$. Strictly speaking, $|\beta_1| = |\beta_2|$ is naturally expected from the boundary condition $|\beta_1|^L \approx |\beta_2|^L$ from Eq. (1.107) [9]. The product of the roots becomes $\beta_1\beta_2 = \frac{t_1-\gamma/2}{t_1+\gamma/2}$, and thus we obtain

$$|\beta_j| = r = \sqrt{\left|\frac{t_1 - \gamma/2}{t_1 + \gamma/2}\right|}. \tag{1.108}$$

Then, we can use the expression $\beta = re^{-ik}$ rigorously, and Eq. (1.107) becomes

$$E^2 = t_1^2 + t_2^2 - \frac{\gamma^2}{4} + t_2\sqrt{|t_1^2 - \gamma^2/4|}[\mathrm{sgn}(t_1 + \gamma/2)e^{ik} + \mathrm{sgn}(t_1 - \gamma/2)e^{-ik}]. \tag{1.109}$$

This solution actually works well. This solution explains the topological transition point $t_1 = \pm\sqrt{t_2^2 + (\gamma/2)^2}$ in OBC.

We next explain the topological invariants in OBC. In Hermitian systems, the topological invariants for the SSH chain is given as

$$w_1 := \int_0^{2\pi} \frac{idk}{2\pi}\mathrm{tr}[q^{-1}\partial_k q], \quad Q(k) = \begin{pmatrix} 0 & q \\ q^\dagger & 0 \end{pmatrix}, \tag{1.110}$$

where Q matrix is a flattened Hamiltonian

$$Q(k) := \sum_\alpha |u_\alpha(k)\rangle\langle u_\alpha(k)| - |u_{\bar{\alpha}}(k)\rangle\langle u_{\bar{\alpha}}(k)|, \tag{1.111}$$

for eigenstates $H(k)|u_\alpha(k)\rangle = E_\alpha(k)|u_\alpha(k)\rangle$ with positive eigenenergy $E_\alpha(k) > 0$ and its chiral-symmetric counterpart $|u_{\bar{\alpha}}\rangle = \sigma_z|u_\alpha\rangle$ with negative eigenenergy $E_{\alpha(\bar{k})} = -E_\alpha(k) < 0$. We note that the Q matrix has eigenvalues ± 1 because $Q(k)^2 = \hat{1}$. Because of the chiral symmetry for the Q matrix: $\sigma_z Q \sigma_z = -Q$, the Q matrix has the form in Eq. (1.110).

In non-Hermitian systems, the topological invariant for the non-Hermitian SSH chain is given as

$$w_1^{\mathrm{nH}} := \int_{C_\beta} \mathrm{tr}[q^{-1}dq], \quad Q(\beta) = \begin{pmatrix} 0 & q \\ q^\dagger & 0 \end{pmatrix}, \tag{1.112}$$

[9] Here $\approx$ means that $|\beta_1|^L = c|\beta_2|^L$ with a factor c that does not scale in the system size L.

where Q matrix is a flattened Hamiltonian

$$Q(\beta) := \sum_{\alpha} |u_\alpha^R(\beta)\rangle \langle u_\alpha^L(\beta)| - |u_{\bar{\alpha}}^R(\beta)\rangle \langle u_{\bar{\alpha}}^L(\beta)|, \tag{1.113}$$

for right-(left-)eigenstates $H(\beta)|u_\alpha^R(\beta)\rangle = E_\alpha(\beta)|u_\alpha^R(\beta)\rangle$ ($H^\dagger(\beta)|u_\alpha^L(\beta)\rangle = E_\alpha(\beta)|u_\alpha^L(\beta)\rangle$) with positive real energy $\mathrm{Re}E_\alpha(k) > 0$ and its chiral-symmetric counterpart $H(\beta)|u_{\bar{\alpha}}^R(\beta)\rangle = E_{\bar{\alpha}}(\beta)|u_{\bar{\alpha}}^R(\beta)\rangle$ ($H^\dagger(\beta)|u_{\bar{\alpha}}^L(\beta)\rangle = E_{\bar{\alpha}}(\beta)|u_{\bar{\alpha}}^L(\beta)\rangle$) with negative imaginary energy $\mathrm{Re}E_{\bar{\alpha}}(k) = -E_\alpha(k) < 0$. We note that the eigenstates are taken in the biorthogonal condition $\langle u_\alpha^L|u_{\alpha'}^R\rangle = \delta_{\alpha,\alpha'}$. Here, $H(\beta)$ is given by the replacement $e^{-ik} \to \beta$ in Eq. (1.104). We note that the Q matrix has eigenvalues ± 1 because $Q(k)^2 = \hat{1}$. Because of the sub-lattice symmetry for the Q matrix: $\sigma_z Q \sigma_z = -Q$, the Q matrix has the form in Eq. (1.112). C_β is the trajectory of β in the complex plane. In this case, we have the form $\beta = re^{-ik}$, and thus the trajectory of β is a circle of radius r.

In general, C_β takes a non-circle structure. Fig. 1.12 is the energy spectrum, w_1^{nH}, and C_β of the modified non-Hermitian SSH

$$H(k) = d_x\sigma_x + (d_y + i\gamma/2)\sigma_y, \tag{1.114}$$

but with $d_x = t_1 + (t_2 + t_3)\cos k$ and $d_y = (t_2 - t_3)\sin k$.

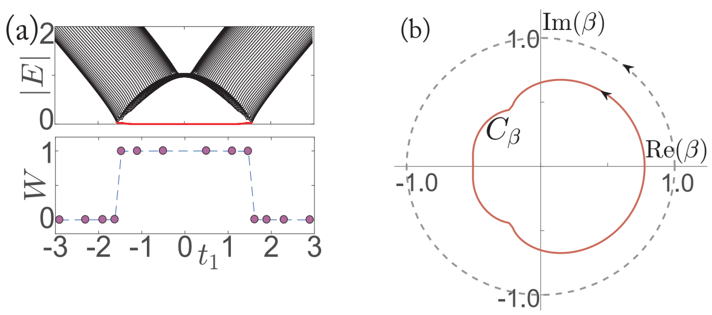

FIGURE 1.12: (a) Energy spectrum, topological invariant w_1^{nH}, (b) and C_β trajectory of Eq. (1.104). Parameters are $t_2 = 1$, $\gamma = 4/3$, $t_3 = 1/5$, and the system size is $L = 100$. (a) Two-fold degenerate zero-energy modes are shown in red. (b) $t_1 = 1.1$ is chosen.
Reproduced from Fig. 5 of Ref. [64]. © 2018 by the American Physical Society.

1.2.3 Examples of point-gapped topological phases

In this section, we review two phenomena related to point-gapped topological phases: skin effect and Anderson localization-delocalization transition.

class A $d = 1$: Anderson localization-delocalization transition

Here, we review the Anderson localization-delocalization transition of the Hatano-Nelson model in 1D [68]. Hatano-Nelson model, which was originally proposed in studying the pinning-depinning transition of vortex lines in superconductors [79–81].

Hatano-Nelson model is a 1D Anderson localization Hamiltonian but with nonsymmetric hopping amplitudes, [10]

$$H = \sum_{j=1}^{N} J_R c_{j+1}^{\dagger} c_j + J_L c_j^{\dagger} c_{j+1} + V_j c_j^{\dagger} c_j, \tag{1.115}$$

where V_j is the random potential, uniformly distributed in the range $[-W, W]$. We take the PBC: $c_{j+N} = c_j$. The matrix expression is given by

$$H = \begin{pmatrix} V_1 & J_R & & & J_L \\ J_L & V_2 & J_R & & \\ & J_L & V_3 & \ddots & \\ & & \ddots & \ddots & J_R \\ J_R & & & J_L & V_N \end{pmatrix}. \tag{1.116}$$

In the Hermitian case ($J_L = J_R$), the Hatano-Nelson model becomes the ordinary 1D Anderson Hamiltonian and shows localization for any $W > 0$. In non-Hermitian systems ($J_L < J_R$), however, for small W, some eigenstates show delocalization [Fig. 1.13,1.14].

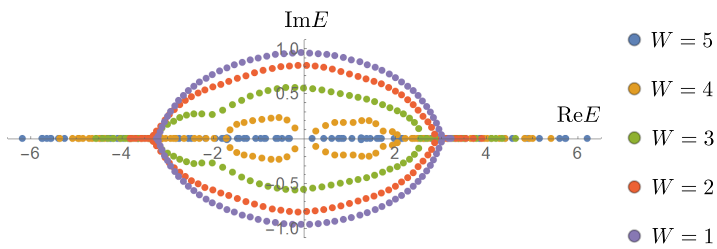

FIGURE 1.13: Energy spectrum of Hatano-Nelson model in Eq. (1.115). The system size is $N = 10^2$. The parameters are $J_R = 2$, $J_L = 1$, and $W = 1, 2, 3, 4, 5$. For small $W \lesssim 4.3$ some part of the energy spectrum becomes complex. We can show $w_1[H(\Phi)] = 1$ for $W \lesssim 4.3$.

This localization-delocalization transition is characterized by a magnetic winding number [68], as shown in the following. In the case of the well-known quantum Hall effect, the robustness of Hall current and the existence of edge modes against impurity scatterings are explained by the Chern numbers under twisted boundary conditions [82]. In the modern view, the twisted boundary conditions can be seen as a kind of flux insertion into the cylinder [11]. There are two well-known methods of flux insertion: (i) to introduce the uniform vector potential $A_x = \Phi/L$ and (ii) to introduce the local vector potential $A_x = \Phi\delta(x)$, where $\delta(x)$ is the delta function. The twisted boundary conditions are realized by the Peierls phase of (ii) the local gauge. But, we use (i) the uniform gauge in the following argument. Any choice of the vector potentials that are equivalent up to gauge transformations produces the same result.

[10] In the original paper [79], the nonsymmetric hoppings are realized by an imaginary vector potential.

[11] The lattice structure with OBC in the x-direction and PBC in the y-direction can be seen as a cylinder.

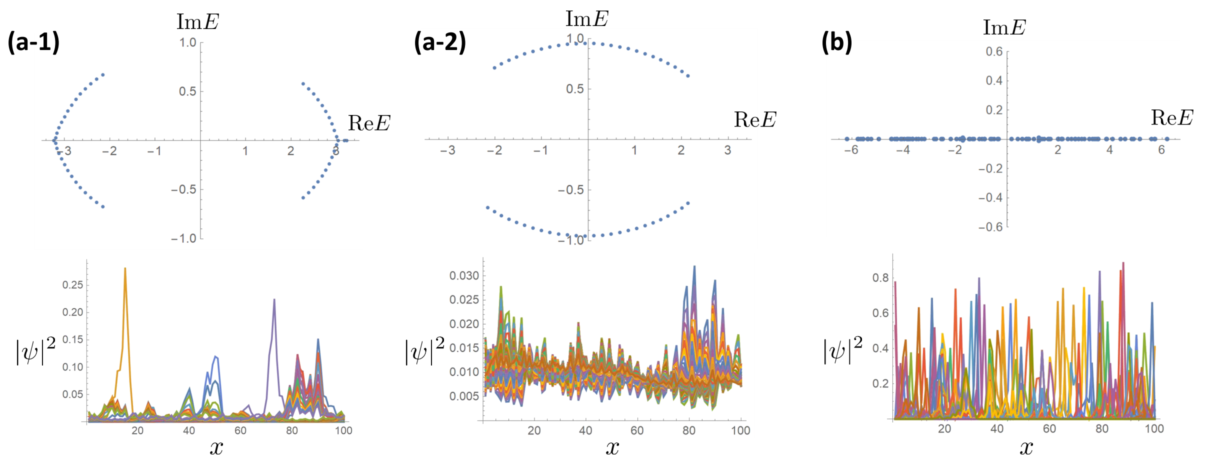

FIGURE 1.14: Energy spectrum and eigenstates of the Hatano-Nelson model in Eq. (1.115. The system size is $L = 10^2$, and the parameters are $J_R = 2$, $J_L = 1$ and (a-1,2) $W = 1$ or (b) $W = 5$. For $W = 1$, We split the eigenstates into two: (a-1) eigenstates with small Im$E = 0$ and (a-2) eigenstates with large Im$E = 0$. (a-1) the eigenstates with small Im$E = 0$ are strongly localized, while (a-2) the eigenstates with large Im$E = 0$ are delocalized. (b) All the eigenstates are strongly localized.

If we introduce the (i) uniform vector potential $A_x = \Phi/L$, the hopping terms changes as $c^\dagger_{j+q}c_j \to e^{-i(\Phi/L)q}c^\dagger_{j+q}c_j$. The Hatano-Nelson model becomes

$$H(\Phi) = \sum_{j=1}^{N} J_R e^{-i\Phi/L} c^\dagger_{j+1}c_j + J_L e^{i\Phi/L} c^\dagger_j c_{j+1} + V_j c^\dagger_j c_j. \tag{1.117}$$

Then, $H(\Phi)$ is periodic in Φ with the period 2π up to the large gauge transformation $\hat{U}_G = e^{-\frac{2\pi i}{L}\hat{x}}$: $H(\Phi + 2\pi) = \hat{U}_G H(\Phi)\hat{U}^\dagger_G$. Then, we can introduce its winding number as

$$w_1[H(\Phi)] := \int_0^{2\pi} \frac{d\Phi}{2\pi} \mathrm{tr}[H^{-1}(\Phi) i\partial_\Phi H(\Phi)] = \int \frac{d\Phi}{2\pi i}\partial_\Phi \log\det H(\Phi). \tag{1.118}$$

Here, we have shown two expressions for convenience. As $\det H = \prod_j E_j$ is a product of all the eigenenergies, $w_1[H(\Phi)]$ has the meaning of energy-winding number. Then, we can see that the delocalization occurs when $w_1[H(\Phi)]$ takes nonzero values [Fig.1.13 and 1.14]. Thus, for the Hatano-Nelson model, the localization-delocalization transition is characterized by the winding number $w_1[H(\Phi)]$, which is the point-gap topological invariant in class A 1D systems.

Class A $d = 1$: Skin effect

Here, we review the skin effect in non-Hermitian systems. Let us consider the Hatano-Nelson model again but without the random disorder in OBC,

$$H = \sum_{j=1}^{N-1} J_R c^\dagger_{j+1}c_j + J_L c^\dagger_j c_{j+1}, \tag{1.119}$$

The matrix expression is

$$H = \begin{pmatrix} 0 & J_R & & & 0 \\ J_L & 0 & J_R & & \\ & J_L & 0 & \ddots & \\ & & \ddots & \ddots & J_R \\ 0 & & & J_L & 0 \end{pmatrix}. \tag{1.120}$$

We can analytically obtain the eigenvalues and eigenvectors. The eigenvalues and eigenvectors are

$$E_k = 2\sqrt{J_L J_R}\cos k,\ v_k(x) = \left(\frac{J_L}{J_R}\right)^{x/2} \sin(kx), \quad k = \frac{s\pi}{L+1},\ s = 1, 2, \cdots, L. \tag{1.121}$$

This can be understood by introducing imaginary gauge transformation

$$S = \begin{pmatrix} 1 & & & & \\ & r & & & \\ & & r^2 & & \\ & & & \ddots & \\ & & & & r^N \end{pmatrix}, \tag{1.122}$$

where S is not unitary due to $r = e^g \lessgtr 1$ for $g \lessgtr 0$. The imaginary gauge transformation by S becomes

$$\bar{H} = S^{-1}HS = \begin{pmatrix} 0 & J_R r & & & 0 \\ J_L r^{-1} & 0 & J_R r & & \\ & J_L r^{-1} & 0 & \ddots & \\ & & \ddots & \ddots & J_R r \\ 0 & & & J_L r^{-1} & 0 \end{pmatrix}, \tag{1.123}$$

which becomes a Hermitian matrix if we choose $r = \sqrt{J_L/J_R}$ as

$$\bar{H} = S^{-1}HS = \begin{pmatrix} 0 & \sqrt{J_L J_R} & & & 0 \\ \sqrt{J_L J_R} & 0 & \sqrt{J_L J_R} & & \\ & \sqrt{J_L J_R} & 0 & \ddots & \\ & & \ddots & \ddots & \sqrt{J_L J_R} \\ 0 & & & \sqrt{J_L J_R} & 0 \end{pmatrix}. \tag{1.124}$$

In Hermitian systems, we know the rule of thumb that the energy spectrum does not change between PBC and OBC [12]. The PBC Hamiltonian of $\bar{H}$ is rewritten as

$$\bar{H} = 2\sqrt{J_L J_R}\cos k, \quad E(k) = 2\sqrt{J_L J_R}\cos k. \tag{1.125}$$

This energy spectrum is compatible with the exact solution in Eq. (1.121). We note that the imaginary gauge transformation does not change the energy spectrum.

[12]except for edge states of topological insulators

In this simplest model, we can see the skin effect. The eigenstates in Eq. (1.121) are exponentially localized at $x = 0$ ($x = N$) for $J_R > J_L$ ($J_L > J_R$). This localization can be understood by the imaginary gauge transformation in Eq. (1.122), which naturally introduces localization factor $r = \sqrt{J_L/J_R}$.

This skin effect was firstly studied in the context of difficulty in bulk-boundary correspondence [Sec.1.2.2]. The non-Hermitian SSH model in Eq. (1.104) also shows the skin effect [Fig. 1.15].

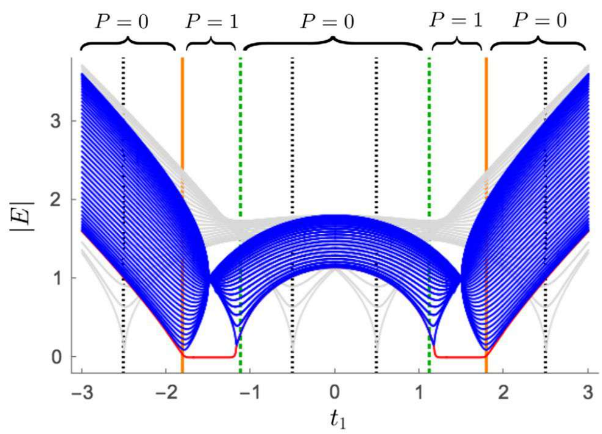

FIGURE 1.15: Energy spectra of the non-Hermitian SSH model in Eq. (1.104). The parameters are $t_1 \in [-3, 3]$, $t_2 = 1$, and $\gamma = 3$. The system size is $N = 46$. The gray lines indicate the PBC spectrum while the blue lines (bulk) and red lines (edge) indicate the OBC spectrum. We can see that the PBC spectrum and the OBC spectrum are different.
Reproduced from Fig. 1 of Ref. [63]. © 2018 by the American Physical Society.

The non-Hermitian skin effect is related to the point-gap topological invariants. For class A 1D systems, the point-gap topological invariant is given by the energy winding number,

$$w_1[H(k)] := \int_0^{2\pi} \frac{dk}{2\pi} \mathrm{tr}[H^{-1}(k) i\partial_k H(k)] = \int \frac{dk}{2\pi i} \partial_k \log\det H(k). \tag{1.126}$$

If the energy winding number is nontrivial, the eigenspectrum has a loop structure in PBC, but the corresponding OBC spectrum cannot have a loop structure, and thus the skin effect (the drastic change of energy spectrum) inevitably occurs [Fig. 1.16(a)]. The OBC spectrum is always inside the PBC loop spectrum [83].

Okuma, *et al.* in Ref. [83] have shown that the skin effect also occurs in class AII† 1D systems:

$$TH^T(k)T^{-1} = H(-k), \quad T^2 = -1. \tag{1.127}$$

The topological invariant of class AII† in 1D is

$$(-1)^\nu := \mathrm{sgn}\left\{ \frac{\mathrm{Pf}[H(\pi)T]}{\mathrm{Pf}[H(0)T]} \times \exp\left[-\frac{1}{2} \int_{k=0}^{k=\pi} d\log\det\{H(k)T\} \right] \right\}. \tag{1.128}$$

They studied a stack of Hatano-Nelson model

$$H(k) = \begin{pmatrix} H^{(HN)}(k) & 2\Delta \sin k \\ 2\Delta \sin k & [H^{(HN)}]^T(-k) \end{pmatrix} = 2t \cos k + 2\Delta \sin k\sigma_x + 2ig \sin k\sigma_z, \tag{1.129}$$

where $H^{(HN)}$ is the Hatano-Nelson model without disorder in the form $H^{(HN)} = (t+g)e^{-ik} + (t-g)e^{ik}$. The eigenenergy takes the form of an ellipse,

$$E_\pm(k) = 2t \cos k \pm 2i\sqrt{g^2 - \Delta^2}. \tag{1.130}$$

The PBC spectrum, the OBC spectrum and the OBC spectrum with symmetry breaking perturbation $\delta h\sigma_z$ is shown in Fig. 1.16.

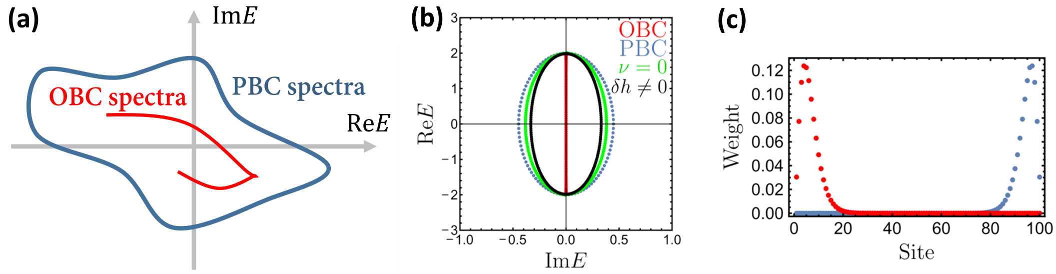

FIGURE 1.16: (a) A picture of typical PBC spectrum and the corresponding OBC spectrum. (b) The energy spectrum and (c) eigenstates of the model Eq. (1.129) with parameters $t = 1$, $g = 0.3$, $\Delta = 0.2$, $\delta = 10^{-3}$ and the system size is $N = 100$. (b) The red line indicates the OBC spectrum and the blue dotted curve indicates the PBC spectrum. The black line indicates the OBC spectrum with symmetry-breaking perturbation. (c) The Kramers doublet eigenstates with $E = 1.948$ in OBC shows localization at opposite edges.
Fig. (b,c) are reproduced from Fig. 2 of Ref. [67]. © 2018 by the American Physical Society.

From the Fig. 1.16(b) and (c), We can see that the skin effect of Kramers doublet occurs in OBC. But, if we add symmetry breaking perturbation $\delta h\sigma_z$, the skin effect disappears. We note that the energy winding number of this model in Eq. (1.129) is zero, and thus the skin effect of class A 1D does not occur.

1.2.4 Examples of point-gapless topological states

In this section, we review a phenomenon related to point-gapless topological states: exceptional points. We also give classifications of exceptional points [84]. Examples are the 2D exceptional point and the PT symmetry breaking point [85].

Exceptional point [13] is a degenerate point, at which not only eigenvalues but also eigenstates coalesce.

Let us consider an example in 2D given as

$$H(\boldsymbol{k}) = \begin{pmatrix} 0 & k_x + ik_y \\ 1 & 0 \end{pmatrix}, \quad E(\boldsymbol{k}) = \pm\sqrt{k_x + ik_y}. \tag{1.131}$$

[13] Exceptional point is mathematically called defective point.

At the origin $\boldsymbol{k} = \boldsymbol{0}$, this model becomes

$$H(\boldsymbol{0}) = \begin{pmatrix} 0 & 0 \\ 1 & 0 \end{pmatrix}, \tag{1.132}$$

and has only one eigenvector $|\psi^R(\boldsymbol{k} = \boldsymbol{0})\rangle = (0,1)^T$ with $E(\boldsymbol{0}) = 0$, i.e., both eigenstates and eigenvalues degenerate at $\boldsymbol{k} = \boldsymbol{0}$.

The exceptional point can be seen as a kind of the point-gapless point. Actually, this gapless point $\boldsymbol{k} = (0,0)$, where the point gap $E = 0$ is closed, is characterized by the energy winding number on S^1 surrounding the origin,

$$w_1 := \oint_{S_1} \frac{d\boldsymbol{k}}{2\pi} \cdot \mathrm{tr}[H^{-1}(\boldsymbol{k}) i \nabla_{\boldsymbol{k}} H(\boldsymbol{k})] = \int \frac{d\boldsymbol{k}}{2\pi i} \cdot \nabla_{\boldsymbol{k}} \log\det H(\boldsymbol{k}). \tag{1.133}$$

$w_1 = 1$ can be pictorially understood from the Fig. 1.17.

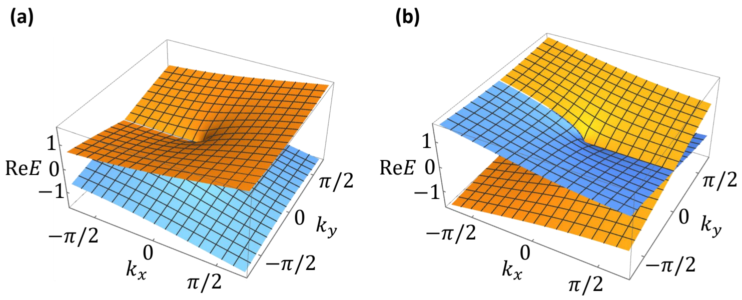

FIGURE 1.17: (a) ReE spectrum and (b) ImE spectrum of $E(k_x, k_y) = \pm\sqrt{k_x + ik_y}$ in Eq. (1.131). They have branch cut structure around $\boldsymbol{k} = \boldsymbol{0}$: Two eigenenergies swap after one-cycle movement around $\boldsymbol{k} = \boldsymbol{0}$.

Another famous exceptional point is the PT symmetry breaking point. Let us consider the following model,

$$H^{(\mathrm{PT})}(k) = \begin{pmatrix} i\gamma & k \\ k & -i\gamma \end{pmatrix}, \quad E(k) = \pm\sqrt{k^2 - \gamma^2}, \tag{1.134}$$

which obeys the PT symmetry

$$(PT)H(k)(PT)^{-1} = H(k), \quad PT = \sigma_x K. \tag{1.135}$$

This model has the PT symmetry breaking points at $k = \pm\gamma$ with only one eigenstate $|\psi^R(k = \pm\gamma)\rangle = (1, \mp i)^T$ and the corresponding eigenenergy $E(k = \pm\gamma) = 0$. We note that the eigenstates of this Hamiltonian are PT-symmetric for $|k| > \gamma$: $PT\,|\psi_j^R\rangle \propto |\psi_j^R\rangle$, while the eigenstates constitute a PT-symmetric pair for $|k| < \gamma$: $PT\,|\psi_1^R\rangle \propto |\psi_2^R\rangle$. In general, the PT symmetry breaking point at $k = k_0$ is characterized by the $\mathbb{Z}_2$ point-gap topological invariant [14]

$$(-1)^\nu = \mathrm{sgn}\det[H(k_0 + \delta)] \cdot \mathrm{sgn}\det[H(k_0 - \delta)], \tag{1.136}$$

[14] Gapless points are often characterized by gapped topological invariants on S^{d-1} surrounding the gapless point. In this case, S^0 indicates two points $k = k_0 \pm \delta$ sandwiching the gapless point $k = k_0$.

where $\delta > 0$ is an infinitesimal real number. As PT symmetry breaking point is $\mathbb{Z}_2$ gapless point, we can trivialize the PT symmetry breaking point by doubling this model as [Fig. 1.18],

$$H(k) = \begin{pmatrix} H^{(\mathrm{PT})} & im\sigma_z \\ im\sigma_z & H^{(\mathrm{PT})} \end{pmatrix} + \lambda \begin{pmatrix} 0 & i\sigma_z \\ i\sigma_z & 0 \end{pmatrix}, \tag{1.137}$$

where the second term is a perturbation preserving the PT symmetry. We can check the point-gapless topological invariant in Eq. (1.136) becomes trivial: $\nu = 0$ for this doubled model.

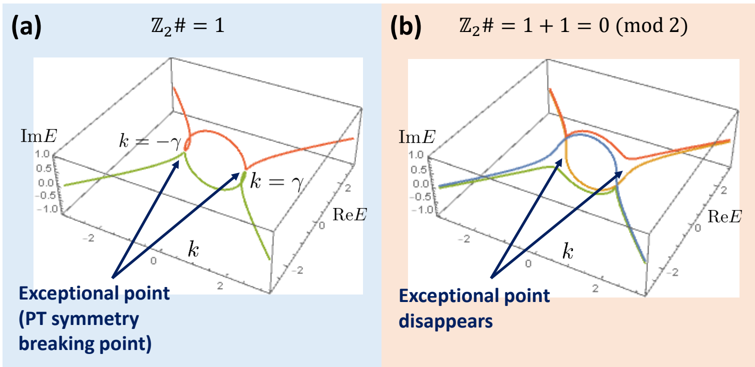

FIGURE 1.18: Complex energy spectrum of (a) a PT-symmetric model Eq. (1.134) and (b) a doubled one Eq. (1.137). (a) The model in Eq. (1.134) has two PT symmetry breaking points characterized by the $\mathbb{Z}_2$ topological invariant in Eq. (1.136), but (b) the PT symmetry breaking points disappear for the doubled one in Eq. (1.137) because the $\mathbb{Z}_2$ topological invariant becomes trivial.

We next explain the topological classification of exceptional points. As shown in the previous two examples, exceptional points are characterized by the topology of point-gapless points. Topological classification of point-gapless points can be obtained from the classification of point-gapped topological phases. Let us remember the classification of gapless states in Hermitian systems. In Hermitian systems, A Weyl point in 3D can be seen as a topological transition point of 2D topological insulators $H(k_x, k_y)$ by regarding k_z as a parameter [Fig. 1.19(a)]. The Chern number Ch of the 2D topological insulator $H(k_x, k_y)$ changes before and after the Weyl point. In non-Hermitian systems, An exceptional point in 2D (the one in Fig. 1.17) can be seen as a topological transition point of 1D point-gapped topological chain $H(k_y)$ by regarding k_x as a parameter [Fig. 1.19(b)]. Energy winding number w_1 in Eq. (1.126) changes before and after the exceptional point.

In general, we have the following relation

"classification of gapless points in d-dim." $\Leftrightarrow$ "classification of gapped phases in $(d-1)$-dim.". (1.138)

We note that this relation is valid in both Hermitian and non-Hermitian systems for both point gap and line gap under k-invariant symmetries. Non-Hermitian systems have seven k-invariant

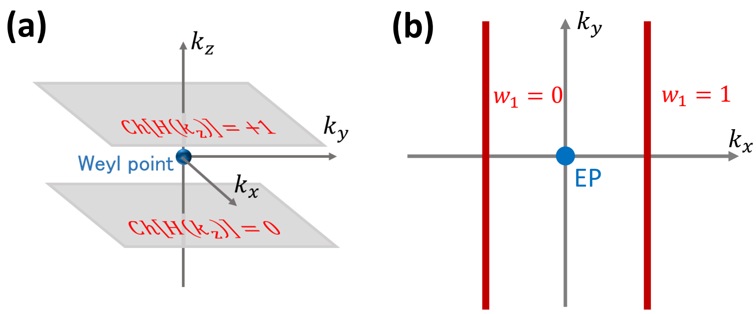

FIGURE 1.19: A gapless point in d-dimensions can be regarded as a topological transition point of $(d-1)$-dimensional gapped topological phases if we regard one momentum as a parameter. (a) A Weyl point in 3D can be seen as a topological transition point of a 2D topological insulator. (b) An exceptional point in 2D can be seen as a topological transition point of a 1D point-gapped topological chain.

symmetries. PT, CP [15] and CS are given as

$$(PT)H(\boldsymbol{k})(PT)^{-1} = H(\boldsymbol{k}), \quad (PT)^2 = \pm 1, \tag{1.139}$$
$$(CP)H^\dagger(\boldsymbol{k})(CP)^{-1} = -H(\boldsymbol{k}), \quad (CP)^2 = \pm 1, \tag{1.140}$$
$$\Gamma H^\dagger(\boldsymbol{k})\Gamma^{-1} = -H(\boldsymbol{k}), \quad \Gamma^2 = 1. \tag{1.141}$$

Here, (PT) and (CP) are anti-unitary operators while Γ is a unitary operator. The Hermitian conjugates of these symmetries: PT†, CP†, and sub-lattice symmetries (SLS) are

$$(PT')H^\dagger(\boldsymbol{k})(PT')^{-1} = H(\boldsymbol{k}), \quad (PT')^2 = \pm 1, \tag{1.142}$$
$$(CP')H(\boldsymbol{k})(CP')^{-1} = -H(\boldsymbol{k}), \quad (CP')^2 = \pm 1, \tag{1.143}$$
$$\mathcal{S}H(\boldsymbol{k})\mathcal{S}^{-1} = -H(\boldsymbol{k}), \quad \mathcal{S}^2 = 1. \tag{1.144}$$

Here, (PT') and (CP') are anti-unitary operators while $\mathcal{S}$ is a unitary operator. The Hermiticity condition is generalized into a symmetry, called pseudo-Hermiticity

$$\eta H(k)^\dagger \eta = H(k), \quad \eta^2 = 1, \tag{1.145}$$

where η is a unitary operator.

The classification of point-gapped topological phases are shown in Sec. 1.2.1. We remark that some of the symmetries we consider in this section (k-invariant symmetries) are different from the ones in Sec. 1.2.1, and thus we have different classification results. The seven symmetries Eqs. (1.139)-(1.145) for the doubled Hamiltonian $\bar{H}(\boldsymbol{k})$ in Eq. (1.102) also have the forms of crystalline symmetries, and thus we can calculate the topological classifications by the methods developed in equilibrium. We explain the classification method by Clifford algebra in Chap. 2.

The following tables 1.6-1.8 are the periodic tables of both point-gapless points and line-gapless points. The point-gapless topological numbers in these periodic tables characterize the exceptional points. The line-gapless states (especially real line-gapless states of Re$E = 0$) can be seen as a natural extension of Hermitian gapless states ($E = 0$), and it is related to the

[15] CP symmetry is a combination of charge-conjugation symmetry (C), or equivalently particle-hole symmetry, and inversion symmetry.

extended Nielsen-Ninomiya theorem.

TABLE 1.6: Periodic table of non-Hermitian gapless points in PAZ symmetry classes. ±1, 1 and 0 in the PT, CP, and Γ columns show the presence or absence of $(PT)^2 = \pm1$, $(CP)^2 = \pm1$, and $\Gamma^2 = 1$. P represents the point gap and L represents the line gap. Under some symmetry classes, real line gap L_r and imaginary line gap L_i give different topological phases.

AZ class	PT	CP	Γ	Gap	$d=1$	$d=2$	$d=3$
A	0	0	0	P	0	$\mathbb{Z}$	0
				L	$\mathbb{Z}$	0	$\mathbb{Z}$
AIII	0	0	1	P	$\mathbb{Z}$	0	$\mathbb{Z}$
				$\mathrm{L_r}$	0	$\mathbb{Z}$	0
				$\mathrm{L_i}$	$\mathbb{Z}\oplus\mathbb{Z}$	0	$\mathbb{Z}\oplus\mathbb{Z}$
PAI	$+1$	0	0	P	$\mathbb{Z}_2$	$\mathbb{Z}_2$	0
				$\mathrm{L_r}$	$\mathbb{Z}$	$\mathbb{Z}_2$	$\mathbb{Z}_2$
				$\mathrm{L_i}$	$\mathbb{Z}_2$	0	$2\mathbb{Z}$
PBDI	$+1$	$+1$	1	P	$\mathbb{Z}_2$	0	$2\mathbb{Z}$
				$\mathrm{L_r}$	$\mathbb{Z}_2$	$\mathbb{Z}_2$	0
				$\mathrm{L_i}$	$\mathbb{Z}_2\oplus\mathbb{Z}_2$	0	$2\mathbb{Z}\oplus2\mathbb{Z}$
PD	0	$+1$	0	P	0	$2\mathbb{Z}$	0
				L	$\mathbb{Z}_2$	0	$2\mathbb{Z}$
PDIII	-1	$+1$	1	P	$2\mathbb{Z}$	0	0
				$\mathrm{L_r}$	0	$2\mathbb{Z}$	0
				$\mathrm{L_i}$	$\mathbb{Z}$	0	$\mathbb{Z}$
PAII	-1	0	0	P	0	0	0
				$\mathrm{L_r}$	$2\mathbb{Z}$	0	0
				$\mathrm{L_i}$	0	0	$\mathbb{Z}$
PCII	-1	-1	1	P	0	0	$\mathbb{Z}$
				$\mathrm{L_r}$	0	0	0
				$\mathrm{L_i}$	0	0	$\mathbb{Z}\oplus\mathbb{Z}$
PC	0	-1	0	P	0	$\mathbb{Z}$	$\mathbb{Z}_2$
				L	0	0	$\mathbb{Z}$
PCI	$+1$	-1	1	P	$\mathbb{Z}$	$\mathbb{Z}_2$	$\mathbb{Z}_2$
				$\mathrm{L_r}$	0	$\mathbb{Z}$	$\mathbb{Z}_2$
				$\mathrm{L_i}$	$\mathbb{Z}$	0	$\mathbb{Z}$

TABLE 1.7: Periodic table of non-Hermitian gapless points in PAZ† symmetry classes. ±1, 1 and 0 in the PT', CP', and Γ columns show the presence or absence of $(PT')^2 = \pm1$, $(CP')^2 = \pm1$, and $\Gamma^2 = 1$. P represents the point gap and L represents the line gap. Under some symmetry classes, real line gap L_r and imaginary line gap L_i give different topological phases.

$\mathcal{P}$AZ† class	PT'	CP'	Γ	Gap	$d=1$	$d=2$	$d=3$
PAI†	$+1$	0	0	P	0	$\mathbb{Z}$	$\mathbb{Z}_2$
				L	$\mathbb{Z}$	$\mathbb{Z}_2$	$\mathbb{Z}_2$
PBDI†	$+1$	$+1$	1	P	$\mathbb{Z}$	$\mathbb{Z}_2$	$\mathbb{Z}_2$
				$\mathrm{L_r}$	$\mathbb{Z}_2$	$\mathbb{Z}_2$	0
				$\mathrm{L_i}$	$\mathbb{Z}\oplus\mathbb{Z}$	$\mathbb{Z}_2\oplus\mathbb{Z}_2$	$\mathbb{Z}_2\oplus\mathbb{Z}_2$
PD†	0	$+1$	0	P	$\mathbb{Z}_2$	$\mathbb{Z}_2$	0
				$\mathrm{L_r}$	$\mathbb{Z}_2$	0	$2\mathbb{Z}$
				$\mathrm{L_i}$	$\mathbb{Z}$	$\mathbb{Z}_2$	$\mathbb{Z}_2$
PDIII†	-1	$+1$	1	P	$\mathbb{Z}_2$	0	$2\mathbb{Z}$
				$\mathrm{L_r}$	0	$2\mathbb{Z}$	0
				$\mathrm{L_i}$	$\mathbb{Z}$	0	$\mathbb{Z}$
PAII†	-1	0	0	P	0	$2\mathbb{Z}$	0
				L	$2\mathbb{Z}$	0	0
PCII†	-1	-1	1	P	$2\mathbb{Z}$	0	0
				$\mathrm{L_r}$	0	0	0
				$\mathrm{L_i}$	$2\mathbb{Z}\oplus2\mathbb{Z}$	0	0
PC†	0	-1	0	P	0	0	0
				$\mathrm{L_r}$r	0	0	$\mathbb{Z}$
				$\mathrm{L_i}$	$2\mathbb{Z}$	0	0
PCI†	$+1$	-1	1	P	0	0	$\mathbb{Z}$
				$\mathrm{L_r}$	0	$\mathbb{Z}$	$\mathbb{Z}_2$
				$\mathrm{L_i}$	$\mathbb{Z}$	0	$\mathbb{Z}$

TABLE 1.8: Periodic table of non-Hermitian gapless points under sub-lattice symmetry (SLS) and chiral symmetry. These unitary symmetry operators obey $\Gamma^2 = 1$ and $S^2 = 1$. P represents the point gap and L represents the line gap. Under some symmetry classes, real line gap L_r and imaginary line gap L_i give different topological phases. The subscript of $S_\pm$ represents the commutation (+) or anticommutation (-) relation with chiral symmetry $\Gamma S_\pm = \pm S_\pm \Gamma$.

SLS	AZ class	Gap	$d=1$	$d=2$	$d=3$
SLS$_+$	AIII	P	0	$\mathbb{Z}$	0
		$\mathrm{L_r}$	0	$\mathbb{Z}\oplus\mathbb{Z}$	0
		$\mathrm{L_i}$	0	$\mathbb{Z}\oplus\mathbb{Z}$	0
SLS	A	P	0	$\mathbb{Z}\oplus\mathbb{Z}$	0
		L	0	$\mathbb{Z}$	0
SLS$_-$	AIII	P	$\mathbb{Z}\oplus\mathbb{Z}$	0	$\mathbb{Z}\oplus\mathbb{Z}$
		$\mathrm{L_r}$	$\mathbb{Z}$	0	$\mathbb{Z}$
		$\mathrm{L_i}$	$\mathbb{Z}$	0	$\mathbb{Z}$

1.2.5 Experimental realization of non-Hermitian Hamiltonians

In this section, we review experimental realizations of non-Hermitian Hamiltonians. We especially explain cold atoms, where the Lindblad equations with post-selection lead to effective non-Hermitian Hamiltonians, and strongly correlated or disordered electron systems where Green's functions lead to effective non-Hermitian Hamiltonians, etc.

Quantum optical method: cold atom systems

We first explain the cold atom case. If a "system" is weakly coupled to an "environment", we can describe the dynamics of the "systems" by a Lindblad equation

$$\frac{d\rho}{dt} = -\frac{i}{\hbar}(H\rho - \rho H) + \sum_m \frac{\gamma_m}{2\hbar}\left(2L_m\rho L_m^\dagger - L_m^\dagger L_m\rho - \rho L_m^\dagger L_m\right), \tag{1.146}$$

where L_m's are Lindblad (jump) operators that describe the coupling of the "systems" with the "environment". We rewrite the equation as

$$\frac{d\rho}{dt} = -\frac{i}{\hbar}\left(H_{\text{eff}}\rho - \rho H_{\text{eff}}^\dagger\right) + \sum_m \frac{\gamma_m}{\hbar} L_m \rho L_m^\dagger, \quad H_{\text{eff}} = H - \frac{i}{2}\sum_m L_m^\dagger L_m. \tag{1.147}$$

where we introduced a non-Hermitian effective Hamiltonian H_{eff}. The Lindblad operator is typically given as an annihilation operator $L_m = a_m$, which describes a loss of particles from the "system" into the "environment". We suppose the Lindblad operators are only annihilation operators in the following.

If we perform a projection measurement of the particle number of the "system", we obtain the measurement results $N_{\text{measured}} = N, N-1, N-2, \cdots$ where we supposed the initial particle number of the "system" is N. We perform the projection measurement every short time step [16] and we concentrate on the no loss case: $N_{\text{measured}} = N$. Then, as a rough discussion, we can forget the loss terms of Eq. (1.147), we have

$$\frac{d\rho}{dt} = -\frac{i}{\hbar}\left(H_{\text{eff}}\rho - \rho H_{\text{eff}}^\dagger\right). \tag{1.148}$$

If the initial state is a pure state $\rho = |\psi\rangle\langle\psi|$, we obtain the following Schrodinger equation

$$\frac{\partial}{\partial t}|\psi\rangle = H_{\text{eff}}|\psi\rangle, \tag{1.149}$$

but with normalization. For completeness, we write the exact form,

$$|\psi(t)\rangle = \frac{1}{\sqrt{\langle\psi_0| e^{iH_{\text{eff}}^\dagger t} e^{-iH_{\text{eff}}t}|\psi_0\rangle}} e^{-iH_{\text{eff}}t}|\psi_0\rangle, \quad H_{\text{eff}} = H - \frac{i}{2}\sum_m L_m^\dagger L_m. \tag{1.150}$$

This is the non-Hermitian Hamiltonian description of cold atoms with post-selection. The rigorous argument is formulated as the quantum trajectory method. See, for example, the Review article [86].

[16] The measurement time step τ needs to satisfy $\gamma\tau \ll 1$ while $\gamma^2\tau$ is finite. If we take $\tau \to 0$ without this condition, the quantum Zeno effect occurs and it prohibits the change of the system and thus the dynamics of the system become trivial.

Green's function method: strongly correlated and disordered systems

We next explain how strongly correlated electron systems induce the description of effective non-Hermitian Hamiltonians. We introduce the retarded/advanced Green's function,

$$iG^R_{\alpha\beta}(\boldsymbol{x},t) := \theta(t)\langle\{\hat{\psi}_\alpha(\boldsymbol{x},t),\hat{\psi}^\dagger_\beta(\boldsymbol{0})\}\rangle \tag{1.151}$$

$$:= \theta(t)\mathrm{tr}[e^{\beta(\Omega-\hat{H})}\{\hat{\psi}_\alpha(\boldsymbol{x},t),\hat{\psi}^\dagger_\beta(\boldsymbol{0})\}], \tag{1.152}$$

$$iG^A_{\alpha\beta}(\boldsymbol{x},t) := -\theta(-t)\langle\{\hat{\psi}_\alpha(\boldsymbol{x},t),\hat{\psi}^\dagger_\beta(\boldsymbol{0})\}\rangle \tag{1.153}$$

$$:= -\theta(-t)\mathrm{tr}[e^{\beta(\Omega-\hat{H})}\{\hat{\psi}_\alpha(\boldsymbol{x},t),\hat{\psi}^\dagger_\beta(\boldsymbol{0})\}], \tag{1.154}$$

Here we used the grand partition function

$$Z_G = e^{-\beta\Omega} := \mathrm{tr}[e^{-\beta\hat{H}}], \tag{1.155}$$

and time-dependent annihilation and creation operator

$$\hat{\psi}_\alpha(\boldsymbol{x},t) := e^{i\hat{H}t}\hat{\psi}_\alpha(\boldsymbol{x})e^{-i\hat{H}t}, \quad \hat{\psi}^\dagger_\alpha(\boldsymbol{x},t) := e^{i\hat{H}t}\hat{\psi}^\dagger_\alpha(\boldsymbol{x})e^{-i\hat{H}t}. \tag{1.156}$$

We next introduce the Fourier transformation of them as

$$G^R(\omega,\boldsymbol{k}) := \int \mathrm{d}^3\boldsymbol{x}\int \mathrm{d}t e^{-i\boldsymbol{k}\cdot\boldsymbol{x}}e^{i\omega t}G^R(\boldsymbol{x},t), \tag{1.157}$$

$$G^A(\omega,\boldsymbol{k}) := \int \mathrm{d}^3\boldsymbol{x}\int \mathrm{d}t e^{-i\boldsymbol{k}\cdot\boldsymbol{x}}e^{i\omega t}G^A(\boldsymbol{x},t). \tag{1.158}$$

We note that $iG^R(\omega,\boldsymbol{k}) = iG(\omega+i\delta,\boldsymbol{k})$ and $iG^A(\omega,\boldsymbol{k}) = iG(\omega-i\delta,\boldsymbol{k})$ with respect to the same function $iG(z,\boldsymbol{k})$ given as

$$G_{\alpha\beta}(z,\boldsymbol{k}) := V\sum_{m,n}\delta(\boldsymbol{k}+\boldsymbol{P}_n-\boldsymbol{P}_m)e^{\beta(\Omega-E_m)} \tag{1.159}$$

$$\times\frac{1+e^{-\beta(E_n-E_m)}}{z+E_n-E_m}\left\langle m\left|\hat{\psi}_\alpha(\boldsymbol{0})\right|n\right\rangle\left\langle n\left|\hat{\psi}^\dagger_\beta(\boldsymbol{0})\right|m\right\rangle. \tag{1.160}$$

We consider the effective non-Hermitian noninteracting Hamiltonian $H_{\text{eff}}(\boldsymbol{k})$ for quasi-particles defined by the retarded Green's function as

$$G^{-1}(\omega+i\delta,\boldsymbol{k}) = (\omega+i\delta) - H(k) - \Sigma(\omega+i\delta,\boldsymbol{k}) \tag{1.161}$$

$$= (\omega+i\delta) - H_{\text{eff}}(\omega,\boldsymbol{k}). \tag{1.162}$$

We usually study the $\omega = 0$ case: $H_{\text{eff}}(\boldsymbol{k}) := H_{\text{eff}}(0,\boldsymbol{k})$ in order to understand the physics of the Fermi surface.

We next explain how disordered electron systems induce the description of effective non-Hermitian Hamiltonians. We introduce the impurity-averaged Green's function as follows. We first consider the following retarded/advanced Green's functions

$$iG^R_{\alpha\beta}(\boldsymbol{x},\boldsymbol{y};t) := \theta(t)\mathrm{tr}[e^{\beta(\Omega-\hat{H})}\{\hat{\psi}_\alpha(\boldsymbol{x},t),\hat{\psi}^\dagger_\beta(\boldsymbol{y})\}] \tag{1.163}$$

$$iG^A_{\alpha\beta}(\boldsymbol{x},\boldsymbol{y};t) := -\theta(-t)\mathrm{tr}[e^{\beta(\Omega-\hat{H})}\{\hat{\psi}_\alpha(\boldsymbol{x},t),\hat{\psi}^\dagger_\beta(\boldsymbol{y})\}] \tag{1.164}$$

Here $\hat{H} := \hat{H}_0 + \hat{V}_{\text{imp}}$ and $\hat{V}_{\text{imp}}$ is impurity potential. Then, the impurity-averaged retarded/advanced Green's function is

$$iG^{R/A}_{\text{imp},\alpha\beta}(\boldsymbol{x}, \boldsymbol{y}; t) := \langle iG^{R/A}_{\alpha\beta}(\boldsymbol{x}, \boldsymbol{y}; t) \rangle_{\text{imp}} \tag{1.165}$$

Here the impurity average is defined as

$$\langle \bullet \rangle_{\text{imp}} := \Pi_i \int \frac{\mathrm{d}^3 \boldsymbol{R}_i}{V} \bullet \tag{1.166}$$

The Feynman rule for impurity scattering is obtained from this definition. The Effective non-Hermitian Hamiltonian from this impurity-averaged retarded Green's function was studied in the previous works [87, 88]. The typical impurity potential is

$$\hat{V}_{\text{imp}} = \sum_{i,\sigma} \int \mathrm{d}^3 \boldsymbol{x} V_{\text{imp}}(\boldsymbol{x} - \boldsymbol{R}_i) \hat{\psi}^\dagger_\sigma(\boldsymbol{x}) \hat{\psi}_\sigma(\boldsymbol{x}) \tag{1.167}$$

with $V_{\text{imp}}(\boldsymbol{x} - \boldsymbol{R}_i) := \delta(\boldsymbol{x} - \boldsymbol{R}_i)$ and σ is spin index. We here show the translational invariance of impurity-averaged Green's function. We introduce a translation operator $\hat{\mathcal{T}}_{\boldsymbol{a}}$ as follows

$$\hat{\mathcal{T}}_{\boldsymbol{a}} \hat{\psi}(\boldsymbol{x}) \hat{\mathcal{T}}^{-1}_{\boldsymbol{a}} = \hat{\psi}(\boldsymbol{x} + \boldsymbol{a}), \tag{1.168}$$

then, we have

$$\begin{aligned}
&\mathrm{tr}[e^{\beta(\Omega - \hat{H})} \hat{\psi}_\alpha(\boldsymbol{x} + \boldsymbol{a}, t) \hat{\psi}^\dagger_\beta(\boldsymbol{y} + \boldsymbol{a})] && (1.169)\\
&= \mathrm{tr}[e^{\beta(\Omega - \hat{H})} e^{i\hat{H}t} \hat{\psi}_\alpha(\boldsymbol{x} + \boldsymbol{a}) e^{-i\hat{H}t} \hat{\psi}^\dagger_\beta(\boldsymbol{y} + \boldsymbol{a})] && (1.170)\\
&= \mathrm{tr}[e^{\beta(\Omega - \hat{H})} e^{i\hat{H}t} \left(\hat{\mathcal{T}}_{\boldsymbol{a}} \hat{\psi}_\alpha(\boldsymbol{x}) \hat{\mathcal{T}}^{-1}_{\boldsymbol{a}} \right) e^{-i\hat{H}t} \left(\hat{\mathcal{T}}_{\boldsymbol{a}} \hat{\psi}^\dagger_\beta(\boldsymbol{y}) \hat{\mathcal{T}}^{-1}_{\boldsymbol{a}} \right)] && (1.171)\\
&= \mathrm{tr}[e^{\beta(\Omega - \hat{\mathcal{T}}_{\boldsymbol{a}}^{-1} \hat{H} \hat{\mathcal{T}}_{\boldsymbol{a}})} e^{i\hat{\mathcal{T}}_{\boldsymbol{a}}^{-1} \hat{H} \hat{\mathcal{T}}_{\boldsymbol{a}}} \hat{\psi}_\alpha(\boldsymbol{x}) e^{-i\hat{\mathcal{T}}_{\boldsymbol{a}}^{-1} \hat{H} \hat{\mathcal{T}}_{\boldsymbol{a}}} \hat{\psi}^\dagger_\beta(\boldsymbol{y})]. && (1.172)
\end{aligned}$$

Here, the translation of the Hamiltonian becomes

$$\begin{aligned}
\hat{\mathcal{T}}^{-1}_{\boldsymbol{a}} \hat{H} \hat{\mathcal{T}}_{\boldsymbol{a}} &= \hat{\mathcal{T}}^{-1}_{\boldsymbol{a}} \left(\hat{H}_0 + \hat{V}_{\text{imp}} \right) \hat{\mathcal{T}}_{\boldsymbol{a}} && (1.173)\\
&= \hat{H}_0 + \sum_{i,\alpha} \int \mathrm{d}^3 \boldsymbol{x} V_{\text{imp},\alpha\beta}(\boldsymbol{x} - \boldsymbol{R}_i) \hat{\psi}^\dagger_\alpha(\boldsymbol{x} - \boldsymbol{a}) \hat{\psi}_\beta(\boldsymbol{x} - \boldsymbol{a}) && (1.174)\\
&= \hat{H}_0 + \sum_{i,\alpha} \int \mathrm{d}^3 \boldsymbol{x} V_{\text{imp},\alpha\beta}(\boldsymbol{x} - \boldsymbol{R}_i + \boldsymbol{a}) \hat{\psi}^\dagger_\alpha(\boldsymbol{x}) \hat{\psi}_\beta(\boldsymbol{x}). && (1.175)
\end{aligned}$$

This is not equal to $\hat{H}$ itself because we do not know the position of impurities, but we can take $\boldsymbol{R}_i \to \boldsymbol{R}_i + \boldsymbol{a}$ after impurity-averaging because $\boldsymbol{R}_i$ is integrated out. Thus we have

$$\langle \mathrm{tr}[e^{\beta(\Omega-\hat{H})}\hat{\psi}_\alpha(\boldsymbol{x}+\boldsymbol{a},t)\hat{\psi}^\dagger_\beta(\boldsymbol{y}+\boldsymbol{a})]\rangle_{\text{imp}} \tag{1.176}$$
$$= \Pi_i \int \frac{\mathrm{d}^3\boldsymbol{R}_i}{V} \mathrm{tr}[e^{\beta(\Omega-\hat{\mathcal{T}}^{-1}\hat{H}\hat{\mathcal{T}})}e^{i\hat{\mathcal{T}}^{-1}\hat{H}\hat{\mathcal{T}}t}\hat{\psi}_\alpha(\boldsymbol{x})e^{-i\hat{\mathcal{T}}^{-1}\hat{H}\hat{\mathcal{T}}t}\hat{\psi}^\dagger_\beta(\boldsymbol{y})] \tag{1.177}$$
$$= \Pi_i \int \frac{\mathrm{d}^3\boldsymbol{R}_i}{V} \mathrm{tr}[e^{\beta(\Omega-\hat{H})}e^{i\hat{H}t}\hat{\psi}_\alpha(\boldsymbol{x})e^{-i\hat{H}t}\hat{\psi}^\dagger_\beta(\boldsymbol{y})] \tag{1.178}$$
$$= \langle \mathrm{tr}[e^{\beta(\Omega-\hat{H})}\hat{\psi}_\alpha(\boldsymbol{x},t)\hat{\psi}^\dagger_\beta(\boldsymbol{y})]\rangle_{\text{imp}}. \tag{1.179}$$

Because of this translational invariance, the impurity-averaged Green's function depends only on $\boldsymbol{x}-\boldsymbol{y}$ and thus we can Fourier transform it as:

$$G^{R/A}_{\text{imp}}(\omega,\boldsymbol{k}) := \int \mathrm{d}^3(\boldsymbol{x}-\boldsymbol{y}) \int \mathrm{d}t e^{-i\boldsymbol{k}\cdot(\boldsymbol{x}-\boldsymbol{y})}e^{i\omega t}G^{R/A}_{\text{imp}}(\boldsymbol{x},\boldsymbol{y};t). \tag{1.180}$$

We note that $iG^R_{\text{imp}}(\omega,\boldsymbol{k}) = iG_{\text{imp}}(\omega+i\delta,\boldsymbol{k})$ and $iG^A_{\text{imp}}(\omega,\boldsymbol{k}) = iG_{\text{imp}}(\omega-i\delta,\boldsymbol{k})$ with respect to a same function $iG_{\text{imp}}(z,\boldsymbol{k})$. Thus, we can consider an effective non-Hermitian non-interacting Bloch Hamiltonian $H_{\text{eff}}(\boldsymbol{k})$ for the quasi-particles defined by the impurity-averaged retarded Green', function:

$$G^{-1}_{\text{imp}}(\omega+i\delta,\boldsymbol{k}) = (\omega+i\delta) - H(k) - \Sigma_{\text{imp}}(\omega+i\delta,\boldsymbol{k}) \tag{1.181}$$
$$= (\omega+i\delta) - H_{\text{eff}}(\omega,\boldsymbol{k}). \tag{1.182}$$

1.3 Organization of the thesis

In this thesis, we construct an extended version of the Nielsen-Ninomiya theorem for Floquet and non-Hermitian systems and provide applications of the theorem for both Floquet systems and non-Hermitian systems. In Chapter 2, we review the properties of Dirac Hamiltonians as theoretical methods. Dirac Hamiltonians give typical models of topological insulators, superconductors, and semimetals in equilibrium. Moreover, Dirac Hamiltonians are closely related to the topological classifications as firstly shown by Kitaev [14].

In Chapter 3, we first see examples of the extended Nielsen-Ninomiya theorem both in Floquet and non-Hermitian systems, which also implies a topological duality between Floquet and non-Hermitian systems. Then, we give general theories. We formulate the topological duality between Floquet and non-Hermitian systems, and provide the extended Nielsen-Ninomiya theorem that is valid in any symmetry classes and dimensions. The proof of the theorem is followed. In Chapter 4, we propose the non-Hermitian chiral magnetic effect as an application of the extended Nielsen-Ninomiya theorem for non-Hermitian systems. We construct a concrete model, and see the wave packets go in the direction of an applied magnetic field. We also find a formula describing the non-Hermitian chiral magnetic effect. In Chapter 5, we propose extrinsic topology in quantum walks as an application of the extended Nielsen-Ninomiya theorem for Floquet systems. According to ordinary bulk-boundary correspondence, the boundary gapless states are determined from the bulk topological invariants. In quantum walks, however, the boundary states depend on both bulk topology and boundary topology.

Chapter 2

Method: Dirac Hamiltonians

2.1 Simplest topological insulator models

In this section, We see that massive Dirac Hamiltonians can be regarded as a simplest topological insulator (superconductor) models.

class A $d = 2$

Let us consider a 2D topological insulator model

$$H(k_x, k_y) = \sin k_x \sigma_x + \sin k_y \sigma_y + (u + \cos k_x + \cos k_y)\sigma_z, \tag{2.1}$$

$$E(k_x, k_y) = \pm\sqrt{\sin^2 k_x + \sin^2 k_y + (u + \cos k_x + \cos k_y)^2}. \tag{2.2}$$

In general, the topological phases of 2D insulators are characterized by the Chern number in Eq. (1.26). For the present model, the Chern number becomes

- $Ch = 0$ for $u < -2$.
- $Ch = -1$ for $-2 < u < 0$.
- $Ch = 1$ for $0 < u < 2$.
- $Ch = 0$ for $u > 2$.

Near the topological transition point $u = -2$ with $\boldsymbol{k} = (0, 0)$, the model becomes a simple massive Dirac Hamiltonian,

$$H(k_x, k_y) = k_x\sigma_x + k_y\sigma_y + m\sigma_z + O(k^2), \quad H(k_x, k_y) = \sqrt{k_x^2 + k_y^2 + m^2} + O(k^2). \tag{2.3}$$

Here we replaced $m = u + 2$. The Chern number of this model in the Brillouin zone $\boldsymbol{k} \in \mathbb{R}^2$ becomes $Ch = \frac{1}{2}\mathrm{sgn}[m]$ [1]. From this result, we can say that $m < 0$ and $m > 0$ are different topological phases.

class AIII $d = 1$

Next, we consider a 1D model with chiral symmetry given as

$$H(k) = \begin{pmatrix} 0 & u + ve^{ik} \\ u + ve^{-ik} & 0 \end{pmatrix}, \quad E(k) = \pm\sqrt{(u + v\cos k)^2 + (v\sin k)^2}, \tag{2.4}$$

[1] The Chern number can take a non-integer value because the Brillouin zone is non-compact.

where the chiral symmetry is given as $\sigma_z H(k)\sigma_z = -H(k)$. The topological phases of 1D chiral-symmetric insulators are characterized by the winding number defined as

$$w := \int_0^{2\pi} \frac{dk}{2\pi i}\mathrm{tr}[q^{-1}\partial_k q], \quad H(k) = \begin{pmatrix} 0 & q \\ q^\dagger & 0 \end{pmatrix}, \tag{2.5}$$

where we assumed the non-diagonal form of Hamiltonians obtained from the chiral symmetry $\sigma_z H \sigma_z = -H$. For the present model, the winding number becomes

- $w = 0$ for $u > v$.
- $w = 1$ for $u < v$.

Near the topological transition point $u = v$ with $k = \pi$, the model becomes a simple massive Dirac Hamiltonian,

$$H(k) = v\delta k\sigma_y + m\sigma_x + O(\delta k^2), \quad E(k) = \pm\sqrt{(v\delta k)^2 + m^2}. \tag{2.6}$$

Here we replaced $m = u - v$ and $\delta k = k - \pi$. The winding number of this model in the Brillouin zone $k \in \mathbb{R}$ becomes $w = \frac{1}{2}\mathrm{sgn}[m]$ [2]. From this result, we can say that $m < 0$ and $m > 0$ are different topological phases.

2.2 Clifford algebra

We first review the Clifford algebra. The Clifford algebra is mathematically a ring, which defines addition and multiplication. The complex Clifford algebra Cl_n has n generators $\{e_1, \ldots, e_n\}$ satisfying

$$\{e_i, e_j\} = \delta_{i,j}, \tag{2.7}$$

and the linear combinations of the products $e_1^{p_1} e_2^{p_2} \cdots e_n^{p_n}$ form a 2^n-dimensional complex vector space. The real Clifford algebra $Cl_{p,q}$ has $p+q$ generators $\{e_1, \ldots, e_p; e_{p+1}, \ldots, e_{p+q}\}$ satisfying

$$\{e_i, e_j\} = 0 \quad \text{for } i \neq j, \tag{2.8}$$

$$e_i^2 = \begin{cases} -1 & \text{for } 1 \leq i \leq p, \\ 1 & \text{for } p+1 \leq i \leq p+q, \end{cases} \tag{2.9}$$

and their products form a 2^{p+q}-dimensional real vector space. For instance, generators of Cl_2 are given by the Pauli matrices,

$$\{e_1, e_2\} = \{\sigma_x, \sigma_y\}, \tag{2.10}$$

the products of which provide the basis of the 2^2-dimensional complex vector space as

$$c_1\hat{1} + c_2\sigma_x + c_3\sigma_y + c_4 i\sigma_z, \quad c_1, c_2, c_3, c_4 \in \mathbb{C}. \tag{2.11}$$

The space coincides with that of 2×2 matrices $\mathbb{C}(2)$, and thus we obtain the isomorphism $Cl_2 \simeq \mathbb{C}(2)$.

[2] The winding number can take a non-integer value because the Brillouin zone is non-compact.

TABLE 2.1: Classifying space C_n.

$n \mod 2$	Classifying space C_n	$\pi_0(C_n)$
0	$[U(k+m)/(U(k)\times U(m))]\times\mathbb{Z}$	$\mathbb{Z}$
1	$U(k)$	0

TABLE 2.2: Classifying space R_q.

$q \mod 2$	Classifying space R_q	$\pi_0(R_q)$
0	$[O(k+m)/(O(k)\times O(m))]\times\mathbb{Z}$	$\mathbb{Z}$
1	$O(k)$	$\mathbb{Z}_2$
2	$O(2k)/U(k)$	$\mathbb{Z}_2$
3	$U(2k)/Sp(k)$	0
4	$[Sp(k+m)/(Sp(k)\times Sp(m))]\times\mathbb{Z}$	$\mathbb{Z}$
5	$Sp(k)$	0
6	$Sp(k)/U(k)$	0
7	$U(k)/O(k)$	0

If a representation of complex Clifford algebra Cl_n is given, we can obtain Cl_{n+1} by adding a generator e_0 satisfying $\{e_0, e_j\} = \delta_{0,j}$. The problem to identify all the possible representations of e_0 is called the extension problem of $Cl_n \to Cl_{n+1}$, and the space of the representations is called the classifying space C_n. In Table 2.1, we summarize the classifying space C_n and the number of connected parts of C_n, i.e., the zeroth homotopy $\pi_0(C_n)$. We note that C_n has the Bott periodicity $C_{n+2} = C_n$.

We also have a similar extension problem for the real Clifford algebras. If a representation of $Cl_{p,q}$ is given, we add a generator e_0 that satisfies $e_0^2 = -1$ ($e_0^2 = 1$), and obtain the real Clifford algebra $Cl_{p+1,q}$ ($Cl_{p,q+1}$). The problem to identify the representation space of e_0 is called the extension problem $Cl_{p,q} \to Cl_{p+1,q}$ ($Cl_{p,q} \to Cl_{p,q+1}$), which defines the classifying space R_{p+2-q} (R_{q-p}). Table 2.2 summarizes the classifying space R_q and the number of connected parts of R_q, i.e., the zeroth homotopy $\pi_0(R_q)$. We note that R_q has the Bott periodicity $R_{q+8} = R_q$.

2.3 Classification of topological insulators and superconductors

As shown in Sec. 2.1, near a topological transition point, the Hamiltonian of topological insulators and superconductors takes the form of massive Dirac Hamiltonian, [3]

$$H(\boldsymbol{k}) = \sum_{j=1}^{d} k_j\gamma_j + \gamma_0, \tag{2.12}$$

where $\gamma_\mu = \gamma_0, \gamma_j$ are gamma matrices satisfying $\{\gamma_\mu\gamma_\nu\} = \delta_{\mu\nu}$. The massive Dirac Hamiltonian needs to satisfy the given symmetries we want to consider. Gamma matrices are mathematically

[3]More strictly, it is believed that we can always deform any model near a topological transition point into a massive Dirac Hamiltonian up to addiction and subtraction of trivial bands.

generators of Clifford algebras introduced in the previous section. The number of connected representations of γ_0 gives the number of topological phases. Mathematically, if we write the representation space of γ_0 as M, then the number of connected parts of M, called the zeroth homotopy group $\pi_0(M)$ gives the number of topological phases.

We see two ways of calculating $\pi_0(M)$ in class A 2D systems. One way is a naive calculation based on its definition. The other way is a formal calculation based on the Clifford algebra extension problem. We first explain a naive calculation. Near a topological transition point, the Hamiltonians of topological insulators take the form of a massive Dirac Hamiltonian

$$H(k_1, k_1) = k_1\gamma_1 + k_2\gamma_2 + \gamma_0 = k_1\sigma_x \otimes 1_{N\times N} + k_2\sigma_y \otimes 1_{N\times N} + \gamma_0, \tag{2.13}$$

where we fixed a representation of gamma matrices of γ_1, γ_2. N is taken to infinity because solids have many trivial bands that does not affect the physics near Fermi surface [4]. The possible representations of γ_0 is given by

$$\gamma_0 = \sigma_z \otimes A, \quad A^2 = 1_{N\times N}, \tag{2.14}$$

where A is Hermitian. A is also rewritten as

$$A = UI_{n,m}U^\dagger, \quad I_{n,m} = \begin{pmatrix} 1_{n\times n} & \\ & -1_{m\times m} \end{pmatrix}, \tag{2.15}$$

where n, m is chosen to satisfy $n + m = N$. We note that A does not change under the gauge transformation of U given as,

$$U \to U \begin{pmatrix} U_n & \\ & U_m \end{pmatrix}. \tag{2.16}$$

U is defined up to this form of gauge transformation. Therefore, the representation space of γ_0 becomes

$$M = [U(n+m)/(U(n) \times U(m))] \times \mathbb{Z} \tag{2.17}$$

in the limit $N \to \infty$. We note that the space M exactly coincides with C_0 in Table 2.1. The number of connected parts of M is

$$\pi_0(M) = \pi_0(C_0) = \mathbb{Z}. \tag{2.18}$$

This result indicates that class A 2D insulators have integer infinity of topological phases. This is compatible with our knowledge that the Chern number is integer-valued.

We next explain a formal calculation based on the Clifford algebra extension problem. Near a topological transition point, the Hamiltonians take the form of a massive Dirac Hamiltonian

$$H(k_1, k_2) = k_1\gamma_1 + k_2\gamma_2 + \gamma_0. \tag{2.19}$$

[4]For example, we have extremely high-energy trivial bands that electrons go outside of solids.

We calculate the representation space of γ_0. The gamma matrices constitute complex Clifford algebra, where the generators are

$$\{e_0, e_1, e_2\} = \{\gamma_0, \gamma_1, \gamma_2\}. \tag{2.20}$$

Then, the problem to obtain the representation space γ_0 for a fixed representation of γ_1 and γ_2 is given as

$$Cl_2 \to Cl_3. \tag{2.21}$$

It's classifying space is $C_2 \simeq C_0$. Therefore, we obtain $\pi_0(\gamma_0) = \pi_0(C_0) = \mathbb{Z}$.

The latter formal calculation is easier to systematically obtain the topological classifications. In the following, we calculate the classifying spaces in all symmetry classes and dimensions.

Complex symmetry classes

We first consider class A. Near a topological transition point, Hamiltonians take the form of a massive Dirac Hamiltonian

$$H(\boldsymbol{k}) = \sum_{j=1}^{d} k_j \gamma_j + \gamma_0. \tag{2.22}$$

The gamma matrices constitute a complex Clifford algebra as

$$\{e_0,\ e_1,\ \cdots, e_{d+1}\} = \{\gamma_0,\ \gamma_1,\ \gamma_2, \cdots, \gamma_d\}. \tag{2.23}$$

Therefore, the problem to obtain the representation space γ_0 is given by the extension problem of

$$Cl_d \to Cl_{d+1}. \tag{2.24}$$

Therefore, the classifying space is given as C_d.

We next consider class AIII. Near a topological transition point, Hamiltonians take the form of a massive Dirac Hamiltonian

$$H(\boldsymbol{k}) = \sum_{j=1}^{d} k_j \gamma_j + \gamma_0, \quad \Gamma H(\boldsymbol{k}) \Gamma = -H(\boldsymbol{k}). \tag{2.25}$$

We note that the massive Dirac Hamiltonian obeys the chiral symmetry. The gamma matrices and the chiral symmetry operator constitute a complex Clifford algebra as

$$\{e_0,\ e_1,\ \cdots, e_{d+2}\} = \{\gamma_0,\ \gamma_1,\ \gamma_2, \cdots, \gamma_d, \Gamma\}. \tag{2.26}$$

Therefore, the problem to obtain the representation space γ_0 is given by the extension problem of

$$Cl_{d+1} \to Cl_{d+2}. \tag{2.27}$$

Therefore, the classifying space is given as C_{d+1}.

Real symmetry classes

In the presence of TRS and PHS,

$$TH(\boldsymbol{k})T^{-1} = H(-\boldsymbol{k}), \quad CH(\boldsymbol{k})C^{-1} = -H(-\boldsymbol{k}), \tag{2.28}$$

anti-unitary operators T and C make the problem difficult. We introduce an operator J that represents the imaginary unit i [5] and anti-commute with T and C. Then, the gamma matrices, symmetry operators, and J constitute a real Clifford algebra as follows.

We first consider classes AI and AII ($T^2 = 1$ and $T^2 = -1$). The generators of the real Clifford algebras for classes AI and AII are

$$\{J\gamma_0;\ T,\ JT,\ \gamma_1,\ \gamma_2, \cdots, \gamma_d\}, \tag{2.29}$$

$$\{J\gamma_0,\ T,\ JT;\ \gamma_1,\ \gamma_2, \cdots, \gamma_d\}. \tag{2.30}$$

Therefore, the representation spaces of γ_0 in classes AI and AII are given by the extension problems of

$$Cl_{0,d+2} \to Cl_{1,d+2}, \quad Cl_{2,d+2} \to Cl_{3,d+2}. \tag{2.31}$$

Their classifying spaces are R_{-d} and R_{4-d} for classes AI and AII.

We next consider classes D and C ($C^2 = 1$ and $C^2 = -1$). The generators of the real Clifford algebra for classes D and C are

$$\{J\gamma_1,\ J\gamma_2, \cdots, J\gamma_d;\ \ C,\ JC,\ \gamma_0\}, \tag{2.32}$$

$$\{J\gamma_1,\ J\gamma_2, \cdots, J\gamma_d,\ \ C,\ JC;\ \gamma_0\}. \tag{2.33}$$

Therefore, the representation space of γ_0 for classes D and C are given by the extension problems of

$$Cl_{d,2} \to Cl_{d,3}, \quad Cl_{d+2,0} \to Cl_{d+2,1}. \tag{2.34}$$

Their classifying spaces are R_{2-d} and R_{6-d} for classes D and C.

We finally consider classes BDI ($T^2 = 1, C^2 = 1$), DIII ($T^2 = -1, C^2 = 1$), CII ($T^2 = -1, C^2 = -1$), and CI ($T^2 = 1, C^2 = -1$). The generators of the real Clifford algebra for classes BDI, DIII, CII and CI are

$$\{J\gamma_0,\ J\Gamma;\ T,\ JT,\ \gamma_1,\ \gamma_2, \cdots, \gamma_d\}, \tag{2.35}$$

$$\{J\gamma_0,\ T,\ JT;\ J\Gamma,\ \gamma_1,\ \gamma_2, \cdots, \gamma_d\}, \tag{2.36}$$

$$\{J\gamma_0,\ T,\ JT,\ J\Gamma;\ \gamma_1,\ \gamma_2, \cdots, \gamma_d\}, \tag{2.37}$$

$$\{J\gamma_0;\ J\Gamma,\ T,\ JT,\ \gamma_1,\ \gamma_2, \cdots, \gamma_d\}. \tag{2.38}$$

Therefore, the representation space of γ_0 for classes BDI, DIII, CII and CI are given by the extension problems of

$$Cl_{1,d+2} \to Cl_{2,d+2}, \quad Cl_{2,d+1} \to Cl_{3,d+1}, \quad Cl_{3,d} \to Cl_{4,d}, \quad Cl_{0,d+3} \to Cl_{1,d+3}. \tag{2.39}$$

Their classifying spaces are R_{1-d}, R_{3-d}, R_{5-d}, and R_{7-d} for classes BDI, DIII, CII and CI.

[5] The 2×2 matrices $\begin{pmatrix} a & -b \\ b & a \end{pmatrix}$ is isomorphic to complex numbers $a + ib$, where $a, b \in \mathbb{R}$.

Combining $\pi_0(C_n)$ and $\pi_0(R_q)$ in Table 2.1 and 2.2, we obtain the periodic table of topological insulators and superconductors as shown in Table 2.3.

TABLE 2.3: Periodic table of topological insulators and superconductors.

AZ class	T	C	Γ	$d=0$	1	2	3	4
A	0	0	0	$\mathbb{Z}$	0	$\mathbb{Z}$	0	$\mathbb{Z}$
AIII	0	0	1	0	$\mathbb{Z}$	0	$\mathbb{Z}$	0
AI	$+1$	0	0	$\mathbb{Z}$	0	0	0	$\mathbb{Z}$
BDI	$+1$	$+1$	1	$\mathbb{Z}_2$	$\mathbb{Z}$	0	0	0
D	0	$+1$	0	$\mathbb{Z}_2$	$\mathbb{Z}_2$	$\mathbb{Z}$	0	0
DIII	-1	$+1$	1	0	$\mathbb{Z}_2$	$\mathbb{Z}_2$	$\mathbb{Z}$	0
AII	-1	0	0	$\mathbb{Z}$	0	$\mathbb{Z}_2$	$\mathbb{Z}_2$	$\mathbb{Z}$
CII	-1	-1	1	0	$\mathbb{Z}$	0	$\mathbb{Z}_2$	$\mathbb{Z}_2$
C	0	-1	0	0	0	$\mathbb{Z}$	0	$\mathbb{Z}_2$
CI	$+1$	-1	1	0	0	0	$\mathbb{Z}$	0

2.4 Bulk-boundary correspondence

Massive Dirac Hamiltonians also give us a clear-cut understanding of the bulk-boundary correspondence. Furthermore, we can see that the effective surface Hamiltonian describing the gapless boundary states takes the form of gapless Dirac Hamiltonians.

2.4.1 2D Chern insulator

Let us first consider the massive Dirac Hamiltonian for 2D Chern insulators again,

$$H(k_x, k_y) = k_x\sigma_x + k_y\sigma_y + m\sigma_z + O(k^2), \quad E(k_x, k_y) = \sqrt{k_x^2 + k_y^2 + m^2} + O(k^2). \tag{2.40}$$

The Chern number of this model is $Ch = \frac{1}{2}\mathrm{sgn}[m]$, which implies that $m < 0$ and $m > 0$ are different topological phases.

We see the surface of two Chern insulators has chiral gapless modes. The surface of two Chern insulators is represented as

$$H = k_x\sigma_x + (-i\partial_y)\sigma_y + m(y)\sigma_z, \tag{2.41}$$

where $m(y)$ is given as

$$m(y) = \begin{cases} -1/2 & \text{for } y > 0, \\ 1/2 & \text{for } y < 0. \end{cases} \tag{2.42}$$

Its solution is [6]

$$\psi \propto e^{\int^y m(y')dy'} v_0, \quad v_0 = \frac{1}{\sqrt{2}} \begin{pmatrix} 1 & 1 \end{pmatrix}^{\mathrm{T}}, \tag{2.43}$$

[6]We note that the spatial factor $\phi(y) \propto e^{\int^y m(y')dy'}$ is a square-integrable function $\int_{-\infty}^{\infty} |\phi(y)|^2 < \infty$.

with eigenenergy $E_{\text{surface}}(k_x) = k_x$, because this solution leads to

$$H\psi = [k_x\sigma_x + m(y)(\sigma_z - i\sigma_y)]\psi \tag{2.44}$$
$$= k_x\psi. \tag{2.45}$$

If we take $m(y) = 1/2$ for $y > 0$ and $m(y) = -1/2$ for $y < 0$, the solution is given by $\psi \propto e^{-\int^y m(y')dy'} v_0'$ with eigenenergy $E_{\text{surface}}(k_x) = -k_x$, where $v_0' = (1/\sqrt{2})(1, -1)^{\mathrm{T}}$.

From this result, we have the bulk-boundary correspondence [7]:

$$Ch_{y<0} - Ch_{y>0} = \sum_{k_x^{p\alpha}} \operatorname{sgn} v_x^{p\alpha}, \tag{2.46}$$

where $k_x^{p\alpha}$ is the α-th Fermi point defined by $E_p(k_x^{p\alpha}) = 0$ for some energy band p, and $v_x^{p\alpha} = (\partial E_p(k_x)/\partial k_x)_{k_x = k_x^{p\alpha}}$ is the group velocity at $k_x^{p\alpha}$. This equation states that the total chirality $\operatorname{sgn} v_x^{p\alpha}$ at the surface $y = 0$ is determined from the difference of the Chern numbers in $y < 0$ region ($Ch_{y<0}$) and the Chern numbers in $y > 0$ region ($Ch_{y>0}$).

2.4.2 General case

In general [36], the topological insulators near topological transition point is given by a massive Dirac Hamiltonian,

$$H(\boldsymbol{k}) = \sum_{j=1}^{d} k_j\gamma_j + m\gamma_0, \tag{2.47}$$

where $\gamma_\mu = \gamma_0, \gamma_j$ are gamma matrices satisfying $\{\gamma_\mu\gamma_\nu\} = \delta_{\mu\nu}$.

We consider the surface at $x_d = 0$ as

$$H = \sum_{j=1}^{d-1} k_j\gamma_j + (-i\partial_{x_d})\gamma_d + m(x_d)\gamma_0. \tag{2.48}$$

where $m(x_d)$ is the one given in Eq. (2.42). From the anti-commutation relations of gamma matrices, we have the commutation relation $[i\gamma_0\gamma_d, \gamma_j] = 0$. Then, we can simultaneously diagonalize $i\gamma_0\gamma_d$ and $\sum_{j=1}^{d-1} k_j\gamma_j$. As we have $(i\gamma_0\gamma_d)^2 = \hat{1}$, its eigenvalues are ± 1. We especially consider the eigenspace of $(i\gamma_0\gamma_d)v = +1v$.

Its solution is given as

$$\psi \propto e^{\int^y m(y')dy'} v \otimes u, \tag{2.49}$$

[7] We have checked that only one nontrivial model satisfies this relation. In general, by stacking this generator model and/or trivial model via a direct sum and performing a smooth deformation, any topological insulator model can be produced. We note that the left-hand side and right-hand side of this relation are invariant during this deformation. Therefore, this relation holds for any gapped model.

which leads to

$$H\psi = \left[\sum_{j=1}^{d-1} k_j\gamma_j + m(x_d)(\gamma_0 - i\gamma_d)\right]\psi \tag{2.50}$$

$$= \sum_{j=1}^{d-1} k_j\gamma_j\psi, \tag{2.51}$$

where we have used $\gamma_0 - i\gamma_d = \gamma_0(\gamma_0^2 - i\gamma_0\gamma_d) = \gamma_0(1-1) = 0$ for v.

If we simultaneously diagonalize $\sum_{j=1}^{d-1} k_j\gamma_j$ by choosing an appropriate u, we have

$$H\psi_\pm = E^\pm_{\text{surface}}(\boldsymbol{k})\psi_\pm, \quad E^\pm_{\text{surface}}(\boldsymbol{k}) = \pm\sqrt{\sum_{j=1}^{d-1} k_j^2}. \tag{2.52}$$

From this result, we see that the boundary gapless states of d-dimensional topological insulators obey the effective surface Hamiltonian of the form of the gapless Dirac Hamiltonian

$$H_{\text{surface}}(\boldsymbol{k}) = \sum_{j=1}^{d-1} k_j\gamma_j. \tag{2.53}$$

This result also implies that the classification of gapless states in $(d-1)$-dimensions is given by the classification of topological insulators in d-dimensions. Therefore, the periodic table of gapless states becomes Table. 2.4.

TABLE 2.4: Periodic table of topological gapless states.

AZ class	T	C	Γ	$d=0$	1	2	3
A	0	0	0	0	$\mathbb{Z}$	0	$\mathbb{Z}$
AIII	0	0	1	$\mathbb{Z}$	0	$\mathbb{Z}$	0
AI	$+1$	0	0	0	0	0	$\mathbb{Z}$
BDI	$+1$	$+1$	1	$\mathbb{Z}$	0	0	0
D	0	$+1$	0	$\mathbb{Z}_2$	$\mathbb{Z}$	0	0
DIII	-1	$+1$	1	$\mathbb{Z}_2$	$\mathbb{Z}_2$	$\mathbb{Z}$	0
AII	-1	0	0	0	$\mathbb{Z}_2$	$\mathbb{Z}_2$	$\mathbb{Z}$
CII	-1	-1	1	$\mathbb{Z}$	0	$\mathbb{Z}_2$	$\mathbb{Z}_2$
C	0	-1	0	0	$\mathbb{Z}$	0	$\mathbb{Z}_2$
CI	$+1$	-1	1	0	0	$\mathbb{Z}$	0

2.5 Topological classification of Floquet systems

In this section, we see how to obtain the topological classification of Floquet topological insulators and Floquet gapless phases by the extension problem of Clifford algebra.

Floquet topological insulators

In Sec. 1.1.1, we discussed the classification of Floquet topological insulators. It is reformulated into the topological classification problem of $C(\boldsymbol{k},t)$ and $L(\boldsymbol{k},t)$ in Eq. (1.18). The topological classification of $C(\boldsymbol{k},t)$ is equivalent to the topological classification of ordinary topological insulators discussed in Sec. 2.3. The topological classification of $L(\boldsymbol{k},t)$ is equivalent to that of $\mathcal{H}_L(\boldsymbol{k},t)$ in Eq. (1.19), which obeys the symmetries in Eqs. (1.20)-(1.23). In Table 2.5, we summarize the generators of Clifford algebra, the extension problem, and the classifying space for the massive Dirac Hamiltonian

$$\mathcal{H}_L(\boldsymbol{k},t) = \sum_{j=1}^{d} k_j\gamma_j + t\gamma_t + \gamma_0, \tag{2.54}$$

for each symmetry class and dimensions. Combining this Table 2.5 with Tables 2.1 and 2.2, we can specify the number of connected components of the classifying space, which gives the topological numbers in Table 1.2.

TABLE 2.5: Clifford algebra extensions and classifying spaces for $\mathcal{H}_L(\boldsymbol{k},t)$.

AZ class	T	C	Γ	Generator	Extension	C_n or R_q
A	0	0	0	$\{\gamma_1,\dots,\gamma_d,\gamma_t,\gamma_0,\Sigma_z\}$	$Cl_{d+2}\to Cl_{d+3}$	C_d
AIII	0	0	1	$\{\gamma_1,\dots,\gamma_d,\gamma_t,\gamma_0,\Sigma_z,J\gamma_t\tilde{\Gamma}\}$	$Cl_{d+3}\to Cl_{d+4}$	C_{d+1}
AI	+1	0	0	$\{J\gamma_0,J\Sigma_z;\gamma_1,\dots,\gamma_d,\gamma_t,\tilde{T},J\tilde{T}\}$	$Cl_{1,d+3}\to Cl_{2,d+3}$	R_{-d}
BDI	+1	+1	1	$\{J\gamma_0,J\Sigma_z,\gamma_t\tilde{\Gamma};\gamma_1,\dots,\gamma_d,\gamma_t,\tilde{T},J\tilde{T}\}$	$Cl_{2,d+3}\to Cl_{3,d+3}$	R_{1-d}
D	0	+1	0	$\{J\gamma_0,J\gamma_t,J\Sigma_z;\gamma_1,\dots,\gamma_d,\tilde{C},J\tilde{C}\}$	$Cl_{2,d+2}\to Cl_{3,d+2}$	R_{2-d}
DIII	−1	+1	1	$\{J\gamma_0,J\Sigma_z,\tilde{T},J\tilde{T};\gamma_1,\dots,\gamma_d,\gamma_t,\gamma_t\tilde{\Gamma}\}$	$Cl_{2,d+2}\to Cl_{3,d+2}$	R_{2-d}
AII	−1	0	0	$\{J\gamma_0,J\Sigma_z,\tilde{T},J\tilde{T};\gamma_1,\dots,\gamma_d,\gamma_t\}$	$Cl_{3,d+1}\to Cl_{4,d+1}$	R_{4-d}
CII	−1	−1	1	$\{J\gamma_0,J\Sigma_z,\gamma_t\tilde{\Gamma},\tilde{T},J\tilde{T};\gamma_1,\dots,\gamma_d,\gamma_t\}$	$Cl_{4,d+1}\to Cl_{5,d+1}$	R_{5-d}
C	0	−1	0	$\{J\gamma_0,J\gamma_t,J\Sigma_z,\tilde{C},J\tilde{C};\gamma_1,\dots,\gamma_d\}$	$Cl_{4,d}\to Cl_{5,d}$	R_{6-d}
CI	+1	−1	1	$\{J\gamma_0,J\Sigma_z;\gamma_1,\dots,\gamma_d,\gamma_t,\gamma_t\tilde{\Gamma},\tilde{T},J\tilde{T}\}$	$Cl_{1,d+4}\to Cl_{2,d+4}$	R_{7-d}

Floquet gapless phases

In Sec. 1.1.3, we discussed the classification of Floquet gapless phases. It is reformulated into the topological classification problem of $\mathcal{H}_U(\boldsymbol{k})$ in Eq. (1.62). We suppose $\mathcal{H}_U(\boldsymbol{k})$ takes the form of Dirac Hamiltonian

$$\mathcal{H}_U(\boldsymbol{k}) = \sum_{j=1}^{d-1} k_j\gamma_j + \gamma_0. \tag{2.55}$$

Then, the gamma matrices γ_μ, symmetry operations for $\mathcal{H}_U(\boldsymbol{k})$ in Eqs. (1.63)-(1.66), and the operator J representing the imaginary unit form the Clifford algebra in Table 2.6. In this table, we also summarized the extension problem and the classifying space C_n or R_q. Combining with Tables 2.1 and 2.2, we can specify the number of connected components of the classifying space, which gives the topological numbers in Table 1.2.

2.6 Topological classification of non-Hermitian systems

In this section, we briefly explain how to obtain the topological classification of non-Hermitian gapped and gapless systems.

TABLE 2.6: Clifford algebra extensions and classifying spaces for $\mathcal{H}_U(\boldsymbol{k}_\parallel)$.

AZ class	T	C	Γ	Generator	Extension	C_n or R_q
A	0	0	0	$\{\gamma_1,\dots,\gamma_{d-1},\gamma_0,\Sigma_z\}$	$Cl_d \to Cl_{d+1}$	C_d
AIII	0	0	1	$\{\gamma_1,\dots,\gamma_{d-1},\gamma_0,\Sigma_z,J\Sigma_z\tilde{\Gamma}\}$	$Cl_{d+1} \to Cl_{d+2}$	C_{d+1}
AI	$+1$	0	0	$\{J\gamma_0;\gamma_1,\dots,\gamma_{d-1},\Sigma_z,\tilde{T},J\tilde{T}\}$	$Cl_{0,d+2} \to Cl_{1,d+2}$	R_{-d}
BDI	$+1$	$+1$	1	$\{J\gamma_0,\tilde{\Gamma}\Sigma_z;\gamma_1,\dots,\gamma_{d-1},\Sigma_z,\tilde{T},J\tilde{T}\}$	$Cl_{1,d+2} \to Cl_{2,d+1}$	R_{1-d}
D	0	$+1$	0	$\{J\gamma_0,J\Sigma_z;\gamma_1,\dots,\gamma_{d-1},\tilde{C},J\tilde{C}\}$	$Cl_{1,d+1} \to Cl_{2,d+1}$	R_{2-d}
DIII	-1	$+1$	1	$\{J\gamma_0,\tilde{T},J\tilde{T};\gamma_1,\dots,\gamma_{d-1},\Sigma_z,\tilde{\Gamma}\Sigma_z\}$	$Cl_{2,d+1} \to Cl_{3,d+1}$	R_{3-d}
AII	-1	0	0	$\{J\gamma_0,\tilde{T},J\tilde{T};\gamma_1,\dots,\gamma_{d-1},\Sigma_z\}$	$Cl_{2,d} \to Cl_{3,d}$	R_{4-d}
CII	-1	-1	1	$\{J\gamma_0,\tilde{T},J\tilde{T},\tilde{\Gamma}\Sigma_z;\gamma_1,\dots,\gamma_{d-1},\Sigma_z\}$	$Cl_{3,d} \to Cl_{4,d}$	R_{5-d}
C	0	-1	0	$\{J\gamma_0,J\Sigma_z,\tilde{C},J\tilde{C};\gamma_1,\dots,\gamma_{d-1}\}$	$Cl_{3,d-1} \to Cl_{4,d-1}$	R_{6-d}
CI	$+1$	-1	1	$\{J\gamma_0;\gamma_1,\dots,\gamma_{d-1},\Sigma_z,\tilde{T},J\tilde{T},\tilde{\Gamma}\Sigma_z\}$	$Cl_{0,d+3} \to Cl_{1,d+3}$	R_{7-d}

In Sec. 1.2.1, we discussed the classification of non-Hermitian gapped phases for both point gap and line gap. As for point-gapped topological phases, the doubled Hamiltonian in Eq. (1.102) has the same structure as the doubled Hamiltonian in Eq. (1.62) for Floquet gapless phases. Thus, its topological classification is obtained in the same manner as that of Floquet gapless phases. As for line-gapped topological phases with respect to real line gap Re$E = 0$, the non-Hermitian gapped Hamiltonian can be continuously deformed into a Hermitian gapped Hamiltonian without closing the real line gap. Thus, its topological classification is obtained in the same manner as that of ordinary topological insulators and superconductors. The classification of imaginary line-gapped phases is obtained from that of real line-gapped phases by $H \to iH$ [8].

In Sec. 1.2.4, we discussed the classification of non-Hermitian gapless points including exceptional points under k-invariant symmetries. It is obtained from the classification of non-Hermitian gapped phases. Topological classification of d-dimensional gapless phases is equivalent to the topological classification of $(d-1)$-dimensional gapped phases.

[8] We also need to change the symmetry classes by the map $H \to iH$

Chapter 3

Extended Nielsen-Ninomiya theorem for Floquet and non-Hermitian systems

The Nielsen-Ninomiya theorem is a fundamental constraint on the realization of chiral fermions in static lattice systems in high-energy and condensed matter physics. Here we see the extension of the theorem in *dynamical systems*, which include the original Nielsen-Ninomiya theorem in the static limit. In contrast to the original theorem, which is a no-go theorem for a single chiral fermion, the new theorem permits it due to bulk topology intrinsic to dynamical systems. The theorem is based on the duality enabling a unified treatment of periodically driven systems (Floquet systems) and non-Hermitian ones. We also present the extended theorem for gapless fermions protected by symmetries. Finally, as an application of our theorem and duality, we propose a non-Hermitian version of the chiral magnetic effect, and also predict the skin effect accompanying it.

3.1 Introduction

The Nielsen-Ninomiya theorem is an essential constraint in realizing chiral fermions on lattice [1, 2, 89]. It initially was a no-go theorem for the lattice realization of the Standard Model in particle physics, but it has been also applied to condensed matter physics. For instance, the Nielsen-Ninomiya theorem demands that bulk Weyl points in Weyl semimetals always appear in a pair so that the net chiral charge of Weyl points vanishes [90–92]. The Nielsen-Ninomiya theorem strongly restricts possible bulk low energy modes in topological materials [37, 93–99].

However, recent studies have declared that the Nielsen-Ninomiya theorem does not hold when considering topological states in dynamical systems [22, 27–31, 33, 40, 42, 51, 52, 63–65, 67, 79, 84, 85, 87, 88, 100–136]: Periodically driven systems (Floquet systems) may support unpaired chiral fermions both in one-[34, 39, 137–139] and three-dimensions[3, 4]. Furthermore, non-Hermitian systems, which are effectively described by non-Hermitian Hamiltonians, also retain unpaired chiral fermions after the long-time dynamics [5]. These examples suggest a reformulation of the Nielsen-Ninomiya theorem in dynamical systems.

In this Letter, we see the extension of the Nielsen-Ninomiya theorem in dynamical systems, which particularly includes the original one in the static limit. A key of our extension is a duality between Floquet systems and non-Hermitian ones. A one-cycle time evolution operator U_F generally describes stroboscopic dynamics in Floquet systems. By identifying iU_F as a non-Hermitian Hamiltonian H, we can treat a Floquet system and a non-Hermitian one in a unified manner. Another key concept is multiple gap structures intrinsic to non-Hermitian systems. The complex energy spectrum of non-Hermitian systems may introduce two different gap structures: point gaps and line gaps [68, 77]. A non-Hermitian Hamiltonian can be gapped in the sense of point gap even if it supports gapless fermions in the sense of the line gap. Because the point gap enables a novel bulk topological invariant, we expect that bulk chiral (so gapless) fermions in dynamical systems may coexist with nontrivial bulk topology; this is similar to the bulk-boundary correspondence, where boundary gapless states coexist with nontrivial bulk topology. This situation never happens in conventional static systems and leads us to reformulate the Nielsen-Ninomiya theorem.

The extended Nielsen-Ninomiya theorem provides an exact relation between the total chiral charge of gapless fermions and the bulk topological invariant. This theorem implies that if the bulk topological invariant is nonzero, so is the net chiral charge, and thus the system realizes unpaired chiral fermions. The extended theorem also applies to systems under symmetries. Symmetry enriches gapless fermions, giving them a topological charge other than chirality. In this case, the bulk topological invariant equals the net topological charge from our theorem.

As an application of our theorem, we propose a non-Hermitian version of the chiral magnetic effect (CME). The CME is an electric current generation parallel to an applied magnetic field in the existence of unpaired Weyl fermions in 3D [7]. While the chiral magnetic effect caNielsen-Ninomiyaot occur in static systems because of the Nielsen-Ninomiya theorem [95], the extended theorem allows it in dynamical systems. Floquet systems can exhibit the CME [3, 4], and thus our duality relation suggests that so do non-Hermitian systems. We see that a wave packet in a non-Hermitian Weyl semimetal moves in the direction of an applied magnetic field, manifesting the CME. This is because the magnetic field changed the effectively single Weyl fermion into 1D right-going chiral mode, which is a kind of dimension reduction. Furthermore, the extended theorem implies a nonzero energy winding number of the non-Hermitian Weyl semimetals under the magnetic field. This result predicts a new type of CME—the chiral magnetic skin effect.

We assume without loss of generality that the Fermi energy E_F, *i.e.* the reference energy of a gap, is zero unless otherwise mentioned. we can recover E_F by replacing the Hamiltonian $H(\boldsymbol{k})$ with $H(\boldsymbol{k}) - E_F$ if necessary.

3.2 Examples

3.2.1 1D chiral fermions in dynamical systems

Let us start with a simple 1D non-Hermitian system hosting a chiral mode:

$$H(k) = \sin k + i \cos k, \tag{3.1}$$

where k is the crystal momentum and $H(k)$ is periodic in k [5]. The energy $E(k)$ of the system is $H(k)$ itself, and the group velocity is $v(k) = \mathrm{Re}[\partial E(k)/\partial k]$. At the Fermi energy $\mathrm{Re}E(k) = 0$, there are two gapless modes with $k = 0, \pi$: A right-going mode $(v(k) > 0)$ with $k = 0$ and a left-going mode $(v(k) < 0)$ with $k = \pi$. While the right-going mode has a positive $\mathrm{Im}E(k)$, the left-going mode has a negative one; thus, the left-going mode decays, and only the right-going mode is amplified and survives after a long-time dynamics. Therefore, the system effectively realizes a single chiral fermion, *i.e.* a right-going chiral mode.

We next consider a simple 1D Floquet model with a chiral mode described by a one-cycle unitary operator [4],

$$U_F(k) = e^{-ik}. \tag{3.2}$$

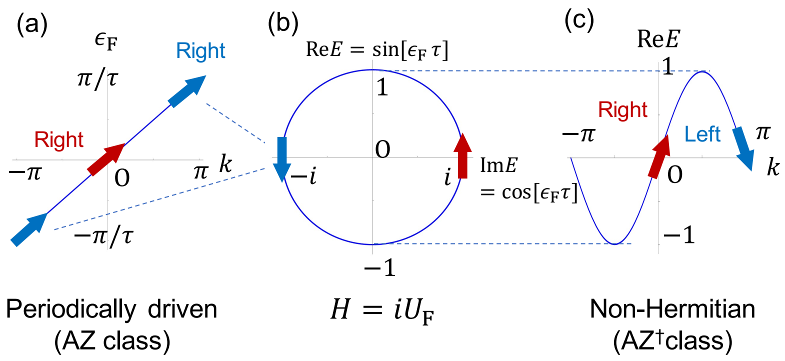

FIGURE 3.1: Duality between a Floquet system and a non-Hermitian one. We illustrate the 1D case here. w_1 is the energy winding number in the complex energy plane in (b). Theorem 1' is evident in the relation between (a) and (b). The duality holds in any dimensions and symmetry classes.

The Floqet Hamiltonian $H_F(k)$ defined by $e^{-iH_F(k)\tau} = U_F(k)$ with a driving period τ describes the stroboscopic time-evolution of the system, $|t+\tau\rangle = U_F(t)|t\rangle = e^{-iH_F(k)\tau}|t\rangle$ as an effective Hamiltonian. The eigenvalue of $H_F(k)$, called the quasi-energy, is $\epsilon_F(k) = k/\tau$ up to an integer multiple of $2\pi/\tau$. Because the group velocity $v_F(k) = \partial\epsilon_F(k)/\partial k$ is positive, the system has a right-going chiral mode.

These chiral modes have a common topological origin. The equation

$$H(k) = iU_F(k), \tag{3.3}$$

relates the above models, then the 1D spectral winding number

$$w_1 = -\int_0^{2\pi} \frac{dk}{2\pi i} \mathrm{tr}[H^{-1}(k)\partial_k H(k)]. \tag{3.4}$$

gives $w_1 = 1$ for both models. (The trace is trivial in these cases.) For the non-Hermitian model in Eq. (3.1), the non-zero spectral winding number results in the so-called non-Hermitian skin effect [64]: For $w_1 > 0$, all bulk states localize to the right end [83, 140]. This effect can be inferred from the unpaired right-going chiral mode because the unidirectional movement forces all the bulk states to accumulate to the right boundary. For the Floquet model in Eq. (3.2), on the other hand, the non-zero spectral winding number implies a non-zero average of the group velocity,

$$w_1 = -\int_0^{2\pi} \frac{dk}{2\pi i} \partial_k \ln \det H(k) = \int_0^{2\pi} \frac{dk}{2\pi} v_F(k)\tau, \tag{3.5}$$

which also indicates a right-going chiral mode.

The above examples suggest a general relation between the spectral winding number and the chirality $\mathrm{sgn}\, v_F(k)$ of gapless modes. For 1D non-Hermitian systems, the exact link is formulated as follows [1]:

[1] See Sec.3.5, which includes Refs. [141–143].

Theorem 1: Let $H(k)$ be a 1D non-Hermitian Hamiltonian and $E_p(k)$ be the complex eigenenergy of a band p. Then, we have

$$w_1 = \sum_{\mathrm{Im}E_p(k_{p\alpha})>0} \mathrm{sgn}\, v_{p\alpha} = -\sum_{\mathrm{Im}E_p(k_{p\alpha})<0} \mathrm{sgn}\, v_{p\alpha}, \tag{3.6}$$

where $k_{p\alpha}$ is the α-th Fermi point of band p defined by $\mathrm{Re}E_p(k_{p\alpha}) = 0$, and $v_{p\alpha} = \mathrm{Re}(\partial E_p(k)/\partial k)_{k=k_{p\alpha}}$ is the group velocity at $k_{p\alpha}$. The summation in Eq. (3.6) is over all p and α.

For a Hermitian Hamiltonian $H(k)$, the above theorem reproduces the Nielsen-Ninomiya theorem. The spectral winding number w_1 is zero for any Hermitian Hamiltonian, and by adding a small imaginary term $i\eta$ to $H(k)$, all the Fermi points can have a positive imaginary part of the energy. Thus, from Eq. (3.6), we have $\sum_{k_{p\alpha}} \mathrm{sgn}\, v_{p\alpha} = 0$, which is the Nielsen-Ninomiya theorem in 1D [1].

Using the relation in Eq. (3.3), we can also derive a counterpart theorem for 1D Floquet systems: Equation (3.3) maps the quasi-energy $\epsilon_p(k)$ of $U_F(k)$ to the complex energy $E_p(k)$ of $H(k)$, $E_p(k) = \sin[\epsilon_p(k)\tau] + i\cos[\epsilon_p(k)\tau]$. Thus, a Fermi point defined by $\epsilon_p(k) = 0$ (π/τ) gives a Fermi point of $E_p(k)$ with a positive (negative) $\mathrm{Im}E_p(k)$. Comparing the group velocities at the Fermi points, we obtain the theorem:

Theorem 1': Let $H_F(k)$ be a 1D Floquet Hamiltonian and $\epsilon_p(k)$ be the quasi-energy of band p. Then, gapless modes of the quasi energy obey

$$w_1 = \sum_{\epsilon_p(k_{p\alpha})=\mu} \mathrm{sgn}\, v_{p\alpha}, \tag{3.7}$$

where $k_{p\alpha}$ is the Fermi point of band p defined by $\epsilon(k_{p\alpha}) = \mu$, and $v_{p\alpha} = (\partial\epsilon_p(k)/\partial k)_{k=k_{p\alpha}}$ is the group velocity at $k_{p\alpha}$ [2].

Here we have shifted the origin of the quasi-energy by $U_F \to e^{i\mu\tau}U_F$ and omitted the term corresponding to the last term in Eq. (3.6) since it is just a particular case of Eq. (3.7).

3.2.2 Non-Hermitian Weyl semimetals

Weyl fermions are 3D massless (or gapless) fermions characterized by a chirality. They are realized as band-crossing points (Weyl points) and behave like magnetic monopoles in the momentum space, of which the magnetic charge provides the chirality charge. In non-Hermitian systems, they have finite lifetimes if the imaginary part of the energies is negative. For Weyl fermions in non-Hermitian systems, we have the following theorem [3]

Theorem 2: Let $H(\boldsymbol{k})$ be a 3D non-Hermitian Hamiltonian and $E_p(\boldsymbol{k})$ be the complex eigenenergy of a band p. Then, gapless modes in the complex energy spectrum obey

$$w_3 = \sum_{\mathrm{Im}E_p(S_{p\alpha})>0} \mathrm{Ch}_{p\alpha} = -\sum_{\mathrm{Im}E_p(S_{p\alpha})<0} \mathrm{Ch}_{p\alpha}. \tag{3.8}$$

Here w_3 is the 3D winding number,

$$w_3 = -\frac{1}{24\pi^2}\int_{\mathrm{BZ}} \mathrm{tr}[H^{-1}dH]^3, \tag{3.9}$$

[2] This result is known as the Brouwer degree in mathematics, and was shown in Ref.[4] in a different manner.

[3] See Sec.3.5.

$S_{p\alpha}$ is the α-th Fermi surface of band p defined by $S_{p\alpha} = \{\boldsymbol{k} \in \mathrm{BZ} | \mathrm{Re}E_p(\boldsymbol{k}) = 0\}$, and $\mathrm{Ch}_{p\alpha}$ is the Chern number on the Fermi surface $S_{p\alpha}$,

$$\mathrm{Ch}_{p\alpha} = \frac{1}{2\pi i} \int_{S_{p\alpha}} (\nabla \times \boldsymbol{A}(\boldsymbol{k})) \cdot \mathrm{d}\boldsymbol{S}, \tag{3.10}$$

where $\boldsymbol{A}(\boldsymbol{k}) = \langle\!\langle \psi_p(\boldsymbol{k}) | \nabla \psi_p(\boldsymbol{k}) \rangle$ with

$$H(\boldsymbol{k})|\psi_p(\boldsymbol{k})\rangle = E_p(\boldsymbol{k})|\psi_p(\boldsymbol{k})\rangle, \quad H^\dagger(\boldsymbol{k})|\psi_p(\boldsymbol{k})\rangle\!\rangle = E_p^*(\boldsymbol{k})|\psi_p(\boldsymbol{k})\rangle\!\rangle, \tag{3.11}$$

and the orientation of $S_{p\alpha}$ is along the direction of the Fermi velocity $\mathrm{Re}(\partial E_p(\boldsymbol{k})/\partial \boldsymbol{k})_{\boldsymbol{k}\in S_{p\alpha}}$. In a sense, $\mathrm{Ch}_{p\alpha}$ counts the total chirality of Weyl points inside $S_{p\alpha}$.

Theorem 2 reproduces the original Nielsen-Ninomiya theorem again when $H(\boldsymbol{k})$ is Hermitian: By adding a tiny positive imaginary term to $H(k)$, we immediately have $w_3 = 0$ and thus $\sum_{p\alpha} \mathrm{Ch}_{p\alpha} = 0$, which is one of the variants of the Nielsen-Ninomiya theorem in 3D [4]. Indeed, this equation prohibits a single Weyl point in Hermitian systems: If an unpaired Weyl point was to exist, we would have a Fermi surface sphere surrounding it by choosing the Fermi energy near the Weyl point. This configuration would give a nonzero $\sum_{p\alpha} \mathrm{Ch}_{p\alpha}$, which contradicts the variant of the original Nielsen-Ninomiya theorem $\sum_{p\alpha} \mathrm{Ch}_{p\alpha} = 0$.

3.3 General theory

3.3.1 Duality

The relation in Eq. (3.3), which enables us a unified treatment of a Floquet system and a non-Hermitian one, is not accidental. This duality relation holds in arbitrary dimensions and symmetry classes. Evidently, we can immediately identify any one-cycle time evolution operator $U_F(\boldsymbol{k})$ with a non-Hermitian Hamiltonian $H(\boldsymbol{k})$ by

$$H(\boldsymbol{k}) = iU_F(\boldsymbol{k}). \tag{3.12}$$

However, the opposite is also true for a class of non-Hermitian systems. Let us consider a non-Hermitian Hamiltonian $H(\boldsymbol{k})$ that has a point gap, i.e., $\mathrm{det}H(\boldsymbol{k}) \neq 0$. Then, we can regard any point-gapped non-Hermitian Hamiltonian as a one-cycle time evolution unitary operator because we can smoothly deform a point-gapped $H(\boldsymbol{k})$ into a unitary matrix without closing the point gap [68, 77].

The duality relation in Eq. (3.12) exposes common properties of Floquet systems and non-Hermitian ones: In terms of the Floquet Hamiltonian $H_F(\boldsymbol{k}) = (i/\tau)\ln U_F(\boldsymbol{k})$, the above relation reads

$$H(\boldsymbol{k}) = \sin[H_F(\boldsymbol{k})\tau] + i\cos[H_F(\boldsymbol{k})\tau]. \tag{3.13}$$

Thus, a gapless state of the form $H_F(\boldsymbol{k}) \sim \boldsymbol{k}\cdot\boldsymbol{\Gamma}$ results in a gapless state in $H(\boldsymbol{k}) \sim \boldsymbol{k}\cdot\boldsymbol{\Gamma} + i$ for $O(k^2)$, and vice versa. ($\boldsymbol{\Gamma}$ are typically Gamma matrices $\{\Gamma_i, \Gamma_j\} = 2\delta_{i,j}$.) Furthermore, the origin of topological invariants in these systems are the same. The topological invariant in these

[4] See Sec.3.7. This form of Nielsen-Ninomiya theorem is closely related to the bulk-boundary correspondence of the 4D Chern insulator. The general form of the net topological charge of gapless boundary states is given in the same form

systems is given by that of the doubled "Hermitian" Hamiltonian [3, 68, 77],

$$\mathcal{H}(\boldsymbol{k}) = \begin{pmatrix} 0 & H(\boldsymbol{k}) \\ H^{\dagger}(\boldsymbol{k}) & 0 \end{pmatrix}. \tag{3.14}$$

From Eq. (3.12), $\mathcal{H}(\boldsymbol{k})$ satisfies $\mathcal{H}^2(\boldsymbol{k}) = 1$ and thus has eigenvalues ± 1. Therefore, $\mathcal{H}(\boldsymbol{k})$ defines insulators, giving well-defined topological invariants established in the extensive previous studies of topological insulators and superconductors.

Note that the above identification links a Floquet system and a non-Hermitian one in corresponding symmetry classes. To see this, consider TRS, PHS, and CS for the Floquet Hamiltonian $H_F(\boldsymbol{k})$, given by

$$TH_F(\boldsymbol{k})T^{-1} = H_F(-\boldsymbol{k}), \tag{3.15}$$

$$CH_F(\boldsymbol{k})C^{-1} = -H_F(-\boldsymbol{k}), \tag{3.16}$$

$$\Gamma H_F(\boldsymbol{k})\Gamma^{-1} = -H_F(\boldsymbol{k}) \tag{3.17}$$

Here T and C are anti-unitary operators with $T^2 = \pm 1$, $C^2 = \pm 1$, and Γ is a unitary operator with $\Gamma^2 = 1$. The presence or absence of these symmetries define Altland-Zirnbauer (AZ) ten symmetry classes [144] of Floquet systems. [5] The relation in Eq. (3.12) maps these symmetries as follows:

$$TH^{\dagger}(\boldsymbol{k})T^{-1} = H(-\boldsymbol{k}), \tag{3.18}$$

$$CH(\boldsymbol{k})C^{-1} = -H(-\boldsymbol{k}), \tag{3.19}$$

$$\Gamma H^{\dagger}(\boldsymbol{k})\Gamma^{-1} = -H(\boldsymbol{k}). \tag{3.20}$$

The latter symmetries define another ten symmetry classes, called AZ† classes [77] of non-Hermitain systems.

3.3.2 Extended Nielsen-Ninomiya theorem

Symmetry enriched gapless fermions characterized with topological charges other than chiralities. We now see the extended Nielsen-Ninomiya theorem, including such symmetry-protected Dirac fermions.

We first consider non-Hermitian systems. Depending on symmetry classes, two different situations may happen: (i) gapless fermions in classes A, AI†, AII† appear as band crossing points at general positions in the complex energy plane, and (ii) those in other AZ† classes appear exactly on the $\mathrm{Re}E = 0$ axis due to PHS and/or CS. To define the topological charge of gapless fermions, we use the Fermi surface at $\mathrm{Re}E = 0$ in the former case (i), and a small sphere encircling a gapless fermion in the latter case (ii) Then, we have the following theorem:

Theorem 3: Let $H(\boldsymbol{k})$ be a point-gapped non-Hermitian Hamiltonian in an AZ† symmetry class. Then, bulk gapless fermions of $H(\boldsymbol{k})$ obeys

$$n = \sum_{\mathrm{Im}E_\alpha > 0} \nu_\alpha = -\sum_{\mathrm{Im}E_\alpha < 0} \nu_\alpha, \tag{3.21}$$

[5] The AZ symmetries for Floquet systems are originally given in the form of time-periodic Hamitlonian $H(\boldsymbol{k}, t)$, and the symmetries for $H(\boldsymbol{k}, t)$ lead to the symmetries for $H_F(\boldsymbol{k})$

As we mentioned above, the point gap topological invariant n originates from the conventional topological invariant of the topological insulator described by the Hermitian Hamiltonian in Eq. (3.14). The explicit form of n is summarized in Ref. [77]. In case (i) in the above, α labels the Fermi surfaces at $\mathrm{Re}E = 0$, ν_α is the net topological charge of gapless fermions inside the α-th Fermi surface, and E_α is the complex energy of the Fermi surface. In case (ii), α labels gapless fermions, ν_α is the topological charge of the α-th gapless fermion defined on the small sphere, and E_α is the complex energy of the gapless fermion. We remark that we can classify all the gapless states into the case of $\mathrm{Im}E_\alpha > 0$ or the case of $\mathrm{Im}E_\alpha < 0$ because we are considering point-gapped Hamiltonians, i.e., $E_\alpha \neq 0$ for any α in the whole Brillouin zone.

Applying the duality relation in Eq. (3.12) for this non-Hermitian formula, we also have a theorem for gapless fermions in Floquet systems. We find that (i') gapless fermions in classes A, AI, AII appear as band crossing points of arbitrary energies in the quasi-energy spectra, and (ii') those in other AZ classes appear with $\epsilon = 0$ or π/τ because of PHS and CS. Then, the theorem for Floquet systems is as follows. We provide the proof of Theorem 3 [6].

Theorem 3': For gapless fermions in a Floquet system in an AZ class, we have

$$n = \sum_{\epsilon_\alpha=\mu} \nu_\alpha^\mu, \qquad \text{in case (i')}, \tag{3.22}$$

$$n = \sum_{\epsilon_\alpha=0} \nu_\alpha^0 = -(-1)^d \sum_{\epsilon_\alpha=\pi/\tau} \nu_\alpha^\pi, \qquad \text{in case (ii')}. \tag{3.23}$$

Here n is the topological invariant of $iU_F(\boldsymbol{k})$ originating from $\mathcal{H}(\boldsymbol{k})$ in Eq. (3.14), and d indicates the dimensions of the system. In case (i'), α labels the Fermi surfaces defined by $\epsilon_\alpha = \mu$, and ν_α^μ is the topological charge of gapless fermions inside the α-th Fermi surface. In case (ii), α labels gapless fermions at $\epsilon = 0, \pi/\tau$, and $\nu_\alpha^{0,\pi}$ is the topological charge of the gapless fermion of the quasi-energy $\epsilon_\alpha = 0, \pi$ [7] .

We note that Eq. (3.23) shows a dependence on the parity of the dimensions d: A gapless fermion at π/τ, $H_F(\boldsymbol{k}) = \boldsymbol{k}\cdot\boldsymbol{\Gamma} + \pi/\tau$, in a Floquet system corresponds to $H(\boldsymbol{k}) = -\boldsymbol{k}\cdot\boldsymbol{\Gamma} - i$, in a non-Hermitian system from Eq. (3.13). Since these Hamiltonians have an opposite topological charge in odd dimensions, we have the additional sign $(-1)^d$. [8] Equation (3.7) is the 1D case of Eq. (3.22) in class A (no symmetry). We have also confirmed Eq. (3.23) using a 2D Floquet model with chiral symmetry (class AIII) [9].

3.4 Gapless structures in non-Hermitian systems

A non-Hermitian Hamiltonian $H(\boldsymbol{k})$ can exhibit an exotic gapless structure that was not seen in Hermitian Hamiltonians. The general gapless structure is composed of two parts: an open region where the real part of the energy gap vanishes, and its boundary where the full complex energy gap vanishes and $H(\boldsymbol{k})$ becomes defective. The open region and the boundary are called "bulk Fermi arc" and "exceptional point" (or their higher dimensional generalization), respectively. (See Fig.3.2.) When $H(\boldsymbol{k})$ is deformed to be diagonalizable, the bulk Fermi arc shrinks, the

[6] See Secs. **??** and 3.5.

[7] See Sec.3.6.

[8] If we apply continuous two-dimensional rotations $(-k_j, -k_{j+1}) \to (k_j, k_{j+1})$ repeatedly, we obtain the topological equivalence $-\boldsymbol{k}\cdot\boldsymbol{\Gamma} \sim \boldsymbol{k}\cdot\boldsymbol{\Gamma}$ for even dimensions. However, we cannot continuously rotate as $-\boldsymbol{k}\cdot\boldsymbol{\Gamma} \sim \boldsymbol{k}\cdot\boldsymbol{\Gamma}$ for odd dimensions, indicating different topological charges between $-\boldsymbol{k}\cdot\boldsymbol{\Gamma}$ and $\boldsymbol{k}\cdot\boldsymbol{\Gamma}$.

[9] See Sec.3.8.

TABLE 3.1: Extended Nielsen-Ninomiya theorem for point gapped Hamiltonians in AZ† symmetry classes for the spatial dimension $d \leq 3$. In the first three AZ† classes, gapless regions are located at an arbitrary position, and in the other seven ones, symmetry-protected gapless regions are located on the $\mathrm{Re}E = 0$ axis. The section numbers for the proof of Theorem are shown for each topological invariant.

AZ† class	$d = 1$	$d = 2$	$d = 3$
A	$\mathbb{Z}$ [Sec.3.5.1]	0	$\mathbb{Z}$ [Sec.3.5.1]
AI†	0	0	$2\mathbb{Z}$ [Sec.3.5.1]
AII†	$\mathbb{Z}_2$ [3.5.1]	$\mathbb{Z}_2$ [Sec.3.5.1]	$\mathbb{Z}$ [Sec.3.5.1]
AIII	0	$\mathbb{Z}$ [Sec.3.5.2]	0
BDI†	0	0	0
D†	$\mathbb{Z}$ [Sec.3.5.2]	0	0
DIII†	$\mathbb{Z}_2$ [Sec.3.5.2]	$\mathbb{Z}$ [Sec.3.5.2]	0
CII†	0	$\mathbb{Z}_2$ [Sec.3.5.2]	$\mathbb{Z}_2$ [Sec.3.5.2]
C†	$2\mathbb{Z}$ [Sec.3.5.2]	0	$\mathbb{Z}_2$ [Sec.3.5.2]
CI†	0	$2\mathbb{Z}$ [Sec.3.5.2]	0

exceptional points are (pair-)annihilated, and the gapless structure reduces to a conventional Dirac or Weyl point. Thus, the topological charge of the Dirac point guarantees the robustness of the general gapless structure.

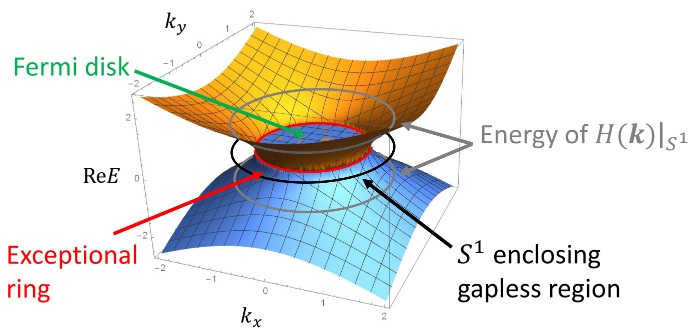

FIGURE 3.2: A general gapless structure in a 2D non-Hermitian system. The gapless structure hosts an open Fermi disk and an exceptional ring, which are the two-dimensional generalizations of bulk Fermi arc and exceptional point, respectively. The gap is open for the real part of the energy spectrum on S^1 enclosing the gapless region.

3.5 Proof of extended Nielsen-Ninomiya theorem

In this section, we prove Theorem 3 in the main text.

Theorem 3 Let $H(\boldsymbol{k})$ be a Hamiltonian with a point gap ($\det(H-E_F)\neq 0$) in an AZ† symmetry class. Then, gapless structures in $H(\boldsymbol{k})$ obey the following relation,

$$n=\sum_{\mathrm{Im}E_\alpha>0}\nu_\alpha=-\sum_{\mathrm{Im}E_\alpha<0}\nu_\alpha, \tag{3.24}$$

where n is the point-gapped topological invariant. In case (i), ν_α is the topological charge on the α-th Fermi surface, and E_α is the complex energy of the α-th Fermi surface. In case (ii), ν_α is the topological charge of the α-th gapless structure, and E_α is the complex energy of the α-th gapless structures.

For class A in 1D and 3D, the above theorem gives Theorem 1 and Theorem 2 in the main text, respectively.

3.5.1 Case (i)

In case (i) (classes A, AI† and AII†), we prove Theorem 3 by directly evaluating n.

Class A

First, we consider a class A non-Hermitian Hamiltonian $H(\boldsymbol{k})$. The point gap topological invariant n in $d=2q+1$ dimensions ($q=0,1,\dots$) is given by the winding number w_{2q+1},

$$n=w_{2q+1}=\left(\frac{i}{2\pi}\right)^{q+1}\frac{q!}{(2q+1)!}\int_{\mathrm{BZ}}\mathrm{tr}[H^{-1}\mathrm{d}H]^{2q+1}. \tag{3.25}$$

To prove Theorem 3 in class A, we use the technique developed in Refs. [141–143]. We first deform the Hamiltonian $H(\boldsymbol{k})$ into a unitary matrix [68, 77]. As $H(\boldsymbol{k})$ remains point-gapped during this deformation, this procedure does not change the point gap topological invariant n. After this deformation, $H(\boldsymbol{k})$ is diagonalizable and can be written in the form of

$$H(\boldsymbol{k})=\sum_p E_p(\boldsymbol{k})|u_p(\boldsymbol{k})\rangle\langle u_p(\boldsymbol{k})|,\quad |E_p(\boldsymbol{k})|=1, \tag{3.26}$$

where $|u_p(\boldsymbol{k})\rangle$ is an eigenstate of the unitary $H(\boldsymbol{k})$ with an corresponding eigenvalue $E_p(\boldsymbol{k})$. We furthermore deform $H(\boldsymbol{k})$ as follows,

$$H(\boldsymbol{k})=\sum_p e^{i\theta_p(\boldsymbol{k})}|u_p(\boldsymbol{k})\rangle\langle u_p(\boldsymbol{k})|, \tag{3.27}$$

with

$$e^{i\theta_p(\boldsymbol{k})}=\frac{\mathrm{Re}E_p(\boldsymbol{k})+\lambda i\mathrm{Im}E_p(\boldsymbol{k})}{|\mathrm{Re}E_p(\boldsymbol{k})+\lambda i\mathrm{Im}E_p(\boldsymbol{k})|} \tag{3.28}$$

where $0<\lambda\leq 1$ is a deformation parameter. When $\lambda=1$, $H(\boldsymbol{k})$ returns to Eq. (3.26). We note that this Hamiltonian is also invertible and has the same value of n as Eq. (3.26). Now take the limit $\lambda\to 0$, where λ is infinitesimally tiny but nonzero. In this limit, the eigenvalue $e^{i\theta_p(\boldsymbol{k})}$ takes a constant value $e^{i\theta_p(\boldsymbol{k})}=\pm 1$ except for the Fermi surfaces $S_{p\alpha}=\{\boldsymbol{k}\in S_{p\alpha}|\mathrm{Re}E_p(\boldsymbol{k})=0\}$.

The Fermi surface generally consists of a set of connected parts, and α labels each connected part of the Fermi surface. Near the Fermi surfaces, $\theta_p(\boldsymbol{k})$ satisfies

$$\nabla_{\boldsymbol{k}}\theta_p(\boldsymbol{k}) = -\pi\mathrm{sgn}[\mathrm{Im}E_p(\boldsymbol{k})]\delta(\mathrm{ReE}_p(\boldsymbol{k}))\nabla_{\boldsymbol{k}}[\mathrm{Re}E_p(\boldsymbol{k})], \tag{3.29}$$

from which the branch of $\theta_p(\boldsymbol{k})$ is determined uniquely. $\mathrm{Im}E_p(\boldsymbol{k})$ takes the same sign on each connected component $S_{p\alpha}$ since $|E_p(\boldsymbol{k})| = 1$, and thus $\mathrm{sgn}[\mathrm{Im}E_p(\boldsymbol{k}))]$ in Eq. (3.29) is well-defined. Substituting Eq. (3.27) with $\lambda \to 0$, we obtain Theorem 3 for each dimensions.

For instance, let us consider the $d = 1$ ($q = 0$) case, where n is especially called energy winding number

$$\begin{aligned} w_1 &= -\frac{1}{2\pi i}\int_{-\pi}^{\pi} dk\mathrm{tr}[H^{-1}(k)\partial_k H(k)] \\ &= -\frac{1}{2\pi i}\int_{-\pi}^{\pi} dk\partial_k \ln\det H(k). \end{aligned} \tag{3.30}$$

Utilizing Eq. (3.27), we obtain

$$\begin{aligned} w_1 &= -\frac{1}{2\pi}\int_{-\pi}^{\pi} dk\sum_p \partial_k\theta_p(k) \\ &= \frac{1}{2}\sum_{p\alpha}\int_{-\pi}^{\pi} dk\,\mathrm{sgn}[\mathrm{Im}E_p(k_{p\alpha})]\delta(k-k_{p\alpha})\mathrm{sgn}[\partial_k[\mathrm{Re}E_p(k_{p\alpha})]] \\ &= \frac{1}{2}\sum_{p\alpha}\mathrm{sgn}[\mathrm{Im}E_p(k_{p\alpha})]\mathrm{sgn}[\partial_k[\mathrm{Re}E_p(k_{p\alpha})]], \end{aligned} \tag{3.31}$$

where $k_{p\alpha}$ is the Fermi point defined by $\mathrm{Re}E_p(k_{p\alpha}) = 0$. Now we use the original Nielsen-Ninomiya theorem since the real part of $H(\boldsymbol{k})$

$$\mathrm{Re}H(\boldsymbol{k}) = \sum_p \mathrm{Re}E_p(\boldsymbol{k})|u_p(\boldsymbol{k})\rangle\langle u_p(\boldsymbol{k})| \tag{3.32}$$

can be seen as a Hermitian Hamiltonian. For $d = 1$, the Nielsen-Ninomiya theorem yields the relation

$$\sum_{p\alpha}\mathrm{sgn}[\partial_k[\mathrm{Re}E_p(k_{p\alpha})]] = 0, \tag{3.33}$$

which is equivalent to

$$\sum_{\mathrm{Im}E_p(k_{p\alpha})>0}\mathrm{sgn}[\partial_k[\mathrm{Re}E_p(k_{p\alpha})]] = -\sum_{\mathrm{Im}E_p(k_{n\alpha})<0}\mathrm{sgn}[\partial_k[\mathrm{Re}E_p(k_{p\alpha})]]. \tag{3.34}$$

Therefore, from Eq. (3.31), we obtain Theorem 3 for $d = 1$ (Theorem 1 in the main text),

$$w_1 = \sum_{\mathrm{Im}E_p(k_{p\alpha})>0}\mathrm{sgn}[\partial_k[\mathrm{Re}E_p(k_{p\alpha})]] = -\sum_{\mathrm{Im}E_p(k_{p\alpha})<0}\mathrm{sgn}[\partial_k[\mathrm{Re}E_p(k_{p\alpha})]]. \tag{3.35}$$

In a similar manner, we can also derive Theorem 3 for $d = 3$ ($q = 1$). In this case, the point gap topological invariant n is given by the 3D winding number, and we can deform its form through tedious calculations [142] into

$$w_3 = \frac{1}{2}\sum_{p\alpha} \mathrm{sgn}[\mathrm{Im}E_p(S_{p\alpha})]\mathrm{Ch}(S_{p\alpha}), \tag{3.36}$$

where $\mathrm{Ch}(S_{p\alpha})$ is the Chern number on $S_{p\alpha}$ defined by

$$\mathrm{Ch}(S_{p\alpha}) = \frac{1}{2\pi i}\int_{S_{p\alpha}} (\nabla \times \boldsymbol{A}_p)\cdot d\boldsymbol{S}. \tag{3.37}$$

Here $\boldsymbol{A}_p = \langle u_p(\boldsymbol{k})|\nabla u_p(\boldsymbol{k})\rangle$ is the Berry connection of the eigenstate $|u_p\rangle$ for $\mathrm{Re}H(\boldsymbol{k})$,

$$\mathrm{Re}H(\boldsymbol{k})|u_p(\boldsymbol{k})\rangle = \mathrm{Re}E_p(\boldsymbol{k})|u_p(\boldsymbol{k})\rangle, \tag{3.38}$$

and the orientation of $S_{p\alpha}$ is chosen as the direction of the Fermi velocity $\partial_{\boldsymbol{k}}[\mathrm{Re}E_p(\boldsymbol{k})]_{\boldsymbol{k}\in S_{p\alpha}}$. In order to prove Theorem 3 from Eq. (3.36), we again use the original Nielsen-Ninomiya theorem for $\mathrm{Re}H(\boldsymbol{k})$. As we shall argue in Sec. 3.7, we have a variation of Nielsen-Ninomiya theorem as

$$\sum_{p\alpha} \mathrm{Ch}(S_{p\alpha}) = 0, \tag{3.39}$$

which is recast into

$$\sum_{\mathrm{Im}E_p(S_{p\alpha})>0} \mathrm{Ch}(S_{p\alpha}) = -\sum_{\mathrm{Im}E_p(S_{p\alpha})<0} \mathrm{Ch}(S_{p\alpha}). \tag{3.40}$$

Using this relation, we finally obtain Theorem 3 for $d = 3$ (Theorem 2 in the main text),

$$w_3 = \sum_{\mathrm{Im}E_p(S_{p\alpha})>0} \mathrm{Ch}(S_{p\alpha}) = -\sum_{\mathrm{Im}E_p(S_{p\alpha})<0} \mathrm{Ch}(S_{p\alpha}). \tag{3.41}$$

Class AI†

A point gapped Hamiltonian in class AI† has the $2\mathbb{Z}$ index in 3D. (See Table.3.1.) The $2\mathbb{Z}$ topological invariant n is given by the winding number in Eq. (3.25) with $q = 1$, and thus we obtain Theorem 3 in the form of Eq. (3.41) in the same manner to class A in 3D.

Class AII†

A Hamiltonian $H(\boldsymbol{k})$ in class AII† satisfies

$$TH^T(\boldsymbol{k})T^\dagger = H(-\boldsymbol{k}), \tag{3.42}$$

where T is a unitary matrix with $TT^* = -1$. As for point gap topological invariants in class AII†, we have the $\mathbb{Z}_2$ invariants in 1D and 2D, and the $\mathbb{Z}$ invariant in 3D. In 3D, the $\mathbb{Z}$ invariant is given by the winding number in Eq. (3.25) with $q = 1$ again, so Theorem 3 holds in the same manner to class A with $d = 3$. We prove Theorem 3 in 1D and 3D in the following.

First, we see the 1D case. The $\mathbb{Z}_2$ invariant is given by

$$(-1)^n = \mathrm{sgn}\left\{\frac{\mathrm{Pf}[H(\pi)T]}{\mathrm{Pf}[H(0)T]}\exp\left[-\frac{1}{2}\int_{k=0}^{k=\pi} dk\partial_k \mathrm{logdet}[H(k)T]\right]\right\}. \tag{3.43}$$

After the unitarization, $H(k)$ is recast into the form of

$$\begin{aligned} H(k) &= \sum_p e^{i\theta_p(k)}|u_p(k)\rangle\langle u_p(k)| \\ &= U(k)\begin{pmatrix} e^{i\theta_1(k)} & & \\ & e^{i\theta_2(k)} & \\ & & \ddots \end{pmatrix} U^\dagger(k) \end{aligned} \tag{3.44}$$

with a unitary matrix $U(\boldsymbol{k}) = (|u_1(k)\rangle, |u_2(k)\rangle, \cdots)$, so we have

$$\mathrm{det}H(k) = \exp(i\sum_p \theta_p(k)). \tag{3.45}$$

Therefore, Eq. (3.29) leads to

$$\begin{aligned} \int_0^\pi dk\partial_k \mathrm{logdet}[H(k)T] &= \int_0^\pi dk\partial_k \left[i\sum_p \theta_p(k)\right] \\ &= -\pi \sum_{p\alpha} \mathrm{sgn}\left[\partial_k \mathrm{Re}E_p(k_{p\alpha})\, \mathrm{Im}E_p(k_{p\alpha})\right], \end{aligned} \tag{3.46}$$

where $0 < k_{p\alpha} < \pi$ is the α-th Fermi point defined by $\mathrm{Re}E_p(k_{p\alpha}) = 0$, and we implicitly assumed that any Fermi point does not exist just at the time-reversal invariant momentum $k = 0, \pi$ without loss of generality. The exponential factor in Eq. (3.43) is evaluated as

$$\exp\left[-\frac{1}{2}\int_0^\pi dk\partial_k \mathrm{logdet}[H(k)T]\right] = \prod_{n\alpha} i\mathrm{sgn}\left[\partial_k \mathrm{Re}E_p(k_{p\alpha})\right] \prod_{p\alpha} \mathrm{sgn}\left[\mathrm{Im}E_p(k_{p\alpha})\right]. \tag{3.47}$$

It should be noted here that each Fermi point with positive (negative) $\partial_k \mathrm{Re}E_p(k_{p\alpha})$ decreases (increases) the number of the occupied state $N_{\mathrm{occ}}(0)$ ($N_{\mathrm{occ}}(\pi)$) at $k = 0$ ($k = \pi$) by 1, where the occupied state is defined as a state with $\mathrm{Re}E_p(k) < 0$. Thus, the first product of the right-hand side in Eq. (3.47) becomes

$$\prod_{p\alpha} i\mathrm{sgn}\left[\partial_k \mathrm{Re}E_p(k_{p\alpha})\right] = i^{N_{\mathrm{occ}}(0)-N_{\mathrm{occ}}(\pi)} = (-1)^{[N_{\mathrm{occ}}(0)-N_{\mathrm{occ}}(\pi)]/2}, \tag{3.48}$$

thus Eq. (3.47) becomes

$$\exp\left[-\frac{1}{2}\int_0^\pi dk\partial_k \mathrm{logdet}[H(k)T]\right] = (-1)^{[N_{\mathrm{occ}}(0)-N_{\mathrm{occ}}(\pi)]/2} \prod_{p\alpha} \mathrm{sgn}\left[\mathrm{Im}E_p(k_{p\alpha})\right]. \tag{3.49}$$

We note that $N_{\mathrm{occ}}(k)$ ($k = 0, \pi$) is an even number because of the generalized Kramers degeneracy in class AII† [77, 104, 113].

We now evaluate the Paffians in Eq. (3.43) in the following. At the time-reversal invariant momentum $k_0 = 0, \pi$, $\theta_p(k_0)$ becomes either 0 or $\pm\pi$, thus $H(k_0)$ is

$$H(k_0) = U(k_0)\Lambda(k_0)U^\dagger(k_0), \quad (k_0 = 0, \pi) \tag{3.50}$$

with

$$\Lambda(k_0) = \begin{pmatrix} 1_{N_{\mathrm{emp}}(k_0)\times N_{\mathrm{emp}}(k_0)} & \\ & -1_{N_{\mathrm{occ}}(k_0)\times N_{\mathrm{occ}}(k_0)} \end{pmatrix}. \tag{3.51}$$

Therefore, the Pfaffian is rewritten as

$$\begin{aligned} \mathrm{Pf}\left[H(k_0)T\right] &= \mathrm{Pf}\left[U(k_0)\Lambda(k_0)U^\dagger(k_0)T\right] \\ &= \mathrm{Pf}\left[U^\dagger(k_0)U(k_0)\Lambda(k_0)U^\dagger(k_0)TU^*(k_0)\right]/\mathrm{det}U^*(k_0) \\ &= \mathrm{Pf}\left[\Lambda(k_0)U^\dagger(k_0)TU^*(k_0)\right]\mathrm{det}U(k_0), \end{aligned} \tag{3.52}$$

where we used the formula $\mathrm{Pf}[B^TAB] = \mathrm{Pf}[A]\mathrm{det}B$ for an antisymmetric matrix A. Because of TRS† in Eq. (3.42), we have

$$\left[U^\dagger(k_0)TU^*(k_0), \Lambda(k_0)\right] = 0, \tag{3.53}$$

so $U^\dagger(k_0)TU^*(k_0)$ becomes block-diagonal. Hence, the Pfaffian is

$$\begin{aligned} \mathrm{Pf}\left[\Lambda(k_0)U^\dagger(k_0)TU^*(k_0)\right] &= (-1)^{N_{\mathrm{occ}}(k_0)/2}\mathrm{Pf}\left[U^\dagger(k_0)TU^*(k_0)\right] \\ &= (-1)^{N_{\mathrm{occ}}(k_0)/2}\mathrm{Pf}[T]\mathrm{det}U^*(k_0), \end{aligned} \tag{3.54}$$

which implies

$$\mathrm{Pf}\left[H(k_0)T\right] = (-1)^{N_{\mathrm{occ}}(k_0)/2}\mathrm{Pf}[T]. \tag{3.55}$$

Substituting the above result and Eq. (3.49) into the right-hand side of Eq. (3.43), we obtain

$$(-1)^n = \prod_{p\alpha}\mathrm{sgn}[\mathrm{Im}E_p(k_{p\alpha})] = (-1)^{\sum_{\mathrm{Im}E_p(k_{p\alpha})>0}}. \tag{3.56}$$

Because of the Kramers degeneracy at $k = 0, \pi$, the number of the Fermi points between $k = 0$ and $k = \pi$ is even, which implies $(-1)^{\sum_{\mathrm{Im}E_p(k_{p\alpha})>0} + \sum_{\mathrm{Im}E_p(k_{p\alpha})<0}} = 1$. Thus, we have

$$(-1)^n = (-1)^{\sum_{\mathrm{Im}E_p(k_{p\alpha})>0}} = (-1)^{\sum_{\mathrm{Im}E_p(k_{p\alpha})<0}}, \tag{3.57}$$

which gives Eq. (3.24) in Theorem 3 for class AII† in 1D:

$$n = \sum_{\mathrm{Im}E_p(k_{p\alpha})>0} = -\sum_{\mathrm{Im}E_p(k_{p\alpha})>0} \quad (\mathrm{mod}\ 2) \tag{3.58}$$

As we illustrate in Fig. 3.3, each Kramers pair of Fermi points always encloses a gapless Dirac point at time-reversal invariant momentum. The middle and the right-hand side in Eq. (3.58) counts the Dirac points enclosed by the Fermi point.

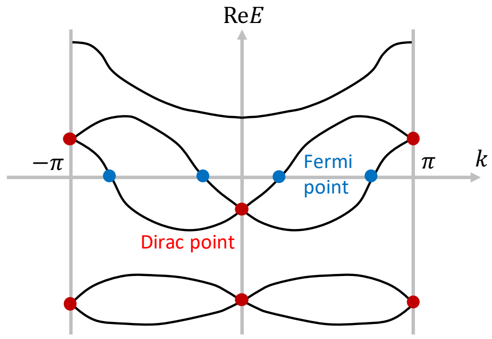

FIGURE 3.3: Typical Dirac and Fermi points in a 1D class AII system. Each Kramers pair of Fermi points encloses a Dirac point at a time-reversal invariant momentum.

Next, we see the 2D case. The $\mathbb{Z}_2$ invariant $(-1)^n$ in 2D is given as the product of the 1D $\mathbb{Z}_2$ invariants,

$$(-1)^n = \mathrm{sgn}\left\{\frac{\mathrm{Pf}[H(\pi,0)T]}{\mathrm{Pf}[H(0,0)T]}\exp\left[-\frac{1}{2}\int_{k_x=0}^{k_x=\pi} dk_x\partial_{k_x}\mathrm{logdet}[H(k_x,0)T]\right]\right\}$$
$$\times\mathrm{sgn}\left\{\frac{\mathrm{Pf}[H(\pi,\pi)T]}{\mathrm{Pf}[H(0,\pi)T]}\exp\left[-\frac{1}{2}\int_{k_x=0}^{k_x=\pi} dk_x\partial_{k_x}\mathrm{logdet}[H(k_x,\pi)T]\right]\right\}. \tag{3.59}$$

Thus, similarly to the 1D case we obtain

$$n = \sum_{\mathrm{Im}E_p(k_{p\alpha},0)>0} + \sum_{\mathrm{Im}E_p(k'_{p\alpha},\pi)>0} = -\left(\sum_{\mathrm{Im}E_p(k_{p\alpha},0)<0} + \sum_{\mathrm{Im}E_p(k'_{p\alpha},\pi)<0}\right) \quad (\mathrm{mod}\ 2), \tag{3.60}$$

where $0 < k_{p\alpha} < \pi$ ($0 < k'_{p\alpha} < \pi$) is the α-th Fermi point of $\mathrm{Re}E_p(k_{p\alpha},0) = 0$ ($\mathrm{Re}E_p(k'_{p\alpha},\pi) = 0$). We note that the Fermi points in the above are the intersection between the Fermi surface $S_{p\alpha}$ defined by $\mathrm{Re}E_p(S_{p\alpha}) = 0$ and the $k_y = 0, \pi$ lines. We also notice that since each Kramers pair of Fermi points enclose a time-reversal invariant momentum, the summation

$$\sum_{\mathrm{Im}E_p(k_{p\alpha},0)>0} + \sum_{\mathrm{Im}E_p(k'_{p\alpha},\pi)>0} \tag{3.61}$$

counts the net number of time-reversal invariant momenta enclosed by the Fermi surfaces with positive $\mathrm{Im}E_p(S_{p\alpha})$. Thus, we have

$$\sum_{\mathrm{Im}E_p(k_{p\alpha},0)>0} + \sum_{\mathrm{Im}E_p(k'_{p\alpha},\pi)>0} = \sum_{\mathrm{Im}E_p(S_{p\alpha})>0} m_{p\alpha}, \tag{3.62}$$

where $m_{p\alpha}$ is the number of time-reversal invariant momenta enclosed by the Fermi surface $S_{p\alpha}$. Consequently, we obtain Eq. (3.24) in Theorem 3 for class AII† in 2D,

$$n = \sum_{\mathrm{Im}E_p(S_{p\alpha})>0} m_{p\alpha} = \sum_{\mathrm{Im}E_p(S_{p\alpha})<0} m_{p\alpha}, \quad (\mathrm{mod}.2). \tag{3.63}$$

Again, since a Fermi surface enclosing a time-reversal invariant momentum also encloses a Dirac point at the time-reversal invariant point, the second and the third terms in Eq. (3.63) count the net number of Dirac points inside the Fermi surfaces.

3.5.2 Case (ii)

We here provide the proof of Theorem 3 in case (ii). The key idea is to use a primitive model that generates all the topological phases. It has been known that by stacking the generator and/or trivial generator via a direct sum and performing a smooth deformation, any point-gapped Hamiltonian can be produced. Therefore, it is enough to prove Eq. (3.24) for the generator. One primitive model with $E_{\mathrm{P}} = 0$ is given as follows [5],

$$H(\boldsymbol{k}) = h(\boldsymbol{k}) + i\gamma(\boldsymbol{k}), \tag{3.64}$$

with

$$h(\boldsymbol{k}) = \sum_{j=1}^{d} \sin k_j \Gamma_j, \quad \gamma(\boldsymbol{k}) = m + \sum_{j=1}^{d} \cos k_j. \tag{3.65}$$

Here we used the gamma matrix Γ_i, which is Hermitian and obeys $\{\Gamma_i, \Gamma_j\} = 2\delta_{ij}$. CS and PHS† imply anti-commutation relations $\{\Gamma, \Gamma_i\} = 0$ and $C\Gamma_i^* + \Gamma_i C = 0$, respectively. We also assume that $-d < m < -d+2$. We need to choose the gamma matrices compatible with the symmetry classes we want to study. Note that $i\gamma(\boldsymbol{k})$ term is consistent with any symmetry of AZ† classes. The energy spectrum of this model is given as

$$E(\boldsymbol{k}) = \pm\sqrt{\sum_{j=1}^{d} \sin^2 k_j} + i(m + \sum_{j=1}^{d} \cos k_j). \tag{3.66}$$

At any time-reversal invariant momentum, this model exhibits a gapless point with real line gap in the form of the Dirac/Weyl point. We note that all the Dirac/Weyl points are forced to appear on the $\mathrm{Re}E = 0$ axis because of CS and/or PHS† in case (ii).

Now we prove Theorem 3 for this generator model. When we choose $-d < m < -d+2$, only a single Dirac/Weyl point with $\boldsymbol{k} = \boldsymbol{0}$ is $\mathrm{Im}E(\boldsymbol{k}) > 0$ in the form of

$$H(\boldsymbol{k}) = \sum_{j=1}^{d} k_j \Gamma_j + i(m+d) \tag{3.67}$$

near $\boldsymbol{k} = 0$, so its topological charge becomes $\nu = 1$. [10] All other $2^d - 1$ Dirac/Weyl points are $\mathrm{Im}E(\boldsymbol{k}) < 0$, and their total topological charge are $\nu = -1$. [11] Therefore, we obtain the second equality of Eq. (3.24). We next see that $n = 1$ in the following. The topological invariant n is given as the topological invariant of the following Hermitian Hamiltonian,

$$\widetilde{H}(\boldsymbol{k}) = \begin{pmatrix} & H(\boldsymbol{k}) \\ H^\dagger(\boldsymbol{k}) & \end{pmatrix} = \tau_x \otimes h(\boldsymbol{k}) - \tau_y \otimes \gamma(\boldsymbol{k}). \tag{3.68}$$

[10] We note that the topological charge of gapless points are always defined to become 1 for $H(\boldsymbol{k}) = \sum_{j=1}^{d} k_j \Gamma_j$.

[11] This is compatible with the original Nielsen-Ninomiya theorem for $ReH(\boldsymbol{k})$.

If we consider $m \to -\infty$ limit, the Hermitain Hamiltonian $\widetilde{H}(\boldsymbol{k})$ becomes atomic insulator with trivial topological invariant $n = 0$. For $m < -d$, $\gamma(\boldsymbol{k})$ is always negative and thus $\widetilde{H}(\boldsymbol{k})$ is always gapped in the whole region of $\boldsymbol{k}$, implying $n = 0$. Then, as one increases m, the point gap closes (i.e. $\mathrm{det}H(\boldsymbol{k}) = 0$) at $m = -d$ in the form of gapless Dirac Hamiltonian, which changes the topological invariant of $\widetilde{H}(\boldsymbol{k})$ by 1. As a result, for $-d < m < -d + 2$, we have $n = 1$. Therefore, the first equality of Eq. (3.24) also holds for the generator model.

We also emphasize that this proof is also a proof of case (i) if we include TRS†. [12]

3.6 Extended Nielsen-Ninomiya theorem in Floquet systems

In this section, we prove the extended Nielsen-Ninomiya Theorem for Floquet systems from the non-Hermitian counterparts by using the duality relation

$$H(\boldsymbol{k}) = iU_F(\boldsymbol{k}). \tag{3.69}$$

Theorem 3' Let $H_F(\boldsymbol{k})$ be a d-dimensional Floquet Hamiltonian in an AZ class of Floquet systems. Then, gapless modes in $H_F(\boldsymbol{k})$ obey the following relations,

$$n = \sum_{\epsilon_\alpha = \mu} \nu_\alpha^\mu, \qquad \text{in case (i')}, \tag{3.70}$$

$$n = \sum_{\epsilon_\alpha = 0} \nu_\alpha^0 = -(-1)^d \sum_{\epsilon_\alpha = \pi/\tau} \nu_\alpha^\pi, \qquad \text{in case (ii')}. \tag{3.71}$$

where n is the bulk topological invariant of $U_F = e^{-iH_F(\boldsymbol{k})\tau}$.

Once we admit Theorem 3 of non-Hermitian systems, the proof of Theorem 3' is straightforward. In the case of (i'), the proof of (i) in non-Hermitian systems is also valid because we deformed non-Hermitian Hamiltonians into unitary operators. We note that the direction of the group velocity $\partial_k[\mathrm{Re}E_p(k_{p\alpha})]$ is flipped for $\epsilon = \pi/\tau$ because a gapless fermion at π/τ, $H_F(\boldsymbol{k}) = \boldsymbol{k}\cdot\boldsymbol{\Gamma} + \pi/\tau$ in a Floquet system corresponds to $H(\boldsymbol{k}) = -\boldsymbol{k}\cdot\boldsymbol{\Gamma} - i$ in a non-Hermitian system as shown in the main text. We also notice that we can neglect the minus sign of n and ν_α^μ for classes A, AII, and, AII in even dimensions because n and $\nu_\alpha^{0(\pi)}$ in those AZ classes are $\mathbb{Z}_2$ numbers in even dimensions. Then, by multiplying $U_F(\boldsymbol{k})$ with an arbitrary phase factor $e^{i\mu\tau}$, we obtain the formula of the form in Eq. (3.70).

In the case of (ii'), we prove it by explicitly relating Floquet and non-Hermitian systems. n as a point gap topological invariant can be seen as a n of Floquet unitary operators by substituting $H = iU_F$. ν_α for $\mathrm{Im}E_\alpha > 0$ in non-Hermitian systems corresponds to ν_α^0 at $\epsilon = 0$ because the primitive gapless Hamiltonian $H_F(\boldsymbol{k}) \sim \boldsymbol{k}\cdot\boldsymbol{\Gamma}$ corresponds to the non-Hermitian Hamiltonian $H(\boldsymbol{k}) \sim \boldsymbol{k}\cdot\boldsymbol{\Gamma} + i$ for $O(k^2)$ as shown in Sec. 3.3. [13] In a similar manner, ν_α for $\mathrm{Im}E_\alpha < 0$ in non-Hermitian systems corresponds to $(-1)^d\nu_\alpha^0$ at $\epsilon = \pi/\tau$ because $H_F(\boldsymbol{k}) \sim \boldsymbol{k}\cdot\boldsymbol{\Gamma} + \pi/\tau$ in Floquet systems corresponds to $H(\boldsymbol{k}) \sim -\boldsymbol{k}\cdot\boldsymbol{\Gamma} - i$ in non-Hermitian systems.

Another proof without utilizing a non-Hermitian counterpart is also given in Appendix. C.

[12] Even in the case of (i), the gapless topological charge is always defined to become 1 for $H(\boldsymbol{k}) = \sum_{j=1}^d k_j\Gamma_j$.

[13] We note that topological charge of gapless points are defined to be compatible with the primitive Dirac Hamiltonian $H(\boldsymbol{k}) = \boldsymbol{k}\cdot\boldsymbol{\Gamma}$.

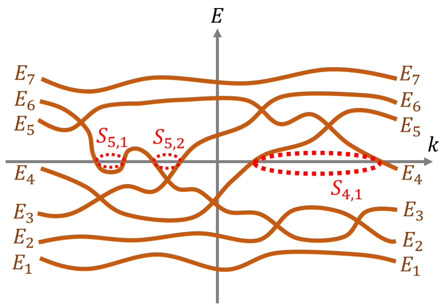

FIGURE 3.4: Typical band dispersion in Hermitian systems. In this case, Eq. (3.72) states $\mathrm{Ch}(S_{5,1}) + \mathrm{Ch}(S_{5,2}) + \mathrm{Ch}(S_{4,1}) = 0$.

3.7 Nielsen-Ninomiya theorem in 3D

The original Nielsen-Ninomiya theorem [1, 2] in Hermitian systems states that the net chirality of Weyl points in the whole Brillouin zone should be zero. Here we reformulate the theorem differently, which is more convenient to describe gapless modes in non-Hermitian and Floquet systems. [14]

Let us consider a Hermitian Hamiltonian $H(\boldsymbol{k})$ with energy bands $E_p(\boldsymbol{k})$ in 3D. For this Hamiltonian, the following relation holds,

$$\sum_{p\alpha} \mathrm{Ch}(S_{p\alpha}) = 0, \tag{3.72}$$

where $S_{p\alpha}$ is the Fermi surface defined by $\{\boldsymbol{k} \in S_{p\alpha} | E_p(\boldsymbol{k}) = 0\}$ and $\mathrm{Ch}(S_{p\alpha})$ is the Chern number on $S_{p\alpha}$, where the orientation of $S_{p\alpha}$ is chosen as the direction of the Fermi velocity $\partial_{\boldsymbol{k}}[\mathrm{Re}E_p(\boldsymbol{k})]_{\boldsymbol{k}\in S_{p\alpha}}$.

Proof: First, we order the bands $E_p(\boldsymbol{k})$ as $E_1(\boldsymbol{k}) \leq E_2(\boldsymbol{k}) \leq E_3(\boldsymbol{k}) \dots$ as illustrated in Fig. 3.4. Then, we continuously deform each energy $E_p(\boldsymbol{k})$ so as to satisfy either $E_p(\boldsymbol{k}) > 0$ or $E_p(\boldsymbol{k}) < 0$ in the whole Brillouin zone. [15] After this deformation, Eq. (3.72) obviously holds because there is no Fermi surface and there is no term on the left-hand side. Therefore, if the left-hand side of Eq. (3.72) is invariant during the above deformation, we obtain Eq. (3.72) for general band structures. We show that by moving bands upward one by one.

Let us consider a gapless band that hosts at least one Fermi surface at the Fermi energy $E = 0$. When we move the band upward, the following four processes may happen. (a) A Fermi surface shrinks and vanishes smoothly. (b) A Fermi surface merges into another Fermi surface or splits into two Fermi surfaces. (c) A new Fermi surface is created smoothly. (d) A Fermi surface shrinks to a Weyl point then moves to a lower band. During the first three processes (a),(b), and (c), the left-hand side of Eq. (3.72) is invariant because the Chern number, a topological invariant, cannot change during such smooth deformations. Notably, the last process also keeps the left-hand side of Eq. (3.72) invariant because we can show

$$\mathrm{Ch}(S_{p_0\alpha}) = \mathrm{Ch}(S_{p_0-1\alpha'}), \tag{3.73}$$

[14] This form of the Nielsen-Ninomiya theorem is also convenient for bulk-boundary correspondence of 4D topological insulator, where Weyl points appear on the boundary.

[15] Weyl points become obstacles during this deformation, but they always appear in a pair and thus we can gap out the pair of Weyl points by the collision of the pair of Weyl points.

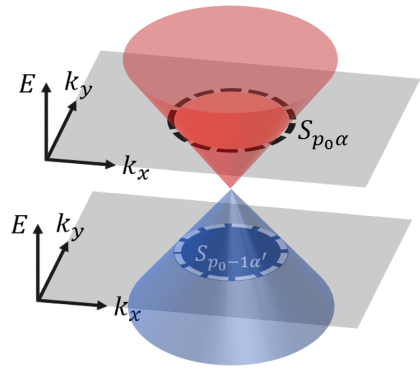

FIGURE 3.5: Energy dispersion near a robust degenerate point (Weyl point). We omit the k_z dependence for illustrative simplicity. The upper (lower) gray plane indicates the Fermi energy $E = 0$ before (after) the Weyl band moves upward. When the band deforms to move upward, the Fermi surface $S_{p_0\alpha}$ shrinks to the Weyl point, then a new Fermi surface $S_{p_0-1\alpha'}$ is created in a lower band $p_0 - 1$. Note that the orientation of $S_{p_0-1\alpha'}$ is opposite to that of $S_{p_0\alpha}$.

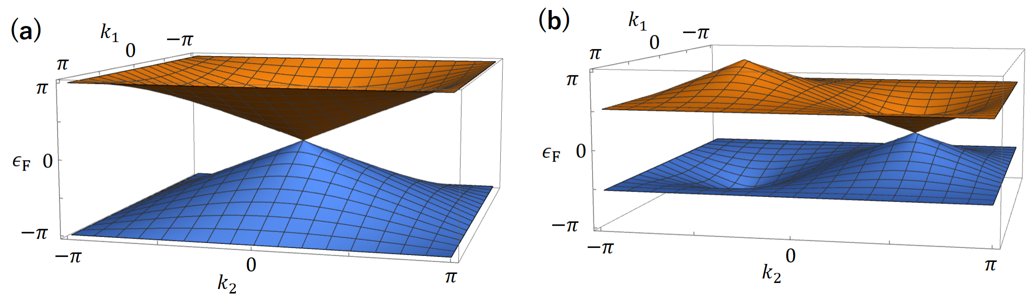

FIGURE 3.6: Floquet energy spectra of $U_F(\boldsymbol{k})$ in Eq. (3.75) with (a) $\theta = 0$ and (b) $\theta = 3/4$.

where $S_{p_0\alpha}$ is the Fermi surface shrinking into the Weyl point and $S_{p_0-1\alpha'}$ is the Fermi surface created on the lower band in this process. (One can directly show this equation for the typical Weyl Hamiltonian $H(\boldsymbol{k}) = \sum_{ij} a_{ij} k_i \sigma_j$.) Therefore, the left-hand side of Eq. (3.72) is invariant when we deform to move all metallic bands upward above the Fermi energy. Consequently, we have Eq. (3.72).

3.8 2D class AIII Floquet system

In this section, we see a nontrivial example of 2D Floquet systems in class AIII. Chiral symmetry for Floquet Hamiltonians $\Gamma H_F \Gamma^{-1} = -H_F$ in class AIII implies the chiral symmetry for one-cycle time evolution operator $\Gamma U_F^\dagger \Gamma^{-1} = U_F$, and thus ΓU_F is Hermitian. The topological invariant n of U_F in 2D class AII systems is the Chern number of ΓU_F. For a gapless mode of H_F at $\epsilon_F = 0$ (π/τ), the topological charge $\nu^{0(\pi)}$ is given by the 1D winding number,

$$\nu^\epsilon = \int_{s_{p\alpha}} \frac{\mathrm{d}\boldsymbol{k}}{4\pi i} \cdot \mathrm{tr}\left[\Gamma(H_\mathrm{F}(\boldsymbol{k}) - \epsilon)^{-1} \nabla (H_\mathrm{F}(\boldsymbol{k}) - \epsilon)\right], \quad (\epsilon = 0, (\pi/\tau)), \tag{3.74}$$

where $s_{p\alpha}$ is a small circle surrounding the gapless point, and the branch cut of $H_\mathrm{F}(\boldsymbol{k})$ is chosen at π/τ (0). For simplicity, we set $\tau = 1$ in the following.

Let us consider the following 2D model in class AIII,

$$U_{\mathrm{F}}(\boldsymbol{k}) = e^{i\theta\sigma_x/2}U_y^-(k_y/2)U_x^-(k_x)U_y^+(k_y/2)U_y^-(k_y/2)U_x^+(k_x)U_y^+(k_y/2)e^{i\theta\sigma_x/2}, \quad \Gamma U_{\mathrm{F}}^\dagger \Gamma^{-1} = U_{\mathrm{F}}, \tag{3.75}$$

where $U_j^\pm(k_j) = P_j^\pm e^{\mp i k_j} + P_j^\mp$ with $P_j^\pm = (\sigma_0 \pm \sigma_j)/2$ and $\Gamma = \sigma_3$. ΓU_F is rewritten as

$$\Gamma U_{\mathrm{F}} = d_x\sigma_x + (d_y\cos\theta - d_z\sin\theta)\sigma_y + (d_z\cos\theta + d_y\sin\theta)\sigma_z \tag{3.76}$$

where $d_x = -\cos^2(k_x/2)\sin k_y$, $d_y = -\sin k_x\cos^2(k_y/2)$, and $d_z = \cos k_x\cos^2(k_y/2) - \sin^2(k_y/2)$. The Chern number of ΓU_F becomes 1 for any θ as the vector $\boldsymbol{d} = (d_x, d_y, d_z)$ wraps the unit sphere once when $\boldsymbol{k}$ covers the whole Brillouin zone.

Figure 3.6 is the quasi-energy spectrum of this model with $\theta = 0, 3/4$. Near the Dirac point at $\epsilon_F = 0$, the Floquet Hamiltonian takes the form

$$H_{\mathrm{F}}(\boldsymbol{k}) \approx (k_x - \theta)\sigma_x + k_y\left(\cos^2\frac{\theta}{2}\right)\sigma_y, \tag{3.77}$$

which gives $\nu^0 = 1$. On the other hand, near the Dirac point at $\epsilon_F = \pi$, the Floquet Hamiltonian becomes

$$H_{\mathrm{F}}(\boldsymbol{k}) \approx \pi + (k_x - \theta - \pi)\sigma_x - \left(\sin^2\frac{\theta}{2}\right)k_y\sigma_y, \tag{3.78}$$

which gives $\nu^\pi = -1$. Thus, this model obeys Eq. (3.23) in Theorem 3'.

Chapter 4

Non-Hermitian chiral magnetic effect

4.1 Chiral magnetic effect

We propose the following model,

$$H(\boldsymbol{k}) = (d_0 + \boldsymbol{d}(\boldsymbol{k}) \cdot \boldsymbol{\sigma})\,\tau_1 + m(\boldsymbol{k})\tau_3 + i\gamma(\tau_3 - \tau_0), \tag{4.1}$$

with $d_i(\boldsymbol{k}) = \sin k_i$, $m(\boldsymbol{k}) = m_0 + \sum_{i=1}^{3} \cos k_i$. This model has a point gap at $E_\mathrm{F} = -i\gamma$ and hosts multiple Weyl points in the complex energy plane as shown in Fig. 4.1(a), satisfying Theorem 2 [1]. Photonic systems [47, 48] and cold atoms [**Takasu20**, 49] may provide the spin-selective (or sublattice selective) loss term in Eq. 4.1, and thus we believe the experimental realization of the following chiral magnetic effect is feasible.

Weyl fermions in a Floquet system can induce the CME [3, 4]. As a non-Hermitian counterpart of this effect, we propose the non-Hermitian CME. Figure 4.1(a) and (b) shows the energy spectrum of the model in Eq. (4.1) without and with a magnetic field B_z. The magnetic field opens the Landau gap at the Weyl point at $k = (0, 0, 0)$ in Fig. 4.1(a), and a right-going chiral mode with $\mathrm{Im}(E - E_\mathrm{F}) > 0$ appears. The chiral mode has a longer lifetime and produces a current parallel to the magnetic field, leading to the CME. We confirm the CME by examining the dynamics of wave packets. Figures 4.1(c) and 4.1(d) show the wave packet dynamics without and with the magnetic field B_z. While wave packets not subject to a magnetic field tend to move into the spin direction as a result of the spin-momentum locking of Weyl fermions, we observe wave packets under magnetic field B_z tend to move in the direction of the magnetic field, which is consistent with the CME.

Using the extended Nielsen-Ninomiya theorem, we can find a general formula that characterizes the non-Hermitian CME: From Theorem 2, a system with nonzero w_3 typically hosts Weyl fermions with the net chiral charge of w_3 with Im$E > 0$. As in Fig. 4.1 (b), a magnetic field B_z opens the Landau gap at each Weyl point, leaving a 1D chiral mode of the Landau degeneracy $(eB_z/2\pi)L_xL_y$ [2], where e is the electric charge of the Weyl fermion and $L_{i=x,y}$ is the system length in the i-direction. Therefore, the system supports 1D chiral modes with the net chiral charge $w_3(eB_z/2\pi)L_xL_y$. From Theorem 1, this result implies that the system also hosts the 1D energy winding number w_1 given by [3]

$$w_1^z = \frac{eB_z}{2\pi} L_x L_y w_3. \tag{4.2}$$

[1] See Sec. 4.2.

[2] See Sec. 4.2

[3] Detailed analysis of this formula is given in Appendix D

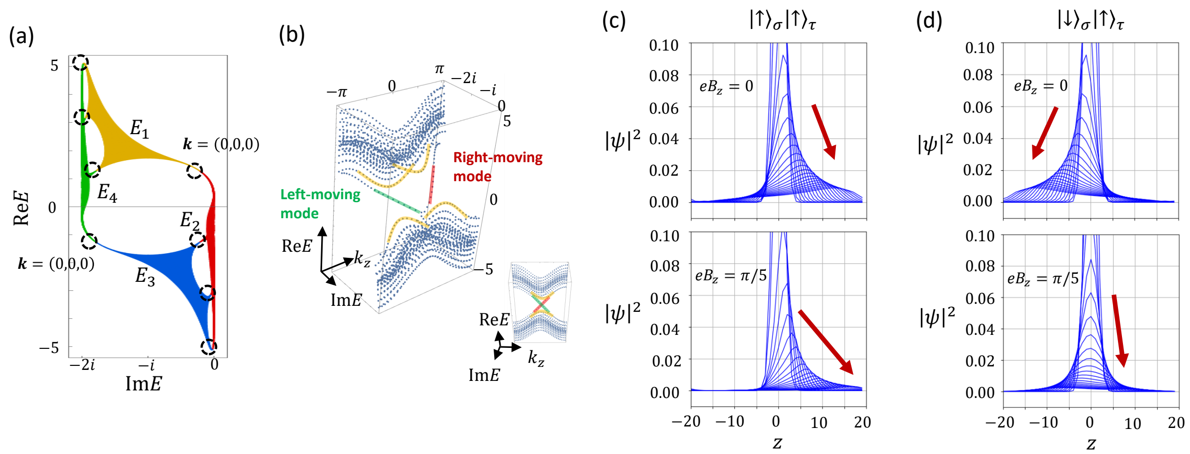

FIGURE 4.1: (a, b) Energy spectrum of the non-Hermitian Weyl semimetal model in Eq. (4.1) (a) without and (b) with a magnetic field B_z in the z direction. (a) Four colors distinguish different bands, and each dotted circle enclose Weyl points. (b) Right-(Left-)going mode has positive (negative) $\mathrm{Im}(E - E_\mathrm{F})$ for $E_\mathrm{F} = -i$. The right- and left-going mode originate from the Weyl points with $\boldsymbol{k} = (0,0,0)$. The inset is the same figure viewed from a different angle, where we can see the crossing of right- and left-going modes. (c,d) Wave packet dynamics in the non-Hermitian Weyl semimetal model of Eq. (4.1) (top) without and (bottom) with magnetic field B_z. We draw snapshots of the probability densities $|\psi(z)|^2$ at each unit cycle, where the red arrows indicate the direction of movement. This is numerically obtained by the fourth-order Runge-Kutta method. The initial wave packets are given by $|\psi_0\rangle = \psi_0 \left|\sigma_z\right\rangle_\sigma \left|\tau_z\right\rangle_\tau$, where ψ_0 is a 3D Gaussian wave packet of the width $2\bar{\sigma}^2 = 5$ and the internal degrees of freedom $\left|\sigma_z\right\rangle_\sigma \left|\tau_z\right\rangle_\tau$ is specified in each figure. Under the magnetic field $B_z = \pi/5$, all the wave packets tend to move in the $+\hat{z}$ direction. The parameters of Eq. (4.1) are $d_0 = \gamma = \gamma_0 = 1$ and $m_0 = -2$. The system size is (b) $L_x = L_y = L_z = 30$ and (c,d) $L_x = L_y = L_z = 40$ with PBC.

Here w_1^z is defined by Eq. (3.4), where $H(k)$ with $k = k_z$ is the Hamiltonian under the magnetic field B_z, and the trace includes the summation of k_x and k_y in the magnetic Brillouin zone. We note that $eB_zL_xL_y/2\pi$ is an integer under the PBC in x- and y-directions[4].

The relation (4.2) gives a profound implication. As mentioned above, a nonzero w_1 implies the occurrence of the non-Hermitian skin effect [83, 140], where extended bulk modes in PBC become localized boundary modes in the OBC. Therefore, Eq. (4.2) indicates that the system with a nonzero w_3 inevitably shows the skin effect under a magnetic field. This prediction is consistent with the CME dynamics we have seen above because bulk modes stack to a boundary in the direction of the magnetic field due to unidirectional CME currents. We have confirmed the chiral magnetic skin effect in the model of Eq. (4.1) in Sec. 4.2.

4.2 Non-Hermitian Weyl semimetal

4.2.1 Extended Nielsen-Ninomiya theorem

In this section, we see the extended Nielsen-Ninomiya theorem holds in the non-Hermitian Weyl semimetal

$$H(\boldsymbol{k}) = \left(d_0 + \boldsymbol{d}(\boldsymbol{k}) \cdot \boldsymbol{\sigma}\right)\tau_1 + \left(m(\boldsymbol{k}) + i\gamma\right)\tau_3 - i\gamma_0\tau_0, \tag{4.3}$$

[4] See Sec. D.2

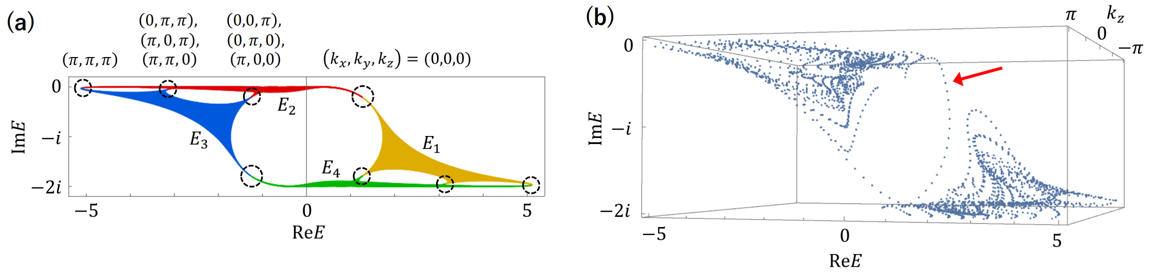

FIGURE 4.2: (a) Complex energy spectrum of the non-Hermitian Weyl semimetal in Eq. (4.3) with $d_0 = \gamma = \gamma_0 = 1$ and $m_0 = -2$. Different colors distinguish different bands in Eq. (4.5), and the black circles emphasize Weyl points. (b) Complex energy spectrum of Eq. (4.3) under a magnetic field B_z. The red arrow points to a right-going mode originating from the Weyl point at $\boldsymbol{k} = (0, 0, 0)$. The system size is $L_x = L_y = L_z = 30$ and the magnetic flux is $eB_z/2\pi = 1/10$.

with

$$d_i(\boldsymbol{k}) = \sin k_i, \quad m(\boldsymbol{k}) = m_0 + \cos k_1 + \cos k_2 + \cos k_3, \tag{4.4}$$

where d_0, m_0, γ, and γ_0 are real constants. The band energies of this model become

$$\begin{aligned}
E_1(\boldsymbol{k}) &= \sqrt{(|\boldsymbol{d}(\boldsymbol{k})| + d_0)^2 + (m(\boldsymbol{k}) + i\gamma)^2} - i\gamma_0, \\
E_2(\boldsymbol{k}) &= \sqrt{(|\boldsymbol{d}(\boldsymbol{k})| - d_0)^2 + (m(\boldsymbol{k}) + i\gamma)^2} - i\gamma_0, \\
E_3(\boldsymbol{k}) &= -\sqrt{(|\boldsymbol{d}(\boldsymbol{k})| + d_0)^2 + (m(\boldsymbol{k}) + i\gamma)^2} - i\gamma_0, \\
E_4(\boldsymbol{k}) &= -\sqrt{(|\boldsymbol{d}(\boldsymbol{k})| - d_0)^2 + (m(\boldsymbol{k}) + i\gamma)^2} - i\gamma_0.
\end{aligned} \tag{4.5}$$

Figure 4.2 illustrates these energy spectrum with Weyl points at $\boldsymbol{k} = (0, 0, 0)$, $(\pi, 0, 0)$, $(0, \pi, 0)$, $(0, 0, \pi)$, $(\pi, \pi, 0)$, $(\pi, 0, \pi)$, $(0, \pi, \pi)$, (π, π, π). The spectrum has a point gap at $E = E_F = -i\gamma_0$. Let us evaluate the topological charge of the Weyl points inside the Fermi surfaces $\mathrm{Re}(E(\boldsymbol{k}) - E_{\mathrm{F}}) = 0$. When $d_0 = \gamma = \gamma_0 = 1$ and $m_0 = -2$, only $E_2(\boldsymbol{k})$ and $E_4(\boldsymbol{k})$ bands have such Fermi surfaces, which we denote by S_2 and S_4, respectively. The Fermi surface S_2 (S_4) has an imaginary part of the energy higher (lower) than $E_{\mathrm{F}} = -i\gamma_0$. For example, the right eigenfunction of $H(\boldsymbol{k})$ with the eigenenergy $E_2(\boldsymbol{k})$ is given by

$$|\psi_2(\boldsymbol{k})\rangle = \frac{1}{\sqrt{2|\boldsymbol{d}(\boldsymbol{k})|(|\boldsymbol{d}(\boldsymbol{k})| - d_3(\boldsymbol{k}))}} \begin{pmatrix} d_3(\boldsymbol{k}) - |\boldsymbol{d}(\boldsymbol{k})| \\ d_1(\boldsymbol{k}) + id_2(\boldsymbol{k}) \end{pmatrix}_\sigma \otimes \begin{pmatrix} m(\boldsymbol{k}) + i\gamma + E_2(\boldsymbol{k}) \\ d_0 - |\boldsymbol{d}(\boldsymbol{k})| \end{pmatrix}_\tau . \tag{4.6}$$

The corresponding left eigenfunction $\langle\!\langle \psi_2(\boldsymbol{k})|$ have a similar expression, which is normalized as $\langle\!\langle \psi_2(\boldsymbol{k})|\psi_2(\boldsymbol{k})\rangle = 1$. The Chern number on the Fermi surface S_2 is

$$\mathrm{Ch}(S_2) = \frac{1}{2\pi i} \int_{S_2} (\nabla \times \boldsymbol{A}(\boldsymbol{k})) \cdot \mathrm{d}\boldsymbol{S}, \tag{4.7}$$

where $\boldsymbol{A}(\boldsymbol{k}) = \langle\!\langle \psi_2(\boldsymbol{k})|\nabla\psi_2(\boldsymbol{k})\rangle$ and the area element $d\boldsymbol{S}$ points to the direction of the Fermi velocity $\nabla \mathrm{Re}E_2(\boldsymbol{k})|_{\boldsymbol{k}\in S_2}$. As S_2 encloses a Weyl point at $\boldsymbol{k} = (0, 0, 0)$ in the upper right side of Fig. 4.2, we obtain $\mathrm{Ch}(S_2) = 1$. Similarly, we also obtain $\mathrm{Ch}(S_4) = -1$. On the other hand, we numerically calculate the 3D winding number w_3 given by

$$w_3 = -\frac{1}{24\pi^2}\int_{\mathrm{BZ}} \mathrm{tr}\left[(H-E_{\mathrm{F}})^{-1}d(H-E_{\mathrm{F}})\right]^3, \tag{4.8}$$

and obtain $w_3 = 1$ for $d_0 = \gamma = \gamma_0 = 1$ and $m_0 = -2$. Therefore, Theorem 2 in the main text holds for this model.

4.2.2 Weyl point under a magnetic field

We review the properties of a Weyl point under an applied magnetic field. We consider the Weyl Hamiltonian with $+1$ chirality,

$$H = k_x\sigma_x + k_y\sigma_y + k_z\sigma_z. \tag{4.9}$$

Under the magnetic field B_z, given by the vector potential $\boldsymbol{A} = (0, B_z x, 0)$, the Hamiltonian reads

$$\hat{H} = -i\partial_x\sigma_x + (k_y - eB_z x)\sigma_y + k_z\sigma_z = \begin{pmatrix} k_z & -i\partial_x - i(k_y - eB_z x) \\ -i\partial_x + i(k_y - eB_z x) & -k_z \end{pmatrix}, \tag{4.10}$$

where e is the electric charge of the Weyl fermion. For $eB_z > 0$, $\hat{H}$ is rewritten as

$$\hat{H} = \begin{pmatrix} k_z & \sqrt{2eB_z}\hat{a}^\dagger \\ \sqrt{2eB_z}\hat{a} & -k_z \end{pmatrix}, \tag{4.11}$$

in terms of the annihilation and creation operators,

$$\hat{a} = \frac{-i\partial_x + i(k_y - eB_z x)}{\sqrt{2eB_z}}, \quad \hat{a}^\dagger = \frac{-i\partial_x - i(k_y - eB_z x)}{\sqrt{2eB_z}}, \quad [\hat{a}, \hat{a}^\dagger] = 1. \tag{4.12}$$

The Hamiltonian $\hat{H}$ has a single right-going chiral mode with $E = k_z$ and gapped modes with $E = \pm\sqrt{k_z^2 + 2eB_z p}$ $(p = 1, 2, 3, \ldots)$, as illustrated in Fig. 4.3. For the right-going mode with $E = k_z$, the Schrödinger equation $\hat{H}|\psi\rangle = E|\psi\rangle$ with $|\psi\rangle = (|\psi_1\rangle, |\psi_2\rangle)$ leads to

$$\hat{a}\,|\psi_1\rangle = 0, \quad |\psi_2\rangle = 0, \tag{4.13}$$

from which we have the wavefunction of the right-going mode,

$$\psi_1(x) = \left(\frac{eB_z}{\pi}\right)^{1/4} \exp\left[-\frac{eB_z}{2}\left(x - \frac{k_y}{eB_z}\right)^2\right], \quad \psi_2(x) = 0. \tag{4.14}$$

The wave function $\psi_1(x)$ is the Gaussian wave packet with the center at $x_c = k_y/eB_z$. In the PBC in the x and y directions, x_c and k_y satisfy $0 < x_c \leq L_x$ and $k_y = 2\pi n_y/L_y$, respectively, leading to $n_y = 1, \ldots, (eB_z/2\pi)L_xL_y$. Therefore, the right-going mode has $(eB_z/2\pi)L_xL_y$-fold degeneracy. Note that $(eB_z/2\pi)L_xL_y$ is an integer in PBC of the magnetic translations [5]. Similarly, for $eB_z < 0$, we have a left-going mode $E = -k_z$ with $-(eB_z/2\pi)L_xL_y$ degeneracy.

[5] See Sec. D.2

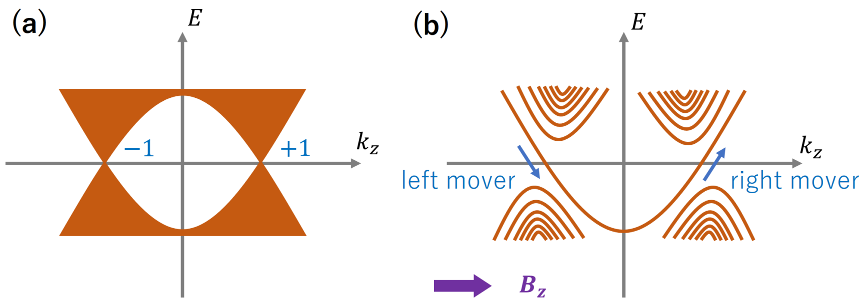

FIGURE 4.3: A typical energy band of Weyl points (a) without and (b) with a magnetic field. (a) Weyl points with ± 1 chiralities. (b) The Weyl point with chirality 1 (-1) becomes a right- (left-)going mode with $(B_z/2\pi)L_xL_y$-fold degeneracy.

For the Weyl Hamiltonian with -1 chirality such as

$$H = k_x\sigma_x + k_y\sigma_y - k_z\sigma_z, \tag{4.15}$$

we have a left-going mode $E = -k_z$ with $(eB_z/2\pi)L_xL_y$-fold degeneracy when $eB_z > 0$, and a right-going mode $E = k_z$ with $-(eB_z/2\pi)L_xL_y$-fold degeneracy when $eB_z < 0$.

4.2.3 Chiral magnetic skin effect

This section compares the complex energy spectra of the non-Hermitian Weyl semimetal in Eq. (4.3) with and without a magnetic field for PBC and OBC in z-direction, and show the chiral magnetic skin effect.

We first see the energy spectra of Eq. (4.3) without a magnetic field in Fig. 4.4 (a). The blue region is the energy spectrum with PBC in all directions, and the red dots are that with OBC in the z-direction and PBC in x and y directions. Skin modes with $E = -i$ and $E = \pm 1 - i$ appear under OBC. This skin effect is nothing to do with the chiral magnetic skin effect. Instead, it originates from the $\mathbb{Z}_2$ topological invariant of the model Hamiltonian in Eq. (4.3). Because of the reciprocity (TRS†) of $H(\boldsymbol{k})$ in Eq. (4.1), $RH^T(\boldsymbol{k})R^{-1} = H(-\boldsymbol{k})$, $R = i\sigma_2\tau_0$, we can define the $\mathbb{Z}_2$ topological invariant for $H(0,0,k_z)$,

$$(-1)^{\nu(E)} = \operatorname{sgn}\left\{\frac{\mathrm{Pf}[(H(0,0,\pi)-E)R]}{\mathrm{Pf}[(H(0,0,0)-E)R]}\exp\left[-\frac{1}{2}\int_{k_z=0}^{\pi} d\log\det[(H(0,0,k_z)-E_F)R]\right]\right\} \tag{4.16}$$

We obtain $\nu(E) = 1$ when E_F is in the center area enclosed by the blue spectrum in Fig. 4.4 (a). Thus, as a 1D system in the z-direction, $H(0,0,k_z)$ shows the $\mathbb{Z}_2$ skin effect protected by the reciprocity [83]. By directly solving the Schrödinger equation, we obtain two skin modes with $E = -i$ as

$$\left|\downarrow\right\rangle_\sigma \otimes \left|\leftarrow\right\rangle_\tau \otimes \left|z=0\right\rangle, \quad \left|\uparrow\right\rangle_\sigma \otimes \left|\leftarrow\right\rangle_\tau \otimes \left|z=L_z\right\rangle, \tag{4.17}$$

each of which has two-fold degeneracy, and the skin modes with $E = \pm 1 - i$ as

$$\begin{aligned}&\mp i\left|\downarrow\right\rangle_\sigma \otimes \left|\rightarrow\right\rangle_\tau \otimes \left|z=0\right\rangle + \left|\downarrow\right\rangle_\sigma \otimes \left|\leftarrow\right\rangle_\tau \otimes \left(2\left|z=0\right\rangle - i\left|z=1\right\rangle\right),\\ &\mp i\left|\uparrow\right\rangle_\sigma \otimes \left|\rightarrow\right\rangle_\tau \otimes \left|z=L_z\right\rangle + \left|\uparrow\right\rangle_\sigma \otimes \left|\leftarrow\right\rangle_\tau \otimes \left(2\left|z=L_z\right\rangle - i\left|z=L_z-1\right\rangle\right),\end{aligned} \tag{4.18}$$

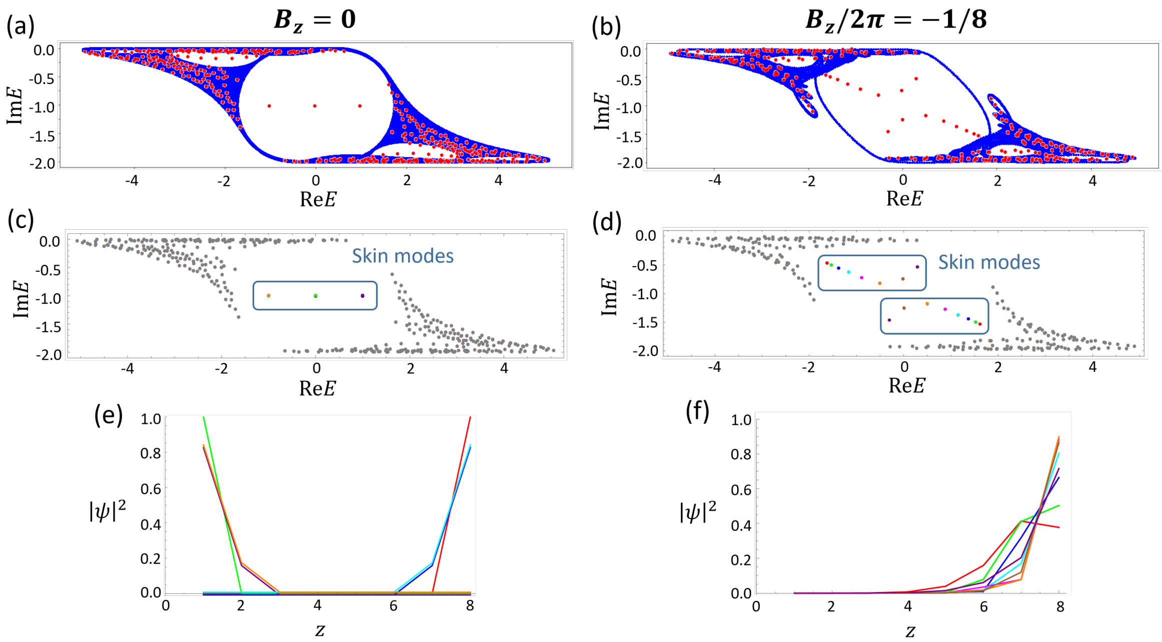

FIGURE 4.4: Chiral magnetic skin effect of the non-Hermitian Weyl semimetal in Eq. (4.3). (a,b) Energy spectra of Eq. (4.3) with $d_0 = \gamma = \gamma_0 = 1$, $m_0 = -2$ (blue) in full PBC and (red) in the OBC in the z direction (zOBC). (c,d,e,f) Skin modes in zOBC with (c,e) $B_z = 0$ and (d,f) $eB_z/2\pi = 1/8$. Colors in (c) and (d) correspond to the same colors in (e) and (f). The zOBC spectra and wavefunctions are calculated in the system size $L_x = L_y = L_z = 8$. All the skin modes in (f) under the magnetic field are localized at the right boundary, as expected from the chiral magnetic current parallel to the magnetic field.

each of which has $(L_z - 1)$-fold degeneracy. Here $|\uparrow\rangle_\sigma$ ($|\downarrow\rangle_\sigma$) and $|\rightarrow\rangle_\tau$ ($|\leftarrow\rangle_\tau$) are the $\sigma_z = 1$ ($\sigma_z = -1$) eigenstate and the $\tau_y = 1$ ($\tau_y = -1$) eigenstate, respectively, and $|z = i\rangle$ is the localized state at the i-th site in the z-direction. The skin modes localized at $z = 0, L_z$ form Kramers pairs of the reciprocity R, and when one applies a magnetic field, they are mixed and disappear into the bulk.

In the presence of a magnetic field B_z, however, different skin modes appear. In Fig. 4.4 (b), we show the energy spectra of Eq. (4.3) with the magnetic field B_z. We can see the skin modes inside the blue spectra. In contrast to the $\mathbb{Z}_2$ skin effect in the above, all the skin modes are localized at $z = L_z$, as shown in Fig. 4.4 (f). The present skin effect originates from the $\mathbb{Z}$-valued 1D energy winding number w_1 [83]. As discussed in Sec. 4.1, a non-zero w_3 induces a non-zero w_1 in the form of Eq. (4.2) under a magnetic field, which induces the skin effect. The existence of the skin modes is also consistent with the CME since the unidirectional motion of wave packets in Figs. 4.1 (c) and (d) results in an accumulation of bulk states at the boundary $z = L_z$.

We have also studied the chiral magnetic skin effect in a different model. Detailed analysis of the chiral magnetic skin effect will be reported elsewhere [145].

Chapter 5

Extrinsic topology in quantum walks

Bulk-boundary correspondence is a fundamental principle, where bulk topological invariants determine gapless boundary states. On the other hand, it has been known that corner or hinge modes in higher-order topological insulators can appear due to the "extrinsic" topology of the boundaries even when the bulk topology is trivial. In this paper, we find that the so-called Floquet anomalous boundary states in quantum walks also have extrinsic topological natures. In contrast to the case of higher-order topological insulators, the extrinsic topology of quantum walks is manifest even for first-order topological phases. We present the periodic table of extrinsic topology in quantum walks and illustrate extrinsic natures of first-order Floquet anomalous boundary states in concrete examples.

5.1 Introduction

Recently, it has become clear that a class of gapless boundary states may appear without bulk topological invariant because of the nontrivial topology of boundaries. Such boundary states have been called "extrinsic" [146]. In particular, in equilibrium, extrinsic topological phases are realized in higher-order topological insulators with gapless corner and hinge modes [147–155]. For example, attaching a one-dimensional (1D) Su-Schrieffer-Heeger (SSH) chain [156] onto an edge of a two-dimensional (2D) chiral-symmetric topologically trivial insulator, extrinsic zero-energy corner states appear. The zero-energy gapless modes are robust against continuous perturbations of the system unless the energy gap closes. The topological invariant of the attached SSH chain determines the types and the numbers of these corner modes.

Floquet systems, where time-dependent Hamiltonians are periodic in time [25, 26, 28, 29, 100, 157–159], and quantum walks, where periodic series of unitary operators describe their dynamics [30, 39–41, 160–173], have attracted uprising interests because of topological phenomena intrinsic to non-equilibrium systems. Both Floquet systems and quantum walks have the $2\pi/T$ quasi-energy periodicity because of the Bloch-Floquet theorem for time translation symmetry of time period T [19]. The $2\pi/T$ periodicity leads to two high-symmetric Fermi energy levels at $\epsilon = 0$ and $\epsilon = \pi/T$ and defines gaps at these energies, which is a feature in these systems. Gapless boundary states at $\epsilon = 0$ and $\epsilon = \pi/T$ have been studied both in Floquet systems [26–29] and quantum walks [30, 39, 40]. Due to the common properties above, quantum walks are studied as a kind of Floquet systems in many previous literatures on topological phases.

However, as we clarify below, there exists a fundamental difference between Floquet systems and quantum walks. To see the difference, we compare quantum walks and Floquet systems in detail. In conventional Floquet systems, the time-evolution operator $U(\boldsymbol{k}, t_1 \to t_2)$ in the momentum space representation is given by a time-dependent microscopic Hamiltonian $H(\boldsymbol{k}, t)$,

$$U(\boldsymbol{k}, t_1 \to t_2) = \mathcal{T} \exp\left[-i \int_{t_1}^{t_2} dt H(\boldsymbol{k}, t)\right], \tag{5.1}$$

where $\mathcal{T}$ indicates the time-ordering operator. The one-cycle time-evolution operator $U_F(\boldsymbol{k}) := U(\boldsymbol{k}, 0 \to T)$ is often called the Floquet operator, where T is the time period of the microscopic Hamiltonian $H(\boldsymbol{k}, t+T) = H(\boldsymbol{k}, t)$. In quantum walks, however, the one-cycle time evolution is given directly as a series of unitary operators $U_j(\boldsymbol{k})$,

$$U_{\mathrm{QW}}(\boldsymbol{k}) = \prod_j U_j(\boldsymbol{k}). \tag{5.2}$$

For both Floquet systems and quantum walks, we define the effective Hamiltonians H_F and H_{QW} as

$$U_F = e^{-iH_F T}, \quad U_{\mathrm{QW}} = e^{-iH_{\mathrm{QW}}}, \tag{5.3}$$

which describe the stroboscopic dynamics in these systems. Therefore, quantum walks can be regarded as a Floquet system of time period $T = 1$. The quasi-energies of these systems are defined as the eigenvalues of the effective Hamiltonians, and thus the periodicity $2\pi/T$ of the quasi-energy can be interpreted as the periodicity in the phases of U_F and U_{QW}. When $U_j(\boldsymbol{k})$'s are written by a microscopic Hamiltonian: $U_j(\boldsymbol{k}) = \mathcal{T} \exp\left[-i \int_{t_j}^{t_{j+1}} dt H(\boldsymbol{k}, t)\right]$, the quantum walk can be regarded as a Floquet system. However, this is not always the case for general quantum walks [Fig. 5.1]. An illustrative example is a quantum walk of only the shift operator $U_{\mathrm{QW}}(k) = S_+(k)$ [39, 161],

$$S_+(k) = \begin{pmatrix} e^{-ik} & 0 \\ 0 & 1 \end{pmatrix}. \tag{5.4}$$

As one can show immediately, this model has a non-trivial winding number $w_1[U_{\mathrm{QW}}(k)] = 1$, where $w_1[U(k)]$ defined by

$$w_1[U(k)] = \int_0^{2\pi} \frac{dk}{2\pi} \mathrm{tr}[U(k)^{-1} i\partial_k U(k)]. \tag{5.5}$$

On the other hand, for any Floquet continuous time evolution $U(k, t_1 \to t_2)$, the winding number inevitably becomes zero:

$$w_1[U(k, t_1 \to t_2)] = w_1[U(k, 0 \to 0)] = 0, \tag{5.6}$$

as $U(k, t_1 \to t_2)$ is continuously deformed into $U(k, 0 \to 0) = 1$. [1] Therefore, the quantum walk $U_{\mathrm{QW}}(k) = S_+(k)$ cannot be written by a form of Floquet continuous time evolution.

In this paper, we argue that this difference enables extrinsic topological phases in quantum walks even in the first order. We see a simple example of the extrinsic topological phase in a quantum walk as follows [Fig. 5.2]. First, let us prepare a topologically trivial bulk model in 2D

[1] During the deformation, the topological invariant w_1 cannot change because $U(k, t_1 \to t_2)$ is always well-defined. This is the basic property of all topological invariants.

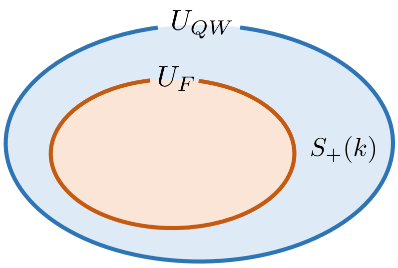

FIGURE 5.1: Relation between the set of quantum walks and the set of Floquet systems. Any Floquet operator U_F can be regarded as a one-step quantum walk U_{QW}. On the other hand, some quantum walks U_{QW} such as $S_+(k)$ in Eq. (5.4) cannot be realized as a form of Floquet operator U_F.

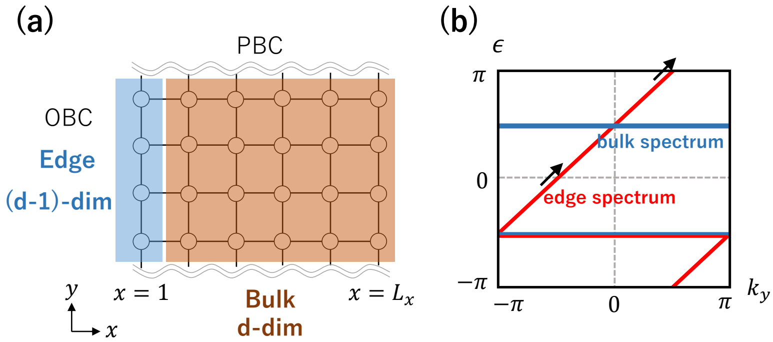

FIGURE 5.2: Lattice construction and quasi-energy spectrum of the simple extrinsic topological model in Eq. (5.13). (a) We attach a topologically nontrivial $(d-1)$-dimensional boundary onto a topologically trivial d-dimensional bulk. In the simple model, we consider $d = 2$. We impose PBC in the y-direction and OBC in the x-direction. (b) The quasi-energy spectrum of Eq. (5.13). The blue (red) line indicates the bulk (edge) quasi-energy spectrum.

with quasi-energy gaps at $\epsilon = 0$ and $\epsilon = \pi/T$ by using the coin operator $C(\theta)$,

$$U_{\text{bulk}}(\boldsymbol{k}) = C(\frac{\pi}{2}),\ C(\theta) := e^{-i\theta\sigma_z}. \tag{5.7}$$

The real space representation of this bulk model becomes

$$U_{\text{bulk}} = \sum_{x=2}^{L_x}\sum_{y=1}^{L_y} -i\,|\boldsymbol{r},+\rangle\,\langle\boldsymbol{r},+| + i\,|\boldsymbol{r},-\rangle\,\langle\boldsymbol{r},-|\,, \tag{5.8}$$

where $\boldsymbol{r}$ is the (x,y) position, and $\pm$ is two orthogonal internal states of the walker. The effective Hamiltonian H_{QW} of this model is

$$H_{\mathrm{QW}} = \frac{\pi}{2}\sigma_z, \tag{5.9}$$

which has the quasi-energies $\epsilon(\boldsymbol{k}) = \pm\pi/2$. Thus, the model has energy gaps both at $\epsilon = 0, \pi$.

Furthermore, as the Hamiltonian is a constant[2], the bulk topological invariant is zero, so no gapless boundary mode is expected from bulk-boundary correspondence.

However, we can obtain a gapless chiral edge mode by decorating the boundary at $x = 1$ of this model with a local unitary operator

$$U_{\text{edge}}(k_y) = S_+(k_y)C(\frac{\pi}{2}), \tag{5.10}$$

where k_y is the momentum along the edge. The effective Hamiltonian $H_{\text{QW}}^{\text{edge}}$ at the edge is

$$H_{\text{QW}}^{\text{edge}} = \begin{pmatrix} k_y + \pi/2 & 0 \\ 0 & -\pi/2 \end{pmatrix}, \tag{5.11}$$

and thus the edge supports a chiral gapless mode with the linear dispersion $\epsilon(k_y) = k_y + \pi/2$. The real space representation of the edge unitary is

$$U_{\text{edge}} = \sum_{y=1}^{L_y} -i\,|1, y+1, +\rangle \langle 1, y, +| + i\,|1, y, -\rangle \langle 1, y, -|\,, \tag{5.12}$$

where PBC is imposed in the y-direction. By attaching this 1D model to the bulk 2D model U_{bulk} in Eq. (5.8) at $x = 1$, we have a edge-decorated bulk model,

$$U_{\text{bulk}} \oplus U_{\text{edge}}. \tag{5.13}$$

In spite of the trivial bulk topological invariant, the decorated model has a nontrivial chiral edge mode, as shown in Fig. 5.2 (b).

The extrinsic gapless chiral mode is understood from the winding number of the edge unitary operator. As shown above, in contrast to conventional Floquet systems, a unitary operator in a quantum walk may have a nonzero winding number, and the edge unitary operator $U_{\text{edge}}(k_y)$ in Eq. (5.10) has $w_1[U_{\text{edge}}(k_y)] = 1$. Following the extended Nielsen-Ninomiya theorem proved in Chapter 3 (Eq. (3.7) in Theorem 1'), nontrivial winding number assures the existence of gapless chiral modes both at $\epsilon = 0, \pi$ at the same time:

$$\sum_{\epsilon_p(k_{p\alpha})=0} \operatorname{sgn} v_{p\alpha} = \sum_{\epsilon_p(k_{p\alpha})=\pi} \operatorname{sgn} v_{p\alpha} = w_1[U_{\text{edge}}(k_y)], \tag{5.14}$$

where $k_{p\alpha}$ is the α-th gapless point of band p of the edge effective Hamiltonian defined by $\epsilon(k_{p\alpha}) = 0$ or π, and $v_{p\alpha} = (\partial\epsilon_p/\partial k_y)_{k_y=k_{p\alpha}}$ is the group velocity of the gapless mode at $k_{p\alpha}$. Since $\operatorname{sgn} v_{p\alpha}$ is the chirality of the gapless mode, a nonzero winding number implies the net nonzero chiral gapless modes both at $\epsilon = 0, \pi$.

Based on the extended Nielsen-Ninomiya theorem in Chapter 3, we classify the extrinsic topological phases in quantum walks in arbitrary dimensions and symmetry classes. Superficially, the classification coincides with that for gapless states in ordinary topological insulators and superconductors [Table 5.2]. This is because the gapless boundary states in quantum walks are characterized by the same topological charges as those in usual topological insulators and superconductors. However, contrary to the conventional gapless modes, gapless modes in the extrinsic topological phases appear even in the absence of bulk topological invariants because of

[2] a kind of atomic insulator

the nontrivial topology of boundary unitary operators. Remarkably, the extrinsic gapless modes always appear in a pair at $\epsilon = 0, \pi/T$. Furthermore, in even (odd) dimensions, the net topological charge of extrinsic gapless modes at $\epsilon = 0$ is the same as (opposite to) the net topological charge of those at $\epsilon = \pi/T$.

The extrinsic topological phase of quantum walks is closely related to the so-called Floquet anomalous topological phase [33]. In Floquet systems, there are two types of topological phases: one is the conventional topological phase characterized by the topology of the effective Hamiltonian in Eq. (5.3), and the other is the anomalous one characterized by the topology of the microscopic Hamiltonian in Eq. (5.1). These two types of topological invariants are needed to fully determine the boundary states both at $\epsilon = 0$ and $\epsilon = \pi/T$. In quantum walks, however, the microscopic Hamiltonian does not always exist, and thus anomalous topological phase is ill-defined in general. As a result, the bulk topology is insufficient to determine the boundary gapless states. Instead, we find that additional boundary unitary operators can be topological, which enables us to fully control gapless states on the boundary.

We also discuss the physical implementations of such extrinsic topological phases. We first numerically and analytically study the robustness of extrinsic chiral gapless modes against disorders using the Anderson localization Hamiltonian [174]. We also show that suitable modulations of boundaries can eliminate gapless boundary states in the split step quantum walk in 1D [39–41] and the five-step model in 2D [27], which clearly illustrates the extrinsic nature of gapless states in the quantum walks.

This paper is organized as follows. In Sec. 5.2, we see the classification of extrinsic topological phases in quantum walks. In Sec. 5.3, we discuss extrinsic topological phases in one-dimensional quantum walks in detail. In Sec. 5.4, the relation between the topological classification of Floquet topological insulators and that of quantum walks is discussed. The relation between Floquet anomalous boundary states and extrinsic boundary states in quantum walks is clarified. In Sec. 5.5, we review the bulk-boundary correspondence for chiral-symmetric quantum walks in 1D through our theory. For chiral symmetric quantum walks in 1D, it has been shown that the bulk topological invariants fully determines the number of boundary zero modes [30], *i.e.* no extrinsic topological phase can appear. On the other hand, our classification indicates the presence of an extrinsic topological phase in this case. We make it clear that this difference comes from the difference in the definitions of chiral symmetry. Indeed, Ref. [30] introduces chiral symmetry for the quantum walks composed from two half-cycle time-evolution operators, and we demonstrate that the extrinsic topological phase becomes trivial under this special realization of chiral symmetry. We also find that class CII 1D quantum walks have a similar property: Using an appropriate realization of symmetries, the bulk topological invariants fully determine the number of boundary zero modes. In Sec. 5.6, we see three physical implementations of extrinsic topological phases, and examine their dynamical properties.

5.2 Classification of extrinsic topology in quantum walks

Let us consider a general one-cycle time-evolution unitary operator $U_{\mathrm{QW}}(\boldsymbol{k})$ and the corresponding effective Hamiltonian $H_{\mathrm{QW}}(\boldsymbol{k})$ defined by $U_{\mathrm{QW}}(\boldsymbol{k}) = e^{-iH_{\mathrm{QW}}(\boldsymbol{k})}$ in d-dimensions with momentum $\boldsymbol{k} = (k_1, k_2, \dots, k_d)$. We first introduce the Altland-Zirnbauer (AZ) symmetry classes [35]. $H_{\mathrm{QW}}(\boldsymbol{k})$ may satisfies time-reversal symmetry (TRS), particle-hole symmetry

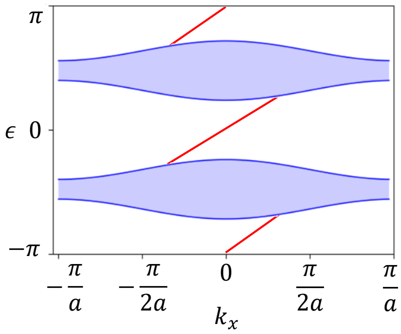

FIGURE 5.3: A typical quasi-energy spectrum of a quantum walk: The quasi-energy has 2π periodicity, we have two high-symmetric bulk energy gaps at $\epsilon = 0$ and π. Gapless boundary states may appear at both energy gaps. Here a is a lattice constant. If we consider a group of people lined up in a grid, the lattice constant needs to be $a \approx 2$ m because of COVID-19 these days.

(PHS) and/or chiral symmetry (CS):

$$TH_{\mathrm{QW}}(\boldsymbol{k})T^{-1} = H_{\mathrm{QW}}(-\boldsymbol{k}), \tag{5.15}$$
$$CH_{\mathrm{QW}}(\boldsymbol{k})C^{-1} = -H_{\mathrm{QW}}(-\boldsymbol{k}), \tag{5.16}$$
$$\Gamma H_{\mathrm{QW}}(\boldsymbol{k})\Gamma^{-1} = -H_{\mathrm{QW}}(\boldsymbol{k}). \tag{5.17}$$

Here, T and C are anti-unitary operators with $T^2 = \pm 1$ and $C^2 = \pm 1$, and Γ is a unitary operator with $\Gamma^2 = 1$. The AZ symmetry classes are defined by the presence or absence of TRS, PHS and/or CS [Table 5.1]. In quantum walks, it is beneficial to rewrite the AZ

$$TU_{\mathrm{QW}}(\boldsymbol{k})T^{-1} = U_{\mathrm{QW}}(-\boldsymbol{k})^{\dagger}, \tag{5.18}$$
$$CU_{\mathrm{QW}}(\boldsymbol{k})C^{-1} = U_{\mathrm{QW}}(-\boldsymbol{k}), \tag{5.19}$$
$$\Gamma U_{\mathrm{QW}}(\boldsymbol{k})\Gamma^{-1} = U_{\mathrm{QW}}(\boldsymbol{k})^{\dagger}. \tag{5.20}$$

When there are particle-hole and/or chiral symmetries, we have a symmetry constraint $\epsilon_n = -\epsilon_m \pmod{2\pi}$ for the quasi-energy bands n, m, and obtain high-symmetric energy gaps at $\epsilon = 0, \pi$. We suppose that these energy gaps are open for bulk bands in the following [Fig. 5.3].

Gapless boundary states can appear at $\epsilon = 0$ and $\epsilon = \pi$ individually. They are described by a gapless Dirac Hamiltonian:

$$H_{\mathrm{QW}}(\boldsymbol{k}_{\parallel}) = \sum_{j=1}^{d-1} k_j \gamma_j + \epsilon_{\mathrm{gap}} \hat{1}, \tag{5.21}$$

up to continuous deformations [3]. Here, we take the OBC in the x_d-direction, and $\boldsymbol{k}_{\parallel} = (k_1, k_2, \ldots, k_{d-1})$ is the momentum along the boundary, and $\epsilon_{\mathrm{gap}} = 0, \pi$ is the energy gaps we consider. The gamma matrix γ_j is a Hermitian matrix satisfying $\{\gamma_i, \gamma_j\} = 2\delta_{ij}$. We note that this boundary Hamiltonian is taken to be compatible with AZ symmetries. The gapless Dirac Hamiltonian Eq. (5.21) has the same form as that for boundary gapless states in conventional topological insulators and superconductors in equilibrium [16, 37, 98, 175]. In equilibrium, owing to the bulk-boundary

[3] and addiction and/or subtraction of trivial bands

TABLE 5.1: Periodic table for $(d-1)$-dimensional gapless boundary states of d-dimensional quantum walks in AZ symmetry class. We assume the existence of bulk gaps at $\epsilon = 0$ and π.

AZ class	T	C	Γ	$d=1$	2	3
A	0	0	0	0	$\mathbb{Z}^2$	0
AIII	0	0	1	$\mathbb{Z}^2$	0	$\mathbb{Z}^2$
AI	$+1$	0	0	0	0	0
BDI	$+1$	$+1$	1	$\mathbb{Z}^2$	0	0
D	0	$+1$	0	$\mathbb{Z}_2^2$	$\mathbb{Z}^2$	0
DIII	-1	$+1$	1	$\mathbb{Z}_2^2$	$\mathbb{Z}_2^2$	$\mathbb{Z}^2$
AII	-1	0	0	0	$\mathbb{Z}_2^2$	$\mathbb{Z}_2^2$
CII	-1	-1	1	$(2\mathbb{Z})^2$	0	$\mathbb{Z}_2^2$
C	0	-1	0	0	$(2\mathbb{Z})^2$	0
CI	$+1$	-1	1	0	0	$(2\mathbb{Z})^2$

correspondence, the topological classification of gapless boundary states in $(d-1)$-dimensions is the same as that of insulators and superconductors in d-dimensions. Therefore, the topological classification of $(d-1)$-dimensional boundary states in quantum walks coincides with that of ordinary insulators and superconductors in d-dimensions [Table. 5.1]. We note that the topological numbers in Table 5.1 are doubled because each gap at $\epsilon = 0, \pi$ may host gapless states individually.

The gapless boundary states of quantum walks have two different topological origins. The first one is the bulk topology of the effective Hamiltonian $H_{\mathrm{QW}}(\boldsymbol{k})$ in the same manner as the bulk-boundary correspondence in equilibrium. The two gaps $\epsilon = 0$ and $\epsilon = \pi$ separate bulk bands of $H_{\mathrm{QW}}(\boldsymbol{k})$ into two, from which one can define "occupied" and "empty" bands like conventional insulators. Therefore, in a manner similar to ordinary topological insulators, $H_{\mathrm{QW}}(\boldsymbol{k})$ can be topological, which gives gapless boundary states at $\epsilon = 0$ through bulk-boundary correspondence. One of the doubled topological numbers $\mathbb{Z}^2$, $\mathbb{Z}_2^2$ and $(2\mathbb{Z})^2$ in Table 5.1 corresponds the boundary gapless states determined from the bulk topological invariant of $H_{\mathrm{QW}}(\boldsymbol{k})$.

Another origin is the main subject of this paper, i.e., extrinsic topology of boundary unitary operators. Below, we see possible lattice terminations of d-dimensional quantum walks, which is given by $(d-1)$-dimensional unitary operators $U_{\mathrm{BDQW}}(\boldsymbol{k}_{\parallel})$.

For this purpose, we employ a theory on gapless states of unitary operators discussed in Chapter 3. For a boundary unitary operator $U_{\mathrm{BDQW}}(\boldsymbol{k}_{\parallel})$ in an AZ symmetry classes, we have gapless states if the unitary operator $U_{\mathrm{BDQW}}(\boldsymbol{k}_{\parallel})$ has a non-trivial topological number. The extended Nielsen-Ninomiya theorem for Floquet systems in Chapter 3 summarizes the exact relation between gapless states and the topological invariant for the $(d-1)$-dimensional unitary operator $U_{\mathrm{BDQW}}(\boldsymbol{k}_{\parallel})$:

$$\sum_{\epsilon_\alpha=0} \nu_\alpha^0 = (-1)^d \sum_{\epsilon_\alpha=\pi} \nu_\alpha^\pi = n, \tag{5.22}$$

where $\nu_\alpha^{0,\pi}$ is the topological charge of α-th gapless states at $\epsilon = 0, \pi$, and n is the topological invariant of $U_{\mathrm{BDQW}}(\boldsymbol{k}_{\parallel})$. Equation (5.14) is an example of the extended Nielsen-Ninomiya theorem for class A with $d = 2$ ($d = 1$ as the boundary dimensions), and explicit forms of $\nu_\alpha^{0,\pi}$ and n for $d = 1$ ($d = 0$ as the boundary dimensions) is discussed in Sec. 5.3. In general, we can

TABLE 5.2: Periodic table of extrinsic topological phases in $(d-1)$-dimensional boundary states of d-dimensional quantum walks. This table shows the presence or absence of the $\mathbb{Z}$ or $\mathbb{Z}_2$ topological number n for $(d-1)$-dimensional boundary unitary operators.

AZ class	T	C	Γ	$d=1$	2	3
A	0	0	0	0	$\mathbb{Z}$	0
AIII	0	0	1	$\mathbb{Z}$	0	$\mathbb{Z}$
AI	$+1$	0	0	0	0	0
BDI	$+1$	$+1$	1	$\mathbb{Z}$	0	0
D	0	$+1$	0	$\mathbb{Z}_2$	$\mathbb{Z}$	0
DIII	-1	$+1$	1	$\mathbb{Z}_2$	$\mathbb{Z}_2$	$\mathbb{Z}$
AII	-1	0	0	0	$\mathbb{Z}_2$	$\mathbb{Z}_2$
CII	-1	-1	1	$2\mathbb{Z}$	0	$\mathbb{Z}_2$
C	0	-1	0	0	$2\mathbb{Z}$	0
CI	$+1$	-1	1	0	0	$2\mathbb{Z}$

define n as follows: We introduce the doubled Hamiltonian $\mathcal{H}_U(\boldsymbol{k}_\parallel)$ [3]:

$$\mathcal{H}_U(\boldsymbol{k}_\parallel) = \begin{pmatrix} 0 & U_{\mathrm{BDQW}}(\boldsymbol{k}_\parallel) \\ U^\dagger_{\mathrm{BDQW}}(\boldsymbol{k}_\parallel) & 0 \end{pmatrix}, \tag{5.23}$$

which is Hermitian and has eigenvalues ± 1 due to $\mathcal{H}_U(\boldsymbol{k}_\parallel)^2 = \hat{1}$. It also obeys the proper CS,

$$\Sigma_z \mathcal{H}_U(\boldsymbol{k}_\parallel)\Sigma_z = -\mathcal{H}_U(\boldsymbol{k}_\parallel),\ \Sigma_z = \begin{pmatrix} \hat{1} & 0 \\ 0 & -\hat{1} \end{pmatrix}. \tag{5.24}$$

The AZ symmetries of $U_{\mathrm{BDQW}}(\boldsymbol{k}_\parallel)$, which has the same form as that of the bulk operator $U_{\mathrm{QW}}(\boldsymbol{k})$ in Eqs. (5.18)-(5.20), lead to the AZ symmetries for the doubled Hamitlonian as

$$\tilde{T}\mathcal{H}_U(\boldsymbol{k}_\parallel)\tilde{T}^{-1} = \mathcal{H}_U(-\boldsymbol{k}_\parallel),\ \tilde{T} = \begin{pmatrix} 0 & T \\ T & 0 \end{pmatrix}, \tag{5.25}$$

$$\tilde{C}\mathcal{H}_U(\boldsymbol{k}_\parallel)\tilde{C}^{-1} = \mathcal{H}_U(-\boldsymbol{k}_\parallel),\ \tilde{C} = \begin{pmatrix} C & 0 \\ 0 & C \end{pmatrix}, \tag{5.26}$$

$$\tilde{\Gamma}\mathcal{H}_U(\boldsymbol{k}_\parallel)\tilde{\Gamma}^{-1} = \mathcal{H}_U(\boldsymbol{k}_\parallel),\ \tilde{\Gamma} = \begin{pmatrix} 0 & \Gamma \\ \Gamma & 0 \end{pmatrix}. \tag{5.27}$$

Therefore, $\mathcal{H}_U(\boldsymbol{k}_\parallel)$ can be regarded as a topological insulator or superconductor with symmetries in Eq. (5.24) and Eqs. (5.25)-(5.27). As shown in Sec 1.1.3, by using the standard Clifford algebra extension method [14, 17], we can obtain the topological classification of $\mathcal{H}_U(\boldsymbol{k}_\parallel)$, which provides a topological classification of the boundary operator $U(\boldsymbol{k}_\parallel)$. The resultant classification of $U_{\mathrm{BDQW}}(\boldsymbol{k}_\parallel)$ in $(d-1)$-dimensions is equivalent to the classification of conventional topological insulators and superconductors in d-dimensions [Table 5.2]. The topological invariant of $\mathcal{H}_U(\boldsymbol{k}_\parallel)$ gives the topological invariant n in Eq. (5.22).

Attaching the boundary unitary operator of nonzero n to any boundary of quantum walks, we can change the number of gapless boundary states, in accordance with the extended Nielsen-Ninomiya theorem in Eq. (5.22): The net number of boundary states changes as

$$\sum_{\epsilon_\alpha=0} \nu_\alpha^0 \to \sum_{\epsilon_\alpha=0} \nu_\alpha^0 + n, \tag{5.28}$$

$$\sum_{\epsilon_\alpha=\pi} \nu_\alpha^\pi \to \sum_{\epsilon_\alpha=\pi} \nu_\alpha^\pi + (-1)^d n. \tag{5.29}$$

On the other hand, for even (odd) dimensions d, the difference (summation) of the boundary states between $\epsilon = 0$ and $\epsilon = \pi$ does not change during this boundary deformation, so it is intrinsically determined by the bulk topological invariant n_{bulk} of $H_{\text{QW}}(\boldsymbol{k})$ as

$$\sum_{\epsilon_\alpha=0} \nu_\alpha^0 - (-1)^d \sum_{\epsilon_\alpha=\pi} \nu_\alpha^\pi = n_{\text{bulk}}. \tag{5.30}$$

Therefore, the bulk-boundary correspondence partially holds in quantum walks.

For classes A, AI, and AII, we can arbitrarily choose the energy gaps because there is no symmetry constraint on the quasi-energy. If there are l energy gaps $\epsilon = \mu_i$ $(i = 1, \dots, l)$, the topological classification of the gapless boundary states in Table 5.1 changes as $\mathbb{Z}^2 \to \mathbb{Z}^l$, $\mathbb{Z}_2^2 \to \mathbb{Z}_2^l$, and $(2\mathbb{Z})^2 \to (2\mathbb{Z})^l$. In these cases, the extended Nielsen-Ninomiya theorem in Eq. (5.22) can be rewritten as

$$\sum_{\epsilon_\alpha=\mu} \nu_\alpha^\mu = n, \tag{5.31}$$

where ν_α^μ is the topological charge of α-th gapless state at $\epsilon = \mu$. We note that this formula is compatible with Eq. (5.22) even for odd d since in class A, AI and AII, the topological invariants n of $U_{\text{BDQW}}(\boldsymbol{k}_\parallel)$ is always 0 or $\mathbb{Z}_2$ for odd d.

5.3 Extrinsic boundary states of quantum walks in 1D

Topological phenomena in quantum walks have been studied mainly in 1D [30, 39, 40, 162–165, 167–170]. In this section, we study extrinsic topological phases of quantum walks in 1D (extrinsic boundary states in 0D). According to the periodic table in Table 5.2, nontrivial extrinsic topological phases exist for classes AIII, BDI, D, DIII, and CII in 1D. We identify the topological invariants n and topological charges $\nu^{0,\pi}$ for these classes, and see that they obey the extended Nielsen-Ninomiya theorem in Eq. (5.22).

5.3.1 class AIII

A boundary quantum walk operator U_{BDQW} in class AIII 1D quantum walks is a unitary matrix obeying

$$\Gamma U_{\text{BDQW}}^\dagger \Gamma^{-1} = U_{\text{BDQW}}, \quad \Gamma^2 = 1, \tag{5.32}$$

with a unitary matrix Γ. $U_{\text{BDQW}}\Gamma$ is Hermitian from this relation, and it has nonzero real eigenvalues because of $\det[U_{\text{BDQW}}\Gamma] \neq 0$. Thus, we can define the $\mathbb{Z}$-valued topological invariant n

in Eq. (5.22) as

$$n = \frac{1}{2}\left[N_{+}(U_{\mathrm{BDQW}}\Gamma) - N_{-}(U_{\mathrm{BDQW}}\Gamma)\right], \tag{5.33}$$

where $N_{+}(U_{\mathrm{BDQW}}\Gamma)$ ($N_{-}(U_{\mathrm{BDQW}}\Gamma)$) is the number of positive (negative) eigenvalues of $U_{\mathrm{BDQW}}\Gamma$. We can also introduce the topological charge $\nu^{0,\pi}$ of gapless modes at $\epsilon = 0, \pi$ as follows. For a gapless mode $|u_0\rangle$ at $\epsilon = 0$, we have

$$U_{\mathrm{BDQW}}|u_0\rangle = |u_0\rangle, \quad U^{\dagger}_{\mathrm{BDQW}}|u_0\rangle = |u_0\rangle, \tag{5.34}$$

and CS implies for the latter relation as

$$U_{\mathrm{BDQW}}\Gamma|u_0\rangle = \Gamma|u_0\rangle. \tag{5.35}$$

Thus, $\Gamma\,|u_0\rangle$ may be $|u_0\rangle$ itself up to phase factor [4]. In other words, the gapless mode may be an eigenstate of Γ,

$$\Gamma\,|u_0\rangle = \pm\,|u_0\rangle\,. \tag{5.36}$$

Then, the eigenvalue of Γ defines the topological charge ν^0 fof $|u_0\rangle$. Similarly, we can also define ν^{π} for a gapless mode $|u_{\pi}\rangle$ at $\epsilon = \pi$. In summary, the topological invariants $\nu^{0,\pi}$ are given as

$$\nu^{0,\pi} = \langle u_{0,\pi}|\,\Gamma\,|u_{0,\pi}\rangle\,. \tag{5.37}$$

When n is nonzero, we have gapless modes according to the extended Nielsen-Ninomiya theorem in Eq. (5.22). To check the theorem, let us consider a general 2×2 unitary matrix in class AIII,

$$U_{\mathrm{BDQW}} = a_0\sigma_0 + ia_1\sigma_1 + ia_2\sigma_2 + a_3\sigma_3, \quad \Gamma = \sigma_3, \tag{5.38}$$

where a_{μ} are real parameters. The unitarity condition $U_{\mathrm{BDQW}}U^{\dagger}_{\mathrm{BDQW}} = 1$ leads to three possible cases:

$$\begin{cases} \text{(i) } a_3 = 0,\ a_0^2 + a_1^2 + a_2^2 = 1, \\ \text{(ii) } a_3 = 1, \\ \text{(iii) } a_3 = -1. \end{cases} \tag{5.39}$$

The eigenvalues of U_{BDQW} in each case are

$$\begin{cases} \text{(i) } \lambda_{\pm} = a_0 \pm i\sqrt{a_1^2 + a_2^2}, \\ \text{(ii), (iii) } \lambda_{\pm} = \pm 1. \end{cases} \tag{5.40}$$

[4] We can take as such by taking an appropriate basis.

The corresponding eigenstates in each case are

$$\begin{cases} \text{(i)} \ |u_\pm\rangle = \frac{1}{\sqrt{2(a_1^2+a_2^2)}} \begin{pmatrix} \pm i\sqrt{a_1^2+a_2^2} \\ ia_1 - a_2 \end{pmatrix}, \\ \text{(ii)} \ |u_+\rangle = (1,0)^{\mathrm{T}}, \ |u_-\rangle = (0,1)^{\mathrm{T}}, \\ \text{(iii)} \ |u_+\rangle = (0,1)^{\mathrm{T}}, \ |u_-\rangle = (1,0)^{\mathrm{T}}. \end{cases} \tag{5.41}$$

which gives topological charges

$$\nu_\pm = \langle u_\pm | \Gamma | u_\pm \rangle = \begin{cases} 0 & \text{for (i)}, \\ \pm 1 & \text{for (ii)}, \\ \mp 1 & \text{for (iii)}, \end{cases} \tag{5.42}$$

Therefore, we have

$$\sum \nu^0 = -\sum \nu^\pi = \begin{cases} 0 & \text{for (i)}, \\ +1 & \text{for (ii)}, \\ -1 & \text{for (iii)}. \end{cases} \tag{5.43}$$

Now we compare this result with the topological invariant n. The Hermitian matrix $U_{\text{BDQW}}\Gamma$ is

$$U_{\text{BDQW}}\Gamma = \begin{cases} a_0\sigma_3 + a_1\sigma_2 - a_2\sigma_1 & \text{for (i)}, \\ +\sigma_0 & \text{for (ii)}, \\ -\sigma_0 & \text{for (iii)}, \end{cases} \tag{5.44}$$

with eigenvalues

$$\mathcal{E} = \begin{cases} \pm 1 & \text{for (i)}, \\ +1 & \text{for (ii)}, \\ -1 & \text{for (iii)}. \end{cases} \tag{5.45}$$

Thus, n in Eq. (D.30) becomes

$$n = \begin{cases} 0 & \text{for (i)}, \\ +1 & \text{for (ii)}, \\ -1 & \text{for (iii)}. \end{cases} \tag{5.46}$$

Equations. (5.43) and (5.46) are compatible with the extended Nielsen-Ninomiya theorem in Eq. (5.22).

5.3.2 class BDI

A boundary unitary operator in class BDI obeys TRS and PHS,

$$\begin{aligned} TU_{\text{BDQW}}T^{-1} &= U_{\text{BDQW}}^\dagger, \\ CU_{\text{BDQW}}C^{-1} &= U_{\text{BDQW}}, \end{aligned} \tag{5.47}$$

where T and C are anti-unitary operators with $CT = TC$ and $T^2 = C^2 = 1$. By combining TRS with PHS, the boundary operator also obeys CS,

$$\Gamma U_{\mathrm{BDQW}}^{\dagger} \Gamma^{-1} = U_{\mathrm{BDQW}}, \quad \Gamma = TC. \tag{5.48}$$

Using CS, the topological invariant n of U_{BDQW} and the topological charge $\nu^{0,\pi}$ of gapless modes at $\epsilon = 0, \pi$ are given in the same manner as the case in class AIII.

The theorem in Eq. (5.22) can be checked in the same way as class AIII. A general 2×2 unitary matrix in class BDI is given by

$$\begin{aligned} &U_{\mathrm{BDQW}} = a_0\sigma_0 + ia_1\sigma_1 + a_3\sigma_3, \\ &T = K, \quad C = \sigma_3 K, \end{aligned} \tag{5.49}$$

where a_μ are real parameters, and K is the complex conjugation operator. From $U_{\mathrm{BDQW}} U_{\mathrm{BDQW}}^{\dagger} = 1$, we have three possible cases:

$$\begin{cases} \text{(i) } a_3 = 0, \ a_0^2 + a_1^2 = 1, \\ \text{(ii) } a_3 = 1, \\ \text{(iii) } a_3 = -1. \end{cases} \tag{5.50}$$

Then, U_{BDQW} in Eq. (5.49) obeys the extended Nielsen-Ninomiya theorem since it is a special case of Eq. (5.38) with $a_2 = 0$.

5.3.3 class D

A boundary operator U_{BDQW} in class D satisfies

$$C U_{\mathrm{BDQW}} C^{-1} = U_{\mathrm{BDQW}}, \quad C^2 = 1, \tag{5.51}$$

with an anti-unitary operator C. This relation implies that $\det(U_{\mathrm{BDQW}})$ is real, and thus it takes only the values ± 1. Therefore, we can define the $\mathbb{Z}_2$-valued topological invariant n of U_{BDQW} by

$$(-1)^n = \det(U_{\mathrm{BDQW}}). \tag{5.52}$$

On the other hand, the topological charge $\nu^{0,\pi}$ is given by the presence or absence of a gapless state at $\epsilon = 0, \pi$. We note that an even number of gapless states trivializes $\nu^{0,\pi}$ as a consequence of the $\mathbb{Z}_2$ structure.

A general 2×2 unitary matrix in class D is given by

$$U_{\mathrm{BDQW}} = a_0\sigma_0 + a_1\sigma_1 + ia_2\sigma_2 + a_3\sigma_3, \quad C = K, \tag{5.53}$$

Then, the unitarity condition for U_{BDQW} leads to two possible cases:

$$\begin{cases} \text{(i) } a_0 = a_2 = 0, \ a_1^2 + a_3^2 = 1, \\ \text{(ii) } a_1 = a_3 = 0, \ a_0^2 + a_2^2 = 1, \end{cases} \tag{5.54}$$

where the eigenvalues of U_{BDQW} are given as

$$\begin{cases} \text{(i) } \lambda_{\pm} = \pm 1, \\ \text{(ii) } \lambda_{\pm} = a_0 \pm i a_2. \end{cases} \tag{5.55}$$

Thus, only for (i), we have a single gapless mode exists at $\epsilon = 0, \pi$. Thus, we obtain

$$\sum \nu^0 = -\sum \nu^\pi = \begin{cases} 1 & \text{for (i)}, \\ 0 & \text{for (ii)}. \end{cases} \tag{5.56}$$

On the other hand, through a direct calculation, we have

$$\det(U_{\text{BDQW}}) = a_0^2 + a_2^2 - a_1^2 - a_3^2, \tag{5.57}$$

and thus, the $\mathbb{Z}_2$-valued invariant n in Eq. (5.52) is

$$n = \begin{cases} 1 & \text{for (i)}, \\ 0 & \text{for (ii)}. \end{cases} \tag{5.58}$$

The topological invariants and the topological charges of gapless states in Eqs. (5.56) and (5.58) satisfy the extended Nielsen-Ninomiya theorem in Eq. (5.22).

5.3.4 class DIII

A boundary unitary operator U_{BDQW} in class DIII obeys

$$\begin{aligned} T U_{\text{BDQW}} T^{-1} &= U_{\text{BDQW}}^\dagger, \\ C U_{\text{BDQW}} C^{-1} &= U_{\text{BDQW}}, \end{aligned} \tag{5.59}$$

where T and C are anti-unitary operators with $T^2 = -1$, $C^2 = 1$ and $CT = TC$. For convenience, we decompose anti-unitary operators T and C into the unitary parts $\mathcal{T}$ and $\mathcal{C}$ and the complex conjugation operator K:

$$T = \mathcal{T} K, \quad C = \mathcal{C} K. \tag{5.60}$$

Then, the matrix $iU_{\text{BDQW}}\mathcal{T}$ is found to be antisymmetric, so we can introduce the Pfaffian $\text{Pf}(U_{\text{BDQW}}\mathcal{T})$. We can also show

$$[\text{Pf}(U_{\text{BDQW}}\mathcal{T})]^* = \det(\mathcal{C}^*)\text{Pf}(iU_{\text{BDQW}}\mathcal{T}), \tag{5.61}$$

and thus, we have $\text{Pf}(U_{\text{BDQW}}\mathcal{T}) = \pm 1$ in the basis with $\det(\mathcal{C}^*) = 1$. Then, the sign of the Pfaffian defines the $\mathbb{Z}_2$-valued invariant n for U_{BDQW}:

$$(-1)^n = -\text{Pf}(U_{\text{BDQW}}\mathcal{T}). \tag{5.62}$$

On the other hand, for gapless states at $\epsilon = 0, \pi$, the presence or absence of a Kramers pair of gapless states defines the $\mathbb{Z}_2$-valued topological charge $\nu^{0,\pi}$. Note that any eigenstate of U_{BDQW} is two-fold degenerates due to the Kramers theorem for TRS.

To obtain a non-trivial example, we need at least a 4×4 unitary matrix in class DIII. We consider a general 4×4 unitary matrix in class DIII,

$$\begin{aligned} U_{\text{BDQW}} = & a_{00}\tau_0\sigma_0 + a_{10}\tau_1\sigma_0 + a_{30}\tau_3\sigma_0 \\ & + ia_{21}\tau_2\sigma_1 + ia_{22}\tau_2\sigma_2 + a_{23}\tau_2\sigma_3, \end{aligned} \tag{5.63}$$

where TRS and PHS are given by $T = \tau_0\sigma_2 K$ and $C = \tau_0\sigma_1 K$. From the unitarity condition $U_{\text{BDQW}}U^{\dagger}_{\text{BDQW}} = 1$, we obtain two possible cases,

$$\begin{cases} \text{(i) } a_{00} = a_{21} = a_{22} = 0, \ a_{30}^2 + a_{10}^2 + a_{23}^2 = 1, \\ \text{(ii) } a_{30} = a_{10} = a_{23} = 0, \ a_{00}^2 + a_{21}^2 + a_{22}^2 = 1. \end{cases} \tag{5.64}$$

The eigenvalues of U_{BDQW} with Kramers degeneracy are

$$\begin{cases} \text{(i) } \lambda_{\pm} = \pm 1, \\ \text{(ii) } \lambda_{\pm} = a_{00} \pm i\sqrt{a_{21}^2 + a_{22}^2}, \end{cases} \tag{5.65}$$

and thus, the system supports a single Kramers pair of gapless states at $\epsilon = 0, \pi$ for (i). Therefore, we have

$$\sum \nu^0 = -\sum \nu^{\pi} = \begin{cases} 1 & \text{for (i)}, \\ 0 & \text{for (ii)}. \end{cases} \tag{5.66}$$

On the other hand, $\text{Pf}(U_{\text{QW}}\mathcal{T})$ becomes

$$\text{Pf}(iU_{\text{BDQW}}\mathcal{T}) = a_{30}^2 + a_{10}^2 + a_{23}^2 - a_{00}^2 - a_{21}^2 - a_{22}^2, \tag{5.67}$$

so the topological invariant n in Eq. (5.62) is evaluated as

$$n = \begin{cases} 1 & \text{for (i)}, \\ 0 & \text{for (ii)}, \end{cases} \tag{5.68}$$

which is compatible wihe the extended Nielsen-Ninomiya theorem in Eq. (5.22).

5.3.5 class CII

We finally examine boundary unitary operators for class CII quantum walks in 1D. The boundary unitary operator obeys

$$\begin{aligned} TU_{\text{BDQW}}T^{-1} &= U^{\dagger}_{\text{BDQW}}, \\ CU_{\text{BDQW}}C^{-1} &= U_{\text{BDQW}}, \end{aligned} \tag{5.69}$$

where T and C are anti-unitary operators with $T^2 = -1$, $C^2 = -1$ and $CT = TC$. Combining TRS and PHS, we also have CS,

$$\Gamma U^{\dagger}_{\text{BDQW}}\Gamma^{-1} = U_{\text{BDQW}}, \quad \Gamma = TC. \tag{5.70}$$

Using CS, we can introduce the topological invariants n and $\nu^{0,\pi}$ in Eqs. (D.30) and (5.37) in the same manner as those in class AIII. However, in contrast to class AIII, because of additional TRS in Eq. (5.69), these topological invariants only take even integers. First, the Hermitian matrix $U_{\mathrm{BDQW}}\Gamma$ has its own TRS for C as

$$C[U_{\mathrm{BDQW}}\Gamma]C^{-1} = U_{\mathrm{BDQW}}\Gamma, \tag{5.71}$$

which results in the Kramers degeneracy for the eigenstates of $U_{\mathrm{BDQW}}\Gamma$. Therefore,

$$n = \frac{1}{2}\left[N_+(U_{\mathrm{BDQW}}\Gamma) - N_-(U_{\mathrm{BDQW}}\Gamma)\right], \tag{5.72}$$

in Eq. (D.30) becomes a $2\mathbb{Z}$-valued topological invariant. Furthermore, gapless modes at $\epsilon = 0, \pi$ also form Kramers pairs due to the original TRS of T. The Kramers pairs have a common eigenvalue of Γ since T commutes with Γ, so the net charges $\sum \nu^{0,\pi}$ of gapless modes with $\nu^{0,\pi}$ defined by Eq. (5.37) also become even integers.

A general 4×4 unitary matrix in class CII is

$$\begin{aligned} U_{\mathrm{BDQW}} = {} & a_{00}\tau_0\sigma_0 + ia_{10}\tau_1\sigma_0 + a_{30}\tau_3\sigma_0 \\ & + ia_{21}\tau_2\sigma_1 + ia_{22}\tau_2\sigma_2 + ia_{23}\tau_2\sigma_3, \end{aligned} \tag{5.73}$$

with $T = \tau_0\sigma_2 K$ and $C = \tau_3\sigma_2 K$. The unitarity condition of $U_{\mathrm{BDQW}}U_{\mathrm{BDQW}}^\dagger = 1$ leads to the following three possible cases:

$$\begin{cases} \text{(i) } a_{30} = 0,\ a_{00}^2 + a_{10}^2 + a_{21}^2 + a_{22}^2 + a_{23}^2 = 1, \\ \text{(ii) } a_{30} = 1,\ a_{00} = a_{10} = a_{21} = a_{22} = a_{23} = 0, \\ \text{(iii) } a_{30} = -1,\ a_{00} = a_{10} = a_{21} = a_{22} = a_{23} = 0. \end{cases} \tag{5.74}$$

The eigenvalues of U_{BDQW} of Kramers degeneracy are

$$\begin{cases} \text{(i) } \lambda_\pm = a_{00} \pm i\sqrt{a_{10}^2 + a_{21}^2 + a_{22}^2 + a_{23}^2}, \\ \text{(ii) } \lambda_\pm = \pm 1, \\ \text{(iii) } \lambda_\pm = \pm 1. \end{cases} \tag{5.75}$$

and thus the boundary supports nontrivial gapless states at $\epsilon = 0, \pi$ for (ii) and (iii). Then, we can see that each Kramers pair satisfies

$$\nu_\pm = \langle u_\pm|\,\Gamma\,|u_\pm\rangle = \begin{cases} 0 & \text{for (i)}, \\ \mp 1 & \text{for (ii)}, \\ \pm 1 & \text{for (iii)}, \end{cases} \tag{5.76}$$

and thus, we have

$$\sum \nu^0 = -\sum \nu^\pi = \begin{cases} 0 & \text{for (i)}, \\ -2 & \text{for (ii)}, \\ +2 & \text{for (iii)}. \end{cases} \tag{5.77}$$

On the other hand, the Hermitian matrix $U_{\mathrm{BDQW}}\Gamma$ has the form

$$\begin{aligned} U_{\mathrm{BDQW}}\Gamma = {} & a_{00}\tau_3\sigma_0 + a_{10}\tau_2\sigma_0 + a_{30}\tau_0\sigma_0 \\ & - a_{21}\tau_1\sigma_1 - a_{22}\tau_1\sigma_2 - a_{23}\tau_1\sigma_3. \end{aligned} \tag{5.78}$$

The eigenvalues are

$$\mathcal{E} = -a_{30} \pm \sqrt{a_{00}^2 + a_{10}^2 + a_{21}^2 + a_{22}^2 + a_{23}^2}, \tag{5.79}$$

with two-fold Kramers degeneracy. Thus, the topological invariant n in Eq. (D.30) is evaluated as

$$n = \begin{cases} 0 & \text{for (i)}, \\ -2 & \text{for (ii)}, \\ +2 & \text{for (iii)}. \end{cases} \tag{5.80}$$

The results in Eqs. (5.77) and (5.80) is compatible with the extended Nielsen-Ninomiya theorem in Eq. (5.22).

5.4 Classification of Floquet systems v.s. quantum walks

In this section, we compare the topological classification of quantum walks with that of Floquet systems. We firstly give a brief review of the topological classification of Floquet topological insulators and superconductors [33]. We consider a general time periodic Hamiltonian $H(\boldsymbol{k}, t+T) = H(\boldsymbol{k}, t)$ and the corresponding time-evolution operator

$$U(\boldsymbol{k}, t) = \mathcal{T} \exp\left[-i \int_0^t dt H(\boldsymbol{k}, t)\right]. \tag{5.81}$$

From the one-cycle time evolution $U_F(\boldsymbol{k}) = U(\boldsymbol{k}, T)$, we define the effective Hamiltonian through $U_F(\boldsymbol{k}) = e^{-iH_F(\boldsymbol{k})T}$. The AZ symmetries, TRS, PHS and CS in Floquet systems are defined for the microscopic Hamiltonian as:

$$TH(\boldsymbol{k}, t)T^{-1} = H(-\boldsymbol{k}, -t), \tag{5.82}$$
$$CH(\boldsymbol{k}, t)C^{-1} = -H(-\boldsymbol{k}, t), \tag{5.83}$$
$$\Gamma H(\boldsymbol{k}, t)\Gamma^{-1} = -H(\boldsymbol{k}, -t). \tag{5.84}$$

Here, T and C are anti-unitary operators with $T^2 = \pm 1$ and $C^2 = \pm 1$, and Γ is a unitary operator of $\Gamma^2 = 1$. These symmetries lead to TRS, PHS and CS for the effective Hamiltonian $H_F(\boldsymbol{k})$:

$$TH_F(\boldsymbol{k})T^{-1} = H_F(-\boldsymbol{k}), \tag{5.85}$$
$$CH_F(\boldsymbol{k})C^{-1} = -H_F(-\boldsymbol{k}), \tag{5.86}$$
$$\Gamma H_F(\boldsymbol{k})\Gamma^{-1} = -H_F(\boldsymbol{k}). \tag{5.87}$$

For convenience, we rewrite the symmetries as those for time-evolution operator $U(\boldsymbol{k}, t)$:

$$TU(\boldsymbol{k}, t)T^{-1} = U(-\boldsymbol{k}, -t), \tag{5.88}$$
$$CU(\boldsymbol{k}, t)C^{-1} = U(-\boldsymbol{k}, t), \tag{5.89}$$
$$\Gamma U(\boldsymbol{k}, t)\Gamma^{-1} = U(\boldsymbol{k}, -t). \tag{5.90}$$

Instead of the microscopic Hamiltonian $H(\boldsymbol{k},t)$, we classify the time-evolution operator $U(\boldsymbol{k},t)$ because it has the same information as $H(\boldsymbol{k},t)$. [5] We then decompose $U(\boldsymbol{k},t)$ into two parts:

$$C(\boldsymbol{k},t) = e^{-iH_F(\boldsymbol{k})t}, \quad L(\boldsymbol{k},t) = U(\boldsymbol{k},t)C(\boldsymbol{k},t)^{-1}, \tag{5.91}$$

where $L(\boldsymbol{k},t)$ is periodic in t. We call $C(\boldsymbol{k},t)$ and $L(\boldsymbol{k},t)$ as the "constant time evolution" and the "loop unitary", each. We have supposed $H_F(\boldsymbol{k})$ is gapped both at $\epsilon = 0,\ \pi/T$ and have taken the branch cut at $\epsilon = \pi/T$, One can show this decomposition is unique up to homotopy equivalence [33]. Thus the topological classification problem of $U(\boldsymbol{k},t)$ reduces to those of the constant time evolution $C(\boldsymbol{k},t)$ and the loop unitary $L(\boldsymbol{k},t)$.

The topological classification of $C(\boldsymbol{k},t)$ is equivalent to that of $H_F(\boldsymbol{k})$, and thus the same as that of usual topological insulators and superconductors. It it the same as the classification of $H_{\mathrm{QW}}(\boldsymbol{k})$ in the previous section.

On the other hand, the loop unitary $L(\boldsymbol{k},t)$ allows the Floquet anomalous topological phase intrinsic to Floquet systems [27]. Remarkably, for a very different reason, the topological classification of $L(\boldsymbol{k},t)$ also coincides with that of usual topological insulators and superconductors as shown below: One can classify $L(\boldsymbol{k},t)$ by introducing the doubled Hamiltonian $\mathcal{H}_L(\boldsymbol{k},t)$,

$$\mathcal{H}_L(\boldsymbol{k},t) = \begin{pmatrix} 0 & L(\boldsymbol{k},t) \\ L^\dagger(\boldsymbol{k},t) & 0 \end{pmatrix}, \tag{5.92}$$

which is Hermitian, gapped due to $\mathcal{H}_L(\boldsymbol{k},t)^2 = \hat{1}$, periodic both in $\boldsymbol{k}$ and t, and obeys the proper CS

$$\Sigma_z \mathcal{H}_L(\boldsymbol{k},t)\Sigma_z = -\mathcal{H}_L(\boldsymbol{k},t),\ \Sigma_z = \begin{pmatrix} \hat{1} & 0 \\ 0 & -\hat{1} \end{pmatrix}. \tag{5.93}$$

Since $L(\boldsymbol{k},t)$ obeys the same symmetries as $U(\boldsymbol{k},t)$ in Eqs. (5.88)-(5.90), $\mathcal{H}_L(\boldsymbol{k},t)$ obeys

$$\tilde{T}\mathcal{H}_L(\boldsymbol{k},t)\tilde{T}^{-1} = \mathcal{H}_L(-\boldsymbol{k},-t),\ \tilde{T} = \begin{pmatrix} T & 0 \\ 0 & T \end{pmatrix}, \tag{5.94}$$

$$\tilde{C}\mathcal{H}_L(\boldsymbol{k},t)\tilde{C}^{-1} = \mathcal{H}_L(-\boldsymbol{k},t),\ \tilde{C} = \begin{pmatrix} C & 0 \\ 0 & C \end{pmatrix}, \tag{5.95}$$

$$\tilde{\Gamma}\mathcal{H}_L(\boldsymbol{k},t)\tilde{\Gamma}^{-1} = \mathcal{H}_L(\boldsymbol{k},-t),\ \tilde{\Gamma} = \begin{pmatrix} \Gamma & 0 \\ 0 & \Gamma \end{pmatrix}. \tag{5.96}$$

Therefore, by regarding t as a momentum k_{d+1} and thus $\mathcal{H}_L(\boldsymbol{k},t)$ as a $(d+1)$-dimensional topological insulator with proper symmetries shown above, we can classify $L(\boldsymbol{k},t)$. As shown in Sec. 1.1.1, one can perform the classification by using the Clifford algebra extension method [14, 17], and find that the classification coincides with that of ordinary topological insulators and superconductors in d-dimensions for each of AZ symmetry classes. Thus, we see the periodic table of $L(\boldsymbol{k},t)$ is the same as that of extrinsic topological phases in quantum walks [Table 5.2].

Therefore, combining the classifications of $C(\boldsymbol{k},t)$ and $L(\boldsymbol{k},t)$, we find that the periodic

[5] If a $H(\boldsymbol{k},t)$ is given, we uniquely obtain $U(\boldsymbol{k},t)$ as the corresponding time-evolution operator. On the other hand, if a $U(\boldsymbol{k},t)$ is given, we uniquely obtain $H(\boldsymbol{k},t)$ by Schrödinger equation.

table of $U(\boldsymbol{k}, t)$ agrees with the boundary classification of quantum walks in Table 5.1. Furthermore, the bulk-boundary correspondence in Floquet systems can be summarized as [33]

$$\sum_{\epsilon_\alpha=0} \nu_\alpha^0 = n_{\mathrm{C}} + n_{\mathrm{L}}, \tag{5.97}$$

$$\sum_{\epsilon_\alpha=\pi/T} \nu_\alpha^\pi = (-1)^d n_{\mathrm{L}}, \tag{5.98}$$

where n_C is the topological invariant calculated from $C(\boldsymbol{k}, t)$ or equivalently $H_F(\boldsymbol{k})$, and n_L is the topological invariant calculated from $L(\boldsymbol{k}, t)$, and $\nu_\alpha^{0,\pi}$ is the topological charge of α-th gapless states at $\epsilon = 0$ or π/T. This formula corresponds to the combination of Eq. (5.29) and Eq. (5.30) in quantum walks.

In summary, extrinsic boundary states determined by the boundary topology of quantum walks correspond to the boundary states determined by $L(\boldsymbol{k}, t)$ of Floquet systems. In other words, the extrinsic gapless boundary states in quantum walks correspond to the Floquet anomalous boundary states. We note that no well-defined loop unitary exists in quantum walks due to the absence of the microscopic Hamiltonian $H(\boldsymbol{k}, t)$: Even though one can introduce $L(\boldsymbol{k}, t)$ for a quantum walk in some ways [166], the constructions are not unique. For instance, the same one-cycle time-evolution operator for the quantum walk can be constructed by the constant microscopic Hamiltonian $H(\boldsymbol{k}, t) = H_{\mathrm{QW}}(\boldsymbol{k})$, for which $L(\boldsymbol{k}, t) = \hat{1}$. As a result, we constructed a microscopic Hamiltonian with $n_{\mathrm{L}} = 0$. Thus, n_{L} cannot be uniquely determined in quantum walks. This observation is also consistent with the extrinsic topological nature of Floquet anomalous boundary states in quantum walks.

5.5 Bulk-boundary correspondence in 1D chiral-symmetric quantum walks

For 1D chiral-symmetric quantum walks, it has been known that the bulk-boundary correspondence holds [30] for a specific definition of CS different from ours. In this section, we explain why the bulk topological invariants fully determine gapless boundary states in their definition of CS, and also discuss another possibility of a similar bulk-boundary correspondence in other symmetry classes.

We first review a specific realization of CS given in Ref. [30]. To define CS, Asbóth and Obuse decomposed the time-evolution unitary operator of a quantum walk into two half-period time evolutions

$$U_{\mathrm{QW}} = U_2 U_1, \tag{5.99}$$

where U_1 and U_2 may also consist of multiple unitary operators. Then, they introduce the decomposed CS as [30],

$$\Gamma U_1 \Gamma^{-1} = U_2^\dagger, \quad \Gamma^2 = 1, \tag{5.100}$$

for a unitary operator $\Gamma^2 = 1$, which leads to the original CS in Eq. (5.20) we have shown. We note that Floquet systems with CS in Eq. (5.84) naturally satisfy Eq. (5.100) by regarding U_1 and U_2 as continuous time-evolution operators as $U_1 = U(0 \to T/2)$ and $U_2 = U(T/2 \to T)$.

Under the decomposed CS, one can see that the bulk-boundary correspondence holds [30, 38]. For this purpose, we take the basis where Γ and U_1 becomes

$$\Gamma = \begin{pmatrix} \hat{1} & 0 \\ 0 & -\hat{1} \end{pmatrix},\; U_1 = \begin{pmatrix} a & b \\ c & d \end{pmatrix}, \tag{5.101}$$

and we note that if the band gap at $\epsilon = 0$ ($\epsilon = \pi$) is open, b and c (a and d) have the well-defined 1D winding number $w_1[b]$ and $w_1[c]$ ($w_1[a]$ and $w_1[d]$) [38]. Then, we have the bulk-boundary correspondence [30],

$$\begin{cases} \displaystyle\sum_{\epsilon_\alpha=0} \nu_\alpha^0 = \frac{w_1[b] - w_1[c]}{2}, \\ \displaystyle\sum_{\epsilon_\alpha=\pi} \nu_\alpha^\pi = \frac{w_1[a] - w_1[d]}{2}, \end{cases} \tag{5.102}$$

where $\nu_\alpha^{0,\pi}$ is the topological charge of boundary zero modes in Eq. (5.37). Therefore, the net topological charges of boundary modes at $\epsilon = 0$ and $\epsilon = \pi$ are determined by the bulk topological invariants. In other words, no extrinsic boundary modes exist under the decomposed CS in Eq. (5.100).

We can easily see why extrinsic boundary modes are prohibited under CS in Eq. (5.100) from our theory. Using the decomposed CS, $U_{\mathrm{QW}}\Gamma$ is recast into

$$U_{\mathrm{QW}}\Gamma = U_2 U_1 \Gamma = U_2(\Gamma^{-1} U_2^\dagger \Gamma)\Gamma = U_2 \Gamma U_2^\dagger, \tag{5.103}$$

which is a unitary transformation of Γ by U_2. Therefore, any boundary operator U_{BDQW} satisfying the decomposed CS in Eq. 5.100 also has the form

$$U_{\mathrm{BDQW}}\Gamma = U_2' \Gamma U_2'^\dagger. \tag{5.104}$$

From this, we can show that the 0D topological number n in Eq. (D.30) becomes zero: Because of the above form, $U_{\mathrm{BDQW}}\Gamma$ has the same eigenvalues as Γ, and thus the occupied states and unoccupied states of $U_{\mathrm{BDQW}}\Gamma$ are the same, so we have

$$n = \frac{1}{2}[N_+(U_{\mathrm{BDQW}}\Gamma) - N_-(U_{\mathrm{BDQW}}\Gamma)] = 0. \tag{5.105}$$

Therefore, the boundary unitary operator cannot give additional zero modes. Thus, in 1D quantum walks with the decomposed CS Eq. (5.100), the bulk topological invariants uniquely determine the net numbers of boundary states at $\epsilon = 0, \pi$.

Whereas the decomposed CS in Eq. (5.100) prohibits the extrinsic gapless states at boundaries of 1D systems, it may allow extrinsic topological phases in other dimensions. For instance, extrinsic gapless boundary states of 3D systems are allowed under the decomposed CS Eq. (5.100). The topological invariant for a 2D boundary operator $U_{\mathrm{BDQW}}(k_x, k_y)$ with CS is the Chern number of $U_{\mathrm{BDQW}}(k_x, k_y)\Gamma$. Equation (5.104) merely implies that $U_{\mathrm{BDQW}}\Gamma$ is diagonalized by U_2', so it should be possible to realize arbitrary Chern numbers by choosing a proper U_2'. Consequently, we can add arbitrary numbers of 2D extrinsic boundary states to three-dimensional quantum walks under the decomposed CS Eq. (5.100).

One may ask a question if there is any other symmetry class that can recover the bulk-boundary correspondence with an appropriate definition of symmetries. The answer is YES! We find 1D quantum walks in class CII have full bulk-boundary correspondence under an appropriate realization of symmetries. To see this, we again decompose the one-cycle time-evolution of a quantum walk into two parts,

$$U_{\mathrm{QW}} = U_2 U_1. \tag{5.106}$$

Then, we introduce decomposed TRS and PHS, which give the original TRS and PHS for U_{QW} in Eq. (5.18) and (5.19),

$$TU_1(k)T^{-1} = U_2^\dagger(-k), \tag{5.107}$$
$$CU_1(k)C^{-1} = U_1(-k),\ CU_2(k)C^{-1} = U_2(-k). \tag{5.108}$$

Here T and C are anti-unitary operators with $CT = TC$ and $T^2 = C^2 = -1$. Combining TRS and PHS, we also have the decomposed CS,

$$\Gamma U_1 \Gamma^{-1} = U_2^\dagger, \quad \Gamma = TC. \tag{5.109}$$

For the decomposed CS, we again take the basis in Eq. (5.101) and then obtain the bulk-boundary correspondence in Eq. (5.102). We note that the decomposed PHS in Eq. (5.108) leads to two-fold Kramers degeneracy, and thus the topological invariants and the topological charges of gapless states in Eq. (5.102) take only even integers. (See Appendix E.1.) Similarly to chiral-symmetric quantum walks, we can also see that 0D extrinsic boundary states are prohibited by Eq. (5.109). The 0D $2\mathbb{Z}$ topological invariant in Eq. (5.72) becomes always zero from the decomposed CS again.

5.6 Physical implementations

In this section, we exemplify three possible physical implementations of the extrinsic topological phases in quantum walks.

5.6.1 2D disordered systems with extrinsic edge modes

In this section, we examine the robustness of extrinsic edge modes against disorders, which is an analog of that of quantum Hall edge states against impurity scatterings [176]. In this section, we consider a simple single-band model with an extrinsic edge mode in quantum walks. The extrinsic edge mode is robust against impurities, and shows a unidirectional pumping along the edge, which is characterized by the topological winding number [26, 32, 42, 137, 168, 177].

We will consider the following single-band tight-binding model with random onsite potentials in 2D, which is typically used for the study of the Anderson localization:

$$\begin{aligned} H_A = \sum_{x,y} & J\,|x+1,y\rangle\langle x,y| + J\,|x,y+1\rangle\langle x,y| \\ & + h.c. + \delta_{x,y}\,|x,y\rangle\langle x,y|, \end{aligned} \tag{5.110}$$

where J is the hopping amplitude and $\delta_{x,y} \in [-W, W]$ is the random potential uniformly distributed on $[-W, W]$. As J and $\delta_{x,y}$ are real, the above Hamiltonian belongs to class AI and is topologically trivial. For class AI 2D cases, it is known that all the eigenstates are localized for

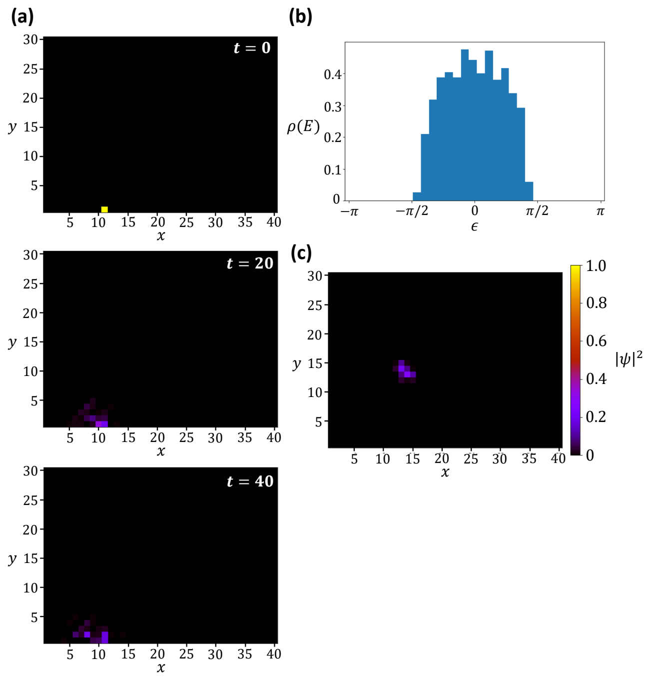

FIGURE 5.4: (a) Dynamics of a wave packet, (b) DOS and (c) a typical distribution of eigenstate of the Anderson model in Eq. (5.110). The parameters are $J = 0.2, W = 1, L_x = 25$ and $L_y = 15$. The initial state of the wave packet is $|x = 10, y = 1\rangle$, localized at an edge. We consider the strongly localized regime $W \gg J$, and thus we see all the eigenstates are localized. (a) We see that a wave packet starting from the edge does not diffuse into the bulk and shows a localization with almost the same radius as a bulk eigenstate. (b) The width of the quasi-energy band is broader than $2J$ due to the existence of random potential $\delta_{x,y} \in [-W, W]$. (c) The density distribution of a typical eigenstate shows the Anderson localization.

any W if the system is large enough [174]. Below, we impose PBC in the x-direction, and OBC in the y-direction.

The one-cycle time evolution by the Hamiltonian Eq. (5.110) is given by

$$U_A = e^{-iH_A T}. \tag{5.111}$$

with $T = 1$. The state at time step t is derived by multiplying the state by U_A^t. Figure 5.4 shows (a) the wave packet dynamics at time step t starting from a localized state at the edge, (b) the density of states (DOS) histogram, and (c) a typical eigenstate of U_A. The Anderson localization occurs for $W/J = 5$ in Fig. 5.4. After long time steps, the wave packet dynamics show a localization with almost the same radius as the typical eigenstate, and thus the wave packets do not diffuse into the bulk.

We next introduce an extrinsic chiral edge mode onto the boundary at $y = 1$. We multiply U_A by a unitary operator A that have a nontrivial anomaly at the edge,

$$A(k_x) = U_{\text{edge}}(k_x) \otimes |y = 1\rangle \langle y = 1| + \sum_{y=2}^{L_y} 1 \otimes |y\rangle \langle y| . \tag{5.112}$$

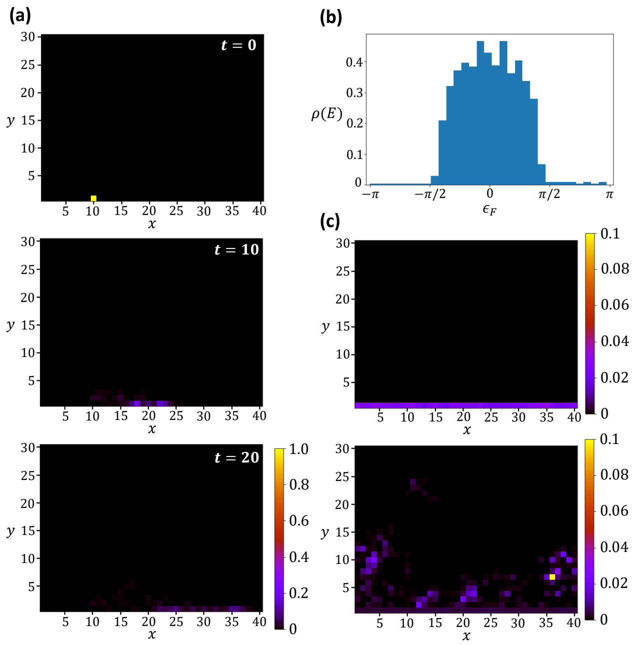

FIGURE 5.5: (a) Dynamics of a wave packet, (b) DOS and (c) adelocalized eigenstates of the decorated Anderson model with a boundary unitary in Eq. (5.113). The parameters are $J = 0.2$, $W = 1$, $L_x = 25$, $L_y = 15$ and $T = 1$. The color scales are different between (a) and (c). The initial state of the wave packet is $|x = 10, y = 1\rangle$. Since $W \gg J$, all bulk eigenstates are strongly localized. (a) The wave packet propagates in the $+x$-direction. (b) The nonzero DOS around $\epsilon = \pi$ implies the presence of an anomalous chiral edge mod. (c) Delocalized eigenstates with quasi-energies $\epsilon = 3.12$ and $\epsilon = 0.06$ are anomalous chiral edge mode.

where the edge unitary operator is given as $U_{\text{edge}}(k_x) = e^{-ik_x}$, and consider the decorated time-evolution operator as

$$U'_A = AU_A. \tag{5.113}$$

In the above sections, we have discussed the attachment of completely decoupled boundary unitary operators. In this section, however, we see attachments of boundary unitary operators coupled with the bulk. As discussed in Sec. 5.1, $U_{\text{edge}}(k_x)$ provides an extrinsic chiral edge mode $\epsilon = k_x$, which is robust against disorders as shown in the following.

Figure 5.5 shows (a) the dynamics of a wave packet starting at the decorated edge with $y = 1$, (b) the DOS histogram, and (c) a typical eigenstate distribution of U'_A. The wave packet propagates in the $+x$-direction, as we expected. Thus, the boundary unitary operator A induces a robust edge mode analogous to a quantum Hall edge state. We also find that the delocalized state along the edge survives even when the quasi-energy of chiral modes inside energy gaps is overlapped with bulk bands. This is due to the Anderson localization of the bulk states, which suppresses the mixing of the bulk states and the chiral edge modes. In Appendix E.4, we also show the extrinsic chiral edge mode is also robust against random phases along the edge at $y = 1$.

In general, we can characterize the unidirectional wave packet movement due to extrinsic chiral edge modes by the winding number in Eq. (5.5). To see this, we first consider the time evolution by $\hat{U}$ in 1D, then apply the result to the extrinsic edge modes in 2D.

For a quantum walk in 1D, we introduce the polarization at x as

$$P_x = \sum_{\alpha} \langle x,\alpha| \hat{x} |x,\alpha\rangle \,, \tag{5.114}$$

where $|x,\alpha\rangle$ represents a state localized at the position x with a internal degree of freedom α representing such as spin, orbital and so on. After one-cycle time evolution by $\hat{U}$, the polarization becomes

$$P_x(T) = \sum_{\alpha} \langle x,\alpha| \hat{U}^\dagger \hat{x} \hat{U} |x,\alpha\rangle \,. \tag{5.115}$$

If $\hat{U}$ obeys translation symmetry, one can show that the position displacement in one cycle equals the winding number [26, 32, 42, 137, 168, 177]

$$P_x(T) - P_x = w_1[U(k)], \tag{5.116}$$

where $U(k)$ is the momentum space representation of $\hat{U}$. The proof is given as follows: From the Fourier transformation, the polarization after one cycle in Eq. (5.115) is rewritten as

$$\begin{aligned}
P_x(T) &= \sum_{\alpha} \langle x| \langle\alpha| \hat{U}^\dagger \hat{x} \hat{U} |x\rangle |\alpha\rangle \\
&= \sum_{\alpha} \left[\frac{1}{\sqrt{L}} \sum_{k} e^{ikx} \langle k|\right] \langle\alpha| \hat{U}^\dagger \left[\sum_{x'} x' |x'\rangle \langle x'|\right] \\
&\quad \times \hat{U} \left[\frac{1}{\sqrt{L}} \sum_{k'} e^{-ik'x} |k'\rangle\right] |\alpha\rangle \\
&= \frac{1}{L^2} \sum_{\alpha,k,k',x'} e^{ikx} \langle\alpha| U^\dagger(k) e^{-ikx'} [-i\partial_{k'} e^{ik'x'}] \\
&\quad \times U(k') e^{-ik'x} |\alpha\rangle \,,
\end{aligned} \tag{5.117}$$

where $U(k)$ is a matrix on the space of internal degrees of freedom α. Using the partial integration and the discrete delta function of the form

$$\frac{1}{L} \sum_{x'} e^{i(k'-k)x'} = \delta_{k,k'}, \tag{5.118}$$

we have

$$\begin{aligned}
P_x(T) &= \frac{1}{L} \sum_{\alpha,k} e^{ikx} \langle\alpha| U^\dagger(k) i\partial_k [U(k) e^{-ikx}] |\alpha\rangle \\
&= \frac{1}{L} \sum_{\alpha,k} \langle\alpha| U^\dagger(k) [i\partial_k U(k)] |\alpha\rangle + \sum_{\alpha} x.
\end{aligned} \tag{5.119}$$

The first term on the right hand side becomes the winding number in Eq. (5.5)

$$\begin{aligned}
&\frac{1}{L}\sum_{\alpha,k}\langle\alpha|\,U^\dagger(k)[i\partial_k U(k)]\,|\alpha\rangle \\
&=\int_0^{2\pi}\frac{dk}{2\pi}\mathrm{tr}[U^\dagger(k)i\partial_k U(k)]=w_1[U(k)],
\end{aligned}\tag{5.120}$$

while the second term reproduces the polarization P_x

$$\sum_\alpha x=\sum_\alpha\langle x,\alpha|\,\hat{x}\,|x,\alpha\rangle=P_x.\tag{5.121}$$

Therefore, we have $P_x(T)=w_1[U(k)]+P_x$, and thus the formula in Eq. (5.116).

We check this formula in Eq. (5.116) for a simple example $U_{\mathrm{QW}}=S_+R(\theta)$ with

$$S_+=\begin{pmatrix}e^{-ik}&0\\0&1\end{pmatrix},\;R(\theta)=\begin{pmatrix}\cos\theta&-\sin\theta\\\sin\theta&\cos\theta\end{pmatrix},\tag{5.122}$$

which has nontrivial winding number $w_1[U_{\mathrm{QW}}(k)]=1$. Let us consider the initial states

$$|x,\uparrow\rangle=\begin{pmatrix}|x\rangle\\0\end{pmatrix},|x,\downarrow\rangle=\begin{pmatrix}0\\|x\rangle\end{pmatrix},\tag{5.123}$$

with the polarization

$$\begin{aligned}
P_x&=\langle x,\uparrow|\,\hat{x}\,|x,\uparrow\rangle+\langle x,\downarrow|\,\hat{x}\,|x,\downarrow\rangle\\
&=2x.
\end{aligned}\tag{5.124}$$

After one cycle, the states become

$$U_{\mathrm{QW}}\begin{pmatrix}|x\rangle\\0\end{pmatrix}=\begin{pmatrix}\cos\theta\,|x+1\rangle\\\sin\theta\end{pmatrix}|x\rangle\,,\tag{5.125}$$

$$U_{\mathrm{QW}}\begin{pmatrix}0\\|x\rangle\end{pmatrix}=\begin{pmatrix}-\sin\theta\,|x+1\rangle\\\cos\theta\,|x\rangle\end{pmatrix},\tag{5.126}$$

and we obtain

$$\begin{aligned}
P_x(T)=&\langle x,\uparrow|\,U^\dagger_{\mathrm{QW}}\hat{x}U_{\mathrm{QW}}\,|x,\uparrow\rangle\\
&+\langle x,\downarrow|\,U^\dagger_{\mathrm{QW}}\hat{x}U_{\mathrm{QW}}\,|x,\downarrow\rangle\\
=&\,2x+1=P_x+1.
\end{aligned}\tag{5.127}$$

Therefore, we have $P_x(T)-P_x=w_1[U_{\mathrm{QW}}]=1$, which is compatible with the formula in Eq. (5.116)

We generalize the above relation between the displacement and the winding number in the presence of disorders. For this purpose, we introduce the flux inserted unitary operator $\hat{U}(\Phi)$, where the hopping terms in $\hat{U}$ are modified by the uniform gauge potential $A_x=\Phi/L$ as

$|x+q\rangle\langle x| \to e^{-i(\Phi/L)q}|x+q\rangle\langle x|$ [82]. Then, we define its winding number [68]

$$w_1[\hat{U}(\Phi)] = \int_0^{2\pi} \frac{d\Phi}{2\pi} \mathrm{tr}[\hat{U}^\dagger(\Phi) i\partial_\Phi \hat{U}(\Phi)]. \tag{5.128}$$

Here we used that the flux inserted unitary operator $\hat{U}(\Phi)$ is periodic in Φ with the period 2π up to the large gauge transformation $\hat{U}_G = e^{-\frac{2\pi i}{L}\hat{x}}$ as $\hat{U}(\Phi+2\pi) = \hat{U}_G \hat{U}(\Phi) \hat{U}_G^\dagger$, and thus the winding number takes an integer. Similarly to Eq. (5.116), one can prove

$$P(T) - P = w_1[\hat{U}(\Phi)], \tag{5.129}$$

where $P(T) - P$ is an spatially averaged version of the one-cycle displacement $P_x(T) - P_x$. See Appendix E.2 for details.

Now, we extend the above results into the 2D systems. Since an extrinsic edge mode is localized along the edge $y = 1$ of the system, we consider the polarization projected along $y = 1$,

$$P_x|_{y=1} = \sum_\alpha \langle x, y=1, \alpha| \hat{x} |x, y=1, \alpha\rangle . \tag{5.130}$$

Then, the polarization after one cycle time evolution becomes

$$P_x(T)|_{y=1} = \sum_\alpha \langle x, y=1, \alpha| \hat{U}^\dagger \hat{x} \hat{U} |x, y=1, \alpha\rangle , \tag{5.131}$$

where $\hat{U}$ is the time-evolution operator in 2D systems. As shown in Appendix E.3, if the system has translation symmetry, the formula in Eq. (5.116) can be generalized as follows,

$$P_x(T)|_{y=1} - P_x|_{y=1} = w_P[U(k_x)], \tag{5.132}$$

where w_P is the winding number projected onto the edge, defined by

$$w_P[U(k_x)] = \int_0^{2\pi} \frac{dk_x}{2\pi} \mathrm{tr}_{y,\alpha} \left[\hat{P}_{\mathrm{edge}} U^\dagger(k_x) i\partial_{k_x} U(k_x)\right], \tag{5.133}$$

with the projection operator $\hat{P}_{\mathrm{edge}} = |y=1\rangle\langle y=1|$ at the edge. Similarly, if the system is subject to disorders, we have a generalization of Eq. (5.129) with the projected winding number for Eq. (5.128).

We remark that the projected winding number is not quantized in general because the wave packet at $y = 1$ diffuses into the bulk. If bulk states are gapped or localized, however, edge modes rarely diffuse into the bulk, so the quantization of the projected winding numbers is almost recovered. In such situations, an extrinsic chiral mode induces a unidirectional movement of wave packets along the edge since it has a non-trivial winding number. For instance, our model in 2D has a strongly localized bulk state as shown in Fig. 5.4 (c), and thus the above mechanism explains the wave packet dynamics in Fig. 5.5 (a). Here we note that the above argument does not require a bulk gap. In Fig. 5.6, we show the wave packet dynamics in the model of Eq. (5.113) with $W = 10, J = 1$, where the bulk band at $\epsilon = \pi$ is closed in the $+x$-direction and there exist delocalized eigenstates along the edge.

Finally, we discuss a noisy environment where the random potential in Eq. (5.110) fluctuates

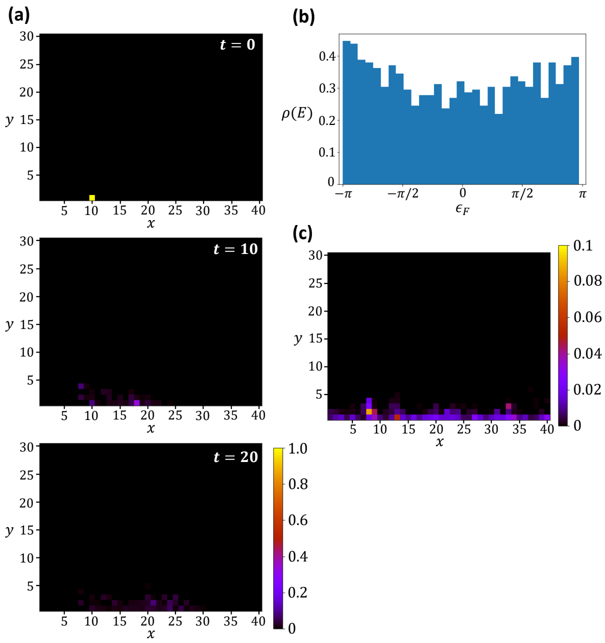

FIGURE 5.6: *In case of no band gap:* (a) Dynamics of a wave packet, (b) DOS and (c) a delocalized eigenstate of the decorated Anderson model with an extrinsic edge mode in Eq. (5.113). The parameters are $J = 1$, $W = 10$, $L_x = 25$, $L_y = 15$ and $T = 1$. The color scales are different between (a) and (c). The initial state of the wave packet is $|x = 10, y = 1\rangle$, localized at the edge. Due to $W \gg J$, all the bulk eigenstates are strongly localized. Whereas no band gap exists due to the strong random potential and the 2π periodicity in energy, the delocalized edge state survives and enables a unidirectional wave packet motion.

in each time step [162, 178–181]. Our numerical simulations show that the unidirectional wave packet motion because of the extrinsic chiral edge mode during the time scale shorter than diffusion. In Fig. 5.7, we compare the t-step dynamics defined as

$$U_{\mathrm{w/o}} = \prod_{s=1}^{t} e^{-iH_A(s)T}, \tag{5.134}$$

with the dynamics with the extrinsic edge mode,

$$U_{\mathrm{w/e}} = \prod_{s=1}^{t} A \cdot e^{-iH_A(s)T}. \tag{5.135}$$

Here $H_A(s)$ at each time step s has the same form as in Eq. (5.110) except for the random potential $\delta_{x,y} \in [-W, W]$ changes at each step s. As shown in Fig. 5.7 (a), the time-dependent randomness leads to diffusive behavior. The details of the diffion is shown in Appendix E.5. In the case with the extrinsic chiral edge mode [Fig. 5.7 (b)], on the other hand, we find again a unidirectional wave packet motion due to the nontrivial winding number $w_1[U_{\mathrm{w/e}}(\Phi)] = t$. Such robustness in a noisy environment may enable extrinsic modes to realize fault-tolerant quantum devices.

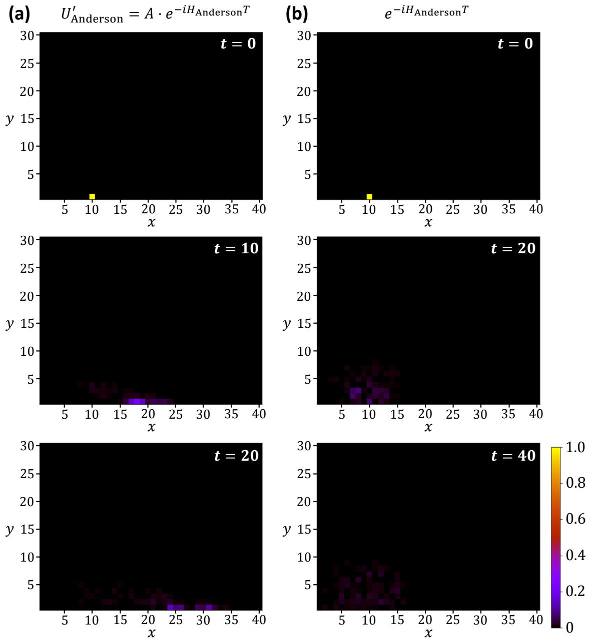

FIGURE 5.7: *In case of noisy environment (spatial and temporal disorder):* Dynamics of a wave packet (a) for the time-dependent Anderson model in Eq. (5.134), and (b) the decorated one with the extrinsic edge mode in Eq. (5.135), where the random potentials change at each time step. The parameters are $J = 0.2$, $W = 1$, $L_x = 25$, $L_y = 15$ and $T = 1$. (a) The time-dependent Anderson model shows the diffusion of a wave packet starting at the edge. (b) For the decorated Anderson model with the extrinsic edge mode, the wave packet propagates in the $+x$-direction during the time scale shorter than that of diffusion.

5.6.2 Class AIII 1D: the split-step quantum walk and the cancellation of its boundary states

Boundary states of chiral-symmetric quantum walks in 1D have been experimentally observed as localization of dynamics [40, 169]. The extrinsic topological phase, however, can cancel out the boundary states, leading to delocalized dynamics.

Let us consider the split step quantum walk model in 1D [39–41]:

$$\begin{aligned} &U_{\text{QW}} = U_2 U_1, \\ &U_1 = R_2^{1/2} S_- R_1^{1/2},\ U_2 = R_1^{1/2} S_+ R_2^{1/2}. \end{aligned} \tag{5.136}$$

Here, S_+ and S_- are the shift operators, and $R_j = R(\theta_j)$ is the spin rotation operator, which are defined as follows:

$$S_+(k) = \begin{pmatrix} e^{-ik} & 0 \\ 0 & 1 \end{pmatrix},\ S_-(k) = \begin{pmatrix} 1 & 0 \\ 0 & e^{ik} \end{pmatrix}, \tag{5.137}$$

$$R(\theta) = \begin{pmatrix} \cos\theta & -\sin\theta \\ \sin\theta & \cos\theta \end{pmatrix}. \tag{5.138}$$

This model has the decomposed CS in Eq. (5.100) for $\Gamma = \sigma_x$. After performing a unitary transformation of the basis that changes Γ into $\Gamma = \sigma_z$, we can calculate the bulk topological

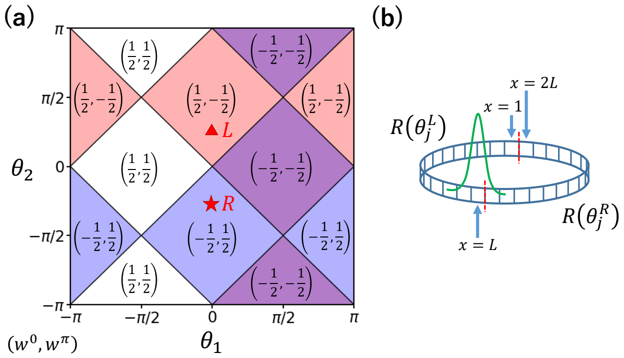

FIGURE 5.8: (a) Topological phase diagram of the split-step quantum walk. (w^0, w^π) are the bulk topological invariants given by Eq. (5.139). The red triangle and star symbol indicate the parameters for the left chain, $(\theta_1^L, \theta_2^L) = (0, \pi/4)$, and those for the right chain, $(\theta_1^R, \theta_2^R) = (0, -\pi/4)$, used in the numerical simulations in Figs. 5.9 and 5.10. (b) The setup of the split-step quantum walk. The left and right chains of the quantum walk are joined at two edges at $x = 1$ and L.

invariants (w^0, w^π) defined by the right hand side of Eq. (5.102),

$$w^0 = \frac{w_1[b] - w_1[c]}{2}, \quad w^\pi = \frac{w_1[a] - w_1[d]}{2}. \tag{5.139}$$

The calculated topological invariants are summarized in the phase diagram in Fig. 5.8 (a).

To examine the boundary states of the system, we introduce the loop configuration shown in Fig. 5.8 (b). The loop consists of left and right half chains with the same length N, where U_{QW} in the left (right) chain has the rotation operators of the parameters $(\theta_1^L, \theta_2^L) = (0, \pi/4)$ ($(\theta_1^R, \theta_2^R) = (0, -\pi/4)$). The boundary states appear at the interfaces $x = 1, N + 1$.

Figure 5.9 (a) shows eigenvalues λ of the eigenequation $U_{\text{QW}} |\psi\rangle = \lambda |\psi\rangle$ in the loop configuration, where $\lambda = 1$ ($\lambda = -1$) indicates the $\epsilon = 0$ ($\epsilon = \pi$) boundary states. Both the interfaces at $x = 1, N + 1$ host a single zero-mode $|\psi^0_{x=1,N+1}\rangle$ and a π-mode $|\psi^\pi_{x=1,N+1}\rangle$ with the topological charges $\nu^{0,\pi}_{x=1,N+1} = \langle \psi^{0,\pi}_{x=1,N+1} | \Gamma | \psi^{0,\pi}_{x=1,N+1} \rangle$ shown in Figs. 5.9 (c)-(f). We note that the boundary gapless states are determined from the bulk-boundary correspondence:

$$\nu^{0,\pi}_{x=1} = -\nu^{0,\pi}_{x=N+1} = w^{0,\pi}_L - w^{0,\pi}_R, \tag{5.140}$$

where $w^{0,\pi}_{R,L}$ are the bulk topological invariants in the right and left chains. Here the original bulk-boundary correspondence in Eq. (5.102) is slightly modified because we are considering the interfaces between two topologically non-trivial chains. Due to the existence of the boundary modes, a wave packet initially localized at one interface remains localized after long time dynamics [Fig. 5.9(b)].

As discussed in Sec. 5.5, if one relaxes the decomposed CS in Eq. (5.100) into the original CS in Eq. (5.20), we can arbitrarily change the number of boundary gapless states by using the extrinsic topology. To see this, we introduce a unitary operator with an anomaly at the boundary as

$$A = \sum_{x \neq N}^{2N} |x\rangle \langle x| \otimes \sigma_0 + |x = N\rangle \langle x = N| \otimes U_{\text{BDQW}}, \tag{5.141}$$

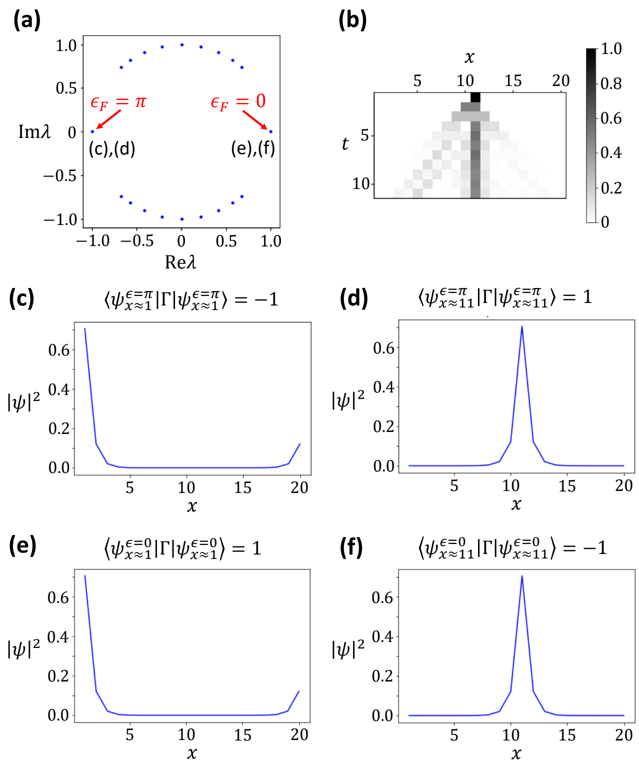

FIGURE 5.9: (a) quasi-energy spectrum, (b) dynamics, and (c-f) the boundary states of the split step walk in Eq. (5.136). The total system length is $2N = 20$. The parameters in the left half chain are $(\theta_1^L, \theta_2^L) = (0, \pi/4)$, and those in the right half chain are $(\theta_1^R, \theta_2^R) = (0, -\pi/4)$. The initial state is located at the interface $|x = N+1, \downarrow\rangle$. At $x = N+1$, we have one gapless state at $\epsilon = 0$ and $\epsilon = \pi$ each. The topological invariant of the zero modes is -1, while that of the π-mode is $+1$.

where the boundary unitary operator U_{BDQW} is 0D nontrivial one,

$$U_{\mathrm{BDQW}} = \sigma_x. \tag{5.142}$$

We insert A between U_1 and U_2 in Eq. (5.136),

$$U_{\mathrm{QW}} = U_2 A U_1. \tag{5.143}$$

Since A obeys $\Gamma A^\dagger \Gamma^{-1} = A$, U_{QW} in the above satisfies the original CS. We can see that U_{BDQW} has nontrivial extrinsic boundary states. From the Hermitian matrix $U_{\mathrm{BDQW}}\Gamma = \sigma_0$, we obtain a nontrivial topological invariant in Eq. (D.30),

$$n = \frac{1}{2}[N_+(U_{\mathrm{BDQW}}\Gamma) - N_-(U_{\mathrm{BDQW}}\Gamma)] = 1. \tag{5.144}$$

Therefore, from the extended Nielsen-Ninomiya theorem in Eq. (5.22), we obtain extrinsic boundary states at $x = N$ of the quasi-energies $\epsilon = 0, \pi$ with the opposite topological charges $\nu^0 = -\nu^\pi = 1$. As we see below, these extrinsic boundary states cancel the original boundary states at the interface at $x = N+1$.

The eigenspectrum of U_{QW} in Eq. (5.143) is shown in Fig. 5.10 (a). The spectrum shows $\epsilon = 0$ and $\epsilon = \pi$ modes, which are localized near the interface at $x = 1$, as shown in Fig. 5.10 (c) and (d). Remarkably, no gapless boundary state exists near the interface at $x = N+1$.

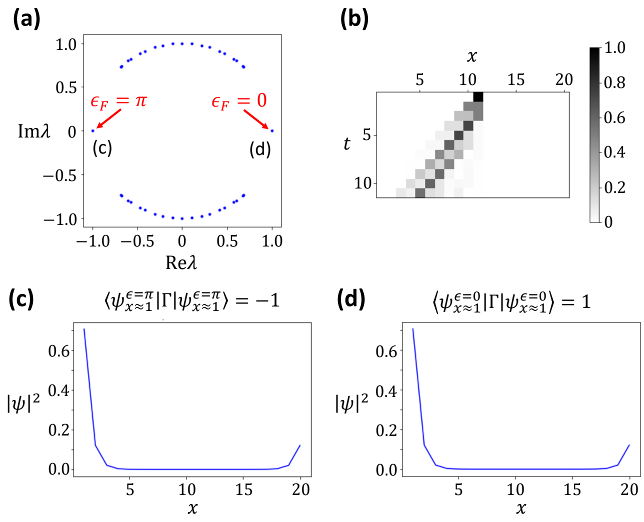

FIGURE 5.10: (a) quasi-energy spectrum, (b) dynamics, and (c,d) the boundary states of the decorated split step walk with the extrinsic boundary states in Eq. (5.143). The total system length is $2N = 20$. The parameters in the left chain is $(\theta_1^L, \theta_2^L) = (0, \pi/4)$, while those in the right chain is $(\theta_1^R, \theta_2^R) = (0, -\pi/4)$. The initial state is $|x = N+1, \downarrow\rangle$, which is localized at the boundary. No localized state at the interface $x = N+1$ is found both in the spectrum and the dynamics.

As a result, in contrast to the previous case, a wave packet initially localized at the interface $x = N+1$ spreads after time evolution [Fig. 5.10 (b)].

5.6.3 Class A in 2D: cancellation of the chiral edge mode

Floquet topological phases may host chiral edge modes with zero Chern number [26, 27, 166]. The Floquet anomalous edge modes originate from the bulk topological invariant defined from the time-evolution operator $U(\boldsymbol{k}, t)$ in Eq. (5.81), and its experimental realizations were given in photonic systems [171, 182, 183]. In this section, we see that the Floquet anomalous edge modes can be eliminated by utilizing the extrinsic topology of quantum walks in 2D.

We consider the 2D model with Floquet anomalous edge states in Ref. [27]:

$$H(t) = H_j,\ t \in [(j-1)T/5, jT/5], \tag{5.145}$$

with

$$\begin{aligned} H_{j=1,2,3,4} &= Je^{i\boldsymbol{b}_j\cdot\boldsymbol{k}}\sigma_+ + Je^{-i\boldsymbol{b}_j\cdot\boldsymbol{k}}\sigma_- + \delta_{AB}\sigma_z, \\ H_5 &= \delta_{AB}\sigma_z. \end{aligned} \tag{5.146}$$

Here we introduced $\boldsymbol{b}_1 = -\boldsymbol{b}_3 = (a, 0)$ and $\boldsymbol{b}_2 = -\boldsymbol{b}_4 = (0, a)$, $\sigma_\pm = (\sigma_x \pm i\sigma_y)/2$, and δ_{AB} is a real parameter. The one-cycle time evolution of the model is

$$U_R = \prod_{j=1}^{5} e^{-iH_jT/5}. \tag{5.147}$$

The quasi-energy spectrum and the wave packet dynamics for the model are shown in Figs. 5.11 (a) and (c). This model has gapless chiral edge modes both at the $\epsilon = 0, \pi$ energy

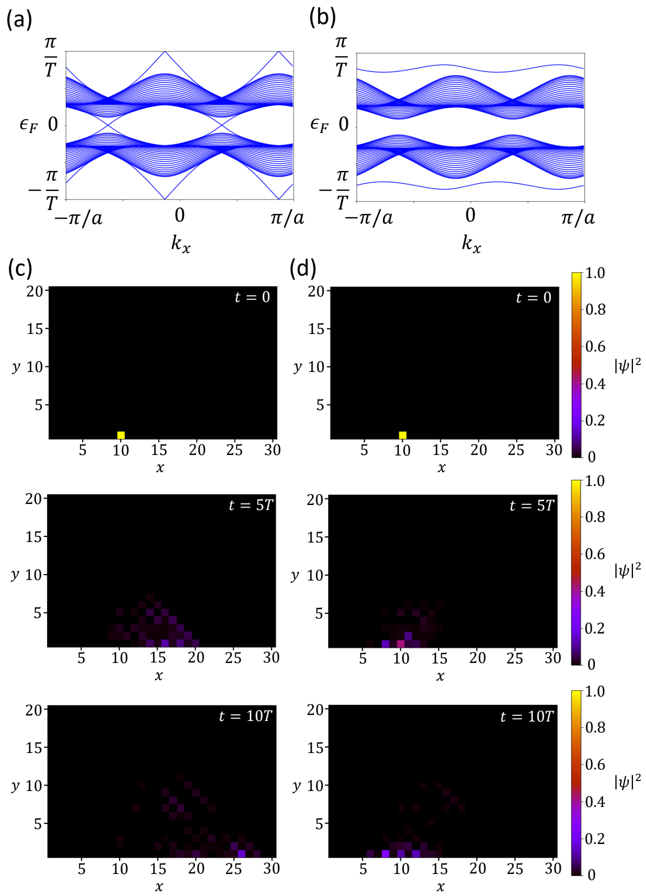

FIGURE 5.11: quasi-energy spectrum and dynamics (a,c) without and (b,d) with the decoration by unitary operator A in Eq. (5.151). We use (a,c) the model U_R in Eq. (5.147) and (b,d) U'_R in Eq. (5.150). The parameters are $J/T = 2.2\pi$, $\delta = 1.3\pi$. For (a) and (b), the length size is $L_y = 30$. For (c) and (d), the system lengths are $L_x = 25$ and $L_y = 15$. The initial state is $|x = 5, y = 1, \downarrow\rangle$, localized at an edge. We take PBC (OBC) in the x-(y-)direction. (a) The model U_R in Eq. (5.147) has Floquet anomalous chiral edge states. (c) Because of the existence of chiral edge modes, a wave packet on the edge at $y = 1$ propagates in the $+x$-direction. (b) The decorated model U'_R in Eq. (5.150) has no chiral edge mode. (d) Because of the disappearance of chiral edge modes, we cannot see the unidirectional movement.

gaps. The existence of the chiral edge modes is pictorially understood for a specific parameter set $JT/5 = \pi/2$ and $\delta_{AB} = 0$. In this case, each time-evolution unitary operator reduces

$$\begin{aligned} &e^{-iH_{j=1,2,3,4}T/5} = -i(e^{i\boldsymbol{b}_j\cdot\boldsymbol{k}}\sigma_+ + e^{-i\boldsymbol{b}_j\cdot\boldsymbol{k}}\sigma_-), \\ &e^{-iH_5T/5} = 1, \end{aligned} \tag{5.148}$$

and thus, the total time-evolution operator becomes trivial $U_R = \hat{1}$ for the bulk, but there exist chiral edge modes as shown in Fig. 5.12. The chiral edge mode remains even if we modify the parameters δ_{AB} and J unless the energy gaps at $\epsilon = 0, \pi$ are closed.

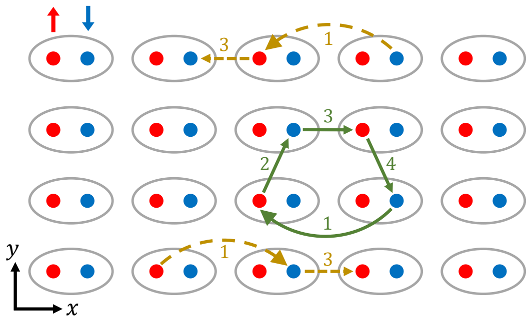

FIGURE 5.12: One-cycle dynamics of the model Eq. (5.147) at a specific set of parameters $JT/5 = \pi/2$ and $\delta_{AB} = 0$. This model has a bipartite lattice structure of spin up (red) and spin down (blue). After the one-cycle time evolution, the bulk state return to the same state, but a spin up (down) edge state at $y = 1$ (L_y) propagates in the $+(-)x$-direction.

The existence of the Floquet anomalous chiral edge state is assured by the three-dimensional winding number defined for the loop unitary $L(\boldsymbol{k}, t)$ in Eq. (5.91),

$$\begin{aligned} w_3[L] = \frac{1}{8\pi^2} \int dk_x dk_y dt \\ \times \operatorname{tr}\left(L^{-1}\partial_t L[L^{-1}\partial_{k_x} L, L^{-1}\partial_{k_y} L]\right). \end{aligned} \tag{5.149}$$

However, as we already pointed out in Sec. 5.4, $L(\boldsymbol{k}, t)$ is well-defined only when the microscopic Hamiltonian $H(\boldsymbol{k}, t)$ is given. If one allows a general deformation of the microscopic Hamiltonian, one can trivialize $L(\boldsymbol{k}, t)$ without closing energy gaps at $\epsilon = 0, \pi$. Therefore, in the framework of quantum walks, where we have no unique microscopic Hamiltonian, the Floquet anomalous edge mode is not protected by the bulk topological invariant.

Actually, we can eliminate the anomalous edge mode in Fig. 5.11 (a) by multiplying U_R a unitary operator A that have nontrivial anomaly at the edge,

$$U'_R = AU_R, \tag{5.150}$$

$$\begin{aligned} A(k_x) = U_{\text{edge}}^{y=1}(k_x) \otimes |y=1\rangle\langle y=1| \\ + U_{\text{edge}}^{y=L_y}(k_x) \otimes |y=L_y\rangle\langle y=L_y| \\ + \sum_{y=2}^{L_y-1} \sigma_0 \otimes |y\rangle\langle y|, \end{aligned} \tag{5.151}$$

$$U_{\text{edge}}^{y=1}(k_x) = \begin{pmatrix} e^{2ik_x} & 0 \\ 0 & 1 \end{pmatrix}, \; U_{\text{edge}}^{y=L_y}(k_x) = \begin{pmatrix} 1 & 0 \\ 0 & e^{-2ik_x} \end{pmatrix}, \tag{5.152}$$

where we impose OBC for U_R at $y = 1, L_y$. As shown in Figs. 5.11 (b) and (d), no chiral edge mode exists in the quasi-particle spectrum of U'_R, and no unidirectional wave packet motion is observed on the edges.

The extrinsic topological nature of $U_{\text{edge}}^{y=1}$ and $U_{\text{edge}}^{y=L_y}$ in A explains the disappearance of the anomalous edge modes. these boundary unitary operators have nonzero winding numbers in Eq. (5.5),

$$w_1\left[U_{\text{edge}}^{y=1}(k_x)\right] = -w_1\left[U_{\text{edge}}^{y=L_y}(k_x)\right] = 2. \tag{5.153}$$

Thus, $U_{\text{edge}}^{y=1}$ and $U_{\text{edge}}^{y=L_y}$ induce extrinsic boundary states. From the the extended Nielsen-Ninomiya theorem in Eq. (5.22), $U_{\text{edge}}^{y=1}$ and $U_{\text{edge}}^{y=L_y}$ provide an additional edge modes on each boundary that has the net chiralities opposite to those in the original model. As a result, the decorated unitary U'_R has net zero topological charges of edge modes, and thus no stable anomalous edge mode remains.

We emphasize again that the unitary operator A affects nontrivially only on the boundary, and it controls the presence and absence of anomalous gapless edge modes, implying the extrinsic nature of the edge states in the context of quantum walks.

Chapter 6

Summary and outlook

In this thesis, we have investigated the topological gapless structures unique to Floquet and non-Hermitian systems based on an extended version of the Nielsen-Ninomiya theorem.

In Chapter 1, we have seen the topological classification of Floquet systems, and have reviewed the previous studies using the classification table. We have also seen the topological classification of non-Hermitian systems, and have reviewed topological phenomena unique to non-Hermitian systems using the classification table.

In Chapter 2, we have overviewed the properties of Dirac Hamiltonians. Dirac Hamiltonians provide minimal models of topological insulators, superconductors, and semimetals. Furthermore, Dirac operators can be regarded as generators of Clifford algebra, then we can relate the classification of topological insulators with the extension problem of Clifford algebra.

In Chapter 3, we have formulated the extended Nielsen-Ninomiya theorem for Floquet and non-Hermitian systems. Both in Floquet and non-Hermitian systems, we have constructed simple models breaking the Nielsen-Ninomiya theorem, and also found formulae that relate the breakdown of the Nielsen-Ninomiya theorem with bulk topological invariant unique to Floquet unitary operators and non-Hermitian point-gapped Hamiltonians. In general, we can establish topological duality between Floquet and non-Hermitian systems by regarding a Floquet unitary operator as a non-Hermitian point-gapped Hamiltonian. We have first formulated the extended Nielsen-Ninomiya theorem for non-Hermitian systems for all the AZ† symmetry classes and dimensions. The general proof is based on the topological properties of Dirac Hamiltonians. Then, topological duality induces the Floquet version of the extended Nielsen-Ninomiya theorem.

The extended Nielsen-Ninomiya theorem summarizes the topological physics unique to Floquet and non-Hermitian systems, and has the potential to provide various exotic phenomena. As applications of this theorem, we have proposed non-Hermitian chiral magnetic effect and extrinsic topology in quantum walks.

We have discussed the extended Nielsen-Ninomiya theorem for Floquet unitary operators. During the argument, however, we did not use any physical properties of Floquet systems other than symmetries. Therefore, if a physical system is described by unitary operators, we can analyze the topological properties of the system by applying the extended Nielsen-Ninomiya theorem. For example, the Wilson loop is a unitary operator, and the dynamics of cellular automatons are described by unitary operators.

In Chapter 4, we have proposed the non-Hermitian chiral magnetic effect with an experimentally practical model. The model is composed of Hermitian terms and a spin-selective loss term. We have numerically simulated the dynamics for this model under a magnetic field, and found that wave packets tend to go in the direction of the magnetic field, which is a non-Hermitian version of the chiral magnetic effect. From the unidirectional dynamics, we can expect that all the wave packets accumulate at one boundary and skin effect occurs. We have numerically confirmed skin modes localize at the boundary where the magnetic field goes out.

We have studied the dynamics of the non-Hermitian chiral magnetic effect while the original chiral magnetic effect indicates the occurrence of current parallel to the magnetic field. This is because it is difficult to define electric current in non-Hermitian systems. In Hermitian systems, electric charge is a conserved quantity, and the measurement of electric current at any part of a wire gives the same result. In non-Hermitian systems, however, particles go in and out of the system, and thus the strongness of electric current depends on the place where we measure it. Therefore, we need to correctly define the electric current. It will need a rigorous understanding of the original systems that yield effective non-Hermitian descriptions.

We have also found a formula that characterizes the non-Hermitian chiral magnetic effect. The formula states that the 1D winding number equals the product of the 3D winding number and the magnetic field, which is a typical dimensional reduction formula. This result may open up the studies of magnetic response in non-Hermitian systems, which have attracted comparably little interest ever.

In Chapter 5, we have argued the bulk-boundary correspondence in quantum walks. Due to the discrete nature of quantum walk dynamics, the bulk topological invariant is insufficient to determine the boundary states. The numbers of boundary states depend on both the bulk topology and the boundary topology. While the conventional topological insulators and superconductors in equilibrium have extrinsic nature in higher-order topological phases, quantum walks can support the extrinsic topology even in the first-order topological phases.

The extrinsic boundary states in quantum walks resemble anomalous boundary states in Floquet systems, but their topological origins are different. For Floquet systems, the anomalous boundary states originate from the non-trivial topology of the bulk continuous time-evolution operator, but for quantum walks, the continuous time-evolution operator is not given. Instead, the boundary states depend on the boundary topological invariants in quantum walks.

In the previous work [30], it was shown that the bulk-boundary correspondence holds for class AIII systems in 1D with a decomposed realization of CS. We have seen how the decomposed CS assures the bulk-boundary correspondence, and discussed a similar bulk-boundary correspondence in other dimensions and symmetry classes. Then, we have found that class CII quantum walks in 1D obey the bulk-boundary correspondence under the decomposed TRS and PHS.

We have also examined the physical implementations of extrinsic topological phases in quantum walks. We have numerically seen that the extrinsic boundary states induce charge pumping and that the pumping is robust against disorders. We have also given general arguments for the robustness of the pumping. Moreover, we have seen that the extrinsic topology can eliminate the pre-existing anomalous boundary states in the class AIII 1D split step walk and a class A 2D model, respectively. We can change the types and the numbers of gapless boundary states without changing the bulk, which implies the breakdown of the bulk-boundary correspondence.

One possible future work is to study higher-order boundary states in quantum walks. Although we have studied only the first-order boundary states in this work, higher-order boundary states may have richer extrinsic topological behaviors. Quantum walks have novel symmetries that have no counterpart in static systems such as time-glide symmetry [38]. Such symmetry may produce extrinsic topological phases unique to dynamical systems.

Roughly speaking, Topology is just a mathematical tool. I believe that this mathematical tool can be used for many systems other than Floquet and non-Hermitian systems to predict exotic phenomena.

Appendix A

Construction of non-Hermitian Weyl semimetal

In this section, we explain how to obtain the non-Hermitian Weyl model Eq. (4.1). We first notice that the following topological equivalence holds with respect to the point gap,

$$H = \begin{pmatrix} & I \\ e^{ik} & \end{pmatrix} \approx \begin{pmatrix} e^{ik} & \\ & I \end{pmatrix}. \tag{A.1}$$

In general, let us consider the following Hamiltonian

$$H(\theta) = \cos\theta \begin{pmatrix} & I \\ H_P & \end{pmatrix} + \sin\theta \begin{pmatrix} H_P & \\ & I \end{pmatrix}, \tag{A.2}$$

where H_P is point-gapped $\det H_P \neq 0$. Then, we can show $\det H(\theta) \neq 0$, and thus $H(\theta)$ is a homotopy for

$$\begin{pmatrix} & I \\ H_P & \end{pmatrix} \approx \begin{pmatrix} H_P & \\ & I \end{pmatrix}, \tag{A.3}$$

with respect to the point gap.

For example, we consider the case

$$H_P(\boldsymbol{k}) = \sin k_x \sigma_x + \sin k_y \sigma_y + \sin k_z \sigma_z + i(m - \cos k_x - \cos k_y - \cos k_z), \tag{A.4}$$

which is a special case of the general nontrivial model given by J. Y. Lee, *et al.* [5]. This model has a 3D nontrivial point-gapped topological invariant in Eq. (3.9) for $1 < m < 3$. From the above relation, this model has the same point-gapped topologcal invariant as the model,

$$\begin{pmatrix} & I \\ \sin k_x \sigma_x + \sin k_y \sigma_y + \sin k_z \sigma_z + i(m - \cos k_x - \cos k_y - \cos k_z) & \end{pmatrix}. \tag{A.5}$$

By adding perturbation to this model, we obtain the non-Hermitian CME model in Eq. (4.1).

Appendix B

Extended Nielsen-Ninomiya theorem in other than AZ† symmetry classes

In this paper, we discussed the extended Nielsen-Ninomiya theorem in 10 AZ† symmetry classes. In non-Hermitian systems, however, there are 38 symmetry classes in total. Then, one naive question is "similar formula as the extended Nielsen-Ninomiya theorem exists in other 28 symmetry classes?"

The answer is yes. It is systematically understood by symmetry forgetting functor in non-Hermitian systems proposed by Ken Shiozaki. Tables of symmetry forgetting functor in all symmetry classes and dimensions are given in the supplemental material of Ref. [83].

B.1 Symmetry forgetting functor

There are some point-gapped (P-gapped) topological phases that can be created by L $\to$ P: a line-gapped (L-gapped) topologically nontrivial phase (including a Hermitian gapped topologically nontrivial phase) can also be a P-gapped topologically nontrivial phase at the same time[1]. If a topologically nontrivial P-gapped topological phase originates from a Hermitian gapped topological phase, we cannot expect novel topological phenomena intrinsic to non-Hermitian systems.

Thus, we have the motivation to know which P-gapped topological phase originate from a L-gapped topological phase and which P-gapped topological phase is the one unique to non-Hermitian systems. It is systematically obtained from the symmetry forgetting functor.

Symmetry forgetting functor is based on the observation that P-gapped classification is obtained by removing a proper chiral symmetry from the L-gapped classification. From the K-theoretic argument, we can obtain periodic tables of symmetry forgetting functors in all the symmetry classes and dimensions. Some of them are shown in TABLE B.1-3. We see how to use this table.

$0 \to \mathbb{Z}$ indicates that there is no L-gapped topological invariant in the symmetry class and dimensions, and thus no P-gapped topologically nontrivial phase originates from a L-gapped topologically nontrivial phase. In other words, the P-gapped topologically nontrivial phase is a novel topological phase unique to non-Hermitian systems.

$\mathbb{Z} \to \mathbb{Z} : n \mapsto n$ indicates that there are one L-gapped topological invariant $n^L \in \mathbb{Z}$ and one P-gapped topological invariant $n^P \in \mathbb{Z}$ in the symmetry class and dimensions, and any L-gapped Hamiltonian of $n^L = n$ is also a P-gapped Hamiltonian of $n^P = n$ at the same time.

[1] We note, for example, if a Hamiltonian is L-gapped for the line gap Re$E = 0$, the Hamiltonian is also P-gapped for the point gap $E = 0$ at the same time.

$\mathbb{Z}_2 \to \mathbb{Z}_2 : n \mapsto 0$ indicates that there are one L-gapped topological invariant $n^L \in \mathbb{Z}_2$ and a P-gapped topological invariant $n^P \in \mathbb{Z}_2$, and any L-gapped Hamiltonian of $n^L = 0, 1$ is a P-gapped Hamiltonian of $n^P = 0$ at the same time. In other words, the P-gapped topologically nontrivial phase ($n^P = 1$) is a novel topological phase unique to non-Hermitian systems.

$\mathbb{Z} \to \mathbb{Z} \oplus \mathbb{Z} : n \to (n, n)$ indicates that there are one L-gapped topological invariant $n^L \in \mathbb{Z}$ and two P-gapped topological invariant $n_1^P, n_2^P \in \mathbb{Z}$, and any L-gapped Hamiltonian of $n^L = n$ is also a P-gapped Hamiltonian of $(n_1^P, n_2^P) = (n, n)$ at the same time. Therefore, the P-gapped topological phase of $n_1^P \neq n_2^P$ is a novel topological phase unique to non-Hermitian systems.

TABLE B.1: Symmetry forgetting functor for AZ symmetry classes.

Symm. class	Gap	$d=0$	$d=1$	$d=2$	$d=3$	$d=4$	$d=5$	$d=6$	$d=7$
A	$\mathrm{L} \to \mathrm{P}$	$\mathbb{Z} \to 0$	$0 \to \mathbb{Z}$	$\mathbb{Z} \to 0$	$0 \to \mathbb{Z}$	$\mathbb{Z} \to 0$	$0 \to \mathbb{Z}$	$\mathbb{Z} \to 0$	$0 \to \mathbb{Z}$
AIII	$\mathrm{L_r} \to \mathrm{P}$	$0 \to \mathbb{Z}$	$\mathbb{Z} \to 0$	$0 \to \mathbb{Z}$	$\mathbb{Z} \to 0$	$0 \to \mathbb{Z}$	$\mathbb{Z} \to 0$	$0 \to \mathbb{Z}$	$\mathbb{Z} \to 0$
	$\mathrm{L_i} \to \mathrm{P}$	$\mathbb{Z} \oplus \mathbb{Z} \to \mathbb{Z}$ $(n,m) \to n-m$	$0 \to 0$	$\mathbb{Z} \oplus \mathbb{Z} \to \mathbb{Z}$ $(n,m) \to n-m$	$0 \to 0$	$\mathbb{Z} \oplus \mathbb{Z} \to \mathbb{Z}$ $(n,m) \to n-m$	$0 \to 0$	$\mathbb{Z} \oplus \mathbb{Z} \to \mathbb{Z}$ $(n,m) \to n-m$	$0 \to 0$
AI	$\mathrm{L_r} \to \mathrm{P}$	$\mathbb{Z} \to \mathbb{Z}_2$ $n \to n$	$0 \to \mathbb{Z}$	$0 \to 0$	$0 \to 0$	$2\mathbb{Z} \to 0$	$0 \to 2\mathbb{Z}$	$\mathbb{Z}_2 \to 0$	$\mathbb{Z}_2 \to \mathbb{Z}_2$ $n \to n$
	$\mathrm{L_i} \to \mathrm{P}$	$\mathbb{Z}_2 \to \mathbb{Z}_2$ $n \to 0$	$\mathbb{Z}_2 \to \mathbb{Z}$	$\mathbb{Z} \to 0$	$0 \to 0$	$0 \to 0$	$0 \to 2\mathbb{Z}$	$2\mathbb{Z} \to 0$	$0 \to \mathbb{Z}_2$
BDI	$\mathrm{L_r} \to \mathrm{P}$	$\mathbb{Z}_2 \to \mathbb{Z}_2$ $n \to n$	$\mathbb{Z} \to \mathbb{Z}_2$ $n \to n$	$0 \to \mathbb{Z}$	$0 \to 0$	$0 \to 0$	$2\mathbb{Z} \to 0$	$0 \to 2\mathbb{Z}$	$\mathbb{Z}_2 \to 0$
	$\mathrm{L_i} \to \mathrm{P}$	$\mathbb{Z}_2 \oplus \mathbb{Z}_2 \to \mathbb{Z}_2$ $(n,m) \to n+m$	$\mathbb{Z}_2 \oplus \mathbb{Z}_2 \to \mathbb{Z}_2$ $(n,m) \to n+m$	$\mathbb{Z} \oplus \mathbb{Z} \to \mathbb{Z}$ $(n,m) \to n+m$	$0 \to 0$	$0 \to 0$	$0 \to 0$	$2\mathbb{Z} \oplus 2\mathbb{Z} \to 2\mathbb{Z}$ $(n,m) \to n+m$	$0 \to 0$
D	$\mathrm{L} \to \mathrm{P}$	$\mathbb{Z}_2 \to 0$	$\mathbb{Z}_2 \to \mathbb{Z}_2$ $n \to n$	$\mathbb{Z} \to \mathbb{Z}_2$ $n \to n$	$0 \to \mathbb{Z}$	$0 \to 0$	$0 \to 0$	$2\mathbb{Z} \to 0$	$0 \to 2\mathbb{Z}$
DIII	$\mathrm{L_r} \to \mathrm{P}$	$0 \to 2\mathbb{Z}$	$\mathbb{Z}_2 \to 0$	$\mathbb{Z}_2 \to \mathbb{Z}_2$ $n \to n$	$\mathbb{Z} \to \mathbb{Z}_2$ $n \to n$	$0 \to \mathbb{Z}$	$0 \to 0$	$0 \to 0$	$2\mathbb{Z} \to 0$
	$\mathrm{L_i} \to \mathrm{P}$	$\mathbb{Z} \to 2\mathbb{Z}$ $n \to n$	$0 \to 0$	$\mathbb{Z} \to \mathbb{Z}_2$ $n \to n$	$0 \to \mathbb{Z}_2$	$\mathbb{Z} \to \mathbb{Z}$ $n \to 2n$	$0 \to 0$	$\mathbb{Z} \to 0$	$0 \to 0$
AII	$\mathrm{L_r} \to \mathrm{P}$	$2\mathbb{Z} \to 0$	$0 \to 2\mathbb{Z}$	$\mathbb{Z}_2 \to 0$	$\mathbb{Z}_2 \to \mathbb{Z}_2$ $n \to n$	$\mathbb{Z} \to \mathbb{Z}_2$ $n \to n$	$0 \to \mathbb{Z}$	$0 \to 0$	$0 \to 0$
	$\mathrm{L_i} \to \mathrm{P}$	$0 \to 0$	$0 \to 2\mathbb{Z}$	$2\mathbb{Z} \to 0$	$0 \to \mathbb{Z}_2$	$\mathbb{Z}_2 \to \mathbb{Z}_2$ $n \to 0$	$\mathbb{Z}_2 \to \mathbb{Z}$	$\mathbb{Z} \to 0$	$0 \to 0$
CII	$\mathrm{L_r} \to \mathrm{P}$	$0 \to 0$	$2\mathbb{Z} \to 0$	$0 \to 2\mathbb{Z}$	$\mathbb{Z}_2 \to 0$	$\mathbb{Z}_2 \to \mathbb{Z}_2$ $n \to n$	$\mathbb{Z} \to \mathbb{Z}_2$ $n \to n$	$0 \to \mathbb{Z}$	$0 \to 0$
	$\mathrm{L_i} \to \mathrm{P}$	$0 \to 0$	$0 \to 0$	$2\mathbb{Z} \oplus 2\mathbb{Z} \to 2\mathbb{Z}$ $(n,m) \to n+m$	$0 \to 0$	$\mathbb{Z}_2 \oplus \mathbb{Z}_2 \to \mathbb{Z}_2$ $(n,m) \to n+m$	$\mathbb{Z}_2 \oplus \mathbb{Z}_2 \to \mathbb{Z}_2$ $(n,m) \to n+m$	$\mathbb{Z} \oplus \mathbb{Z} \to \mathbb{Z}$ $(n,m) \to n+m$	$0 \to 0$
C	$\mathrm{L} \to \mathrm{P}$	$0 \to 0$	$0 \to 0$	$2\mathbb{Z} \to 0$	$0 \to 2\mathbb{Z}$	$\mathbb{Z}_2 \to 0$	$\mathbb{Z}_2 \to \mathbb{Z}_2$ $n \to n$	$\mathbb{Z} \to \mathbb{Z}_2$ $n \to n$	$0 \to \mathbb{Z}$
CI	$\mathrm{L_r} \to \mathrm{P}$	$0 \to \mathbb{Z}$	$0 \to 0$	$0 \to 0$	$2\mathbb{Z} \to 0$	$0 \to 2\mathbb{Z}$	$\mathbb{Z}_2 \to 0$	$\mathbb{Z}_2 \to \mathbb{Z}_2$ $n \to n$	$\mathbb{Z} \to \mathbb{Z}_2$ $n \to n$
	$\mathrm{L_i} \to \mathrm{P}$	$\mathbb{Z} \to \mathbb{Z}$ $n \to 2n$	$0 \to 0$	$\mathbb{Z} \to 0$	$0 \to 0$	$\mathbb{Z} \to 2\mathbb{Z}$ $n \to n$	$0 \to 0$	$\mathbb{Z} \to \mathbb{Z}_2$ $n \to n$	$0 \to \mathbb{Z}_2$

TABLE B.2: Symmetry forgetting functor for AZ† symmetry classes.

Symm. class	Gap	$d=0$	$d=1$	$d=2$	$d=3$	$d=4$	$d=5$	$d=6$	$d=7$
AI†	$\mathrm{L} \to \mathrm{P}$	$\mathbb{Z} \to 0$	$0 \to 0$	$0 \to 0$	$0 \to 2\mathbb{Z}$	$2\mathbb{Z} \to 0$	$0 \to \mathbb{Z}_2$	$\mathbb{Z}_2 \to \mathbb{Z}_2$ $n \mapsto 0$	$\mathbb{Z}_2 \to \mathbb{Z}$
BDI†	$\mathrm{L_r} \to \mathrm{P}$	$\mathbb{Z}_2 \to \mathbb{Z}$	$\mathbb{Z} \to 0$	$0 \to 0$	$0 \to 0$	$0 \to 2\mathbb{Z}$	$2\mathbb{Z} \to 0$	$0 \to \mathbb{Z}_2$	$\mathbb{Z}_2 \to \mathbb{Z}_2$ $n \mapsto 0$
	$\mathrm{L_i} \to \mathrm{P}$	$\mathbb{Z} \oplus \mathbb{Z} \to \mathbb{Z}$ $(n,m) \mapsto n+m$	$0 \to 0$	$0 \to 0$	$0 \to 0$	$2\mathbb{Z} \oplus 2\mathbb{Z} \to 2\mathbb{Z}$ $(n,m) \mapsto n+m$	$0 \to 0$	$\mathbb{Z}_2 \oplus \mathbb{Z}_2 \to \mathbb{Z}_2$ $(n,m) \mapsto n+m$	$\mathbb{Z}_2 \oplus \mathbb{Z}_2 \to \mathbb{Z}_2$ $(n,m) \mapsto n+m$
D†	$\mathrm{L_r} \to \mathrm{P}$	$\mathbb{Z}_2 \to \mathbb{Z}_2$ $n \mapsto 0$	$\mathbb{Z}_2 \to \mathbb{Z}$	$\mathbb{Z} \to 0$	$0 \to 0$	$0 \to 0$	$0 \to 2\mathbb{Z}$	$2\mathbb{Z} \to 0$	$0 \to \mathbb{Z}_2$
	$\mathrm{L_i} \to \mathrm{P}$	$\mathbb{Z} \to \mathbb{Z}_2$ $n \mapsto n$	$0 \to \mathbb{Z}$	$0 \to 0$	$0 \to 0$	$2\mathbb{Z} \to 0$	$0 \to 2\mathbb{Z}$	$\mathbb{Z}_2 \to 0$	$\mathbb{Z}_2 \to \mathbb{Z}_2$ $n \mapsto n$
DIII†	$\mathrm{L_r} \to \mathrm{P}$	$0 \to \mathbb{Z}_2$	$\mathbb{Z}_2 \to \mathbb{Z}_2$ $n \mapsto 0$	$\mathbb{Z}_2 \to \mathbb{Z}$	$\mathbb{Z} \to 0$	$0 \to 0$	$0 \to 0$	$0 \to 2\mathbb{Z}$	$2\mathbb{Z} \to 0$
	$\mathrm{L_i} \to \mathrm{P}$	$\mathbb{Z} \to \mathbb{Z}_2$ $n \mapsto n$	$0 \to \mathbb{Z}_2$	$\mathbb{Z} \to \mathbb{Z}$ $n \mapsto 2n$	$0 \to 0$	$\mathbb{Z} \to 0$	$0 \to 0$	$\mathbb{Z} \to 2\mathbb{Z}$ $n \mapsto n$	$0 \to 0$
AII†	$\mathrm{L} \to \mathrm{P}$	$2\mathbb{Z} \to 0$	$0 \to \mathbb{Z}_2$	$\mathbb{Z}_2 \to \mathbb{Z}_2$ $n \mapsto 0$	$\mathbb{Z}_2 \to \mathbb{Z}$	$\mathbb{Z} \to 0$	$0 \to 0$	$0 \to 0$	$0 \to 2\mathbb{Z}$
CII†	$\mathrm{L_r} \to \mathrm{P}$	$0 \to 2\mathbb{Z}$	$2\mathbb{Z} \to 0$	$0 \to \mathbb{Z}_2$	$\mathbb{Z}_2 \to \mathbb{Z}_2$ $n \mapsto 0$	$\mathbb{Z}_2 \to \mathbb{Z}$	$\mathbb{Z} \to 0$	$0 \to 0$	$0 \to 0$
	$\mathrm{L_i} \to \mathrm{P}$	$2\mathbb{Z} \oplus 2\mathbb{Z} \to 2\mathbb{Z}$ $(n,m) \mapsto n+m$	$0 \to 0$	$\mathbb{Z}_2 \oplus \mathbb{Z}_2 \to \mathbb{Z}_2$ $(n,m) \mapsto n+m$	$\mathbb{Z}_2 \oplus \mathbb{Z}_2 \to \mathbb{Z}_2$ $(n,m) \mapsto n+m$	$\mathbb{Z} \oplus \mathbb{Z} \to \mathbb{Z}$ $(n,m) \mapsto n+m$	$0 \to 0$	$0 \to 0$	$0 \to 0$
C†	$\mathrm{L_r} \to \mathrm{P}$	$0 \to 0$	$0 \to 2\mathbb{Z}$	$2\mathbb{Z} \to 0$	$0 \to \mathbb{Z}_2$	$\mathbb{Z}_2 \to \mathbb{Z}_2$ $n \mapsto 0$	$\mathbb{Z}_2 \to \mathbb{Z}$	$\mathbb{Z} \to 0$	$0 \to 0$
	$\mathrm{L_i} \to \mathrm{P}$	$2\mathbb{Z} \to 0$	$0 \to 2\mathbb{Z}$	$\mathbb{Z}_2 \to 0$	$\mathbb{Z}_2 \to \mathbb{Z}_2$ $n \mapsto n$	$\mathbb{Z} \to \mathbb{Z}_2$ $n \mapsto n$	$0 \to \mathbb{Z}$	$0 \to 0$	$0 \to 0$
CI†	$\mathrm{L_r} \to \mathrm{P}$	$0 \to 0$	$0 \to 0$	$0 \to 2\mathbb{Z}$	$2\mathbb{Z} \to 0$	$0 \to \mathbb{Z}_2$	$\mathbb{Z}_2 \to \mathbb{Z}_2$ $n \mapsto 0$	$\mathbb{Z}_2 \to \mathbb{Z}$	$\mathbb{Z} \to 0$
	$\mathrm{L_i} \to \mathrm{P}$	$\mathbb{Z} \to 0$	$0 \to 0$	$\mathbb{Z} \to 2\mathbb{Z}$ $n \mapsto n$	$0 \to 0$	$\mathbb{Z} \to \mathbb{Z}_2$ $n \mapsto n$	$0 \to \mathbb{Z}_2$	$\mathbb{Z} \to \mathbb{Z}$ $n \mapsto 2n$	$0 \to 0$

TABLE B.3: Symmetry forgetting functor for AZ+SLS+pH symmetry classes.

AZ class	Add. symm.	Gap	$d=0$	$d=1$	$d=2$	$d=3$	$d=4$	$d=5$	$d=6$	$d=7$
A	S	$\mathrm{L} \to \mathrm{P}$	$0 \to 0$	$\mathbb{Z} \to \mathbb{Z} \oplus \mathbb{Z}$ $n \mapsto (n,n)$	$0 \to 0$	$\mathbb{Z} \to \mathbb{Z} \oplus \mathbb{Z}$ $n \mapsto (n,n)$	$0 \to 0$	$\mathbb{Z} \to \mathbb{Z} \oplus \mathbb{Z}$ $n \mapsto (n,n)$	$0 \to 0$	$\mathbb{Z} \to \mathbb{Z} \oplus \mathbb{Z}$ $n \mapsto (n,n)$
AIII	S_-, η_-	$\mathrm{L_r} \to \mathrm{P}$	$\mathbb{Z} \to \mathbb{Z} \oplus \mathbb{Z}$ $n \mapsto (n,n)$	$0 \to 0$	$\mathbb{Z} \to \mathbb{Z} \oplus \mathbb{Z}$ $n \mapsto (n,n)$	$0 \to 0$	$\mathbb{Z} \to \mathbb{Z} \oplus \mathbb{Z}$ $n \mapsto (n,n)$	$0 \to 0$	$\mathbb{Z} \to \mathbb{Z} \oplus \mathbb{Z}$ $n \mapsto (n,n)$	$0 \to 0$
		$\mathrm{L_i} \to \mathrm{P}$	$\mathbb{Z} \to \mathbb{Z} \oplus \mathbb{Z}$ $n \mapsto (n,-n)$	$0 \to 0$	$\mathbb{Z} \to \mathbb{Z} \oplus \mathbb{Z}$ $n \mapsto (n,-n)$	$0 \to 0$	$\mathbb{Z} \to \mathbb{Z} \oplus \mathbb{Z}$ $n \mapsto (n,-n)$	$0 \to 0$	$\mathbb{Z} \to \mathbb{Z} \oplus \mathbb{Z}$ $n \mapsto (n,-n)$	$0 \to 0$
AI	S_-	$\mathrm{L_r} \to \mathrm{P}$	$0 \to 0$	$0 \to \mathbb{Z}$	$0 \to 0$	$2\mathbb{Z} \to \mathbb{Z}$ $n \mapsto 2n$	$0 \to 0$	$\mathbb{Z}_2 \to \mathbb{Z}$	$\mathbb{Z}_2 \to 0$	$\mathbb{Z} \to \mathbb{Z}$ $n \mapsto n$
		$\mathrm{L_i} \to \mathrm{P}$	$0 \to 0$	$\mathbb{Z}_2 \to \mathbb{Z}$	$\mathbb{Z}_2 \to 0$	$\mathbb{Z} \to \mathbb{Z}$ $n \mapsto n$	$0 \to 0$	$0 \to \mathbb{Z}$	$0 \to 0$	$2\mathbb{Z} \to \mathbb{Z}$ $n \mapsto 2n$
BDI	S_{-+}, η_{+-}	$\mathrm{L_r} \to \mathrm{P}$	$\mathbb{Z} \to \mathbb{Z}$ $n \mapsto n$	$0 \to 0$	$0 \to \mathbb{Z}$	$0 \to 0$	$2\mathbb{Z} \to \mathbb{Z}$ $n \mapsto 2n$	$0 \to 0$	$\mathbb{Z}_2 \to \mathbb{Z}$	$\mathbb{Z}_2 \to 0$
		$\mathrm{L_i} \to \mathrm{P}$	$\mathbb{Z}_2 \to \mathbb{Z}$	$\mathbb{Z}_2 \to 0$	$\mathbb{Z} \to \mathbb{Z}$ $n \mapsto n$	$0 \to 0$	$0 \to \mathbb{Z}$	$0 \to 0$	$2\mathbb{Z} \to \mathbb{Z}$ $n \mapsto 2n$	$0 \to 0$
D	S_+	$\mathrm{L} \to \mathrm{P}$	$\mathbb{Z}_2 \to 0$	$\mathbb{Z} \to \mathbb{Z}$ $n \mapsto n$	$0 \to 0$	$0 \to \mathbb{Z}$	$0 \to 0$	$2\mathbb{Z} \to \mathbb{Z}$ $n \mapsto 2n$	$0 \to 0$	$\mathbb{Z}_2 \to \mathbb{Z}$
DIII	S_{-+}, η_{-+}	$\mathrm{L_r} \to \mathrm{P}$	$\mathbb{Z}_2 \to \mathbb{Z}$	$\mathbb{Z}_2 \to 0$	$\mathbb{Z} \to \mathbb{Z}$ $n \mapsto n$	$0 \to 0$	$0 \to \mathbb{Z}$	$0 \to 0$	$2\mathbb{Z} \to \mathbb{Z}$ $n \mapsto 2n$	$0 \to 0$
		$\mathrm{L_i} \to \mathrm{P}$	$\mathbb{Z} \to \mathbb{Z}$ $n \mapsto n$	$0 \to 0$	$0 \to \mathbb{Z}$	$0 \to 0$	$2\mathbb{Z} \to \mathbb{Z}$ $n \mapsto 2n$	$0 \to 0$	$\mathbb{Z}_2 \to \mathbb{Z}$	$\mathbb{Z}_2 \to 0$
AII	S_-	$\mathrm{L_r} \to \mathrm{P}$	$0 \to 0$	$\mathbb{Z}_2 \to \mathbb{Z}$	$\mathbb{Z}_2 \to 0$	$\mathbb{Z} \to \mathbb{Z}$ $n \mapsto n$	$0 \to 0$	$0 \to \mathbb{Z}$	$0 \to 0$	$2\mathbb{Z} \to \mathbb{Z}$ $n \mapsto 2n$
		$\mathrm{L_i} \to \mathrm{P}$	$0 \to 0$	$0 \to \mathbb{Z}$	$0 \to 0$	$2\mathbb{Z} \to \mathbb{Z}$ $n \mapsto 2n$	$0 \to 0$	$\mathbb{Z}_2 \to \mathbb{Z}$	$\mathbb{Z}_2 \to 0$	$\mathbb{Z} \to \mathbb{Z}$ $n \mapsto n$
CII	S_{-+}, η_{+-}	$\mathrm{L_r} \to \mathrm{P}$	$2\mathbb{Z} \to \mathbb{Z}$ $n \mapsto 2n$	$0 \to 0$	$\mathbb{Z}_2 \to \mathbb{Z}$	$\mathbb{Z}_2 \to 0$	$\mathbb{Z} \to \mathbb{Z}$ $n \mapsto n$	$0 \to 0$	$0 \to \mathbb{Z}$	$0 \to 0$
		$\mathrm{L_i} \to \mathrm{P}$	$0 \to \mathbb{Z}$	$0 \to 0$	$2\mathbb{Z} \to \mathbb{Z}$ $n \mapsto 2n$	$0 \to 0$	$\mathbb{Z}_2 \to \mathbb{Z}$	$\mathbb{Z}_2 \to 0$	$\mathbb{Z} \to \mathbb{Z}$ $n \mapsto n$	$0 \to 0$
C	S_+	$\mathrm{L} \to \mathrm{P}$	$0 \to 0$	$2\mathbb{Z} \to \mathbb{Z}$ $n \mapsto 2n$	$0 \to 0$	$\mathbb{Z}_2 \to \mathbb{Z}$	$\mathbb{Z}_2 \to 0$	$\mathbb{Z} \to \mathbb{Z}$ $n \mapsto n$	$0 \to 0$	$0 \to \mathbb{Z}$
CI	S_{-+}, η_{-+}	$\mathrm{L_r} \to \mathrm{P}$	$0 \to \mathbb{Z}$	$0 \to 0$	$2\mathbb{Z} \to \mathbb{Z}$ $n \mapsto 2n$	$0 \to 0$	$\mathbb{Z}_2 \to \mathbb{Z}$	$\mathbb{Z}_2 \to 0$	$\mathbb{Z} \to \mathbb{Z}$ $n \mapsto n$	$0 \to 0$
		$\mathrm{L_i} \to \mathrm{P}$	$2\mathbb{Z} \to \mathbb{Z}$ $n \mapsto 2n$	$0 \to 0$	$\mathbb{Z}_2 \to \mathbb{Z}$	$\mathbb{Z}_2 \to 0$	$\mathbb{Z} \to \mathbb{Z}$ $n \mapsto n$	$0 \to 0$	$0 \to \mathbb{Z}$	$0 \to 0$

B.2 Relation between point-gapped structures and line-gapless structures

In this section, we discuss the relation between P-gapped topological structures and L-gapless topological structures, which can be seen a natural extension of the extended Nielsen-Ninomiya theorem [2]. For the P-gapped topological phases that do not originate from L-gapped topological phases, we can always find L-gapless structures accompanying it. In some symmetry classes, we need to differentiate the real line gap ($\mathrm{L_r}$-gap) for $\mathrm{Re}E = 0$ and the imaginary line gap ($\mathrm{L_i}$-gap) for $\mathrm{Im}E = 0$. For convenience, we call the P-gapped topological phase that **does not originate** from $\mathrm{L_{r(i)}}$-gapped topological phases as *$L_{r(i)} \to P$ trivial phase*, and we call the P-gapped topological phase that **originate** from $\mathrm{L_{r(i)}}$-gapped topological phases as *$L_{r(i)} \to P$ nontrivial phase* in the following.

In general, we find the following statements 1 and 2.

1. $\mathrm{L_{r(i)}} \to$ P trivial phase has robust $\mathrm{L_{r(i)}}$-gapless structure with $\mathrm{Im}E \lesseqgtr 0$ ($\mathrm{Re}E \lesseqgtr 0$).
2. $\mathrm{L_{r(i)}} \to$ P nontrivial phase do not have robust $\mathrm{L_{r(i)}}$-gapless structure with $\mathrm{Im}E \lesseqgtr 0$ ($\mathrm{Re}E \lesseqgtr 0$).

The $\mathrm{L_{r(i)}}$-gapless structure typically takes the form of Dirac point.

B.3 Examples

In this section, we check the statement 1 through examples.

B.3.1 AZ† class

In AZ† symmetry classes, all the P-gapped topologically nontrivial phases are $\mathrm{L}_r \to$ P trivial phases according to the tables of symmetry forgetting functors. In other words, P-gapped topologically nontrivial phases do not originate from $\mathrm{L_r}$-gapped topological phases. In class AZ†, we know the extended Nielsen-Ninomiya theorem, which is a relation between P-gapped topological invariants and $\mathrm{L_r}$-gapless structures with $\mathrm{Im}E \lesseqgtr 0$. Therefore, the $\mathrm{L_{r(i)}} \to$ P trivial phase actually has robust $\mathrm{L_{r(i)}}$-gapless structure with $\mathrm{Im}E \lesseqgtr 0$.

We also note that the same result is obtained for the i multiplied counterparts of AZ† symmetry classes.

B.3.2 class A +SLS

According to the table, 1D systems in class A + sublattice symmety (SLS) have the symmetry forgetting functor L$\to$ P: $\mathbb{Z} \to \mathbb{Z} \oplus \mathbb{Z} : n \to (n, n)$. We construct the concrete P-gapped topological numbers. From the sublattice symmetry, the non-Hermitian Hamiltonian has the form of

$$H(k) = \begin{pmatrix} & b \\ c & \end{pmatrix}, \quad SHS^{-1} = -H, \quad S = \sigma_z. \tag{B.1}$$

[2]The general statements we provide here is weaker than the extended Nielsen-Ninomiya theorem. For specific symmetry classes, however, we can construct stronger statements like the extended Nielsen-Ninomiya theorem.

Thus, we can obtain two P-gapped topological invariants

$$n_1^P = -\int_0^{2\pi} \frac{dk}{2\pi i} \mathrm{tr}[b^{-1}\partial_k b], \quad n_2^P = \int_0^{2\pi} \frac{dk}{2\pi i} \mathrm{tr}[c^{-1}\partial_k c]. \tag{B.2}$$

On the other hand, the L-gapped topological invariant is

$$n^L = \int_0^{2\pi} \frac{dk}{4\pi i} \mathrm{tr}[S\tilde{H}^{-1}\partial_k \tilde{H}]. \tag{B.3}$$

where $\tilde{H}$ is the Hermitian flattended Hamiltonian of H [64, 77].

For example, we can see the P-gapped topological phase of $(n_1^P, n_2^P) = (1,1)$ originates from a L-gapped topological phase. Let us consider a simple model,

$$H = \begin{pmatrix} & e^{-ik} \\ e^{ik} & \end{pmatrix}, \tag{B.4}$$

which is a L-gapped Hamiltonian with $n^L = 1$. We can also check $n_1^P = n_2^P = 1$.

On the other hand, the P-gapped topological phase of $(n_1^P, n_2^P) = (1,0)$ do not originate from a L-gapped topological phase, and we can also see this P-gapped topological phase has $\mathrm{L_r}$-gapless structure with $\mathrm{Im}E \lesseqgtr 0$. Let us consider the following model

$$H = \begin{pmatrix} & e^{ik} \\ 1 & \end{pmatrix}, E_{\pm} = \pm e^{ik/2}, \tag{B.5}$$

which has $(n_1^P, n_2^P) = (1,0)$. As any L-gapped topological phases cannot be the origin of this P-gapped topological phase, this model is in the $\mathrm{L}_r \to$ P trivial phase. We note that this model has energy winding number, the P-gapped topological invariant for class A 1D P-gapped systems,

$$w = \int_0^{2\pi} \frac{dk}{2\pi i} \mathrm{tr}[H^{-1}\partial_k H] = \frac{1}{2\pi} \oint \mathrm{d}k \partial_k \mathrm{arg}[E_+ E_-] = 1. \tag{B.6}$$

Therefore, from the extended Nielsen-Ninomiya theorem in class A 1D systems, we have the following formula,

$$w = n_1^P - n_2^P = \sum_{\mathrm{Im}E_j > 0} \nu_j^{\mathrm{R}} = -\sum_{\mathrm{Im}E_j < 0} \nu_j^{\mathrm{R}}, \tag{B.7}$$

where $\nu_j^R = \mathrm{sign}[\mathrm{Re}[\mathrm{d}E/\mathrm{d}k]$ characterize $\mathrm{L_r}$-gapless structures. Therefore, the $\mathrm{L}_r \to$ P trivial phase actually has robust $\mathrm{L_r}$-gapless structure with $\mathrm{Im}E \lesseqgtr 0$. We obtained more detailed formula than the statement 1 in this specific case.

B.4 Proof of statements 1 and 2

The proofs of statements 1 and 2 are almost evident from its definition, but we give the proofs for completeness.

Proof of statement 1

We prove by contradiction. Let us consider a $\mathrm{L}_{\mathrm{r(i)}} \to$ P trivial phase, i.e., a P-gapped topological phase that do not originate from any L-gapped topological phase. Assume that there is no robust $\mathrm{L}_{\mathrm{r(i)}}$-gapless structure with Im$E \lesseqgtr 0$ (Re$E \lesseqgtr 0$). Then, if we consider a model in $\mathrm{L}_{\mathrm{r(i)}} \to$ P trivial phase, we can be continuously deform the model to be $\mathrm{L}_{\mathrm{r(i)}}$-gapped without closing the point gap. This is contrary to the fact that we are considering a $\mathrm{L}_{\mathrm{r(i)}} \to$ P trivial phase, i.e., a P-gapped topological phase that do not originate from any $\mathrm{L}_{\mathrm{r(i)}}$-gapped phase.

Hence, $\mathrm{L}_{\mathrm{r(i)}} \to$ P trivial phase has robust $\mathrm{L}_{\mathrm{r(i)}}$-gapless structure with Im$E \lesseqgtr 0$ (Re$E \lesseqgtr 0$).

Proof of statement 2

We prove by contradiction. Let us consider $\mathrm{L}_{\mathrm{r(i)}} \to$ P nontrivial phase, i.e., a P-gapped topological phase that originates from L-gapped topological phases. Assume that there exists robust $\mathrm{L}_{\mathrm{r(i)}}$-gapless structure with Im$E \lesseqgtr 0$ (Re$E \lesseqgtr 0$). Then, if we consider a model in $\mathrm{L}_{\mathrm{r(i)}} \to$ P nontrivial phase, we cannot continuously deform the model to be $\mathrm{L}_{\mathrm{r(i)}}$-gapped. This is contrary to the fact that we are considering a $\mathrm{L}_{\mathrm{r(i)}} \to$ P nontrivial phase, i.e., a P-gapped topological phase that originate from $\mathrm{L}_{\mathrm{r(i)}}$-gapped phase.

Hence, $\mathrm{L}_{\mathrm{r(i)}} \to$ P nontrivial phase do not have robust $\mathrm{L}_{\mathrm{r(i)}}$-gapless structure with Im$E \lesseqgtr 0$ (Re$E \lesseqgtr 0$).

Appendix C

Extended Nielsen-Ninomiya theorem for Floquet systems: another proof

In the main text, we proved the Theorem 3',

$$n = \sum_{\epsilon_\alpha = 0} \nu_\alpha^0 = -(-1)^d \sum_{\epsilon_\alpha = \pi/\tau} \nu_\alpha^\pi, \tag{C.1}$$

In this section, we directly show this theorem for class A and AIII without using the non-Hermitian counterparts.

Firstly, we give an intuitive proof of the first equality, $n = \sum_{\epsilon_\alpha=0} \nu_\alpha^0$. We suppose a model has $n = 0$, which means the model can be continuously deformed into a trivial model such as $U_F(\boldsymbol{k}) = -\hat{1}$. Then, there is no robust zero-energy gapless mode, and thus we obtain $\sum_{\epsilon_\alpha=0} \nu_\alpha^0 = 0$. We next suppose a model has $n = 1$. Then, there exist robust zero-energy gapless structures; otherwise, we can gap out $\epsilon = 0$ and continuously deform the energy spectrum and the resulting Floquet unitary operator becomes a trivial one, $U_F = -1$ again. The robust zero-energy gapless structures should be characterized by some topological invariant, i.e., the topological charge of gapless states, ν_α^0. As a result, we obtained $n^F = \sum_j \nu_j^0 = 0$ and $n^F = \sum_j \nu_j^0 = 1$ [1]. For general n, we can obtain by considering direct sums of $n = 1$ models.

Next, we prove the second equality, $\sum_{\epsilon_\alpha=0} \nu_\alpha^0 = -(-1)^d \sum_{\epsilon_\alpha=\pi/\tau} \nu_\alpha^\pi$. An important observation is that the Floquet Hamiltonian $H_{\mathrm{F}} := \frac{i}{\tau} \ln U_{\mathrm{F}}$ and ordinary Hermitian Hamiltonian has the same property except for the $2\pi/\tau$-periodicity in Floquet energy spectrum.

We split the Brillouin zone (BZ) into two regions [Fig. C.1] such that one region $\mathcal{M}$ does not include π-energy gapless structures, while the complementary region $\bar{\mathcal{M}} :=$ BZ $- \mathcal{M}$ does not include zero-energy gapless structures [2]. In the case where some regions in BZ have both zero-energy gapless structures and π-energy gapless structures at the same time, we need to add some perturbation to the model to obtain the above situation. This is possible for class A and AIII, but impossible for other symmetry classes in general: We cannot move Dirac points from time-reversal invariant momenta. Then, inside the region $\mathcal{M}$, the Floquet Hamiltonian H_F has an energy gap at $\epsilon = \pi/\tau$, and thus H_F can be seen as an ordinary Hermitian Hamiltonian by taking the branch within $-\pi/\tau < \epsilon < \pi/\tau$. We focus on $\partial\mathcal{M}$, where both $\epsilon = 0, \pi$ are gapped.

[1] Here, we implicitly supposed $\nu_\alpha^0 = 1$ for the gapless structures accompanying the bulk topology of $n = 1$. For class A and AIII, we know the gapless structures take the form of gapless Dirac Hamiltonians up to continuous deformations.

[2] $\mathcal{M}$ and/or $\bar{\mathcal{M}}$ may be disconnected in general, but that does not change the problem.

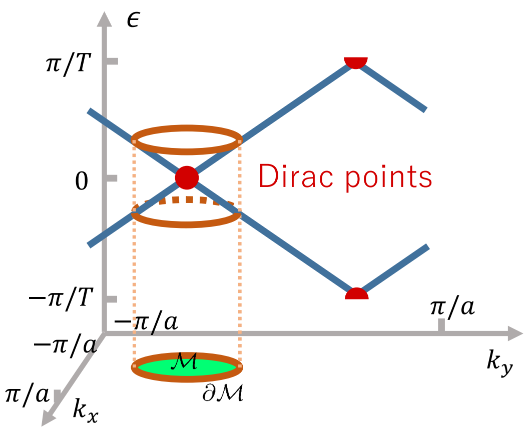

FIGURE C.1: Sketch of the proof. The region $\mathcal{M}$ does not include π-energy gapless regions. The complementary region $\bar{\mathcal{M}} = \mathrm{BZ} - \mathcal{M}$ does not include zero-energy gapless regions.

We can rewrite the Floquet Hamiltonian on $\partial\mathcal{M}$ as

$$H_F^\pi(\boldsymbol{k}) = \sum_{-\pi/\tau<\epsilon_j(\boldsymbol{k})<0} \epsilon_j(\boldsymbol{k})P_j(\boldsymbol{k}) + \sum_{0<\epsilon_j(\boldsymbol{k})<\pi/\tau} \epsilon_j(\boldsymbol{k})P_j(\boldsymbol{k}) \tag{C.2}$$

where $H_F^\pi(\boldsymbol{k})$ has the branch cut at $\epsilon = \pm\pi/\tau$ and the energy spectrum is within $-\pi/\tau < \epsilon < \pi/\tau$ [100]. $\epsilon_j(\boldsymbol{k})$ is the Floquet energy eigenvalue of the band j. $P_j(\boldsymbol{k}) = |\psi_j(\boldsymbol{k})\rangle\langle\psi_j(\boldsymbol{k})|$ is the projection operator on to the band j. We took summation of energy bands j for lower bands $\epsilon_j < 0$ and upper bands $\epsilon_j > 0$. Here, we implicitly used the fact that $\epsilon_j(\boldsymbol{k}) \neq 0, \pi/\tau$ on $\partial\mathcal{M}$. Then the $H_F^\pi(\boldsymbol{k})$ can be seen as Hermitian Hamiltonian with zero-energy gap, i.e., a topological insulator, thus we can calculate a topological invariant $Q[H_F^\pi]$ for this topological insulator. In class A and AIII, nontrivial topological insulators on $\partial\mathcal{M}$ indicates the existence of Dirac/Weyl points inside $\mathcal{M}$,

$$Q[H_F^\pi] = \sum_j \nu_j^0, \tag{C.3}$$

where ν_j^0 is the topological charge of the zero-energy gapless region j (or simply the chirality of Dirac/Weyl zero-modes) and $Q[H_F^\pi]$ is the topological invariant of the topological insulator H_F^π. We can continuously flatten the energy spectrum of $H_F^\pi(\boldsymbol{k})$ without closing energy gap $\epsilon = 0$ as

$$H_F^\pi(\boldsymbol{k}) = \sum_{-\pi/\tau<\epsilon_j(\boldsymbol{k})<0} \left(-\frac{\pi}{2T}\right) P_j(\boldsymbol{k}) + \sum_{0<\epsilon_j(\boldsymbol{k})<\pi/\tau} \left(\frac{\pi}{2T}\right) P_j(\boldsymbol{k}). \tag{C.4}$$

This Hamiltonian on the boundary $\partial\mathcal{M}$ can also be seen as a Hamiltonian on the boundary of $\bar{\mathcal{M}}$ but inside out. In this case, we need to take the branch cut at $\epsilon = 0$ and take $0 < \epsilon < 2\pi/\tau$ because there are π/τ-gapless regions inside $\bar{\mathcal{M}}$. So, we rewrite $H_F^\pi(\boldsymbol{k})$ in Eq. (C.4) by using $2\pi/\tau$-energy periodicity as,

$$H_F^\pi(\boldsymbol{k}) = \sum_{-\pi/\tau<\epsilon_j(\boldsymbol{k})<0} \left(\frac{3\pi}{2T}\right) P_j(\boldsymbol{k}) + \sum_{0<\epsilon_j(\boldsymbol{k})<\pi/\tau} \left(\frac{\pi}{2T}\right) P_j(\boldsymbol{k}), \tag{C.5}$$

the energy spectrum of which is within $0 < \epsilon < 2\pi/\tau$. In order to shift the energy gap from $\epsilon = \pi/\tau$ to $\epsilon = 0$, we redefine the Hamiltonian with energy shift π/τ,

$$H_F^0(\boldsymbol{k}) := H_F^\pi(\boldsymbol{k}) - \frac{\pi}{T} = \sum_{-\pi/\tau<\epsilon_j(\boldsymbol{k})<0} \frac{\pi}{2T} P_j(\boldsymbol{k}) + \sum_{0<\epsilon_j(\boldsymbol{k})<\pi/\tau} \left(-\frac{\pi}{2T}\right) P_j(\boldsymbol{k}). \tag{C.6}$$

This can be seen as a Hermitian Hamiltonian with $\epsilon = 0$ gap. We note that the topological invariant $Q[H_F^0]$ for this topological insulator indicates the existence of Dirac/Weyl points inside $\mathcal{M}$ at π-energy,

$$Q[H_F^0] = \sum_j \nu_j^\pi, \tag{C.7}$$

because we shifted the energy π/τ.

Comparing Eq. (C.4) and Eq. (C.6), we find

$$H_F^0(\boldsymbol{k}) = -H_F^\pi(\boldsymbol{k}) \tag{C.8}$$

In general, topological invariants of topological insulators has the following properties,

$$Q[-H] = (-1)^{d+1} Q[H]. \tag{C.9}$$

We will explain this relation later. If we accept this relation, we have

$$Q[H_F^0(\boldsymbol{k})] = Q[-H_F^\pi(\boldsymbol{k})] = (-1)^{d+1} Q[H_F^\pi(\boldsymbol{k})]. \tag{C.10}$$

Then, combining with Eq. (C.3) and Eq. (C.7), we obtain the second equiality of Theorem 3' as

$$\sum_j \nu_j^0 = (-1)^{d+1} \sum_j \nu_j^\pi. \tag{C.11}$$

For completeness, we explain the relation in Eq. (C.9). For example in class A $d = 2$, the massive Dirac Hamiltonian [3] is given by [**KitaevTable**, 15, 16, 37]:

$$H(\boldsymbol{k}) = k_1\sigma_1 + k_2\sigma_2 + m\sigma_3, \quad m > 0 \tag{C.12}$$

This model has $Ch = +1/2$, but $-H$ has $Ch = -1/2$ because

$$-H = -k_1\sigma_1 - k_2\sigma_2 - m\sigma_3 \approx k_1\sigma_1 + k_2\sigma_2 - m\sigma_3, \tag{C.13}$$

where, $\approx$ means the topological equivalence (we can continuously deform from left-hand side into right-hand side without closing zero-energy gap). Here, we continuously rotated $(-k_1, -k_2)$ into (k_1, k_2) by

$$\begin{pmatrix} \cos\theta & -\sin\theta \\ \sin\theta & \cos\theta \end{pmatrix} \begin{pmatrix} k_1 \\ k_2 \end{pmatrix}, \quad \theta = \pi \to 0. \tag{C.14}$$

[3] We note that the massive Dirac Hamiltonian represents topological insulators near topological transition points as discussed in Chapter. 2.

We can also a give different explanation for class A $d = 2$. If a topological insulator has the form

$$H = d_1\sigma_1 + d_2\sigma_2 + d_3\sigma_3, \tag{C.15}$$

the covering number of the $\boldsymbol{d}$ vector around $\boldsymbol{d} = \boldsymbol{0}$ becomes the Chern number. As $\boldsymbol{d}$ and $-\boldsymbol{d}$ has an opposite covering number, we obtain the relation $Q[-H] = -Q[H]$.

In general, massive Dirac Hamiltonians of topological insulators can be written as [4],

$$H = \sum_{j=1}^{d} k_j\Gamma_j + m\Gamma_0, \tag{C.16}$$

by using gamma matrices $\{\Gamma_i, \Gamma_j\} = 2\delta_{ij}$ [**KitaevTable**, 15, 16, 37]. Then, $-H$ has the following topological equivalence,

$$-H = \sum_{j=1}^{d}(-k_j)\Gamma_j - m\Gamma_0 \approx \begin{cases} \sum_{j=1}^{d} k_j\Gamma_j - m\Gamma_0 & (d = 2n) \\ \sum_{j=1}^{d} k_j\Gamma_j + m\Gamma_0 & (d = 2n+1) \end{cases} \tag{C.17}$$

Here we repeated the continuous rotation $(-k_j, -k_{j+1}) \to (k_j, k_{j+1})$. We note that $\sum_{j=1}^{d} k_j\Gamma_j - m\Gamma_0$ has the opposite topological invariant from $H = \sum_{j=1}^{d} k_j\Gamma_j + m\Gamma_0$. This is because the covering number of the generalized $\boldsymbol{d}$ vector for $H = \sum_{j=1}^{d} d_j\Gamma_j$ takes opposite values between them. Therefore, we obtain

$$Q[-H] = \begin{cases} -Q[H] & (d = 2n) \\ Q[H] & (d = 2n+1) \end{cases}, \tag{C.18}$$

or equivalently Eq. (C.9).

[4] See Chapter 2 why it is enough to consider only massive Dirac Hamiltonians.

Appendix D

Details for non-Hermitian chiral magnetic effect

We give miscellaneous arguments about the formula of non-Hermitian CME in Eq. (4.2),

$$\frac{w_1^z}{L_x L_y} = \frac{eB_z}{2\pi} w_3. \tag{D.1}$$

We see detailed properties of this formula by using a minimal model

$$H(k_x, k_y, k_z) = e^{-ik_x\sigma_x} + e^{-ik_y\sigma_y} + e^{-ik_z\sigma_z}, \tag{D.2}$$

which is a special case of the general model proposed by Lee, *et al.*, [5]. This model has $w_3 = 1$ for the 3D point-gapped topological invariant given in Eq. (3.9).

D.1 Lattice realization of magnetic field

In order to study the CME formula in detail, we review Peierls substitution method. Magnetic field on a lattice is realized by multiplying Peierls phase onto translation operators (hopping terms) as

$$\sum_{x,y} |x+1, y\rangle \langle x, y| \to T_x := \sum_{x,y} |x+1, y\rangle \langle x, y| \, e^{ie\int_{(x,y)}^{(x+1,y)} \boldsymbol{A}\cdot d\boldsymbol{x}}, \tag{D.3}$$

$$\sum_{x,y} |x, y+1\rangle \langle x, y| \to T_y := \sum_{x,y} |x, y+1\rangle \langle x, y| \, e^{ie\int_{(x,y)}^{(x,y+1)} \boldsymbol{A}\cdot d\boldsymbol{x}}. \tag{D.4}$$

Here the vector potential $\boldsymbol{A}$ is chosen to satisfy

$$\int_{(x,y)}^{(x+1,y)} \boldsymbol{A}\cdot d\boldsymbol{x} + \int_{(x+1,y)}^{(x+1,y+1)} \boldsymbol{A}\cdot d\boldsymbol{x} + \int_{(x+1,y+1)}^{(x,y+1)} \boldsymbol{A}\cdot d\boldsymbol{x} + \int_{(x,y+1)}^{(x,y)} \boldsymbol{A}\cdot d\boldsymbol{x} = \iint_{S_{x,y}} B_z dS, \tag{D.5}$$

where the area $S_{x,y}$ is a square plaquette with vertices (x, y), $(x+1, y)$, $(x+1, y+1)$ and $(x, y+1)$. We also introduce the magnetic flux per area $2\pi\phi_{x,y} = e\iint_{S_{x,y}} B_z dS$. Correspondingly, the translation operators satisfy

$$T_y^\dagger T_x^\dagger T_y T_x |x, y\rangle = e^{i2\pi\phi_{x,y}} |x, y\rangle\,. \tag{D.6}$$

Thus, we have a nontrivial commutation relation $T_y T_x = e^{i2\pi\phi_{x,y}} T_x T_y$. We suppose the magnetic flux is uniform and takes a rational number: $\phi_{x,y} = \phi = p/q$, where p and q are coprime integers. Then, successive application of the above commutation relation leads to $T_x^q T_y = e^{i2\pi q\phi_{x,y}} T_y T_x^q$, and thus we obtain

$$T_x^q T_y = T_y T_x^q. \tag{D.7}$$

If a Hamiltonian is composed of the hoppings T_x and T_y, the Hamiltonian commute with T_x^q and T_y, and from the same argument as Bloch theorem, the eigenstates are characterized by magnetic momentum (k_x^0, k_y) as

$$H \left| u_n(k_x^0, k_y) \right\rangle = E_n(k_x^0, k_y) \left| u_n(k_x^0, k_y) \right\rangle, \tag{D.8}$$

$$T_x^q \left| u_n(k_x^0, k_y) \right\rangle = e^{-ik_x^0 q} \left| u_n(k_x^0, k_y) \right\rangle, \tag{D.9}$$

$$T_y \left| u_n(k_x^0, k_y) \right\rangle = e^{-ik_y} \left| u_n(k_x^0, k_y) \right\rangle, \tag{D.10}$$

and the magnetic Brillouin zone is $(k_x^0, k_y) \in [-\pi/q, \pi/q] \times [-\pi, \pi]$. From the relation $T_y T_x = e^{i2\pi\phi} T_x T_y$, we have

$$T_y T_x \left| u_n(k_x^0, k_y) \right\rangle = e^{i2\pi\phi} T_x T_y \left| u_n(k_x^0, k_y) \right\rangle = e^{-i(k_y - 2\pi\phi)} T_x \left| u_n(k_x^0, k_y) \right\rangle. \tag{D.11}$$

Thus we have $T_x \left| u_n(k_x^0, k_y) \right\rangle = \left| u_{n'}(k_x^0, k_y - 2\pi\phi) \right\rangle$. Then, we have the energy periodicity

$$E_n(k_x^0, k_y) = E_{n'}(k_x^0, k_y - 2\pi\phi). \tag{D.12}$$

As a result, the energy spectra of all bands have the periodicity [1]

$$\{E_n(k_x^0, k_y)\}_n = \{E_n(k_x^0, k_y - 2\pi/q)\}_n. \tag{D.13}$$

We choose the Landau gauge $(A_x, A_y) = (0, B_z x)$ in the following. Then the translation operators become

$$T_x := \sum_{x,y} |x+1, y\rangle \langle x, y|, \quad T_y := \sum_{x,y} |x, y+1\rangle \langle x, y| e^{i2\pi\phi x}. \tag{D.14}$$

They are Fourier transformed into [2]

$$\begin{aligned} T_x &= \int_{-\pi}^{\pi} dk_x \int_{-\pi}^{\pi} dk_y e^{-ik_x} |k_x, k_y\rangle \langle k_x, k_y| \\ &= \sum_{n=0}^{q-1} \int_{-\pi/q}^{\pi/q} dk_x^0 \int_{-\pi}^{\pi} dk_y e^{-i(k_x^0 + 2\pi\phi n)} |k_x^0 + 2\pi\phi n, k_y\rangle \langle k_x^0 + 2\pi\phi n, k_y|, \end{aligned} \tag{D.15}$$

$$\begin{aligned} T_y &= \int_{-\pi}^{\pi} dk_x \int_{-\pi}^{\pi} dk_y e^{-ik_y} |k_x + 2\pi\phi, k_y\rangle \langle k_x, k_y| \\ &= \sum_{n=0}^{q-1} \int_{-\pi/q}^{\pi/q} dk_x^0 \int_{-\pi}^{\pi} dk_y e^{-ik_y} |k_x^0 + 2\pi\phi(n+1), k_y\rangle \langle k_x^0 + 2\pi\phi n, k_y|. \end{aligned} \tag{D.16}$$

[1] We have not used Hermiticity, so this relation is valid even for non-Hermitian Hamiltonians.
[2] The wave numbers in Fourier transformation is a realization of magnetic momenta.

We apply the above relations onto the model in Eq. (D.2) for $k_z = 0$,

$$H'(k_x, k_y) = e^{-ik_x\sigma_x} + e^{-ik_y\sigma_z}, \tag{D.17}$$

where we subtracted a trivial term $-\hat{1}$ and interchanged $\sigma_y \leftrightarrow \sigma_z$ [3]. We note that this model has pseudo-Hermiticity

$$\sigma_y H'(k_x, k_y)^\dagger \sigma_y = H'(k_x, k_y). \tag{D.18}$$

Under uniform magnetic flux $\phi = p/q$ for coprime integers p and q, this model becomes

$$H' = \sum_{n=0}^{q-1} \int_{-\pi/q}^{\pi/q} dk_x^0 \int_{-\pi}^{\pi} dk_y \; e^{-i(k_x^0+2\pi\phi n)\sigma_x} \left|k_x^0 + 2\pi\phi n, k_y\right\rangle \left\langle k_x^0 + 2\pi\phi n, k_y\right| \tag{D.19}$$

$$+ \begin{pmatrix} e^{-ik_y} \left|k_x^0 + 2\pi\phi(n+1), k_y\right\rangle \left\langle k_x^0 + 2\pi\phi n, k_y\right| & 0 \\ 0 & e^{ik_y} \left|k_x^0 + 2\pi\phi n, k_y\right\rangle \left\langle k_x^0 + 2\pi\phi(n+1), k_y\right| \end{pmatrix}. \tag{D.20}$$

We can rewrite it by regarding n as a sublattice degree of freedom

$$\mathcal{H}' = \int_{-\pi/q}^{\pi/q} dk_x^0 \int_{-\pi}^{\pi} dk_y \tag{D.21}$$

$$= \left[\begin{array}{c|c|c|c|c}
e^{-ik_x^0\sigma_x} & \begin{matrix}0 & 0\\ 0 & e^{-ik_y}\end{matrix} & O & \cdots & \begin{matrix}e^{ik_y} & 0\\ 0 & 0\end{matrix} \\ \hline
\begin{matrix}e^{ik_y} & 0\\ 0 & 0\end{matrix} & ie^{-i(k_x^0+2\pi\phi)\sigma_x} & \begin{matrix}0 & 0\\ 0 & e^{-ik_y}\end{matrix} & \cdots & O \\ \hline
O & \begin{matrix}e^{ik_y} & 0\\ 0 & 0\end{matrix} & \ddots & \ddots & \vdots \\ \hline
\vdots & \vdots & \ddots & ie^{-i(k_x^0+2(q-2)\pi\phi)\sigma_x} & \begin{matrix}0 & 0\\ 0 & e^{-ik_y}\end{matrix} \\ \hline
\begin{matrix}0 & 0\\ 0 & e^{-ik_y}\end{matrix} & O & \cdots & \begin{matrix}e^{ik_y} & 0\\ 0 & 0\end{matrix} & ie^{-i(k_x^0+2(q-1)\pi\phi)\sigma_x}
\end{array}\right]. \tag{D.22}$$

Here $(\mathcal{H}')_{nn'}$ is a block matrix on the basis $\left|k_x^0 + 2\pi\phi n, k_y\right\rangle \left\langle k_x^0 + 2\pi\phi n', k_y\right|$.

D.2 Exact quantization of total flux

As w_1^z and w_3 are integers, we expect the factor $\frac{eB_z}{2\pi} L_x L_y$ is also an integer. This expectation is correct. From the periodic boundary condition (PBC) for the vector potential (A_x, A_y), we obtain the quantization of total flux $\frac{e}{2\pi} \iint dxdyB_z \in \mathbb{Z}$ in general.

The Peierls substitutions

$$T_x := \sum_{x,y} |x+1, y\rangle \langle x, y| \, e^{ie\int_{(x,y)}^{(x+1,y)} \boldsymbol{A}\cdot d\boldsymbol{x}}, \quad T_y := \sum_{x,y} |x, y+1\rangle \langle x, y| \, e^{ie\int_{(x,y)}^{(x,y+1)} \boldsymbol{A}\cdot d\boldsymbol{x}} \tag{D.23}$$

[3] Strictly speaking, we need to flip $k_y \to -k_y$ when we realize the interchange $\sigma_y \leftrightarrow \sigma_z$ as a unitary transformation.

indicate that $A_x(x,y) := e\int_{(x,y)}^{(x+1,y)} \boldsymbol{A}\cdot d\boldsymbol{x}$ and $A_y(x,y) := e\int_{(x,y)}^{(x,y+1)} \boldsymbol{A}\cdot d\boldsymbol{x}$ are defined mod 2π. As a magnetic flux on a cell is given by

$$eA_x(x,y) + eA_y(x+1,y) - eA_x(x,y+1) - eA_y(x,y) = 2\pi\phi_{x,y} \text{ (mod } 2\pi), \tag{D.24}$$

the total flux on a lattice of system size $L_x \times L_y$ is becomes

$$e\iint dxdyB_z = \sum_{x=0}^{L_x-1}\sum_{y=0}^{L_y-1} 2\pi\phi_{x,y} \tag{D.25}$$
$$= \sum_{x=0}^{L_x-1}\sum_{y=0}^{L_y-1} [eA_x(x,y) + eA_y(x+1,y) - eA_x(x,y+1) - eA_y(x,y)] \tag{D.26}$$
$$= \sum_{x=0}^{L_x-1} [eA_x(x,0) - eA_x(x,L_y)] + \sum_{y=0}^{L_y-1} [eA_y(L_x,y) - eA_y(0,y)] \text{ (mod } 2\pi). \tag{D.27}$$

If we use the PBC $A_x(x,0) = A_x(x,L_y)$ and $A_y(0,y) = A_y(L_x,y)$, we obtain the constraint on the total magnetic flux; $e\iint dxdyB_z = 0$ (mod 2π), or equivalently

$$\frac{e}{2\pi}\iint dxdyB_z = n \; (n\in\mathbb{Z}). \tag{D.28}$$

For completeness, we see the explicit realization of unit flux: $\frac{eB_z}{2\pi}L_xL_y = 1$ in PBC [Fig. D.1]. It is given by

$$eA_x^0(x,y) = \begin{cases} 0 & (y = 0,\cdots,L_y-2) \\ \frac{2\pi y}{L_y} & (y = L_y-1). \end{cases}, \quad eA_y^0(x,y) = \frac{2\pi x}{L_xL_y}. \tag{D.29}$$

D.3 w_3 with and without magnetic field

One naive question is "does w_3 change before and after inserting a magnetic field?" In the CME formula, w_3 is calculated for a model without a magnetic field, while w_1 is calculated for the model with a magnetic field. We found the answer is NO! We checked the minimal model in Eq. (D.2) has $w_3 = 1$ after inserting magnetic field. [4]

We remember the non-Hermitian model Eq. (D.2) has $w_3 = 1$. Let us consider the case $\phi = 1/5$ for $k_z = 0$ [5]. The energy spectra are shown in Fig. D.2. We can see that one of the spectra is a Fermi surface of Im$E_n = 0$ with Re$E_n > 0$. We numerically calculated the Chern number of the Fermi surface and obtained $Ch = 1$. From the extended Nielsen-Ninomiya theorem in Eq. (3.8), we can say that the winding number is $w_3 = 1$ [6]. Therefore, w_3 does not change after inserting a magnetic field.

[4]Any other models can be continuously deformed into direct sums of this minimal model and trivial models. Therefore, this result assures that w_3 does not change with and without a magnetic field for any model.

[5]Strictly speaking, we need to check $w_3 = 1$ for any ϕ.

[6]We need to transform as $H \to iH$ in this case.

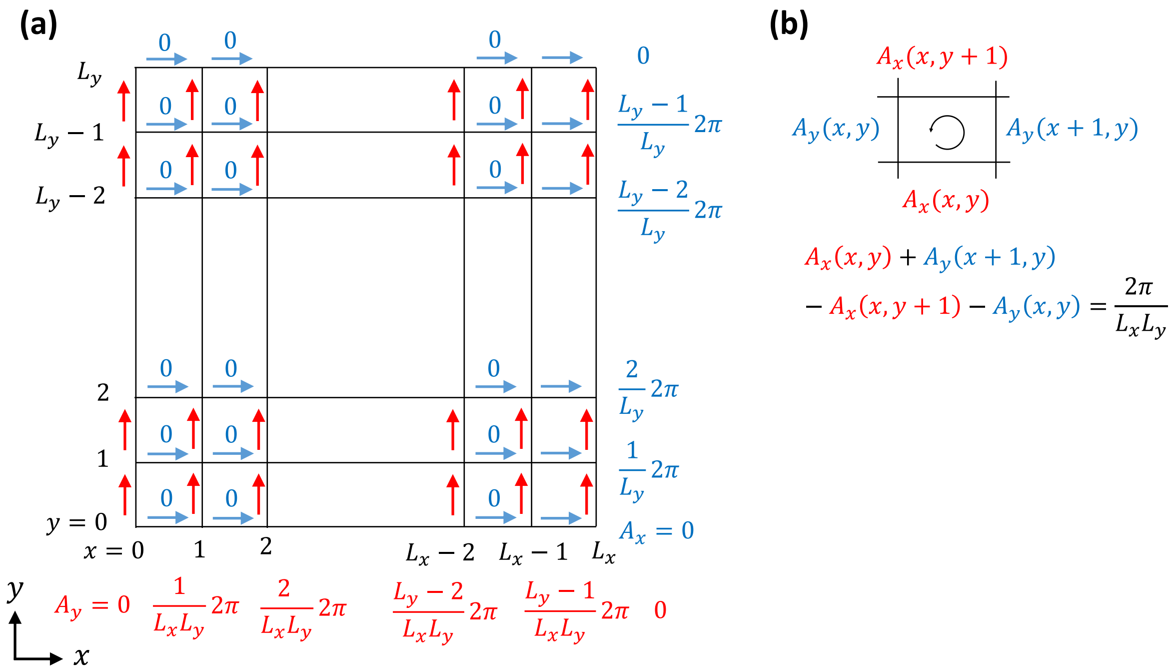

FIGURE D.1: (a) A lattice realization of a unit magnetic flux $(eB_z/2\pi)L_xL_y = 1$. F (b) These Peierls phases are chosen to satisfy $A_x(x, y) + A_y(x + 1, y) - A_x(x, y + 1) - A_y(x, y) = 2\pi/L_xL_y$. For simplicity, we have chosen the unit $e = 1$.

D.4 Finite magnetic field case

The proof of the non-Hermitian CME formula $\frac{w_1^z}{L_xL_y} = \frac{eB_z}{2\pi}w_3$ used the fact that a Weyl point becomes a ϕL_xL_y-degenerate chiral mode under an applied magnetic field $eB_z = 2\pi\phi$. The Landau degeneracy (ϕL_xL_y-degeneracy) is explained by semiclassical arguments. However, this semiclassical method may not be rigorous, especially for strong (not infinitesimally small) magnetic fields. Thus, we need to numerically confirm this formula for finite B_z. We can numerically find that this formula is exact for $\phi = p/q < 23/81$ at most for the model Eq. (D.2). For a strong enough magnetic field $\phi = p/q > 23/81$, the point gap of this model is closed.

We explain the numerical method in detail. The model $iH'(k_x, k_y) = ie^{-ik_x\sigma_x} + ie^{-ik_y\sigma_z}$, where $H'(k_x, k_y)$ is given in Eq. (D.17), has chiral symmetry $\Gamma(iH')^\dagger\Gamma = -iH'$ with $\Gamma = \sigma_y$. We apply the extended Nielsen-Ninomiya theorem for class AIII $d = 0$. It is obtained by recasting the Floquet version in Sec. 5.3.1 into a non-Hermitian version by $H = iU_F$ [7]. The point-gapped topological invariant is given by

$$n = \frac{1}{2}\left[N_+(iH\Gamma) - N_-(iH\Gamma)\right], \tag{D.30}$$

where $N_+(iH\Gamma)$ ($N_-(iH\Gamma)$) is the number of positive (negative) eigenvalues of $iH\Gamma$. The topological charge of gapless state is the chirality $\mathrm{sgn}[\langle\psi^R|\Gamma|\psi^R\rangle] = \pm 1$, where $|\psi^R\rangle$ is a right-eigenstate satisfying $H|\psi^R\rangle = E|\psi^R\rangle$ with $\mathrm{Re}E = 0$.

From this extended Nielsen-Ninomiya theorem, if the zero-dimensional point-gapped topological invariant n takes a nontrivial value, iH' has a nontrivial net number of real line-gapless modes with the chirality $\mathrm{sgn}[\langle\psi^R|\sigma_y|\psi^R\rangle] = \pm 1$.

[7] For detailed arguments about the topological duality $H = iU_F$, see Chapter 3.

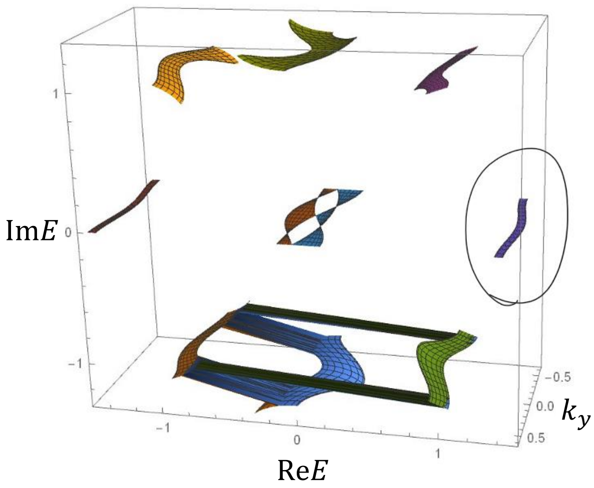

FIGURE D.2: The energy spectra of a minimal non-Hermitian Weyl model Eq. (D.2) under magnetic field $\phi = 1/5$ in z-direction for fixed $k_z = 0$. One band encircled black is imaginary line-gapless satisfying $\mathrm{Im}E_n(k_x^0, k_y, k_z = 0) = 0$ with $\mathrm{Re}E_n(k_x^0, k_y, k_z = 0) > 0$. Due to the difficulty of numerical calculations, there are meaningless planes around $\mathrm{Im}E = -1$.

If we add perturbation $k_z\sigma_y$ to $iH'(k_x, k_y)$, the real line-gapless modes have additional real energy

$$\Delta E = \langle \psi^R | k_z \sigma_y | \psi^R \rangle = \pm k_z, \tag{D.31}$$

from the first-order perturbation theory. We note that the energy takes the form of chiral modes, i.e., the real line-gapless modes, of class A $d = 1$.

According to the extended Nielsen-Ninomiya theorem for class A $d = 1$ (Eq. (3.6)), we have the relation $w_1 =$ (the number of $+k_z$ modes with Im $E > 0$) $-$ (the number of $-k_z$ modes with Im $E > 0$) for Eq. (D.2). Therefore, we have

$$\begin{aligned} w_1 &= (\text{the number of} + k_z \text{ modes with } \mathrm{Im}E > 0) \\ &\quad - (\text{the number of} - k_z \text{ modes with } \mathrm{Im}E < 0) \quad (\text{for Eq. (D.2)}) \qquad \text{(D.32)} \\ &= (\text{the number of } \langle \psi^R | \sigma_y | \psi^R \rangle = +1 \text{ modes with } \mathrm{Im}E > 0) \\ &\quad - (\text{the number of } \langle \psi^R | \sigma_y | \psi^R \rangle = -1 \text{ modes with } \mathrm{Im}E > 0 \quad (\text{for Eq. (D.17)}) \qquad \text{(D.33)} \\ &= n. \qquad \text{(D.34)} \end{aligned}$$

We can numerically check $n = \phi L_x L_y$ for $\phi = p/q < 23/81$ with $-10^2 < p, q < 10^2$.

Appendix E

Details in extrinsic quantum walks

E.1 The winding numbers $w_1[a]$, $w_1[b]$, $w_1[c]$, and $w_1[d]$ in class CII 1D

In this section, we prove that the winding number $w_1[a]$ in Sec. 5.5 takes an even integer for class CII in 1D under decomposed TRS and PHS in Eqs. (5.107) and (5.108). The following argument also holds for $w_1[b]$ $w_1[c]$, and $w_1[d]$.

For this purpose, we take the basis where CS and PHS becomes

$$\Gamma = \begin{pmatrix} \hat{1} & 0 \\ 0 & -\hat{1} \end{pmatrix}, \quad C = \begin{pmatrix} \sigma_2 & 0 \\ 0 & -\sigma_2 \end{pmatrix} K. \tag{E.1}$$

Then, PHS in Eq. (5.108) leads to the following constraints

$$\begin{pmatrix} \sigma_2 a^*(k)\sigma_2 & -\sigma_2 b^*(k)\sigma_2 \\ -\sigma_2 c^*(k)\sigma_2 & \sigma_2 d^*(k)\sigma_2 \end{pmatrix} = \begin{pmatrix} a(-k) & b(-k) \\ c(-k) & d(-k) \end{pmatrix}. \tag{E.2}$$

When the system has a energy gap at $\epsilon = 0$, one can show $\det[a(k)] \neq 0$ [38] and thus define the winding number $w_1[a]$. To see that $w_1[a]$ is an even integer, we first deform $a(k)$ into a unitary matrix [68, 77]. This deformation keeps the condition $\det[a(k)] \neq 0$, and so $w_1[a]$ does not change. After the deformation, $a(k)$ becomes diagonalizable. Because of the constraint $\sigma_2 a^*(k)\sigma_2 = a(-k)$ in Eq. (E.2) [1], any eigenstate of $a(k)$ has a Kramers partner, and thus $a(k)$ has the form of

$$\begin{aligned} a(k) = \sum_n \big[&\lambda_n(k) \left|\psi_n(k)\right\rangle \left\langle\psi_n(k)\right| \\ &+ \lambda_n^*(-k)\sigma_2 \left|\psi_n^*(-k)\right\rangle \left\langle\psi_n^*(-k)\right| \sigma_2 \big], \end{aligned} \tag{E.3}$$

[1]This constraint can be seen as TRS with $T^2 = -1$ for non-Hermitian Hamiltonians. In the periodic table in Table. 1.3, we see the point-gap topological number in class AII 1D is $2\mathbb{Z}$. This indicates that $w_1[a(k)]$ takes only even integers.

where $|\psi_n(k)\rangle$ is an eigenstate of $a(k)$ with the eigenvalue $\lambda_n(k)$. Then, we obtain

$$\begin{aligned}\mathrm{tr}[a(k)^\dagger \partial_k a(k)] &= \partial_k \log \det[a(k)] \\ &= \partial_k \log \left[\prod_n \lambda_n(k)\lambda_n^*(-k)\right] \\ &= \partial_k \left[\sum_n \log \lambda_n(k) + \sum_n \log \lambda_n^*(-k)\right],\end{aligned} \tag{E.4}$$

which leads to

$$\begin{aligned}w_1[a] &= \int_0^{2\pi i} \frac{dk}{2\pi} \mathrm{tr}[a(k)^\dagger \partial_k a(k)] \\ &= \int_0^{2\pi i} \frac{dk}{2\pi} \partial_k \left[\sum_n \log \lambda_n(k) + \sum_n \log \lambda_n^*(-k)\right] \\ &= 2\int_0^{2\pi i} \frac{dk}{2\pi} \partial_k \sum_n \log \lambda_n(k).\end{aligned} \tag{E.5}$$

As the integral

$$\int_0^{2\pi i} \frac{dk}{2\pi} \partial_k \sum_n \log \lambda_n(k) \tag{E.6}$$

takes an integer due to the periodicity of $a(k)$ in k, $w_1[a]$ is an even integer.

The same argument also holds for $w_1[b]$, $w_1[c]$, and $w_1[d]$.

E.2 Proof of Eq. (5.129)

In this section, we prove the formula in Eq. (5.129) in Chapter 5. For a rigorous argument, instead of the original quantum walk operator $\hat{U}$ having L sites, we introduce N copies of $\hat{U}$ arranged in a line, $\hat{U}_N$. Whereas $\hat{U}$ does not have translation symmetry in the presence of disorder potentials, $\hat{U}_N$ has translation invariance of L-sites translations. We also assume PBC for $\hat{U}_N$. Below we see that the position displacement in one-cycle by $\hat{U}_N$ equals the winding number of $\hat{U}(\Phi)$:

$$\begin{aligned}&\sum_{x=1}^{L}\sum_\alpha \langle x,\alpha|\, \hat{U}_N^\dagger \frac{\hat{x}}{L} \hat{U}_N \,|x,\alpha\rangle - \sum_{x=1}^{L}\sum_\alpha \langle x,\alpha|\, \frac{\hat{x}}{L} \,|x,\alpha\rangle \\ &= \int_0^{2\pi} \frac{d\Phi}{2\pi} \mathrm{tr}\left[\hat{U}^\dagger(\Phi) i\partial_\Phi \hat{U}(\Phi)\right].\end{aligned} \tag{E.7}$$

The left hand side of the above equation defines $P(T) - P$, i.e., an position-averaged version of $P_x(T) - P_x$. Equation (E.7) is the exact description of Eq. (5.129) in Chapter 5.

To show the above formula, we introduce a flux insertion to the N-copied systems

$$\hat{U}_N(\Phi) = e^{-i(\Phi/L)\hat{x}} \hat{U}_N e^{i(\Phi/L)\hat{x}}, \tag{E.8}$$

where Φ takes the discrete values of $\Phi = 2\pi p/N$ with integers p. For these values of Φ, $e^{-i(\Phi/L)\hat{x}}$ has NL-periodicity for $\hat{x}$ and thus $\hat{U}_N$ is well-defined. We note that this form of flux insertion is equivalent to the flux insertion by the uniform gauge potential $A_x = \Phi/L$. Below, we assume the large N limit, and we treat Φ as a continuous real number.

The flux inserted operator satisfies the Heisenberg equation

$$i\partial_\Phi \hat{U}_N(\Phi) = \left[\frac{\hat{x}}{L}, \hat{U}_N\right]. \tag{E.9}$$

Thus, we have

$$\hat{U}_N^\dagger(\Phi) i\partial_\Phi \hat{U}_N(\Phi) = \hat{U}_N^\dagger(\Phi)\frac{\hat{x}}{L}\hat{U}_N(\Phi) - \frac{\hat{x}}{L}, \tag{E.10}$$

which leads to

$$\begin{aligned}
&\sum_{x=1}^{L}\sum_{\alpha} \langle x,\alpha|\, \hat{U}_N^\dagger(\Phi) i\partial_\Phi \hat{U}_N(\Phi)\, |x,\alpha\rangle \\
&= \sum_{x=1}^{L}\sum_{\alpha} \langle x,\alpha|\, \hat{U}_N^\dagger(\Phi)\frac{\hat{x}}{L}\hat{U}_N(\Phi)\, |x,\alpha\rangle \\
&\qquad - \sum_{x=1}^{L}\sum_{\alpha} \langle x,\alpha|\, \frac{\hat{x}}{L}\, |x,\alpha\rangle .
\end{aligned} \tag{E.11}$$

From the translation invariance for $\hat{U}_N(\Phi)$ under L-sites translations $\mathcal{T}_L$,

$$\mathcal{T}_L^\dagger \hat{U}_N(\Phi)\mathcal{T}_L = \hat{U}_N(\Phi), \tag{E.12}$$

the left hand side of Eq. (E.11) is rewritten as

$$\begin{aligned}
&\sum_{x=1}^{L}\sum_{\alpha} \langle x,\alpha|\, \hat{U}_N^\dagger(\Phi) i\partial_\Phi \hat{U}_N(\Phi)\, |x,\alpha\rangle \\
=&\frac{1}{N}\sum_{x=1}^{L}\sum_{n=1}^{N}\sum_{\alpha} \langle x,\alpha|\, \left(\mathcal{T}_L^\dagger\right)^n \hat{U}_N^\dagger(\Phi) i\partial_\Phi \hat{U}_N(\Phi)\, (\mathcal{T}_L)^n\, |x,\alpha\rangle \\
=&\frac{1}{N}\sum_{x=1}^{NL}\sum_{\alpha} \langle x,\alpha|\, \hat{U}_N^\dagger(\Phi) i\partial_\Phi \hat{U}_N(\Phi)\, |x,\alpha\rangle \\
=&\frac{1}{N}\mathrm{tr}_N\left[\hat{U}_N^\dagger(\Phi) i\partial_\Phi \hat{U}_N(\Phi)\right],
\end{aligned} \tag{E.13}$$

where tr_N is the trace over the Hilbert space for $\hat{U}_N$. On the other hand, the first term of the right hand side of Eq. (E.11) becomes

$$\begin{aligned}
&\sum_{x=1}^{L}\sum_{\alpha}\langle x,\alpha|\,\hat{U}_N^\dagger(\Phi)\frac{\hat{x}}{L}\hat{U}_N(\Phi)\,|x,\alpha\rangle\\
=&\sum_{x=1}^{L}\sum_{\alpha}\langle x,\alpha|\,e^{-i(\Phi/L)\hat{x}}\hat{U}_N^\dagger e^{i(\Phi/L)\hat{x}}\frac{\hat{x}}{L}e^{-i(\Phi/L)\hat{x}}\\
&\qquad\times\hat{U}_N(\Phi)e^{i(\Phi/L)\hat{x}}\,|x,\alpha\rangle\\
=&\sum_{x=1}^{L}\sum_{\alpha}\langle x,\alpha|\,\hat{U}_N^\dagger\frac{\hat{x}}{L}\hat{U}_N\,|x,\alpha\rangle\,.
\end{aligned}\tag{E.14}$$

Thus, Eq. (E.11) rewritten as

$$\begin{aligned}
&\frac{1}{N}\int_0^{2\pi}\frac{d\Phi}{2\pi}\mathrm{tr}_N\left[\hat{U}_N^\dagger(\Phi)i\partial_\Phi\hat{U}_N(\Phi)\right]\\
=&\sum_{x=1}^{L}\sum_{\alpha}\langle x,\alpha|\,\hat{U}_N^\dagger\frac{\hat{x}}{L}\hat{U}_N\,|x,\alpha\rangle\\
&-\sum_{x=1}^{L}\sum_{\alpha}\langle x,\alpha|\,\frac{\hat{x}}{L}\,|x,\alpha\rangle\,.
\end{aligned}\tag{E.15}$$

Finally, we have the relation that [2]

$$\begin{aligned}
&\frac{1}{N}\int_0^{2\pi}\frac{d\Phi}{2\pi}\mathrm{tr}_N\left[\hat{U}_N^\dagger(\Phi)i\partial_\Phi\hat{U}_N(\Phi)\right]\\
&=\int_0^{2\pi}\frac{d\Phi}{2\pi}\mathrm{tr}\left[\hat{U}^\dagger(\Phi)i\partial_\Phi\hat{U}(\Phi)\right],
\end{aligned}\tag{E.16}$$

and thus we obtain Eq. (E.7).

E.3 Proof of Eq. (5.132)

The proof is almost the same as that of the formula in Eq. 5.116.

[2] Note that Eq. (E.16) can be easily shown for $U(k)=e^{\pm ik}$. In general, any model can be continuously deformed into a direct product of $U(k)=e^{\pm ik}$ and trivial models, and thus Eq. (E.16) holds.

The polarization at $t = T$ becomes

$$
\begin{aligned}
P_x(T)|_{y=1} &= \sum_\alpha \langle x, y=1, \alpha| \hat{U}^\dagger \hat{x} \hat{U} |x, y=1, \alpha\rangle \\
&= \sum_\alpha \left[\frac{1}{\sqrt{L_x}} \sum_{k_x} e^{ik_x x} \langle k_x|\right] \langle y=1, \alpha| \hat{U}^\dagger \left[\sum_{x'} x' |x'\rangle \langle x'|\right] \\
&\quad \times \hat{U} \left[\frac{1}{\sqrt{L_x}} \sum_{k'_x} e^{-ik'_x x} |k'_x\rangle\right] |y=1, \alpha\rangle \\
&= \frac{1}{L_x^2} \sum_{\alpha, k_x, k'_x, x'} e^{ik_x x} \langle y=1, \alpha| U^\dagger(k_x) e^{-ik_x x'} [-i\partial_{k'_x} e^{ik'_x x'}] \\
&\quad \times U(k'_x) e^{-ik'_x x} |y=1, \alpha\rangle \\
&= \frac{1}{L_x} \sum_{\alpha, k_x} e^{ik_x x} \langle y=1, \alpha| U^\dagger(k_x) i\partial_{k_x} [U(k_x) e^{-ik_x x}] |y=1, \alpha\rangle \\
&= \frac{1}{L_x} \sum_{\alpha, k_x} \langle y=1, \alpha| U^\dagger(k_x) [i\partial_{k_x} U(k_x)] |y=1, \alpha\rangle + \sum_\alpha x \\
&= \int_0^{2\pi} \frac{dk_x}{2\pi} \mathrm{tr}_{y,\alpha} \left[\hat{P}_{\mathrm{edge}} U^\dagger(k_x) i\partial_{k_x} U(k_x)\right] + P_x|_{y=1},
\end{aligned}
\tag{E.17}
$$

where we introduced the projection operator $\hat{P}_{\mathrm{edge}} = |y=1\rangle\langle y=1|$. Thus we obtain Eq. (5.132).

As an example for the formula in Eq. (5.132), we consider a model with 2 sites in the y-direction,

$$
\begin{aligned}
&U(k_x) \\
&= e^{-ik_x} \cos\theta |y=1\rangle \langle y=1| - e^{-ik_x} \sin\theta |y=1\rangle \langle y=2| \\
&+ \sin\theta |y=2\rangle \langle y=1| + \cos\theta |y=2\rangle \langle y=2| .
\end{aligned}
\tag{E.18}
$$

The model provides one-site displacement in the x-direction when a particle is located along $y = 1$ after one-cycle time evolution. If the particle starts at $y = 1$, only the first term in the right hand side of Eq. (E.18) affects the dynamics. Thus, the particle is expected to move in the x-direction along $y = 1$ at rate $\cos^2\theta$.

Equation (5.132) reproduces the same result. From direct calculations, we have

$$
\begin{aligned}
\hat{P}_{\mathrm{edge}} U^\dagger(k_x) &= e^{ik_x} \cos\theta |y=1\rangle \langle y=1| \\
&\quad + \sin\theta |y=1\rangle \langle y=2| , \\
i\partial_{k_x} U(k_x) &= e^{-ik_x} \cos\theta |y=1\rangle \langle y=1| \\
&\quad - e^{-ik_x} \sin\theta |y=1\rangle \langle y=2| ,
\end{aligned}
\tag{E.19}
$$

and thus the projected winding number becomes

$$
\begin{aligned}
w_P[U(k_x)] &= \int_0^{2\pi} \frac{\mathrm{d}k_x}{2\pi} \mathrm{tr}_{y,\alpha} \left[\hat{P}_{\mathrm{edge}} U^\dagger(k_x) i\partial_{k_x} U(k_x) \right] \\
&= \int_0^{2\pi} \frac{\mathrm{d}k_x}{2\pi} \mathrm{tr}_{y,\alpha} \left[\cos^2\theta \left| y=1 \right\rangle \left\langle y=1 \right| \right] \\
&= \cos^2\theta.
\end{aligned} \tag{E.20}
$$

E.4 Robustness of extrinsic chiral edge modes against random phase

In this section, we numerically check that the extrinsic edge mode in Eq. (5.113) is also robust against random phases along the edge. For this purpose, we consider U_A'' as follows,

$$
\begin{aligned}
U_A'' &= A' \cdot e^{-iH_A T}, \\
A' &= \sum_{x=1}^{L_x} e^{-i\phi_x} \left| x+1 \right\rangle \left\langle x \right| \otimes \left| y=1 \right\rangle \left\langle y=1 \right| \\
&\quad + \sum_{x=1}^{L_x} \sum_{y=2}^{L_y} \left| x \right\rangle \left\langle x \right| \otimes \left| y \right\rangle \left\langle y \right|,
\end{aligned} \tag{E.21}
$$

where ϕ_x is uniformly distributed in the range $[0, 2\pi]$. The resultant dynamics of a wave packet starting at an edge, the DOS histogram, and a edge mode distribution are shown in Fig. E.1. We can see the unidirectional wave packet motion along $y = 1$ even in this case. Actually, this behavior is ensured from the formulae Eqs. (5.129) and (5.132).

E.5 Diffusive behavior of the time-dependent Anderson model

Here we see diffusive behaviors of the time-dependent Anderson models in Eqs. (5.134) and (5.135). For this purpose, we numerically calculate $\rho(y,t)$ and $\langle y^2 \rangle$ defined by

$$
\begin{aligned}
\rho(y,t) &= \int \rho(x,y,t) dx, \\
\langle y^2 \rangle &= \int y^2 \rho(x,y,t) dx dy,
\end{aligned} \tag{E.22}
$$

where $\rho(x,y,t) = |\psi(x,y,t)|^2$ is the density distribution. If $\rho(x,y)$ obeys the diffusion equation

$$
\frac{\partial \rho}{\partial t} = \frac{D}{2} \left(\frac{\partial^2 \rho}{\partial x^2} + \frac{\partial^2 \rho}{\partial y^2} \right), \tag{E.23}
$$

with a diffusion constant D, then the solution takes the form of the Gaussian distribution:

$$
\rho(x,y,t) = \frac{1}{2\pi\sigma_t^2} \exp\left[-\frac{x^2+y^2}{2\sigma_t^2} \right], \ \sigma_t = \sqrt{Dt}, \tag{E.24}
$$

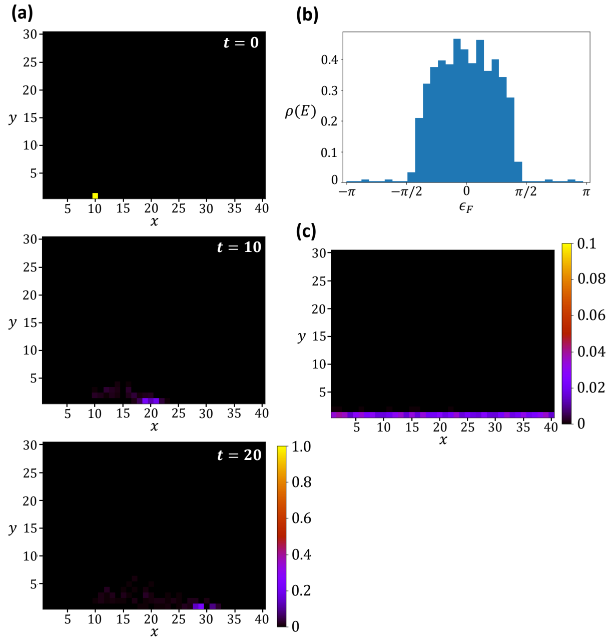

FIGURE E.1: (a) A wave packet Dynamics, (b) DOS and (c) a delocalized edge mode of the decorated Anderson model with the disordered extrinsic edge mode in Eq. (E.21). The parameters are $J = 0.2$, $W = 1$, $L_x = 25$, $L_y = 15$ and $T = 1$. The color scales are different between (a) and (c). The initial state of the wave packet is the localized state at an edge $|x = 10, y = 1\rangle$. We take the PBC (OBC) in the x-(y-)direction. Even in the presence of random phases on the boundary unitary operator, the anomalous edge state survives, and enables a unidirectional wave packet motion.

and thus we have

$$\rho(y, t) = \frac{1}{\sqrt{2\pi\sigma_t^2}} \exp\left[-\frac{y^2}{2\sigma_t^2}\right], \quad \langle y^2 \rangle = Dt. \tag{E.25}$$

We obtain the numerical results of $\rho(y, t = 100T)$ and $\langle y^2 \rangle$ for the time-dependent Anderson models in Eqs. (5.134) and (5.135) in Figs. E.2 and E.3, respectively. These numerical results show Gaussian tails for $\rho(y, t = 100T)$ and nearly linear behaviors of $\langle y^2 \rangle$ in time t, which are consistent with the diffusive behaviors in Eq. (E.25). Similar results have been reported for similar models in Refs. [178–181].

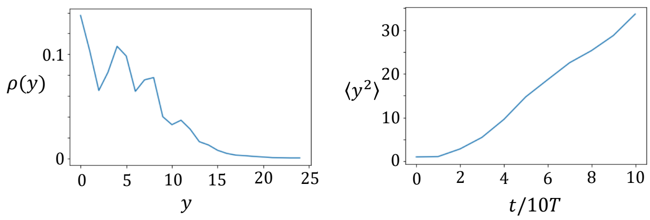

FIGURE E.2: Density distribution $\rho(y) = \rho(y, t = 100T)$ and the mean squared distance $\langle y^2 \rangle$ of the time-dependent Anderson model in Eq. (5.134). The system lengths are $L_x = 40$ and $L_y = 25$. The parameters are $J = 0.2$, $W = 1$, and $T = 1$. The initial state of the wave packet is the edge localized one $|x = 20, y = 1\rangle$. The density distribution $\rho(y)$ exhibits a Gaussian tail, and the mean squared distance $\langle y^2 \rangle$ shows a nearly linear behavior in time.

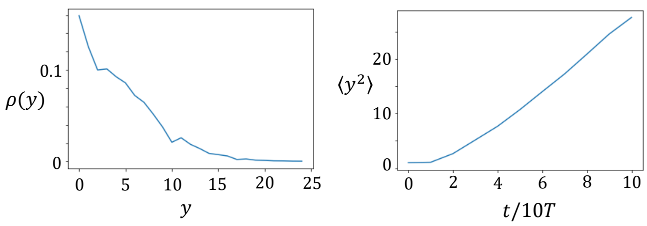

FIGURE E.3: Density distribution $\rho(y) = \rho(y, t = 100T)$ and the mean squared distance $\langle y^2 \rangle$ of the time-dependent Anderson model with the extrinsic edge mode in Eq. (5.135). System lengths are $L_x = 40$ and $L_y = 25$. The parameters are $J = 0.2$, $W = 1$, and $T = 1$. The initial state of the wave packet is the localized state at an boundary $|x = 20, y = 1\rangle$. Even in this case, we see the density distribution $\rho(y, t)$ exhibits a Gaussian tail, and the mean squared distance $\langle y^2 \rangle$ shows a nearly linear behavior in time.

Bibliography

[1] H. B. Nielsen and M. Ninomiya, “Absence of neutrinos on a lattice: (I). Proof by homotopy theory”, Nuclear Physics B **185**, 20 (1981).

[2] H. B. Nielsen and M. Ninomiya, “Absence of neutrinos on a lattice: (II). Intuitive topological proof”, Nuclear Physics B **193**, 173 (1981).

[3] S. Higashikawa, M. Nakagawa, and M. Ueda, “Floquet chiral magnetic effect”, Phys. Rev. Lett. **123**, 066403 (2019).

[4] X.-Q. Sun, M. Xiao, T. Bzdušek, S.-C. Zhang, and S. Fan, “Three-dimensional chiral lattice fermion in floquet systems”, Phys. Rev. Lett. **121**, 196401 (2018).

[5] J. Y. Lee, J. Ahn, H. Zhou, and A. Vishwanath, “Topological correspondence between hermitian and non-hermitian systems: anomalous dynamics”, Phys. Rev. Lett. **123**, 206404 (2019).

[6] T. Bessho and M. Sato, “Nielsen-ninomiya theorem with bulk topology: duality in floquet and non-hermitian systems”, Phys. Rev. Lett. **127**, 196404 (2021).

[7] K. Fukushima, D. E. Kharzeev, and H. J. Warringa, “Chiral magnetic effect”, Phys. Rev. D **78**, 074033 (2008).

[8] T. Bessho, K. Mochizuki, H. Obuse, and M. Sato, “Extrinsic topology of floquet anomalous boundary states in quantum walks”, arXiv preprint arXiv:2112.03167 (2021).

[9] K. v. Klitzing, G. Dorda, and M. Pepper, “New method for high-accuracy determination of the fine-structure constant based on quantized hall resistance”, Phys. Rev. Lett. **45**, 494 (1980).

[10] D. J. Thouless, M. Kohmoto, M. P. Nightingale, and M. den Nijs, “Quantized hall conductance in a two-dimensional periodic potential”, Phys. Rev. Lett. **49**, 405 (1982).

[11] M. Kohmoto, “Topological invariant and the quantization of the hall conductance”, Annals of Physics **160**, 343 (1985).

[12] C. L. Kane and E. J. Mele, “Quantum spin hall effect in graphene”, Phys. Rev. Lett. **95**, 226801 (2005).

[13] A. P. Schnyder, S. Ryu, A. Furusaki, and A. W. W. Ludwig, “Classification of topological insulators and superconductors in three spatial dimensions”, Phys. Rev. B **78**, 195125 (2008).

[14] A. Kitaev, “Periodic table for topological insulators and superconductors”, AIP Conference Proceedings **1134**, 22 (2009).

[15] S. Ryu, A. P. Schnyder, A. Furusaki, and A. W. Ludwig, “Topological insulators and superconductors: tenfold way and dimensional hierarchy”, New Journal of Physics **12**, 065010 (2010).

[16] C.-K. Chiu, J. C. Y. Teo, A. P. Schnyder, and S. Ryu, "Classification of topological quantum matter with symmetries", Rev. Mod. Phys. **88**, 035005 (2016).

[17] T. Morimoto and A. Furusaki, "Topological classification with additional symmetries from clifford algebras", Phys. Rev. B **88**, 125129 (2013).

[18] K. Shiozaki and M. Sato, "Topology of crystalline insulators and superconductors", Phys. Rev. B **90**, 165114 (2014).

[19] H. Sambe, "Steady states and quasienergies of a quantum-mechanical system in an oscillating field", Phys. Rev. A **7**, 2203 (1973).

[20] J. H. Shirley, "Solution of the schrödinger equation with a hamiltonian periodic in time", Phys. Rev. **138**, B979 (1965).

[21] T. Oka and H. Aoki, "Photovoltaic hall effect in graphene", Phys. Rev. B **79**, 081406 (2009).

[22] T. Kitagawa, T. Oka, A. Brataas, L. Fu, and E. Demler, "Transport properties of nonequilibrium systems under the application of light: photoinduced quantum hall insulators without landau levels", Phys. Rev. B **84**, 235108 (2011).

[23] Y. Wang, H. Steinberg, P. Jarillo-Herrero, and N. Gedik, "Observation of floquet-bloch states on the surface of a topological insulator", Science **342**, 453 (2013).

[24] G. Jotzu, M. Messer, R. Desbuquois, M. Lebrat, T. Uehlinger, D. Greif, and T. Esslinger, "Experimental realization of the topological haldane model with ultracold fermions", Nature **515**, 237 (2014).

[25] M. Bukov, L. D'Alessio, and A. Polkovnikov, "Universal high-frequency behavior of periodically driven systems: from dynamical stabilization to floquet engineering", Advances in Physics **64**, 139 (2015).

[26] T. Kitagawa, E. Berg, M. Rudner, and E. Demler, "Topological characterization of periodically driven quantum systems", Physical Review B **82**, 235114 (2010).

[27] M. S. Rudner, N. H. Lindner, E. Berg, and M. Levin, "Anomalous edge states and the bulk-edge correspondence for periodically driven two-dimensional systems", Phys. Rev. X **3**, 031005 (2013).

[28] L. Jiang, T. Kitagawa, J. Alicea, A. R. Akhmerov, D. Pekker, G. Refael, J. I. Cirac, E. Demler, M. D. Lukin, and P. Zoller, "Majorana fermions in equilibrium and in driven cold-atom quantum wires", Phys. Rev. Lett. **106**, 220402 (2011).

[29] D. Carpentier, P. Delplace, M. Fruchart, and K. Gawędzki, "Topological index for periodically driven time-reversal invariant 2d systems", Phys. Rev. Lett. **114**, 106806 (2015).

[30] J. K. Asbóth and H. Obuse, "Bulk-boundary correspondence for chiral symmetric quantum walks", Phys. Rev. B **88**, 121406 (2013).

[31] T. Morimoto, H. C. Po, and A. Vishwanath, "Floquet topological phases protected by time glide symmetry", Phys. Rev. B **95**, 195155 (2017).

[32] D. J. Thouless, "Quantization of particle transport", Phys. Rev. B **27**, 6083 (1983).

[33] R. Roy and F. Harper, "Periodic table for floquet topological insulators", Phys. Rev. B **96**, 155118 (2017).

[34] L. Privitera, A. Russomanno, R. Citro, and G. E. Santoro, "Nonadiabatic breaking of topological pumping", Phys. Rev. Lett. **120**, 106601 (2018).

[35] A. Altland and M. R. Zirnbauer, “Nonstandard symmetry classes in mesoscopic normal-superconducting hybrid structures”, Phys. Rev. B **55**, 1142 (1997).

[36] C.-K. Chiu, H. Yao, and S. Ryu, “Classification of topological insulators and superconductors in the presence of reflection symmetry”, Phys. Rev. B **88**, 075142 (2013).

[37] C.-K. Chiu and A. P. Schnyder, “Classification of reflection-symmetry-protected topological semimetals and nodal superconductors”, Phys. Rev. B **90**, 205136 (2014).

[38] K. Mochizuki, T. Bessho, M. Sato, and H. Obuse, “Topological quantum walk with discrete time-glide symmetry”, Phys. Rev. B **102**, 035418 (2020).

[39] T. Kitagawa, M. S. Rudner, E. Berg, and E. Demler, “Exploring topological phases with quantum walks”, Phys. Rev. A **82**, 033429 (2010).

[40] T. Kitagawa, M. A. Broome, A. Fedrizzi, M. S. Rudner, E. Berg, I. Kassal, A. Aspuru-Guzik, E. Demler, and A. G. White, “Observation of topologically protected bound states in photonic quantum walks”, Nat. Commun. **3**, 1 (2012).

[41] H. Obuse, J. K. Asbóth, Y. Nishimura, and N. Kawakami, “Unveiling hidden topological phases of a one-dimensional hadamard quantum walk”, Phys. Rev. B **92**, 045424 (2015).

[42] M. Nakagawa, R.-J. Slager, S. Higashikawa, and T. Oka, “Wannier representation of floquet topological states”, Phys. Rev. B **101**, 075108 (2020).

[43] M. J. Rice and E. J. Mele, “Elementary excitations of a linearly conjugated diatomic polymer”, Phys. Rev. Lett. **49**, 1455 (1982).

[44] B. A. Bernevig, *Topological insulators and topological superconductors* (Princeton University Press, 2013).

[45] J. K. Asbóth, L. Oroszlány, and A. Pályi, “A short course on topological insulators”, Lecture notes in physics **919**, 166 (2016).

[46] M. V. Berry, “Quantal phase factors accompanying adiabatic changes”, Proceedings of the Royal Society of London. A. Mathematical and Physical Sciences **392**, 45 (1984).

[47] A. Cerjan, S. Huang, M. Wang, K. P. Chen, Y. Chong, and M. C. Rechtsman, “Experimental realization of a weyl exceptional ring”, Nat. Photonics **13**, 623 (2019).

[48] A. Guo, G. J. Salamo, D. Duchesne, R. Morandotti, M. Volatier-Ravat, V. Aimez, G. A. Siviloglou, and D. N. Christodoulides, “Observation of $\mathcal{PT}$-symmetry breaking in complex optical potentials”, Phys. Rev. Lett. **103**, 093902 (2009).

[49] J. Li, A. K. Harter, J. Liu, L. de Melo, Y. N. Joglekar, and L. Luo, “Observation of parity-time symmetry breaking transitions in a dissipative floquet system of ultracold atoms”, Nat. commun. **10**, 1 (2019).

[50] V. Kozii and L. Fu, “Non-hermitian topological theory of finite-lifetime quasiparticles: prediction of bulk fermi arc due to exceptional point”, arXiv preprint arXiv:1708.05841 (2017).

[51] T. Yoshida, R. Peters, and N. Kawakami, “Non-hermitian perspective of the band structure in heavy-fermion systems”, Phys. Rev. B **98**, 035141 (2018).

[52] T. Yoshida, R. Peters, N. Kawakami, and Y. Hatsugai, “Symmetry-protected exceptional rings in two-dimensional correlated systems with chiral symmetry”, Phys. Rev. B **99**, 121101(R) (2019).

[53] M. Papaj, H. Isobe, and L. Fu, “Nodal arc of disordered dirac fermions and non-hermitian band theory”, Phys. Rev. B **99**, 201107 (2019).

[54] H. Shen and L. Fu, “Quantum oscillation from in-gap states and a non-hermitian landau level problem”, Phys. Rev. Lett. **121**, 026403 (2018).

[55] M. Ezawa, “Non-hermitian higher-order topological states in nonreciprocal and reciprocal systems with their electric-circuit realization”, Phys. Rev. B **99**, 201411 (2019).

[56] X.-X. Zhang and M. Franz, “Non-hermitian exceptional landau quantization in electric circuits”, Phys. Rev. Lett. **124**, 046401 (2020).

[57] G. Gamow, “Zur quantentheorie des atomkernes”, Zeitschrift für Physik **51**, 204 (1928).

[58] E. Majorana, “Scattering of an α particle by a radioactive nucleus”, EJTP **3**, 293 (2006).

[59] H. Feshbach, “Unified theory of nuclear reactions”, Ann. Phys. **5**, 357 (1958).

[60] H. Feshbach, “Unified theory of nuclear reactions”, Ann. Phys. **19**, 287 (1962).

[61] C. M. Bender and S. Boettcher, “Real spectra in non-hermitian hamiltonians having $\mathcal{PT}$ symmetry”, Phys. Rev. Lett. **80**, 5243 (1998).

[62] Y. C. Hu and T. L. Hughes, “Absence of topological insulator phases in non-hermitian PT-symmetric hamiltonians”, Phys. Rev. B **84**, 153101 (2011).

[63] F. K. Kunst, E. Edvardsson, J. C. Budich, and E. J. Bergholtz, “Biorthogonal bulk-boundary correspondence in non-hermitian systems”, Phys. Rev. Lett. **121**, 026808 (2018).

[64] S. Yao and Z. Wang, “Edge states and topological invariants of non-hermitian systems”, Phys. Rev. Lett. **121**, 086803 (2018).

[65] S. Yao, F. Song, and Z. Wang, “Non-hermitian chern bands”, Phys. Rev. Lett. **121**, 136802 (2018).

[66] K. Yokomizo and S. Murakami, “Non-bloch band theory of non-hermitian systems”, Phys. Rev. Lett. **123**, 066404 (2019).

[67] N. Okuma and M. Sato, “Topological phase transition driven by infinitesimal instability: majorana fermions in non-hermitian spintronics”, Phys. Rev. Lett. **123**, 097701 (2019).

[68] Z. Gong, Y. Ashida, K. Kawabata, K. Takasan, S. Higashikawa, and M. Ueda, “Topological phases of non-hermitian systems”, Phys. Rev. X **8**, 031079 (2018).

[69] Z. Lin, H. Ramezani, T. Eichelkraut, T. Kottos, H. Cao, and D. N. Christodoulides, “Unidirectional invisibility induced by $\mathcal{PT}$-symmetric periodic structures”, Phys. Rev. Lett. **106**, 213901 (2011).

[70] A. Regensburger, C. Bersch, M.-A. Miri, G. Onishchukov, D. N. Christodoulides, and U. Peschel, “Parity–time synthetic photonic lattices”, Nature **488**, 167 (2012).

[71] L. Feng, Y.-L. Xu, W. S. Fegadolli, M.-H. Lu, J. E. Oliveira, V. R. Almeida, Y.-F. Chen, and A. Scherer, “Experimental demonstration of a unidirectional reflectionless parity-time metamaterial at optical frequencies”, Nat. Mater. **12**, 108 (2013).

[72] B. Peng, Ş. K. Özdemir, F. Lei, F. Monifi, M. Gianfreda, G. L. Long, S. Fan, F. Nori, C. M. Bender, and L. Yang, “Parity–time-symmetric whispering-gallery microcavities”, Nature Physics **10**, 394 (2014).

[73] J. Wiersig, "Enhancing the sensitivity of frequency and energy splitting detection by using exceptional points: application to microcavity sensors for single-particle detection", Phys. Rev. Lett. **112**, 203901 (2014).

[74] Z.-P. Liu, J. Zhang, i. m. c. K. Özdemir, B. Peng, H. Jing, X.-Y. Lü, C.-W. Li, L. Yang, F. Nori, and Y.-x. Liu, "Metrology with $\mathcal{PT}$-symmetric cavities: enhanced sensitivity near the $\mathcal{PT}$-phase transition", Phys. Rev. Lett. **117**, 110802 (2016).

[75] H. Hodaei, A. U. Hassan, S. Wittek, H. Garcia-Gracia, R. El-Ganainy, D. N. Christodoulides, and M. Khajavikhan, "Enhanced sensitivity at higher-order exceptional points", Nature **548**, 187 (2017).

[76] W. Chen, Ş. K. Özdemir, G. Zhao, J. Wiersig, and L. Yang, "Exceptional points enhance sensing in an optical microcavity", Nature **548**, 192 (2017).

[77] K. Kawabata, K. Shiozaki, M. Ueda, and M. Sato, "Symmetry and topology in non-hermitian physics", Phys. Rev. X **9**, 041015 (2019).

[78] H. Zhou and J. Y. Lee, "Periodic table for topological bands with non-hermitian symmetries", Phys. Rev. B **99**, 235112 (2019).

[79] N. Hatano and D. R. Nelson, "Localization transitions in non-hermitian quantum mechanics", Phys. Rev. Lett. **77**, 570 (1996).

[80] N. Hatano and D. R. Nelson, "Vortex pinning and non-hermitian quantum mechanics", Phys. Rev. B **56**, 8651 (1997).

[81] N. Hatano and D. R. Nelson, "Non-hermitian delocalization and eigenfunctions", Phys. Rev. B **58**, 8384 (1998).

[82] Q. Niu, D. J. Thouless, and Y.-S. Wu, "Quantized hall conductance as a topological invariant", Physical Review B **31**, 3372 (1985).

[83] N. Okuma, K. Kawabata, K. Shiozaki, and M. Sato, "Topological origin of non-hermitian skin effects", Phys. Rev. Lett. **124**, 086801 (2020).

[84] K. Kawabata, T. Bessho, and M. Sato, "Classification of exceptional points and non-hermitian topological semimetals", Phys. Rev. Lett. **123**, 066405 (2019).

[85] H. Shen, B. Zhen, and L. Fu, "Topological band theory for non-hermitian hamiltonians", Phys. Rev. Lett. **120**, 146402 (2018).

[86] Y. Ashida, Z. Gong, and M. Ueda, "Non-hermitian physics", Advances in Physics **69**, 249 (2020).

[87] A. A. Zyuzin and A. Y. Zyuzin, "Flat band in disorder-driven non-hermitian weyl semimetals", Phys. Rev. B **97**, 041203(R) (2018).

[88] T. Matsushita, Y. Nagai, and S. Fujimoto, "Disorder-induced exceptional and hybrid point rings in weyl/dirac semimetals", Phys. Rev. B **100**, 245205 (2019).

[89] L. H. Karsten, "Lattice fermions in euclidean space-time", Physics Letters B **104**, 315 (1981).

[90] H. B. Nielsen and M. Ninomiya, "The adler-bell-jackiw anomaly and weyl fermions in a crystal", Physics Letters B **130**, 389 (1983).

[91] S. Murakami, "Phase transition between the quantum spin hall and insulator phases in 3d: emergence of a topological gapless phase", New Journal of Physics **9**, 356 (2007).

[92] X. Wan, A. M. Turner, A. Vishwanath, and S. Y. Savrasov, "Topological semimetal and fermi-arc surface states in the electronic structure of pyrochlore iridates", Phys. Rev. B **83**, 205101 (2011).

[93] A. A. Burkov, M. D. Hook, and L. Balents, "Topological nodal semimetals", Phys. Rev. B **84**, 235126 (2011).

[94] A. A. Zyuzin and A. A. Burkov, "Topological response in weyl semimetals and the chiral anomaly", Phys. Rev. B **86**, 115133 (2012).

[95] M. M. Vazifeh and M. Franz, "Electromagnetic response of weyl semimetals", Phys. Rev. Lett. **111**, 027201 (2013).

[96] S.-Y. Xu, I. Belopolski, N. Alidoust, M. Neupane, G. Bian, C. Zhang, R. Sankar, G. Chang, Z. Yuan, C.-C. Lee, S.-M. Huang, H. Zheng, J. Ma, D. S. Sanchez, B. Wang, A. Bansil, F. Chou, P. P. Shibayev, H. Lin, S. Jia, and M. Z. Hasan, "Discovery of a weyl fermion semimetal and topological fermi arcs", Science **349**, 613 (2015).

[97] N. P. Armitage, E. J. Mele, and A. Vishwanath, "Weyl and dirac semimetals in three-dimensional solids", Rev. Mod. Phys. **90**, 015001 (2018).

[98] S. Kobayashi, K. Shiozaki, Y. Tanaka, and M. Sato, "Topological blount's theorem of odd-parity superconductors", Phys. Rev. B **90**, 024516 (2014).

[99] C. Fang, Y. Chen, H.-Y. Kee, and L. Fu, "Topological nodal line semimetals with and without spin-orbital coupling", Phys. Rev. B **92**, 081201(R) (2015).

[100] F. Nathan and M. S. Rudner, "Topological singularities and the general classification of floquet–bloch systems", New Journal of Physics **17**, 125014 (2015).

[101] L. Zhou, C. Chen, and J. Gong, "Floquet semimetal with floquet-band holonomy", Phys. Rev. B **94**, 075443 (2016).

[102] C. Dembowski, H.-D. Gräf, H. L. Harney, A. Heine, W. D. Heiss, H. Rehfeld, and A. Richter, "Experimental observation of the topological structure of exceptional points", Phys. Rev. Lett. **86**, 787 (2001).

[103] M. S. Rudner and L. S. Levitov, "Topological transition in a non-hermitian quantum walk", Phys. Rev. Lett. **102**, 065703 (2009).

[104] M. Sato, K. Hasebe, K. Esaki, and M. Kohmoto, "Time-Reversal Symmetry in Non-Hermitian Systems", Progress of Theoretical Physics **127**, 937 (2012).

[105] Y. C. Hu and T. L. Hughes, "Absence of topological insulator phases in non-hermitian PT-symmetric hamiltonians", Phys. Rev. B **84**, 153101 (2011).

[106] K. Esaki, M. Sato, K. Hasebe, and M. Kohmoto, "Edge states and topological phases in non-hermitian systems", Phys. Rev. B **84**, 205128 (2011).

[107] H. Schomerus, "Topologically protected midgap states in complex photonic lattices", Opt. Lett. **38**, 1912 (2013).

[108] J. M. Zeuner, M. C. Rechtsman, Y. Plotnik, Y. Lumer, S. Nolte, M. S. Rudner, M. Segev, and A. Szameit, "Observation of a topological transition in the bulk of a non-hermitian system", Phys. Rev. Lett. **115**, 040402 (2015).

[109] T. E. Lee, "Anomalous edge state in a non-hermitian lattice", Phys. Rev. Lett. **116**, 133903 (2016).

[110] D. Leykam, K. Y. Bliokh, C. Huang, Y. D. Chong, and F. Nori, "Edge modes, degeneracies, and topological numbers in non-hermitian systems", Phys. Rev. Lett. **118**, 040401 (2017).

[111] L Xiao, X Zhan, Z. Bian, K. Wang, X Zhang, X. Wang, J Li, K Mochizuki, D Kim, N Kawakami, et al., "Observation of topological edge states in parity–time-symmetric quantum walks", Nature Physics **13**, 1117 (2017).

[112] M. Chernodub, "The nielsen-ninomiya theorem, pt-invariant non-hermiticity and single 8-shaped dirac cone", Journal of Physics A: Mathematical and Theoretical **50**, 385001 (2017).

[113] H. Zhou and J. Y. Lee, "Periodic table for topological bands with non-hermitian symmetries", Phys. Rev. B **99**, 235112 (2019).

[114] K. Kawabata, K. Shiozaki, and M. Ueda, "Anomalous helical edge states in a non-hermitian chern insulator", Phys. Rev. B **98**, 165148 (2018).

[115] H. Xu, D. Mason, L. Jiang, and J. Harris, "Topological energy transfer in an optomechanical system with exceptional points", Nature **537**, 80 (2016).

[116] S. Longhi, "Topological phase transition in non-hermitian quasicrystals", Phys. Rev. Lett. **122**, 237601 (2019).

[117] R. Okugawa and T. Yokoyama, "Topological exceptional surfaces in non-hermitian systems with parity-time and parity-particle-hole symmetries", Phys. Rev. B **99**, 041202(R) (2019).

[118] F. Song, S. Yao, and Z. Wang, "Non-hermitian skin effect and chiral damping in open quantum systems", Phys. Rev. Lett. **123**, 170401 (2019).

[119] Z.-Y. Ge, Y.-R. Zhang, T. Liu, S.-W. Li, H. Fan, and F. Nori, "Topological band theory for non-hermitian systems from the dirac equation", Phys. Rev. B **100**, 054105 (2019).

[120] F. Song, S. Yao, and Z. Wang, "Non-hermitian topological invariants in real space", Phys. Rev. Lett. **123**, 246801 (2019).

[121] K.-I. Imura and Y. Takane, "Generalized bulk-edge correspondence for non-hermitian topological systems", Phys. Rev. B **100**, 165430 (2019).

[122] K. Kimura, T. Yoshida, and N. Kawakami, "Chiral-symmetry protected exceptional torus in correlated nodal-line semimetals", Phys. Rev. B **100**, 115124 (2019).

[123] W. B. Rui, M. M. Hirschmann, and A. P. Schnyder, "$\mathcal{PT}$-symmetric non-hermitian dirac semimetals", Phys. Rev. B **100**, 245116 (2019).

[124] K. Moors, A. A. Zyuzin, A. Y. Zyuzin, R. P. Tiwari, and T. L. Schmidt, "Disorder-driven exceptional lines and fermi ribbons in tilted nodal-line semimetals", Phys. Rev. B **99**, 041116(R) (2019).

[125] Z. Yang and J. Hu, "Non-hermitian hopf-link exceptional line semimetals", Phys. Rev. B **99**, 081102(R) (2019).

[126] L. Jin and Z. Song, "Bulk-boundary correspondence in a non-hermitian system in one dimension with chiral inversion symmetry", Phys. Rev. B **99**, 081103(R) (2019).

[127] L. Zhou, "Non-hermitian floquet topological superconductors with multiple majorana edge modes", Phys. Rev. B **101**, 014306 (2020).

[128] T. Ohashi, S. Kobayashi, and Y. Kawaguchi, “Generalized berry phase for a bosonic bogoliubov system with exceptional points”, Phys. Rev. A **101**, 013625 (2020).

[129] S. Longhi, “Non-bloch-band collapse and chiral zener tunneling”, Phys. Rev. Lett. **124**, 066602 (2020).

[130] Z. Yang, C.-K. Chiu, C. Fang, and J. Hu, “Jones polynomial and knot transitions in hermitian and non-hermitian topological semimetals”, Phys. Rev. Lett. **124**, 186402 (2020).

[131] C. C. Wojcik, X.-Q. Sun, T. Bzdušek, and S. Fan, “Homotopy characterization of non-hermitian hamiltonians”, Phys. Rev. B **101**, 205417 (2020).

[132] Z. Yang, A. Schnyder, J. Hu, and C.-K. Chiu, “Fermion doubling theorems in 2d non-hermitian systems”, arXiv:1912.02788.

[133] K. Kawabata and S. Ryu, “Nonunitary scaling theory of non-hermitian localization”, arXiv:2005.00604.

[134] F. Terrier and F. K. Kunst, “Dissipative analogue of four-dimensional quantum hall physics”, arXiv:2003.11042.

[135] M. N. Chernodub and A. Cortijo, “Non-hermitian chiral magnetic effect in equilibrium”, Symmetry **12**, 761 (2020).

[136] D. S. Borgnia, A. J. Kruchkov, and R.-J. Slager, “Non-hermitian boundary modes and topology”, Phys. Rev. Lett. **124**, 056802(R) (2020).

[137] P. Titum, E. Berg, M. S. Rudner, G. Refael, and N. H. Lindner, “Anomalous floquet-anderson insulator as a nonadiabatic quantized charge pump”, Phys. Rev. X **6**, 021013 (2016).

[138] J. C. Budich, Y. Hu, and P. Zoller, “Helical floquet channels in 1d lattices”, Phys. Rev. Lett. **118**, 105302 (2017).

[139] M. M. Wauters, A. Russomanno, R. Citro, G. E. Santoro, and L. Privitera, “Localization, topology, and quantized transport in disordered floquet systems”, Phys. Rev. Lett. **123**, 266601 (2019).

[140] K. Zhang, Z. Yang, and C. Fang, “Correspondence between winding numbers and skin modes in non-hermitian systems”,

[141] M. Sato, “Topological properties of spin-triplet superconductors and fermi surface topology in the normal state”, Phys. Rev. B **79**, 214526 (2009).

[142] X.-L. Qi, T. L. Hughes, and S.-C. Zhang, “Topological invariants for the fermi surface of a time-reversal-invariant superconductor”, Phys. Rev. B **81**, 134508 (2010).

[143] M. Sato, Y. Tanaka, K. Yada, and T. Yokoyama, “Topology of andreev bound states with flat dispersion”, Phys. Rev. B **83**, 224511 (2011).

[144] A. Altland and M. R. Zirnbauer, “Nonstandard symmetry classes in mesoscopic normal-superconducting hybrid structures”, Phys. Rev. B **55**, 1142 (1997).

[145] D. Nakamura, T. Bessho, and M. Sato, in preparation (2021).

[146] M. Geier, L. Trifunovic, M. Hoskam, and P. W. Brouwer, “Second-order topological insulators and superconductors with an order-two crystalline symmetry”, Phys. Rev. B **97**, 205135 (2018).

[147] W. A. Benalcazar, B. A. Bernevig, and T. L. Hughes, "Electric multipole moments, topological multipole moment pumping, and chiral hinge states in crystalline insulators", Phys. Rev. B **96**, 245115 (2017).

[148] W. A. Benalcazar, B. A. Bernevig, and T. L. Hughes, "Quantized electric multipole insulators", Science **357**, 61 (2017).

[149] W. A. Benalcazar, T. Li, and T. L. Hughes, "Quantization of fractional corner charge in C_n-symmetric higher-order topological crystalline insulators", Phys. Rev. B **99**, 245151 (2019).

[150] Z. Song, Z. Fang, and C. Fang, "$(d-2)$-dimensional edge states of rotation symmetry protected topological states", Phys. Rev. Lett. **119**, 246402 (2017).

[151] J. Langbehn, Y. Peng, L. Trifunovic, F. von Oppen, and P. W. Brouwer, "Reflection-symmetric second-order topological insulators and superconductors", Phys. Rev. Lett. **119**, 246401 (2017).

[152] F. Schindler, A. M. Cook, M. G. Vergniory, Z. Wang, S. S. Parkin, B. A. Bernevig, and T. Neupert, "Higher-order topological insulators", Science advances **4**, eaat0346 (2018).

[153] M. Ezawa, "Higher-order topological insulators and semimetals on the breathing kagome and pyrochlore lattices", Phys. Rev. Lett. **120**, 026801 (2018).

[154] E. Khalaf, "Higher-order topological insulators and superconductors protected by inversion symmetry", Phys. Rev. B **97**, 205136 (2018).

[155] A. Matsugatani and H. Watanabe, "Connecting higher-order topological insulators to lower-dimensional topological insulators", Phys. Rev. B **98**, 205129 (2018).

[156] W. P. Su, J. R. Schrieffer, and A. J. Heeger, "Solitons in polyacetylene", Phys. Rev. Lett. **42**, 1698 (1979).

[157] A. Eckardt, "Colloquium: atomic quantum gases in periodically driven optical lattices", Rev. Mod. Phys. **89**, 011004 (2017).

[158] T. Oka and S. Kitamura, "Floquet engineering of quantum materials", Annual Review of Condensed Matter Physics **10**, 387 (2019).

[159] M. H. Kolodrubetz, F. Nathan, S. Gazit, T. Morimoto, and J. E. Moore, "Topological floquet-thouless energy pump", Physical review letters **120**, 150601 (2018).

[160] Y. Aharonov, L. Davidovich, and N. Zagury, "Quantum random walks", Phys. Rev. A **48**, 1687 (1993).

[161] J Kempe, "Quantum random walks: an introductory overview", Contemporary Physics **44**, 307 (2003).

[162] H. Obuse and N. Kawakami, "Topological phases and delocalization of quantum walks in random environments", Physical Review B **84**, 195139 (2011).

[163] D. Gross, V. Nesme, H. Vogts, and R. F. Werner, "Index theory of one dimensional quantum walks and cellular automata", Communications in Mathematical Physics **310**, 419 (2012).

[164] J. K. Asbóth, "Symmetries, topological phases, and bound states in the one-dimensional quantum walk", Phys. Rev. B **86**, 195414 (2012).

[165] B. Tarasinski, J. K. Asbóth, and J. P. Dahlhaus, "Scattering theory of topological phases in discrete-time quantum walks", Phys. Rev. A **89**, 042327 (2014).

[166] J. K. Asboth and J. M. Edge, “Edge-state-enhanced transport in a two-dimensional quantum walk”, Phys. Rev. A **91**, 022324 (2015).

[167] C Cedzich, F. Grünbaum, C Stahl, L Velázquez, A. Werner, and R. Werner, “Bulk-edge correspondence of one-dimensional quantum walks”, Journal of Physics A: Mathematical and Theoretical **49**, 21LT01 (2016).

[168] F. Cardano, M. Maffei, F. Massa, B. Piccirillo, C. De Lisio, G. De Filippis, V. Cataudella, E. Santamato, and L. Marrucci, “Statistical moments of quantum-walk dynamics reveal topological quantum transitions”, Nature communications **7**, 1 (2016).

[169] S. Barkhofen, T. Nitsche, F. Elster, L. Lorz, A. Gábris, I. Jex, and C. Silberhorn, “Measuring topological invariants in disordered discrete-time quantum walks”, Phys. Rev. A **96**, 033846 (2017).

[170] C Cedzich, T Geib, F. Grünbaum, C Stahl, L Velázquez, A. Werner, and R. Werner, “The topological classification of one-dimensional symmetric quantum walks”, in Annales henri poincaré, Vol. 19, 2 (Springer, 2018), pp. 325–383.

[171] C. Chen, X. Ding, J. Qin, Y. He, Y.-H. Luo, M.-C. Chen, C. Liu, X.-L. Wang, W.-J. Zhang, H. Li, L.-X. You, Z. Wang, D.-W. Wang, B. C. Sanders, C.-Y. Lu, and J.-W. Pan, “Observation of topologically protected edge states in a photonic two-dimensional quantum walk”, Phys. Rev. Lett. **121**, 100502 (2018).

[172] C Cedzich, T Geib, C Stahl, L Velázquez, A. Werner, and R. Werner, “Complete homotopy invariants for translation invariant symmetric quantum walks on a chain”, Quantum **2**, 95 (2018).

[173] C Cedzich, T Geib, A. Werner, and R. Werner, “Chiral floquet systems and quantum walks at half-period”, in Annales henri poincaré, Vol. 22, 2 (Springer, 2021), pp. 375–413.

[174] P. W. Anderson, “Absence of diffusion in certain random lattices”, Physical review **109**, 1492 (1958).

[175] S. Matsuura, P.-Y. Chang, A. P. Schnyder, and S. Ryu, “Protected boundary states in gapless topological phases”, New Journal of Physics **15**, 065001 (2013).

[176] B. I. Halperin, “Quantized hall conductance, current-carrying edge states, and the existence of extended states in a two-dimensional disordered potential”, Physical Review B **25**, 2185 (1982).

[177] Z. Fedorova, H. Qiu, S. Linden, and J. Kroha, “Observation of topological transport quantization by dissipation in fast thouless pumps”, Nature communications **11**, 1 (2020).

[178] N. Konno, “A path integral approach for disordered quantum walks in one dimension”, arXiv preprint quant-ph/0406233 (2004).

[179] A. Joye and M. Merkli, “Dynamical localization of quantum walks in random environments”, Journal of Statistical Physics **140**, 1025 (2010).

[180] A. Joye, “Random time-dependent quantum walks”, Communications in mathematical physics **307**, 65 (2011).

[181] D. Evensky, R. Scalettar, and P. G. Wolynes, “Localization and dephasing effects in a time-dependent anderson hamiltonian”, Journal of Physical Chemistry **94**, 1149 (1990).

[182] L. J. Maczewsky, J. M. Zeuner, S. Nolte, and A. Szameit, “Observation of photonic anomalous floquet topological insulators”, Nature communications **8**, 1 (2017).

[183] S. Mukherjee, A. Spracklen, M. Valiente, E. Andersson, P. Öhberg, N. Goldman, and R. R. Thomson, “Experimental observation of anomalous topological edge modes in a slowly driven photonic lattice”, Nature communications **8**, 1 (2017).

Acknowledgements

I would like to thank my supervisor Masatoshi Sato for his support during my master and doctoral courses. He provided me with plentiful opportunities to join many conferences, giving me various advice on the direction of my study, which greatly helped me to advance my research. It was also a great pleasure that he refined the papers written in my ugly English, otherwise many readers could have encountered difficulty reading my papers.

I also appreciate Kohei Kawabata at the University of Tokyo, Ken Mochizuki and Hideaki Obuse at Hokkaido University for many fruitful and stimulating discussions through collaborations. I appreciate Ken Shiozaki, Nobuyuki Okuma, Masaya Kunimi, Shimpei Goto, Ippei Danshita, Yukihisa Imamura, Kazuhiko Tanimoto, and Kazuma Nagao for fruitful discussions and support in academic affairs.

I would also like another Condensed Matter Theory Group including Norio Kawakami, Yoichi Yanase, Ryusuke Ikeda, Robert Peters, and Masaki Tezuka and their students for plentiful discussions during undergraduate and graduate courses.

I have greatly benefited from my colleagues in YITP for everyday discussions on physics and other topics. I am especially grateful to Taigen Kawano and Yutaro Akahoshi in the high-energy physics group for a lot of stimulating discussions and many other things as friends. I also thank some of my off-campus friends, Masashi Hashimoto, Tomohiro Yonezu, Yasuhiro Ibata, and Hiroto Mori, for non-academic affairs.

I appreciate the Kumano dormitory, which is an inexpensive apartment for students. If this dormitory were not to exist, I might have given up entering master and doctoral courses due to financial constraints. As for financial support, I also need to thank JASSO during master courses, and the Japan Society for the Promotion of Science (JSPS) through the WISE program and the research fellowship for young scientists.

When I was about ten years old, I read "Manga: Atom hakase no soutaisei-riron" (*comic: Theory of relativity explained by Dr. Atom*) written by Osamu Tezuka. This book has strongly motivated me to study theoretical physics.